THE EFFECT OF TERNARY ADDITIONS ON THE ORDERING REACTIONS IN IRON - ALUMINIUM ALLOYS

A thesis submitted for the degree

of

DOCTOR OF PHILOSOPHY

in the

University of London

by

RICHARD ADAMS

May 1971

Department of Metallurgy,
Royal School of Mines,
Imperial College of Science
and Technology,
London, S.W.7.

All things began in order, so shall they end and so shall they begin again; according to the ordainer of order and mystical mathematics in the city of heaven.

Sir Thomas Browne 1605 - 1682

ABSTRACT

The microstructure and magnetic properties of iron - aluminium alloys containing additions of copper or titanium have been studied with particular reference to the ordering reactions in the system. The alloys contained between 17·5 and 30 atomic % Al and the ternary addition in each case was 5 atomic %. The experimental techniques used were transmission electron microscopy and thermomagnetic analysis.

The addition of copper to alloys on the iron rich side of stoichiometric Fe_3Al produces a precipitate in the structure, which has been identified as Cu_3Al. On the aluminium rich side of stoichiometry, however, the copper is taken into solid solution in both the $L2_0$ and DO_3 ordered phases. This has the effect of elevating the $L2_0$ critical temperature by about 250°C whilst the corresponding temperature for the DO_3 phase is raised by 15°C. The transition from $\alpha_2(L2_0)$ to α_1 (DO_3) was found to be a non-classical phase change showing critical point fluctuations, as in the binary system.

The addition of copper results in an increase in magnetization of alloys with the DO_3 structure and an increase in the $L2_0$ Curie temperature. This second feature was largely responsible for the disappearance of the $\alpha + \alpha_2(L2_0)$ phase field observed in the binary alloy system. These effects were found to be consistent with the proposal that copper atoms substitute for iron on the wholly iron sublattice in the $L2_0$ structure and hence, on one of the two equivalent sublattices in the DO_3 structure.

It has been shown that the titanium addition, which is in solid solution in all the alloys studied, stabilizes the $L2_0$ and DO_3 phases to a comparable extent, elevating the critical temperature by 250°C in each case. The $\alpha + \alpha_1$ (DO_3)

phase field has been considerably expanded and electron microscopy has revealed modulated structures in this region, which have been attributed to spinodal decomposition. At higher temperatures a region in which the $L2_0$ and DO_3 structures coexist has been established.

The magnetization of the ordered phases is substantially reduced by the titanium addition and this has enabled coercivities of the order of 200 Oe to be obtained in alloys with the $\alpha + \alpha_1$ structure.

The potent magnetic and structural effects of the titanium addition are attributed to a specific site substitution mechanism whereby titanium replaces iron atoms in the alternate body centre positions of the DO_3 structure. Thus, a continuous transition from Fe_3Al with the DO_3 structure to Fe_2TiAl with the $L2_1$ structure is predicted.

TABLE OF CONTENTS

CHAPTER I

INTRODUCTION

Iron - aluminium alloys have been shown to exhibit some interesting magnetic properties[1,2]. In the early part of this century alloys containing up to 10 atomic % aluminium received much attention as a possible alternative to iron - silicon alloys for use in transformer cores, but were rejected on the basis of higher cost and greater difficulty of manufacture. In view of their inherent hard and brittle characteristics, the alloys have only found applications where specific combinations of properties or economic considerations have outweighed the production problems.

These two factors may be illustrated as follows:-

(i) High electrical resistivity combined with good oxidation resistance have made the alloys suitable for use as resistance heating elements.

(ii) The development of iron - aluminium alloys as a substitute for nickel-iron alloys was carried out by the Japanese in World War II who introduced "Alfer" and later by the Americans leading to "16-Alfenol". In both cases the cost and difficulty of obtaining nickel was a primary consideration. Despite these limited practical applications, the system has been the subject of many experimental and theoretical investigations with particular regard to the nature of the ordering reactions occuring.

Two types of superlattice are formed with stoichiometric compositions FeAl and Fe_3Al, but both exist over a wide composition range. In fact, alloys in the region of

25 atomic % Al first form FeAl type order, and then at a lower temperature Fe_3Al type order, the transition occuring at about 550°C. The exact shape of the equilibrium diagram in the area where this transition occurs is still a matter of some controversy but recent investigations[3,4,5] have done much to clarify the situation.

It has been shown[6] that there is an interaction between ordering and the magnetic transition occuring in these alloys and this has led to the discovery of a small region of the diagram in which magnetic heat treatments have a marked influence on microstructure[6,7]. This feature is of great importance in the closely related alnico permanent magnet alloys in which this important region has been considerably enlarged by the addition of nickel.

The complex alnico alloys of today have been produced as a result of systematic studies aimed at determining empirically the optimum compositions and their most appropriate thermomagnetic treatments. A typical composition for a present day magnet alloy (Alnico 450) is Fe-34Co-14Ni-7.5Al-3.5Cu-5Ti (weight percent).

Recent investigations[8,9,10] have been able to establish the main outlines of the relationship between microstructure and magnetic properties, but there are many details which still require clarification. Notable in this respect is the marked effect of titanium and other minor additions.

The present investigation was undertaken with two main objectives:

(i) To establish the effect of small additions of a) copper and b) titanium on the ordering reactions in iron-

aluminium alloys.

(ii) To use these results to make a contribution to the understanding of the properties of the more complex commercial magnet alloys.

With regard to the first objective, it was hoped that by choosing two such alloying additions as copper and titanium, both of which form compounds of the type M_3Al, the interaction between the ordering and magnetic transitions would be changed in a way which would further clarify the situation in the binary alloy.

The alloying addition was chosen to be 5 atomic % in each case, and the experimental techniques used are transmission electron microscopy of thin foils and magnetic analysis.

CHAPTER II

2:1 Description of phases

As a preface to a discussion of the literature on the nature of the iron rich portion of the iron - aluminium equilibrium diagram, a brief description of the phases existing in this region is necessary. The disordered, bcc α phase may form two ordered structures based on the stoichiometric compositions FeAl and Fe_3Al. The respective Strukturbericht[11] notations for these superlattices are $L2_0$ and DO_3. A brief description of each is given below, a more detailed account of their features is given by Marcinkowski and Brown[12].

2:1:1 The $L2_0$ type superlattice

A diagram of the unit cell of the $L2_0$ superlattice is shown in Fig. 2:1a. It will be seen that the lattice points have been divided equally into two interpenetrating sublattices. Thus, in the case of perfect long range order for FeAl, all the sites associated with one sublattice are occupied exclusively by iron atoms, while the other sublattice is wholly occupied by aluminium atoms. It is apparent from the diagram that the nearest neighbours of any Fe atom are all Al atoms and vice versa.

The ordering process which leads to a fully ordered structure may occur at different points in a crystal almost simultaneously. This gives rise to relative displacements of atoms in different regions of the crystal and the occurence of antiphase boundaries. Associated

FIG 2:1a

$L2_0$ SUPERLATTICE

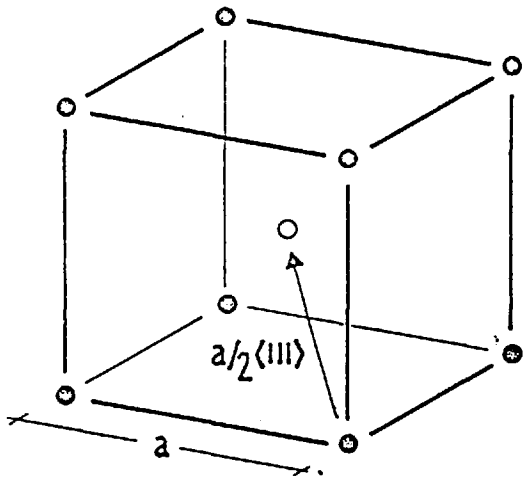

TYPE I SITE

TYPE II SITE

FIG 2:1b

DO_3 SUPERLATTICE

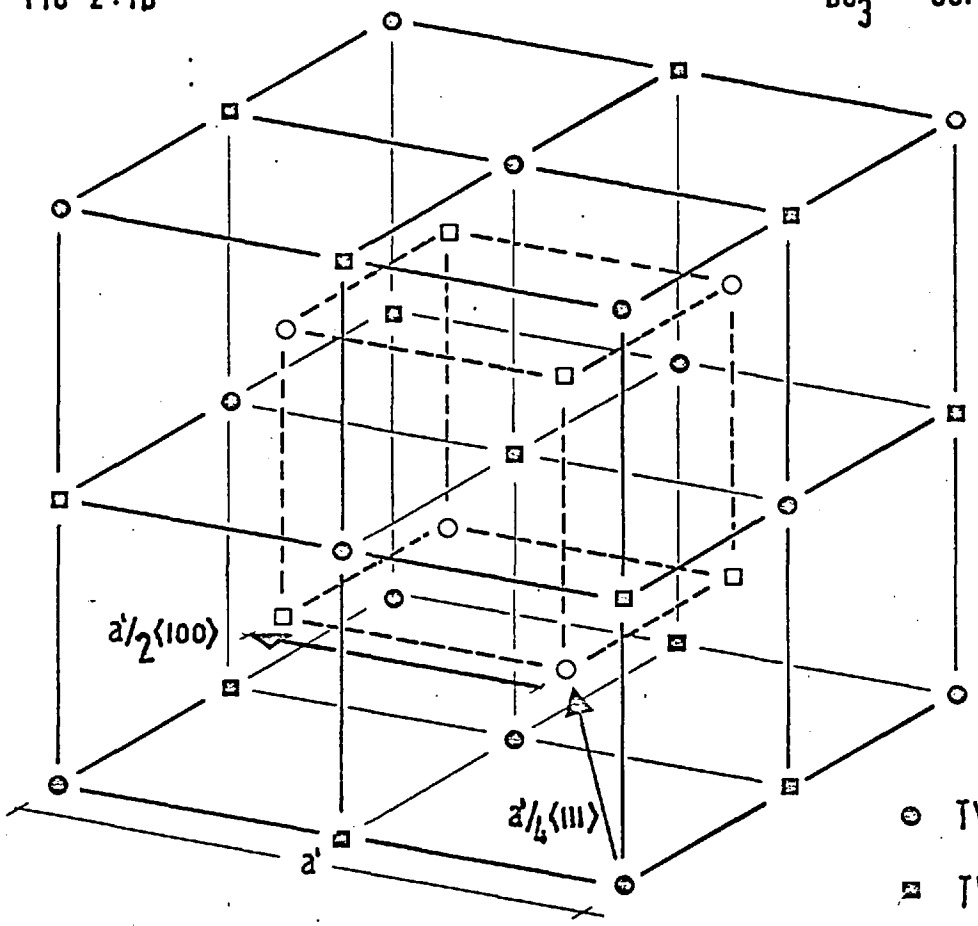

TYPE I SITE

TYPE II SITE

TYPE III SITE

TYPE IV SITE

NOTE: a'= 2 x a

with these boundaries is an antiphase vector describing the displacement which is, in this case, of the type $\bar{p} = \pm \frac{1}{2}a$ [III]. (It will be appreciated that there are four vectors of this type).

In the case of $L2_0$ ordering there are only two possibilities of occupation of the sublattices i.e. defining the sublattices throughout the crystal as I and II, domain I represents Fe on I, Al on II; domain II represents Fe on II, Al on I.

The $L2_0$ type superlattice extends over a range of composition in iron - aluminium alloys, and for the composition Fe_3Al it exists from about 550°C to 800°C. The arrangement of atoms is such that Fe atoms occupy type I sites exclusively, while type II sites are occupied at random by the remaining Fe atoms and an equal number of Al atoms. Below about 550°C the structure undergoes a further ordering reaction to give the DO_3 superlattice which is described below:

2:1:2 The DO_3 type superlattice

A diagram of the DO_3 structure is shown in Fig. 2:1b Comparison of Figs. 2:1a and 2:1b indicates the similarity of the $L2_0$ and DO_3 superlattices, but it will be noted that the lattice parameter associated with DO_3 is twice the size of the corresponding $L2_0$ parameter. The lattice may be divided into four interpenetrating fcc lattices as shown. In Fe_3Al, Fe atoms occupy the sites on sublattices I, II and III while Al atoms occupy type IV lattice sites.

A most important feature of the DO_3 structure is that the atoms are arranged such that the maximum number

of unlike first as well as unlike second nearest neighbour pairs are formed. There are 2 distinct types of antiphase vectors for this structure characterised by the following displacements of Al atoms,
i) from type I sites to type III or IV sites i.e. $\frac{1}{4}a'[\bar{1}\bar{1}1]$
ii) from type I sites to type II sites i.e. $\frac{1}{2}a'[0\bar{1}0]$.
Vectors of this type are marked in Fig. 2:1b. It should be noted that the translation described in (i) above may be expressed in terms of the $L2_0$ lattice parameter (a) giving $\frac{1}{2}a[\bar{1}\bar{1}1]$, which is the same as the antiphase vector for the $L2_0$ structure.

The significance of these antiphase vectors in the observation of antiphase domains by electron microscopy will be discussed in section 3:6.

2:1:3 The magnetic transition

Iron - aluminium alloys containing less than about 33 atomic % aluminium are ferromagnetic at room temperature. The variation of Curie point with composition is shown on the equilibrium diagram as a dotted line.

2:1:4 Notation

In order to discuss the nature of the equilibrium diagram relating the above mentioned phases the following notation will be adopted (from Metals Handbook)[13].

α	-	disordered bcc.
α_1	-	DO_3 type order.
α_2	-	$L2_0$ type order.

The subscripts m and n will be used to denote magnetic and non-magnetic phases.

LITERATURE SURVEY

2:2 The binary equilibrium diagram

A considerable amount of literature has been published in recent years on the iron rich portion of the iron - aluminium system. Despite the diversity of the techniques used and the undoubted experimental care taken, the exact nature of the ordering reactions in this system, and hence the shape of the diagram, are still a matter of some controversy. It is proposed in this survey to review some of the more recent diagrams, indicating the experimental technique used in each case, and it is hoped that this will indicate the development of the reasoning underlying the latest revisions of the diagram.

2:2:1 X-ray diffraction

The first comprehensive X-ray investigation of the system was carried out by Bradley and Jay[14] in 1932. This study established the existance of the two long range ordered phases based on the stoichiometric compositions FeAl and Fe_3Al, in addition to the disordered phase, in alloys containing up to about 50 atomic % aluminium. On the basis of this work Hansen and Anderko[15] prepared a simple phase diagram, the main feature of which is a vertical boundary separating the α and α_2 phase fields (see previous section for explanation of notation).

The results of this work have been superceded by a more recent investigation by Taylor and Jones[16] who used a more sophisticated technique and materials of a higher purity. The priciples, however, were the same, and involved precision measurements of lattice parameters at high temperatures, using powder specimens. The phase

boundaries were indicated by discontinuities in the slopes of isothermal plots of lattice parameter vs. composition. From these results they constructed the diagram shown in Fig 2:2a. The exact boundaries of the proposed two phase fields could not be determined by the limited number of lattice parameter measurements made at elevated temperatures. In fact, the presence of the $\alpha_{1m} + \alpha_{2n}$ phase field at temperatures up to 500°C was inferred from the general shape of the lattice parameter isotherm at 25°C.

In a similar, but more comprehensive, investigation, Lihl and Ebel[17] obtained lattice parameter vs. composition isothersm showing more definite discontinuities. In addition they reported pronounced broadening of the fundamental reflections in the proposed two-phase regions. The diagram they produced indicates that the authors consider α_1 to form by a peritectoid reaction (Fig. 2:2e). It should be noted that in both these investigations[16,17] evidence for the $\alpha + \alpha_1$ phase field is much more conclusive than that for the $\alpha_1 + \alpha_2$ field.

Lawley and Cahn[18] repeated the lattice parameter measurements of Taylor and Jones[16] and found anomalies in the slopes of lattice parameter Vs temperature plots for alloys with compositions outside the limits of the two phase field proposed. They therefore concluded that anomalies in the slope of parameter plots are no sure indication of the formation of long range order, and concentrated their efforts on intensity measurements of superlattice lines. The apparatus used was a Geiger counter diffractometer used at high temperatures, and measurements were made of

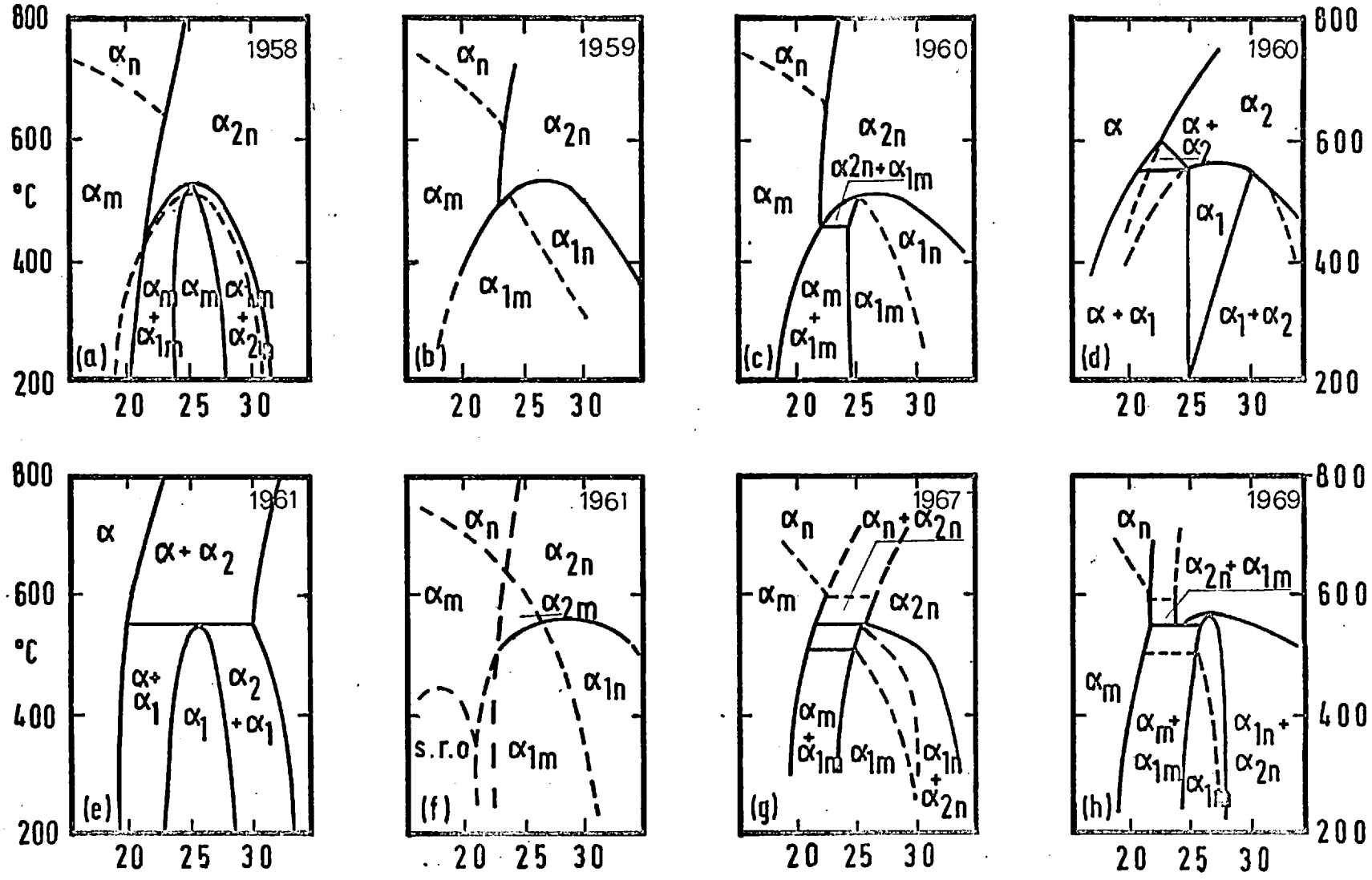

FIG 2·2

Evolution of the iron-rich portions of the FeAl equilibrium diagram since 1958

the variation of the relative intensity of superlattice lines and fundamental lines. On the basis of these measurements and a review of the results of previous measurements of physical properties (see sections 2:2:2 to 2:2:4) they proposed the diagram shown in Fig. 2:2f.

The most recent diagram proposed on the basis of X-ray results was that of Rimlinger et al[19] shown in Fig. 2:2g. Using a technique similar to that of Lawley and Cahn[18] they compared the intensity of superlattice lines characteristic of the $L2_0$ and DO_3 structures with the intensity of fundamental reflections. By ploting isothermal curves of this ratio as a function of composition they were able to detect diecontinuities corresponding to the boundaries of the proposed two phase fields.

In most cases where diagrams have been proposed on the basis of X-ray investigations the authors have examined the correlation between their X-ray data and the changes which occur in physical properties in the vicinity of the ordering reactions. Investigations dealing with these physical properties will now be considered.

2:2:2 Specific heat

The first determination of the variation of specific heat with temperature for these alloys was carried out by Sykes and Evans[2] in 1935. Their specific heat vs. temperature curves showed pronounced maxima which, in the light of present knowledge, must be associated with the α_2 to α_1 ordering reaction. Subsidiary maxima corresponding to magnetic transitions were also noted. Similar curves were obtained more recently by Eguchi et al[20], who found anomaloue results in the region of 23 atomic %

aluminium. They therefore suggested the possible existance of a two phase field of either $\alpha_1 + \alpha_2$ or $\alpha + \alpha_1$ in alloys with less than 23 atomic % aluminium.

2:2:3 Electrical resistivity

Sykes and Evans[2] found good agreement between their specific heat data and maxima occuring in resisitivity vs. temperature curves. These early experiments have been repeated by various workers for example Bennett[21] 1952, Marcinkowski and Smoluchowski[22] 1965 and Eguchi et al[20] 1967. Discrepancies between the results of these workers are attributed to the close proximity of the ordering and magnetic transformations, both of which can affect such measurements to a marked extent. This makes interpretation of the various maxima in the resistivity vs. temperature curves very difficult.

2:2:4 Dilatometry

In an attempt to avoid complications due to magnetic transitions McQueen and Kuczynski[23] made measurements using a sensitive dilatometer. On the basis of their readings they proposed the diagram shown in Fig. 2:2b. Resistivity measurements were made only to indicate when the specimens had reached equilibrium. On this basis it was found that the time to reach equilibrium between 400°C and 550°C was of the order of a few minutes. This is insufficient time to allow for a decomposition by any precipitation reaction. For this reason no two phase regions are shown on the diagram.

The failure to allow for the possible existance of two phase fields is also a feature of the investigation by Davies[24]. A comparison is made between his dilatometry data and the results of Seybolt[25] (resistivity) Showak (specific heat) and McQueen and Kuczynski[23] (dilatometry). These combined results show reasonable agreement regarding the α to α_2 transition temperature above 620°C, but considerable scatter in alloys between 23 atomic % aluminium and 25 atomic % aluminium at temperatures in the region of 500°C.

The dilatometric results of Rimlinger[26] are quoted as confirmation of the authors diagram shown in Fig. 2:2g. It is again noted that evidence for the $\alpha_m + \alpha_{1m}$ phase field is much more conclusive than that for the coexistance of the α_{1n} and α_{2n} phases. It is reported that there were differences in the heating and cooling curves for an alloy containing 23·8 atomic % aluminium. With reference to Rimlinger's diagram this would be associated with changes in the $\alpha_m + \alpha_{1m}$ structure but on this basis similar hysteresis would be expected in the curves for the alloy with 24·7 atomic % aluminium. This is not, however, reported.

It can be seen from the foregoing sections that interpretation of the results of measurements of these physical properties has proved very difficult. This is mainly due to uncertainties in the phase diagram which remain despite the extensive X-ray analysis. Direct observation of the microstructures of quenched specimens by transmission electron microscopy has shown considerable promise in resolving these difficulties. However, as indicated in the next section, the results of independant investigations are still not in perfect agreement.

2:2:5 Electron Microscopy

The crystallography of the $L2_0$ and DO_3 structures has been outlined in sections 2:1 from the work of Marcinkowski and Brown[12]. These authors thoroughly investigated the antiphase domain structures, formed in iron - aluminium alloys, by dark field microscopy. As was noted previously there are two types of antiphase vector in the DO_3 structure i.e. $\frac{1}{2}a'$ <100> and $\frac{1}{4}a'$ <111>. Boundaries with either type of vector are visible in dark field images using superlattice reflections of the type h + k + 1 = odd integer, whilst only those with $\frac{1}{4}a'$ <111> vectors are revealed by superlattice reflections of the type (h + k + 1)/2 = odd integer. In the $L2_0$ structure only boundaries having an antiphase vector $\frac{1}{2}a$ <111> occur, (equivalent to $\frac{1}{4}a'$ <111> in the DO_3 structure) and whilst these are visible for all $L2_0$ superlattice reflections, (100) type reflections are normally used because of their high intensity. In their exacting analysis of these domain structures, however, Marcinkowski and Brown[12] do not deal with the mode of transformation between the two superlattice types and make no predictions as regards the equilibrium diagram.

The application of dark field microscopy to the phase diagram was first performed by Lutjering and Warlimont[27,28] in 1964, when they confirmed the existance of the two phase field ($\alpha_m + \alpha_{1m}$). In a subsequent publication Warlimont[29] proposed the diagram shown in Fig.2:2h (which results from a more comprehensive study of the system). It can be seen that there is some measure of agreement between this diagram and that of Rimlinger (Fig. 2:2g) in that both

contain extensive (α_{1n} + α_{2n}) phase fields. However, basic differences in the mode of transformation from α_2 to α_1, in the composition range 21 atomic % to 26 atomic % aluminium, are evident.

Rimilinger[30] has produced several electron micrographs by hot stage microscopy which he offers as confirmation of his diagram but has not undertaken any detailed study of the system by this method. It is noticeable that Rilinger does not give any details of the thermal history of his specimens in this investigation, merely the temperature at which the micrographs were taken.

In their electron microscopical examinations of quenched specimens Morgand and Gjurasevic[31,32,33] and Morgand, Mouturat and Sainfort[34] examined the α_m to α_{1m} and α_1 to α_2 transitions. Their results concerning the former are in agreement with those of Lutjering and Warlimont[27,28] and Rimlinger[30] i.e. that this transition occurs by a classical, first order, reaction involving the passage through a two phase field. In the case of the α_1 to α_2 transition, however, they conclude that the mechanism is completely different. On heating a fully ordered α_1 structure, they found that the long range order decreased continously, and homogeneously, to zero at the transition temperature. Thus no stable two phase field was found to exist, and it was suggested that the reaction was not a classical phase change.

This conclusion is in full agreement with the work of Swann, Duff and Fisher[4], who have examined this reaction in great detail by dark field microscopy, using quenched specimens. Earlier work by Swann and Fisher[6] had shown that magnetization has a marked effect on the α to α_2 ordering reaction. These two observations play an

important part in the revision of the equilibrium diagram by Swann et al[4,6], proposed on evidence from a systematic electron microstructural investigation[3]. The diagram (Fig. 2:3) is markedly different from Fig. 2:2g in that there are two non-classical reactions incorporated, where Rimlinger maintains all reactions are of the classical, first order, type.

It will be noted that in Fe. 2:3 shaded areas are shown in the region of the proposed, non-classical, ordering reactions. This shading denotes the transition range and dark field micrographs of specimens quenched from this region show a very fine inhomogeneous structure. These "speckled" structures are thought, by the authors[14], to indicate critical point fluctuations in the degree of long range order. The analogy is drawn between these observations and the familiar opalescence phenomenon near critical points in vapour - liquid systems. The occurrence of these speckled structures is not considered evidence of a narrow two phase field since the small ordered zones present do not grow with increased ageing time, and their volume fraction does not obey the lever rule.

Ordering reactions exhibiting these fluctuations are observed for the transition α_1 to α_2 in alloys containing more than 25·3 atomic % aluminium and also in the case of the α_n to α_{2n} transition. Below the Curie point of the disordered structure, this latter reaction is shown to become a classical phase change in a manner predicted by theoretical considerations[35].

2:2:6 Correlation of experimental observations

The discussion, so far, has introduced the various versions of the equilibrium diagram based on experimental

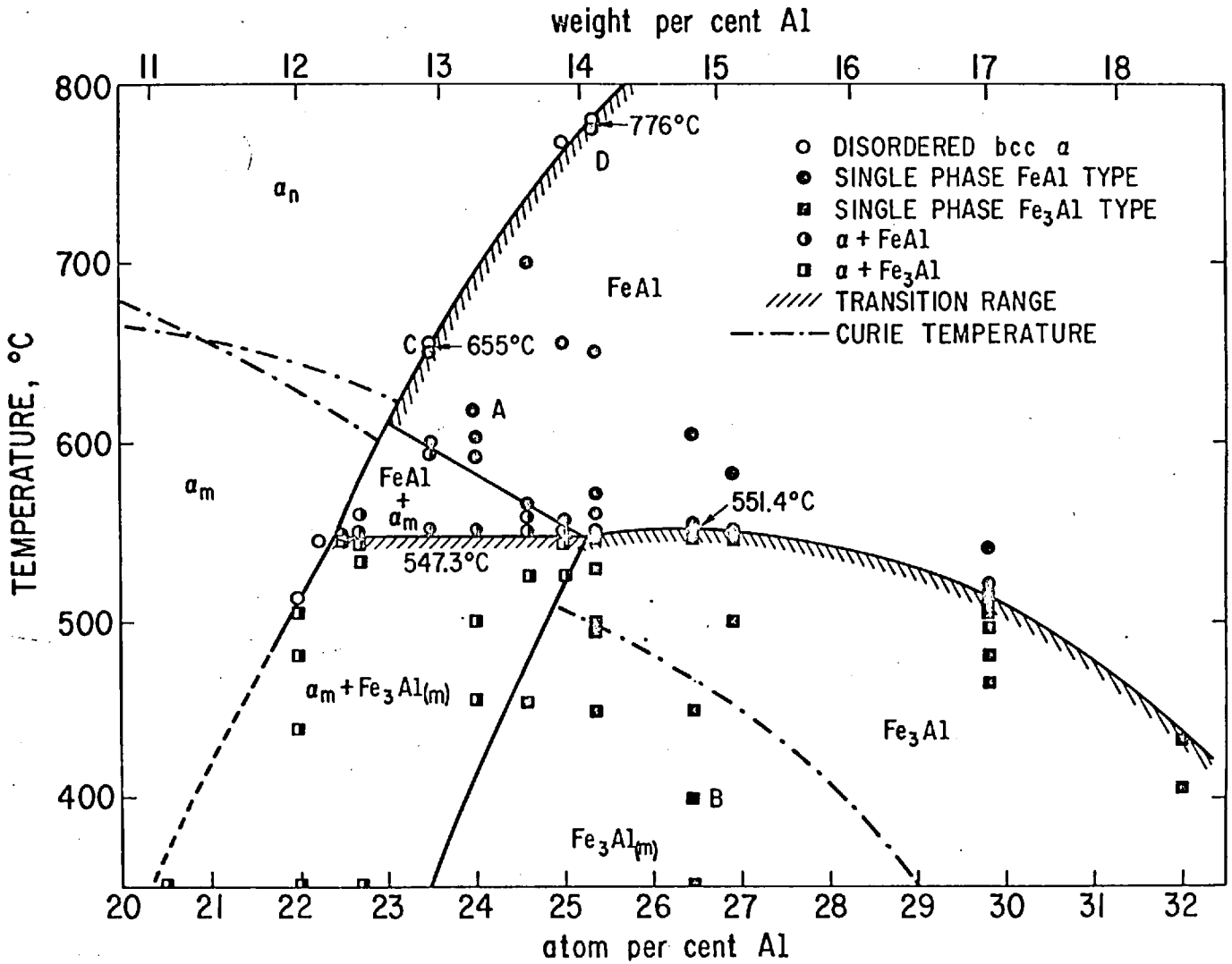

Fig 2:3 THE IRON-RICH PORTION OF THE Fe-Al BINARY PHASE DIAGRAM PROPOSED BY SWANN et al [3] (1969)

observations, as far as possible in chronological order. It is now proposed to attempt a correlation of the results and thus to indicate which diagram most nearly satisfies all the data. In such a comparison the following points emerge:

(i) There is considerable evidence[3,14,17,27,28,29,36] for the existance of the $\alpha_m + \alpha_{1m}$ phase field indicating that the α_m to α_{1m} reaction is of the first order, classical type.

(ii) There is a shift in the maximum ordering temperature for the α_1 (DO_3) structure, away from the stoichiometric Fe_3Al composition to higher aluminium contents[2,23,18,3,5].

(iii) There is general agreement on the positions of lines denoting where crystallographic order is first observed. In assesing the agreement here, consideration should be given to the fact that accurate chemical analyses of these alloys are difficult to obtain.

From a comparison of the diagrams based on X-ray measurements it is apparent that Rimlinger's diagram Fig.2:2g is the logical successor of the earlier versions, Figs.2:2a and 2:2c. This diagram does not, however, show the maximum in the DO_3 ordering temperature noted in point (ii) above. This feature is, however, incorporated in fig.2:2h and agreement between these two diagrams on other points is quite good. The diagram proposed by Warlimont[29] will therefore be considered as representing the views of those who consider that the ordering reactions in this system are all classical, first order, phase changes. Opposed to this view are Swann et al[3-6] and Morgand et al[31-34] whose observations indicate that higher order phase changes occur.

In order to evaluate the relative merits of the two schools of thought it is necessary to consider two topics as yet unmentioned. They are:

(i) The magnetic properties of the alloys and (where applicable) the influence of magnetization on the ordering reactions.

(ii) The theoretical predictions concerning the nature of the ordering reactions in this system.

2:2:7 Magnetic Properties

There has been considerable interest in the magnetic properties of iron - aluminium alloys since Sykes and Evans'[2] initial invesitigation in 1935. The technique used here, was to observe the general shape of thermomagnetic curves using rather weak fields (15 oersted). In alloys containing between 13 and 14 wt % Al (23·5 to 25·2 atomic %) the curve obtained could be described as follows. A sharp rise in magnetization was observed on cooling the alloys below 650°C to 600°C as is normal in ferromagnetic materials. This was followed by a fall in the curve to almost zero at about 550°C the magnetization remaining at this level until the temperature had fallen to between 500°C and 450°C when it again began to rise. The alloy was described as having "two ferromagnetic Curie points", one corresponding to the disordered state and one to the ordered α_1 state. The drop between these two points was explained by the transformation from a ferromagnetic disordered phase to a paramagnetic ordered phase. The inadequacy of this explanation was demonstrated by Bennett[21] and Ivanovskii and Denisov[37] who showed that alloys of this composition exhibited an anomalous increase in coercive force, by

a factor of the order of 100, in the temperature range 450°C to 550°C. This would obviously account for the difficulty of magnetizing the alloys at low fields in this temperature range.

The existance of the anomalous increase in coercive was also deduced from the work of Pal and Tarnoczi[38] who used a technique similar to Sykes and Evans[2]. They found that the unusual shape of the magnetization vs temperature curve was sensitive to cooling rate and also to the magnitude of the magnetic field, in fact, at high fields (1000 Oe) the extensive "minimum" in the curves of Sykes and Evans could be reduced to a kink, in an otherwise smoothly falling magnetization vs. temperature curve. This result was also noted by Shinohara[39].

The most important investigation of the magnetic properties of iron-aluminium alloys was carried out by Zusman[40,41], who produced comprehensive data on the change of shape of the hysteresis loop during heat treatment. These results showed the marked influence of thermomagnetic treatment on alloys containing less than 25 atomic % aluminium and also the existance of "perminvar loops" for alloys in this system. The results obtained from an alloy containing 23·2 atomic % aluminium are most interesting. For this alloy there is a sharp maximum in the coercive force (H_c) vs. temperature curve corresponding to a kink in the saturation magnetization (I_s) vs. temperature curve.

Isothermol measurements of magnetic and electrical properties by Zusman and Aptekar[42] showed that there were two diffusion processes occuring at elevated temperatures with different activation energies. The first process occured between 300°C and 450°C and was associated with

the formation of perfect order in the α_1 phase. The second, occuring between 500°C and 575°C was regarded as evidence for the existance of two phases with differing magnetic properties, in particular different Curie points. In order to explain the existance of the two phase state above 550°C a theroretical analysis of the system was performed by Aptekar[43] who produced the diagram shown in Fig. 2:2d. (At this time there had been no direct observation of $\alpha_m + \alpha_{2n}$ structures.) This type of diagram, which explains the magnetic results outlined above, bears a marked resemblance of Fig. 2:3 determined experimentally by Swann et al. The theoretical basis for Aptekar's diagram will be discussed in the next section, it is sufficient to note here that the general shape depends on estimates of the relative values of 'ordering energy' and 'energy of mixing' and that agreement between the theoretical diagram and Swann's diagram may be even better if slightly different values of these parameters are chosen.

From this discussion it appears that the shape of the two phase field $\alpha_m + \alpha_{2n}$ suggested by Swann is more compatible with the results than is that of Warlimont. The other basic difference between the two diagrams is the presence of the two phase $\alpha_{1n} + \alpha_{2n}$ phase field suggested by Warlimont. The theoretical predictions for the α_1 to α_{2n} transition will now be considered.

2:2:8 Theoretical treatment of ordering

a) The degree of order - disorder transformations.

In the previous sections the terms first order, second order or alternatively classical and non classical have been used to describe ordering reactions. The meaning of

these terms will now be discussed.

Contrary to pure metals, with a perfect crystal lattice, alloys do not exhibit translational symmetry. The only exception is the case of complete order. In an incompletly ordered alloy the symmetry does, however, present a probability that different sites will be occupied by different types of atom. This symmetry changes during an order - disorder reaction and when this happens we may consider two cases. In the first case, the probability of site substitution at the transition point changes discontinuously and a first order phase transition occurs. In the second case, the probability changes continuously and the transition is called a second order phase transition. In the first case, as originally noted by Ehrenfest[44], discontuities are observed in the first derivatives of the thermodynamic potential Φ (P,T,) with respect to temperature T and pressure P i.e.

$$\text{entropy } S = -\frac{\partial \Phi}{\partial T} \quad \text{and volume } V = \frac{\partial \Phi}{\partial P}$$

Thus there is a latent heat associated with a first order transformation. Second order phase transformations are those in which the thermodynamic potential and its first derivatives remain continuous, while the second derivatives of Φ with respect to T and P change discontinuously. Consequently a discontinuous change will occur in :-

$$\text{specific heat } C_p = T\frac{\partial S}{\partial T} = -T\frac{\partial^2 \Phi}{\partial T^2}$$

$$\text{compressibility} = -\frac{1}{V}\frac{\partial V}{\partial P} = -\frac{1}{V}\frac{\partial^2 \Phi}{\partial P^2}$$

$$\text{coefficient of thermal expansion} = \frac{1}{V}\frac{\partial V}{\partial T} = \frac{1}{V}\frac{\partial^2 \Phi}{\partial T \partial P}$$

In binary alloys it is possible to establish some general relationships between the discontinuities at the equilibrium surface. (See, for example, ref (45) pp 97-99). From these relationships, and from the condition that for a first order reaction the chemical potentials of alloy components A and B must be equal in the first and second phase, it is possible to predict the presence of a two phase region seperating the ordered and disordered phases on the equilibrium diagram. For a second order phase transition the chemical potentials change continuously through the reaction and the transition is possible without the appearance of a two phase region.

b) Second order phase transitions.

The general theory of second order phase transitions was developed by Landau and Lifshits[35]. Two approaches to the problem were adopted by these authors. In the first, the possibility of second order transition is postulated and the symmetry of the ordered and disordered phase is regarded as known. An investigation of the temperature and concentration dependance of the degree of long range order near the phase transition point is carried out, and the variation of different thermodynamic quantities during the transition is considered. Using this approach to predict the variations in degree of long range order with temperature they obtained curves which showed good agreement with X-ray results of Chipman and Warren[46] for β brass.

The second approach does not assume the existance of a second order transition but uses the general symmetry of the density probability function to predict whether such a transformation will occur in an alloy of given

structure. Included in the list of predictions[47], are the transformations A2 (bcc) to $L2_0$ and A2 to DO_3, however, transitions involving face centred and hexagonal close packed are also indicated.

Guttman[48], in his extensive review of order disorder phenomena in metals, explains the difficulties involved determining the order of a reaction from experimental measurements but concludes that from the results available.

(i) transitions from $L2_0$ or DO_3 to A2 are second order and

(ii) all others are first order.

Christian[49], supports this view and states that a feature of second order transitions is that both the superlattice and disordered phases are non - close packed structures. Guttman[48] suggests that the reason for the differentiation between the $L2_0$ to A2 and DO_3 to A2, and transformations involving fcc and hcp is the greater degree of atomic interconnection in the latter case. This, he suggests, leads to a more abrupt order - disordered change i.e. a first order transition.

c) Statistical theories of ordering.

Guttman's[48] review deals not only with experimental data but makes comparisons between this and the various "statistical theories" of ordering. These theories are all based on an expression for the potential energy of an alloy obtained by considering nearest neighbour interactions, using what is commonly called the Ising model. This model may be made the basis of a statistical thermodynamic calculation but an exact solution for 3 dimensional crystals

is a formidable task. The various "theories" by Bragg and Williams[50], Bethe[51], Yang[52] and others are merely different mathematical techniques employed to yield approximate solutions of the problem.

d) The particular case of iron - aluminium alloys.

These methods have been applied to the particular case of iron - aluminium alloys and the results are shown in diagrams 2:2c and 2:2d. Fig. 2:2c was proposed by Rudman[53] who reviewed experimental data and combined these results with his own calculations using the quasi-chemical method. These calculations indicated that at aluminium contents less than 25 atomic % the transition from α_1 to disorder was a first order transition, whereas above 25% the transition α_1 to α_2 was second order. The former conclusion is not in agreement with Guttman[48] and Rudman suggests that Guttman's rules should be restricted to systems with only one independent order parameter. In the iron - aluminium system below 25 atomic % aluminium the reaction α to α_1 occurs necessitating changes in two long range order parameters, which involve both first nearest and second nearest neighbour interactions. Above 25 atomic % aluminium the ordering reaction may be considered in two parts:- α to α_2 as ordering of a body centred cubic lattice at a given composition to the CsCl structure; and α_2 to α_1 as ordering of a simple cubic lattice to an NaCl structure at the composition existing on the sublattice involved. (The CsCl structure may be considered as consisting of two interpenetrating sublattices,- see section 1 - one of which is involved in the second ordering reaction).

The diagram produced by Aptekar[43] Fig. 2:2d has already been mentioned with particular reference to the

shape of the $\alpha + \alpha_2$ phase field. This diagram was produced by a generalisation of the Bragg - Williams method involving three energy parameters, the energy of long range order of the AB and A_3B types and what is described, in translation, as the energy of displacement. The first two terms are denoted V_1 and V_2 respectively whilst the latter is given the symbol U and appears in a contribution to the overall free energy of the system of the form $+ C_A C_B U$, where C_A and C_B are the atomic fractions of the A and B alloy components. It would thus seem more reasonable to identify the energy parameter U with the free energy of mixing, which would provide a contribution of this form.

These energies, which are based on nearest neighbour, and next nearest neighbour interactions, may be described by the following relationships:

$$V_1 = 2N[2v'_{AB} - (v'_{AA} + v'_{BB})]$$

$$V_2 = \tfrac{3}{2}N[2v''_{AB} - (v''_{AA} + v''_{BB})]$$

$$U = 4V_1 + 16V_2$$

where v'_{AA}, v'_{BB} and v'_{AB} are the energies of nearest neighbour interaction in the first co-ordination sphere, while v''_{AA}, v''_{BB} and v''_{AB} are interactions with the second sphere. N in these equations is the total number of lattice points. Aptekar notes that in the general case, when other components of the bonding energy are taken into consideration, the ratio between V_1 and V_2 and also between U and V_1 and V_2 may vary from system to system. This means that the

generalised Bragg - Williams theory can be applied to a particular system and a whole family of equilibrium diagrams predicted, depending on the absolute and relative values of the energy parameters chosen. For the particular case of iron - aluminium alloys the analysis predicts that, for the case where $U > 4V_1 + 16V_2$, decomposition at the extremities of the DO_3 phase field will occur and the $\alpha + DO_3$ and $DO_3 + L2_0$ two phase structures will be stable, whilst for $U \leqslant 4V_1 + 16V_2$ such decomposition will not occur. The diagram shown in Fig. 2:2d is for the case where $U = 0$ $V_1 = -500R$ $V_2 = -163R$ i.e. $U > 4V_1 + 16V_2$.

The particular components of the bonding energy which give rise to the variation in U are not specified. In this connection it should be noted that alloys with aluminium contents less than 33 atomic % are ferromagnetic at room temperature while those above are not. The ferromagnetic state would be expected to favour Fe - Fe bonds and the energy associated with these would be in opposition to the mixing energy. This would favour the condition $U > 4V_1 + 16V_2$ and hence stabilise the $\alpha + DO_3$ structure. At higher aluminium contents there is no contribution from magnetic energy and it is suggested that decomposition to the $L2_0 + DO_3$ structure is not energetically favourable. Under these conditions where the ratio of U to V_1 and V_2 is considered to vary within the system, the theoretical predictions would seem to be in excellent agreement with the results of Swann et al.

The revision of Aptekar's diagram, outlined above, is based on the suggestion that interactions between magnetization and order can affect phase stability. Such interactions have been proposed by Sato[54], Houska[55] and Lavis and Bell[56] in similar theoretical analyses of this problem.

e) Summary

If the effects of interaction between magnetization and crystallographic order are taken into consideration then it may be predicted, from Aptekar's analysis[43], that the $\alpha + \alpha_1$ phase field will be stable but the coexistance of α_1 and α_2 will not be observed. This is in agreement with the work of Rudman[53] who concludes that below 25 atomic % aluminium the α_m to α_1 reaction is first order, and above 25 atomic % the α_2 to α_1 reaction is second order.

A second important feature of Aptekar's diagram is the prediction of a triangular $\alpha_m + \alpha_2$ phase field, and considering these results jointly it can be seen that these theoretical analyses are in good agreement with the experimental observations of Swann et al.

2:2:9 Conclusion regarding the phase diagram

This review of the literature concerning the iron rich portion of the iron - aluminium system indicates that the equilibrium diagram proposed by Swann et al[3] shows the best agreement with experimental data and theoretical predictions for these alloys. In particular, it explains many of the anomalies in physical properties found in the range 22 atomic % to 25 atomic % aluminium, shows the type of ordering reactions expected, and is based on extensive electron microscopical evidence[3,4,5] corroborated by other workers[31-34]. In the light of this conclusion, the following points may help to explain the diversity of opinion regarding this system.

i) Electrical resistivity and specific heat results for this system would be difficult to interpret because of the proximity of magnetic and ordering reactions.
ii) X-ray investigations using the lattice parameter method are unsuitable for detecting second order phase changes as they do not give sufficiently sharp evidence of phase boundaries.
iii) In considering the conflicting evidence produced by electron microscopy. It should be emphasised that Swann et al[3,4,5] worked with specimens held at a certain temperature and the quenched, whilst Warlimont[29] worked with slowly cooled specimens. It is suggested that Warlimonts results do not correspond to alloys in the equilibrium condition.

2:3 Commercial magnet alloys containing iron and aluminium

In their investigation of the binary iron - aluminium system Swann and Fisher[6] have shown that the microstructure of alloys heat treated in the ($\alpha_m + \alpha_{2n}$) phase field can be influenced by an externally applied magnetic field. They observed that α_m particles in an α_2(FeAl) matrix or α_2 particles in an α_m matrix could both be aligned and elongated in the field direction. These particular results have been confirmed in a recent investigation by Warlimont[7]. Swann's observations[5] indicate that in this composition range, the α_m phase forms as a product of spinodal decomposition. He suggests that the proximity of the spinodal and the Curie temperature accounts for the good response of these alloys to magnetic ageing in agreement with the theoretical predictions of Cahn[57]. Alloys

possessing this structure of aligned ferromagnetic particles in a paramagnetic or weakly ferromagnetic matrix show good magnetic properties, e.g. high values of coercive force (H_c), at temperature. When cooled to room temperature the beneficial effect of the aligned precipitates is lost as the matrix becomes strongly ferromagnetic. The addition of nickel to these alloys has the effect of greatly expanding the $\alpha_m + \alpha_{2n}$ phase field, depressing the Curie points of α_2 and α_1, and these factors have been of major importance in the development of the present range of magnetic materials based on the Fe-Ni-Al system.

2:3:1 The Development of Alnico alloys

a) Composition.

It should not be concluded from the foregoing section that the development of magnetic alloys has been achieved by theoretical predictions and careful studies of the phase diagram. On the contrary, since Mishima[58] introduced 'MK' or Alnico 3 (63 Fe 25Ni 12AL) in 1931, found during a routine investigation of alloys for use at high temperatures, most improvements have been achieved as a result of routine trial and error investigation. Briefly, the developments since 1931 have been as follows:

Copper has been found to give a slight increase in coercive force when added on its own. Additions of cobalt, to elevate the Curie point, together with copper enabled simplifications in heat treatments to be made, and produced marked improvements in magnetic properties. The beneficial effect of magnetic field treatment was discovered in 1938[59,60] and this was found to be due to preferential precipitation of a second phase along the <100> crystal axes nearest to the direction of the applied field. This

led to the idea of using unidirectional solidification to encourage the growth of columnar crystals with their <100> major growth directions aligned, prior to magnetic heat treatment. Titanium was found to be a grain refiner but had the advantage of increasing the coercive force. Alloys containing titanium were much improved by substantially increasing the cobalt content, in fact the alloys of this type, with the highest energy products today, contain as much as 8%Ti and 40%Co (by weight).

The history of the development of these alloys is summarized in the table (Fig. 2:4) and further details may be found in recent review articles[61,62].

Although substantial improvements have been made in the magnetic properties of Alnico type alloys by careful control of alloying additions and complicated heat treatments, the microsturctural changes occuring in the alloys and the relationship between these changes and magnetic properties are not completely understood.

b) Heat treatment.

The heat treatment used for a typical titanium free Alnico alloy (Ticonal 600*) will now be considered with reference to the simplified quasi-binary diagram shown in Fig. 2:5. After the alloy has homogenized at 1300°C it is subjected to a rapid cooling down to 920°C to avoid the precipitation of the γ (fcc) phase. The next stage is slow cooling at about 0·5°C/sec in a magnetic field to 600°C followed by double tempering at 640°C and 550°C. In alloys containing titanium e.g. Ticonal 1500**

*Ticonal 600 Fe-24Co-14Ni-8Al-3Cu (Wt %)

**Ticonal 1500 Fe-34Co-15Ni-7.5Al-4Cu-5Ti (Wt %)

FIG 2·4 THE DEVELOPMENT OF HIGH COERCIVE FORCE ALLOYS IN THE Fe-Co-Ni-Al SYSTEM (from ref. 61)

Date of introduction	Alloy	Nominal composition						Treatment*	Magnetic properties		
		Ni	Co	Cu	Al	Ti	Nb		B_r, G	H_c, Oe	$(BH)_{max}$, M.G.O.
1931	Alni	25	—	5	12·5	—	—	A	5600	580	1·3
1934	Alnico	18	12	5	9·5	—	—	A	7250	560	1·7
1939	Ticonal G Alnico V	14	24	3	8	—	—	B	13500	580	5·7
1939	Ticonal E Alnico VI	14	24	3	8	1·5	—	B	11100	740	4·1
1947	Alcomax III	13·5	24	3	8	—	0·6	B	12600	650	5·4
1947	Alcomax IV	13·5	24	3	7·8	—	2·5	B	11500	750	4·5
1948	Ticonal K Koerzit 350	15	30	4	7	5	—	B	8500	1150	3·6
1955	Hycomax III Ticonal X Alnico VIII	14	34	4	7	5	—	C	8800	1500	5·3
1960	Hycomax II	14	29	3	7	4	2	B	8500	1200	4·0
1964	Hycomax IV Sermalloy A_1	14	40	3	7·5	8	—	C	7400	2100	6·0

* A Continuous cool without field, followed by tempering.
B Continuous cool in magnetic field, followed by tempering.
C Isothermal treatment in magnetic field, followed by tempering.

FIG 2·5 PSEUDO-BINARY SECTION

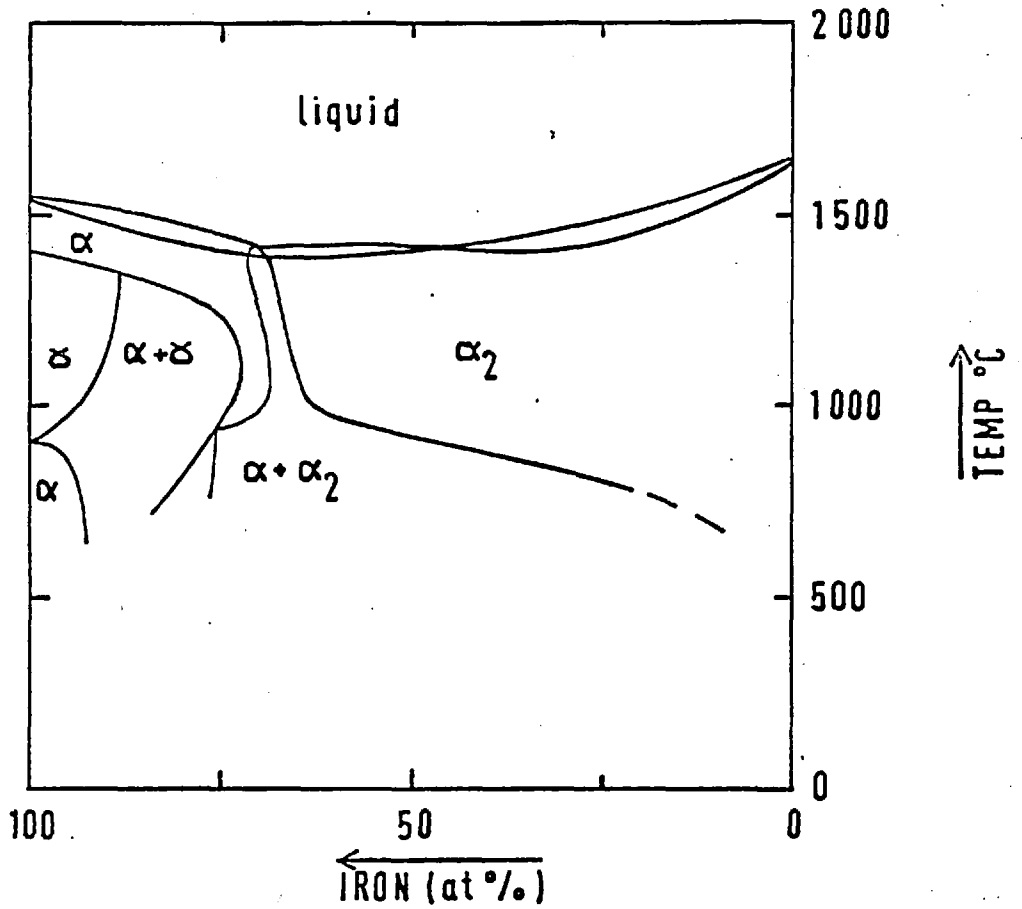

Fe-NiAl Psuedo-Binary Vertical Section of
Fe-Ni-Al Ternary Diagram
(from ref.62)

the optimum magnetic properties are obtained by inserting a magnetic anneal in the heat treatment sequence, immediately after the controlled cooling in a magnetic field.

2:3:2 The microstructure of alnico alloys.

During cooling in the magnetic field from 920°C to 600°C the disordered bcc solid solution decomposes into two phases normally denoted α_1 and α_2. To maintain continuity of notation with the phases occuring in the binary system the α_1 phase will simply be referred to as α. It has been shown by Heidenreich and Nesbitt[63] using X-ray analysis, that both phases have body centred cubic structures with slightly different lattice parameters, and that one of the phases is ordered. The morphology of these alloys was studied by de Vos[8] who used transmission electron microscopy of oxide replicas and by this method showed that the $\alpha + \alpha_2$ structure forms by means of a spinodal decomposition. This technique had the disadvantage that the phases involved could not be identified by electron diffraction analysis, and this prompted an investigation using thin foils by Bronner et al[9]. The aim of their study was to compare the microstructural changes occuring in Ticonal 600 and Ticonal 1500 during their industrial heat treatments and to relate these to their magnetic properties. The results were interpreted according to de Vos's assertion that the α phase is rich in iron and cobalt and is strongly ferromagnetic, whilst the α_2 phase is rich in nickel and aluminium and only weakly ferromagnetic.

Electron diffraction showed that the α_2 phase possesses the ordered CsCl structure characteristic of NiAl (and FeAl) and thus the $\alpha + \alpha_2$ phase field in these complex alloys may be regarded as an enlargement of the $\alpha_m + \alpha_{2n}$ region of the binary alloy system.

The alloys owe their good magnetic properties to a structure consisting of a fine, uniform dispersion of elongated single -domain ferromagnetic particles in a non - magnetic matrix. The theory concerning the coercivity of such a structure has been proposed by Stoner and Wohlfarth[69] who derived the following relationship for a group of ellipsoidal single - domain particles, all orientated in the same direction.

$$H_c = p(1 - p)\ (N_2 - N_1)\ \frac{(I_1 - I_2)^2}{I_s}$$ where N_1 and N_2 are, respectively, the demagnetization factors along the major and minor axes of the ellipsoid, I_1 and I_2 the saturation magnetization of the ellipsoid and the surrounding matrix, p the packing factor of the precipitated phase and I_s the average saturation magnetization of the assembly as a whole. It may be seen from this equation that the coercivity is a function of the precipitate shape, volume percentage and composition and also of the composition of the matrix.

It has been established that the fine distribution of precipitates in alnico alloys is achieved by spinodal decomposition and the application of a magnetic field during the transformation promotes the shape anisotropy. A quantitative study of the shape and volume fraction of the precipitate has been made by Bronner et al[9] but determination

of the exact composition of the phases has proved to be a more difficult problem. The annealing treatments given to alnico alloys permit diffusion between the precipitate and matrix leading to a sharper difference in composition, and hence saturation magnetization, than that present in the initial stages of decomposition. This fact has been illustrated by the Mössbauer measurements reported by Pfeiffer[10]. After such annealing treatments the structure of Ticonal 1500 was examined by Bronner et al[9]. By comparison with Ticonal 600 it was possible to conclude that titanium refines the spinodal structure, however, it was further observed that additional superlattice spots was present in the diffraction patterns of the alloy containing titanium. Similar diffraction patterns were obtained from a two phase structure occuring in a specially produced alloy of composition Fe-8Al-3.2Ti (weight percent) but the second phase was not identified.

In an investigation by electron microscopy similar to that of Bronner et al Pfeiffer[10] suggested that the extra spots observed could be attributed to the presence of the α_1 phase based on Fe_3Al. The reasons why this phase should occur only in alloys containing titanium were not clarified and several other interpretations of structural features were based on a version of the iron - aluminium binary diagram (Fig. 2:2h) which, in the light of the preceeding survey is considered incorrect. The uncertainty regarding the interpretation of these extra superlattice spots has been resolved only very recently by Mason, Ashall and Dean[70] who managed to extract one of the phases in a titanium containing alnico alloy and determine its composition by electron - probe microanalysis.

The results, when taken in conjunction with magnetic analysis, showed that the precipitate was disordered and rich in iron and cobalt, as is the case for titanium free alloys. The matrix, however, was found to have the $L2_1$ structure, characteristic of Heusler alloys of the type Cu_2MnAl. The composition found was close to $(NiCo)_2(TiFeCu)Al$. This is a contrast with the results for titanium free alloys in which the matrix has the $L2_0$ structure. It should be emphasised that the $L2_1$ and DO_3 structures are very similar the distinction being one of common usage of the Strukturbericht notation. In this particular $L2_1$ structure, with reference to Fig. 2:1b, sublattices I and II are equivalent and are occupied by Ni and Co atoms, sublattice III is occupied by Fe, Ti and Cu atoms and sublattice IV by Al atoms. Thus the notation $L2_1$ is used where three different types or groups of atoms are involved (e.g. Cu_2MnAl) and DO_3 where three sublattices are equivalent and only two types of atom are involved e.g. Fe_3Al.

It may be seen from the above that Pfeiffer's interpretation of the diffraction pattern involves the correct symmetry of the structure present, but his conclusion that it is Fe_3Al is incorrect. The additional spots are explained by the matrix having the $L2_1$ structure and not by the existance of additional coherent phases as suggested by earlier workers[9,10].

Investigations of the magnetic properties of the matrix phase by Mason Ashall and Dean[70] have indicated that this is virtually non - magnetic in alloys containing 5 weight % Ti. The substantial improvement in coercivity obtained by increasing this addition to 8 wt % cannot therefore, be explained in terms of further reduction in

magnetization of the matrix, nor is any appreciable increase in packing factor observed. It has been proposed[70], therefore, that titanium effects the shape anisotropy of the precipitate, possibly by altering the lattice mismatch between matrix and precipitate.

The influence of lattice mismatch, elastic anistropy and general thermodynamic considerations are considered in the next section.

2:4 Spinodal decomposition

2:4:1 General theory

The theory of the spinodal decomposition occuring in these alloys has been thoroughly investigated by Hillert[64] and Cahn and Hilliard[65,66] and was the subject of a recent review paper by Cahn[67]. It has been shown that the spinodal instability sets in when certain infinitesimal composition fluctuations result in a decrease in overall free energy. This statement implies that the new phase forms by a continuous process, and thus spinodal decomposition involves only crystallographically similar phases. The continuity criterion also requires coherency to be maintained during the first stages of the reaction, and for this reason elastic energy must be included in the calculations[66], which yield the following result.

A solid solution inside the spinodal is unstable to sinusoidal fluctuations of wavelength $2\pi/\beta$ when

$$\frac{\delta^2 f'}{\delta c^2} + 2k\beta^2 + \frac{2\eta^2 E}{1-\nu} < 0$$

where $f'(c)$ is the free energy of a unit volume of homogeneous material of composition c, k is a constant

determined by the surface energy between the two phases, E is Young's modulus and η is the linear expansion of the lattice per unit composition change. The first term in the expression corresponds to the thermodynamic condition for spinodal decomposition ($\frac{\delta^2 f'}{\delta c^2} < 0$) and the second and third terms are modifications which account for the creation of interfaces and the coherency strain respectively. Solution of this equation for given values of $\frac{\delta^2 f'}{\delta c^2}$ and η yields a minimum wavelength (λ_c) above which all waves are stable. Consideration of the exponential amplification factors for these waves shows that those with wavelength $\sqrt{2}\ \lambda_c$ grow most rapidly at the expense of all others. The equation above applies to an isotropic solid and considerations of elastic anisotropy in the case of alnico alloys indicates that three orthogonal <100> composition waves will occur preferentially. The application of a magnetic field during cooling has the effect of causing the values of k and η to become different along the three <100> directions, leading to a prefered orientation corresponding to the most favourable <100> direction.

2:4:2 The application of the theory to magnetic materials.

Nicholson and Tufton[68] have compared these theoretical predictions with microstructural evidence from several systems, by transmission electron microscopy. They conclude that the theory of spinodal decomposition provides a good explanation of the microstructure of the various

permanent magnet alloys examined. With regard to the development of improved magnetic alloys they note that the relationship between magnetic properties and microstructure is not yet sufficiently well understood to enable quantitative correlations to be made. The suggestions made for further work include investigation of minor microstructural changes such as the perfection of the precipitate rods, and it was emphasized that detailed experiments with simple alloys may lead to significant advances.

It is in the light of such recomendations as these that the present work has been undertaken.

CHAPTER III

Experimental Method

3:1 Materials

The materials used in this investigation were as listed below:

Iron — This was purchased from B.I.S.R.A. in the form of 3/8" (9·425mm) rod and consisted of Japanese electrolytic iron deoxidised and refined by controlled additions of carbon. The outside surface of the rod was removed by grinding, and it was sawn into 2cm lengths. The cut faces were thoroughly cleaned.

Aluminium — High purity 99·999% Al. was cut up into small pieces about 10mm x 5mm x 5mm and cleaned in caustic soda solution.

Copper — Small pieces of electrolytic copper, of a similar size to that mentioned above, were used together with 0·1mm copper sheet. Both were thoroughly cleaned in dilute nitric acid.

Titanium — This was donated by I.M.I. in the form of high purity sponge. It was necessary to premelt this sponge, in the arc furnace, to remove chlorine and subsequently cut the resulting ingot into very small fragments.

FIGURE 3:1

Chemical analysis of materials used in alloy preparation.

IRON (wt %)

basic material - Si < ·006 Mn < ·01 Ni < ·01
Cr < ·01 Cu < ·01 Co < ·01 S ·007 P ·004
C ·009 All others < ·005
after refining C ·013 O·006

ALUMINIUM

Commercially available high purity 99·999%Al

COPPER (wt %)

Ag ·001 S ·003 O ·04
As ·0015 Sb ·002 Ni ·0015 Fe ·0025

TITANIUM (wt %)

C ·01 H ·002 Fe ·02 N ·003
O ·04 Na ·09 Cl ·14

The relevant chemical analyses are shown in Fig. 3:1. The figures for iron apply to a typical analysis of the base material with the exception of the particular carbon and oxygen contents which are for this batch after refining.

3:2 Alloy preparation

The materials, prepared as outlined in section 3:1 were carefully weighed out to within ·0001gm of the weight calculated to give a 45gm melt of each of the compositions listed in Fig. 3:2. The constituents were then placed, with the iron rods uppermost, in a hemispherical depression in the water cooled copper hearth of an argon arc furnace. The furnace was operated under a pressure of 1/3 atmosphere of argon and at first an arc current of only 100 amps was used to melt the iron, allowing it to run down and dissolve the other constituents. The alloy was 'flipped' over and remelted at a higher arc current three times, to promote good mixing, before it was cast in a long depression in the hearth, with a rectangular cross section. The dimensions of the ingots produced in this way were approximately 75mm x 12mm x 12mm.

Ingots weighed after melting showed weight differences of the order of 0·1% over the combined weights of the constituents. In view of these negligible differences and the fact that reliable analyses of iron - aluminium alloys are difficult to obtain, it was assumed that the composition of each ingot was as calculated from the weights of the constituents.

3:3 Homogenisation.

The ingots were lightly ground to remove the surface oxide film which formed during melting and were then sealed

FIGURE 3:2

Chemical composition of alloys used in this investigation

ALLOYS CONTAINING COPPER

Composition (at %)			Code
Fe	Al	Cu	
77·5	17·5	5·0	175C
75·0	20·0	5·0	20C
73·25	21·75	5·0	2175C
72·5	22·5	5·0	225C
72·0	23·0	5·0	23C
70·0	25·0	5·0	25C
67·5	27·5	5·0	275C
65·0	30·0	5·0	30C

ALLOYS CONTAINING TITANIUM

Composition (at %)			Code
Fe	Al	Ti	
77·5	17·5	5·0	175T
75·0	20·0	5·0	20T
72·5	22·5	5·0	225T
72·0	23·0	5·0	23T
70·0	25·0	5·0	25T
67·5	27·5	5·0	275T
65·0	30·0	5·0	30T

in silica capsules under a protective atmosphere of argon. The capsules were suspended in a vertical crusilite furnace at 1200°C ± 10°C for 24hrs, and subsequently dropped onto a sand tray, where they were allowed to cool in air. It would have been more normal, at this latter stage, to quench the capsules into water, however, this approach resulted in severe cracking of the ingots. For this reason the heat treatments described later (section 3:5) are all designed to minimise the temperature range through which it is necessary to quench these alloys.

3:4 Sectioning the ingots.

The homogenised ingots were mounted on a slit grinding machine and slices were cut using a 0·25mm thick carborundum wheel. The slices were of varying thickness according to their application (see Fig. 3:3). For electron microscopy a thickness of 0·4mm was used, while for magnetic measurements the thicknesses were 0·5mm for use on the magnetic balance and 1·8mm for vibrating sample magnetometer measurements.

3:5 Heat treatments.

As the ingots were all air cooled in their silica capsules, it was necessary to give each specimen a short solution treatment prior to ageing at the requisite temperature. In view of the fragmentation of the alloys on quenching, specimens were loosely retained in an iron gauze envelope spot welded to a weighted stainless steel rod (Fig. 3:4a). The rods were suspended in a vertical crusilite furnace at a temperature of 1100°C ± 5°C for 1hr unless other wise

FIG 3:3. SPECIMEN PREPARATION.

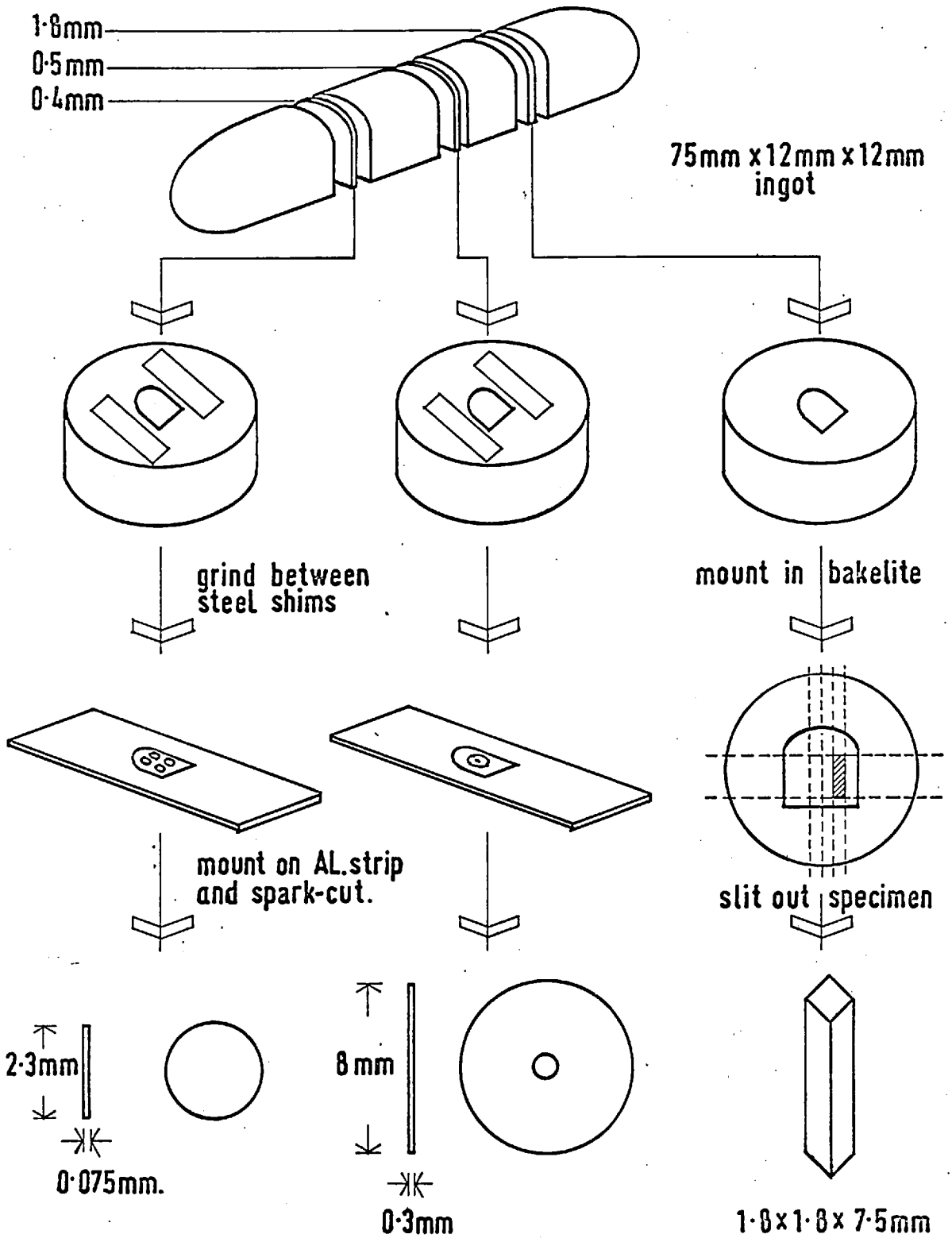

FIG 3·4

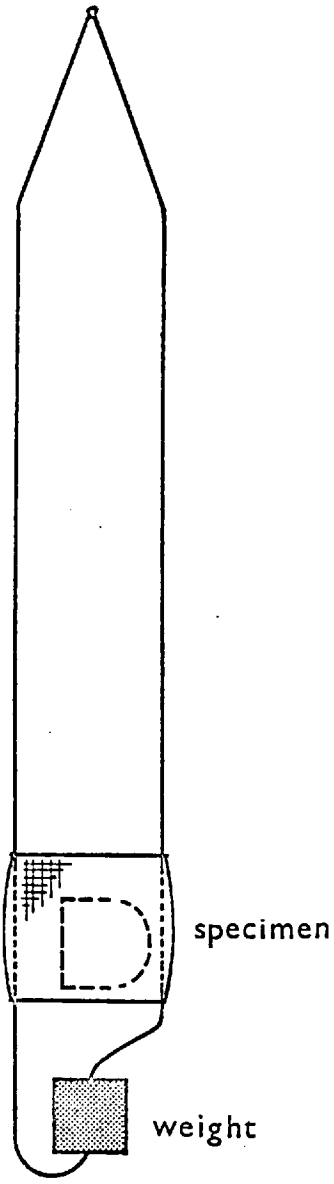

SPECIMEN HOLDER

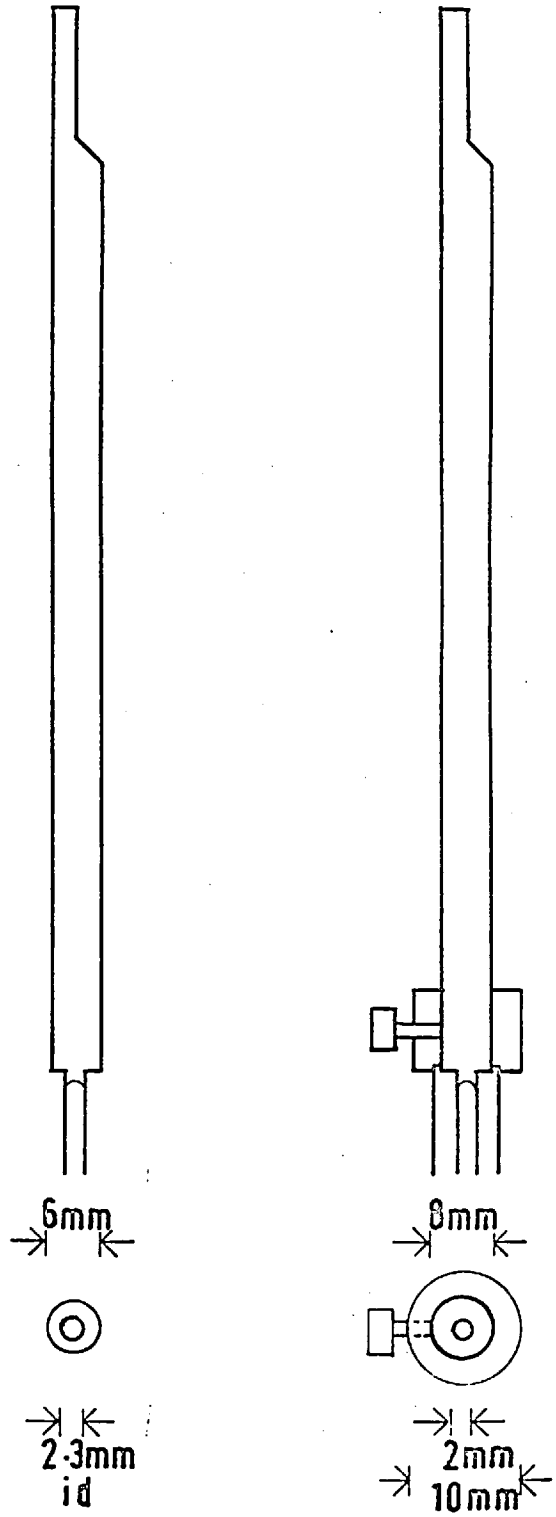

SPARK CUTTERS

stated. A 95% argon - 5% hydrogen gas mixture was circulated through the furnace to inhibit oxidation of the specimens.

On completion of the solution treatment the weighted rod was quenched into a salt bath situated below the vertical furnace, at the required ageing temperature. This technique proved successful for ageing temperatures in the range 400°C to 850°C as suitable salt mixtures were readily available. For ageing temperatures above 850°C, however, it was found preferable to use a second furnace in place of the salt bath. In this latter method the speed of transfer between the two temperatures was inferior to that when using the salt bath, as the ageing furnace was mounted alongside rather than below the solution treatment furnace. Despite this only 2-3 seconds were required for the transfer and a thermocouple attached to the specimen support indicated that the temperature did not drop more than 20°C to 30°C during this time. In both types of ageing treatment the temperature was measured using a chromel - alumel thermocouple in close contact with the specimen support. The thermocouple was checked against the melting point of pure lead and phase angle temperature controllers were used on both the salt bath and furnace, consequently heat treatment temperatures are considered accurate to $\pm$ 2°C. It will be noted that in these ageing treatments no precautions were taken to prevent oxidation of the specimen. Such measures were unnecessary in view of the good oxidation resistance of the alloys themselves.

On completion of the ageing treatment, in either the furnace or salt bath, the specimens were quenched into

water at 20°C. This inevitably produced quench cracking which was more pronounced the higher the aluminium content and the ageing temperature.

3:6 Electron microscopy.

The fragmented specimens were lightly rubbed on a silicon carbide paper to remove the oxidized layer which had formed during ageing, and affixed to a steel block using 'Twinstik' double sided adhesive tape. They were then ground between hardened steel shims of varying thickness on water lubricated silicon carbide papers commencing with 220 grade and finishing on 600 grade. By this means the thickness of the slices was reduced from 0·4mm to 0·075mm and the steel shims ensured that the slices remained parallel sided. At this stage the specimens were rather fragile and were carefully removed from the steel block by dissolving the adhesive in acetone. It was obvious that these small fragments could not be electropolished by the window technique, and consequently a disc method was developed.

Each small piece was smeared with 'Durofix' adhesive and stuck to an aluminium backing strip. While the adhesive was setting slight pressure was maintained to ensure good electrical contact between the two metal surfaces. The aluminium strip was held in the vice of a 'Servomet' spark cutting machine and 2·3mm discs were cut using a tubular tool as shown in Fig. 3:4b. The best results were obtained using a fine cutting rate and a tool of wall thickness 0·05mm to minimise structural damage at the periphery of the disc. The discs were seperated from the backing strip

by soaking in acetone and were lightly rubbed on 600 grade silicon carbide paper to remove all traces of adhesive. The final thickness of the discs prior to electropolishing was thus 0·062mm.

The preparation of electron microscope specimens from these discs formed an important part of this investigation and to ensure rapid and reliable results, the apparatus described in Appendix A was developed. This is based on the jetted electrolyte technique and incorporates a detection system to enable polishing to be stopped automatically when initial perforation of the disc occurs. The application of the apparatus is not specific to the alloys used in the present investigation, but optimum valves of the critical parameters for iron - aluminium alloys are given. Using the apparatus under these conditions good flat electro-polishing profiles were obtained, leading to specimens with large electron transparent areas. The basic composition of the electrolyte was 50gm chromium trioxide, 266ml glacial acetic acid and 14ml of water, however, small additions of water were made at the time of use, as described in the appendix.

The 2·3mm discs were loaded into the apparatus and polished at a fixed current density of 0·01A/mm^2 corresponding to applied voltage of between 25V and 30V. The polishing time was about 7 minutes and on perforation the current was automatically switched off and the alarm sounded. The specimen holder was thoroughly washed in methanol and the specimen removed, rewashed and dried on absorbant tissue.

The discs were examined in a Siemens Elmiskop IA electron microscope fitted with a double tilt goniometer stage. This facility enable full use to be made of high

REFLECTION	ANTIPHASE BOUNDARIES		PHASES		
(Indexed with respect to a')	$a'/2\langle 100\rangle$	$a'/4\langle 111\rangle$	α	$\alpha_1 (DO_3)$ i.e. Fe_3Al type	$\alpha_2 (L2_0)$ i.e. FeAl type
Fundamental	invisible	invisible	bright	bright	Bright
S_1 h + k + l = odd (typically 111)	visible	visible	dark	bright	dark
S_2 $\frac{h + k + l}{2}$ = odd (typically 200)	invisible	visible	dark	bright	bright

FIGURE 3:5 Visibility criteria for phases and antiphase boundaries encountered in this investigation.

resolution dark field microscopy, hence comparison of micrographs taken using fundamental and particular superlattice spots enabled the phases present to be identified. The criteria used in this identification are summarised in Fig. 3:5. The normal magnification and rotation cablibrations were performed on the microscope.

3:7 Magnetic balance measurements (σ_s vs temperature curves)

The slices cut for this purpose were ground down from 0·5mm to 0·3mm and mounted on aluminium backing strips in a similar manner to that described in section 3:6. Specimens, in the form of discs with a hole in the middle, were spark cut from the slices in a two stage operation using the tool shown in Fig. 3:4c. These discs were 8·0mm in diameter, 0·3mm thick and the diameter of the hole was 2mm. The measurements were made on a Sucksmith Ring Balance constructed by H.Smith (PhD thesis London University 1968) and a full description of the basic instrument has already been given.

3:7:1 Description of apparatus.

The apparatus consists of an electromagnet with pole pieces shaped to produce a non-uniform field with constant field gradient (see Fig. 3:6). A ferromagnetic specimen placed in the pole gap experiences a downward force which produces a distortion of the copper - beryllium support ring, the magnitude of which is measured by a small displacement transducer. The force on the specimen at saturation, is given by

$$F = \sigma_s m \frac{dH}{dx}$$

FIG 3·6 SPECIMEN HOLDER AND POLE PIECES

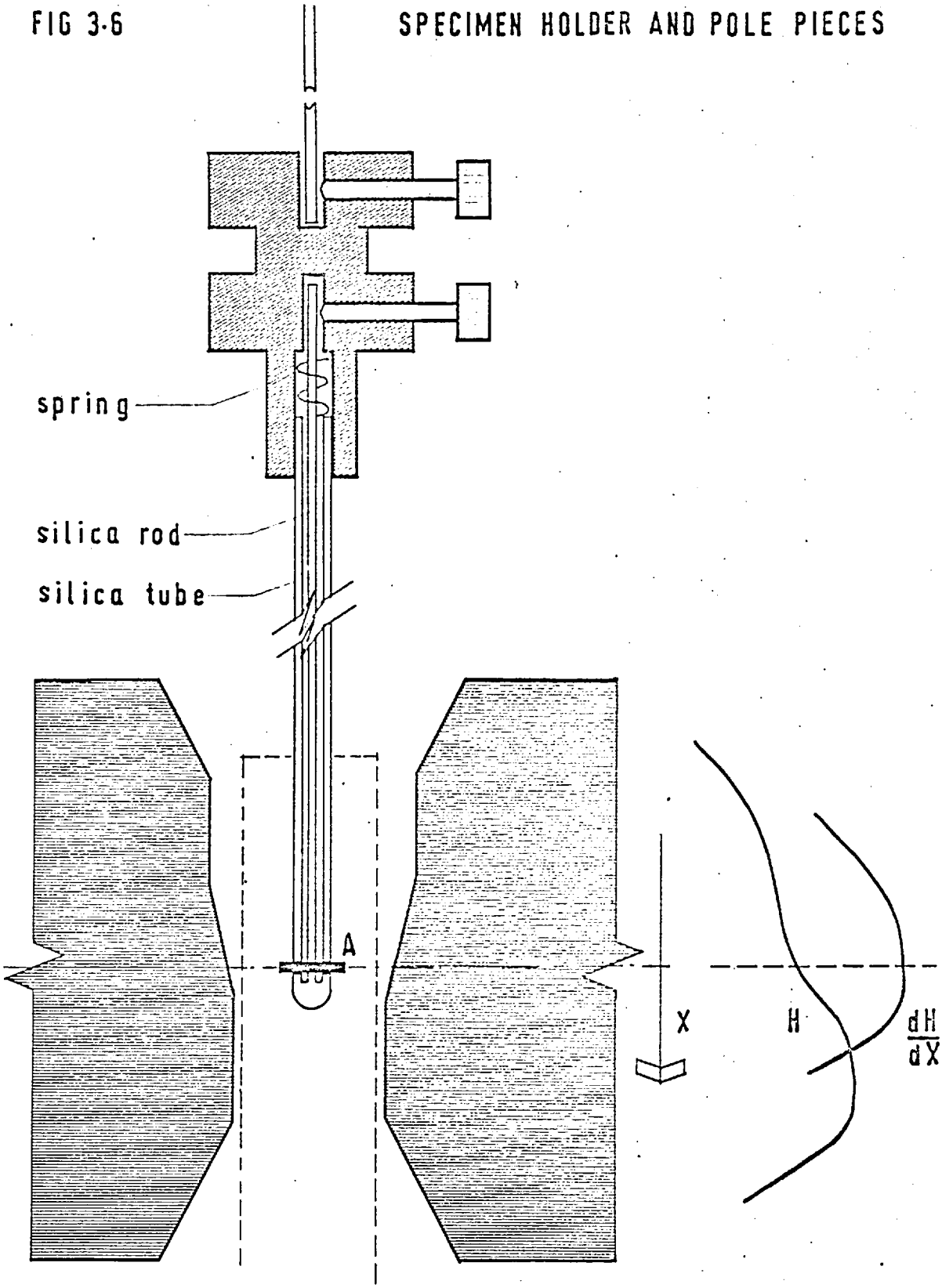

A : Specimen

which is proportional to the displacement measured at the centre of the ring (D). In this expression H is the field strength, x the vertical displacement, m the mass of the specimen and σ_s the saturation magnetic moment per unit mass or specific magnetic intensity i.e. the intensity of magnetization at saturation (I_s) divided by the density (d). The validity of this proportionality for the apparatus was established by Smith.

For the present investigation the apparatus was modified to enable high temperature measurements to be made (see Fig. 3:7). A small furnace with a non - inductive winding was inserted in the pole gap. The phase angle controller, used in conjunction with this furnace, was fitted with a mechanical drive giving continuous temperature variation. The original brass specimen holder was replaced by the spring loaded silica suspension shown Fig. 3:6. A Pt/Pt-13%Rh thermocouple was strapped to the side of the suspension and, to minimise drag, the thermocouple connections were made by means of mercury contacts. Tests indicated that these modifications in no way impaired the satisfactory operation of the balance. The outputs of the thermocouple and transducer meter were connected to an X - Y recorder which enabled direct plots of deflection vs temperature to be made.

3:7:2 Field calibration

With the furnace in position, measurements were made of the field produced by certain magnet coil currents using a Hall effect fluxmeter. The probe of this instrument was taped to the suspension at the specimen position but

FIG 3:7. HIGH TEMPERATURE MAGNETIC BALANCE

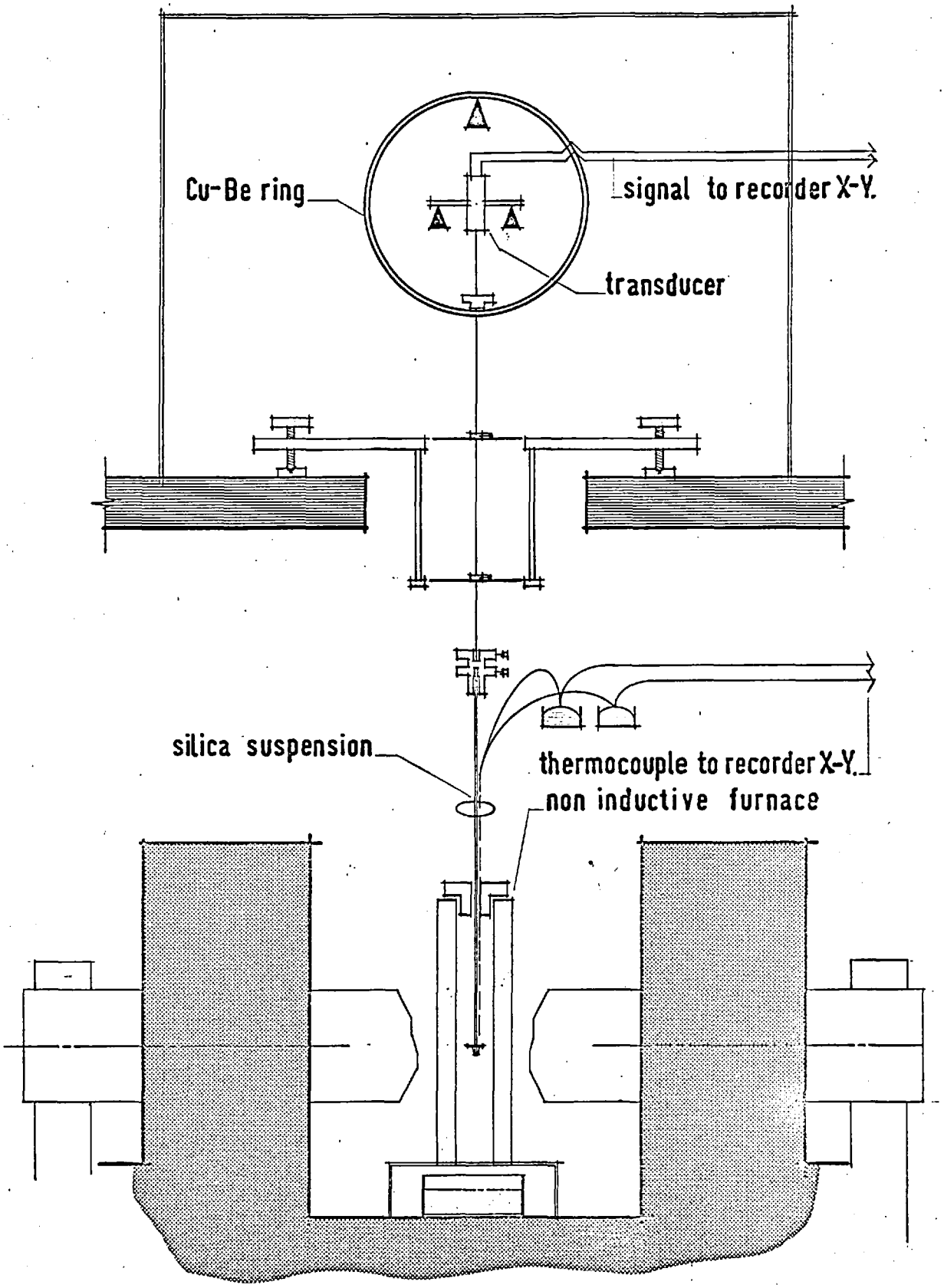

because of the size of the measuring crystal (4mm x 4mm) the readings were only average values over this area. The specimen is situated at the position of maxium dH/dx (see Fig. 3:6) as determined by the variation of reading on the transducer meter with vertical displacement of the specimen. From this procedure it was noted that the charge in dH/dx over the area of the Hall effect probe was less than 1%, however, the variation of H was somewhat greater, hence field measurements are considered accurate to $\pm$ 2% as indicated by several different calibration checks. In view of this inaccuracy in absolute field values readings were always taken at fixed magnet coil currents and using an accurate ammeter the resetability was within 0·02 amps corresponding to a maxium field error of 0·6%.

3:7:3 Experimental Procedure

The disc shaped specimens were first weighed and then fitted into the apparatus, on the silica suspension. A series of deflection readings were taken at room temperature corresponding to coil currents of 0 to 14 amps (i.e. 0-11,315Oe) in 1 amp increments. These results were compared with similar readings for a pure iron specimen, made from the base material used in the preparation of these alloys, after applying a weight correction. The ratio between these two values was found to reach a constant value above a certain current, indicating saturation of the magnetically harder alloy specimen. The absolute value of this ratio, found by averaging the results obtained above saturation, was compared with the published value for pure iron and a σ_s value characteristic of the specimen was obtained.

Magnetization vs temperature curves were then produced using a fixed heating rate of 15°C per minute at three fixed currents: 3 amps (4,530 Oe $\pm$ 90 Oe)
7 amps (8,590 Oe $\pm$ 170 Oe)
10 amps (10,110 Oe $\pm$ 200 Oe)
It should be noted that at the lowest field the specimens were not completely saturated at low temperatures, however, near the Curie point all specimens were completely saturated.

3:7:4 Curie point determination

The change from the ferromagnetic to the paramagnetic state is not perfectly sharp, and it is difficult to define and determine the Curie point exactly. The subject has been studied by Weiss and the method devised in accordance with his theory may be found in Appendix B. Also included is the simplified extrapolation technique used in this investigation. Tests with pure iron and nickel specimens indicate the validity of this procedure and the results are considered accurate to $\pm$ 3°C. Although the technique used is not as rigorous as that proposed by Weiss it is a considerable improvement over the more arbitrary methods in common use (e.g. taking the Curie point as the point of inflexion in the σ_s vs T curve).

3:8 Vibrating sample magnetometer measurements

Although the magnetic balance measurements gave information concerning the variation of specific magnetic intensity with temperature, no data on other magnetic properties could be obtained by this method. In order to obtain complete hysteresis loops for these alloys at

elevated temperatures, measurements were made on a vibrating sample magnetometer in the School of Physics at the University of Newcastle upon Tyne.

3:8:1 Description of the apparatus

A range of vibrating sample magnetometers for measurements between 4 and 1000°k have been described by Creer, de Sa and O'Reilly[71]. The particular variant used in this case is mentioned, but not described in detail. However, the main principles involved are those used in the low temperature design.

An electric motor and drive belt is used to impart a reciprocating, simple harmonic vibration to a vertical silica tube via a scotch crank system. The specimen holder is secured to the lower end of the tube and oscillates in the constant field region of an air cored solenoid, between the centres of two detecting coils. The major axis of the specimen, the axis of the detecting coils and that of the solenoid are thus coincident as outlined by Creer et al. The amplitude of the vibration was 5cm and the frequency 10 c.p.s. A non-inductive resistance heating furnace and water jacket is positioned between the specimen and the detecting coils and the whole specimen region is evacuated during high temperature measurements The electronic circuitry is exactly as described by Creer et al.

3:8:2 Preparations of specimens.

The size and shape of specimens used in this apparatus was to some extent a compromise between theoretical

considerations and limitations imposed by the apparatus. The maximum length of specimen which the specimen holder could accomodate was about 9mm and to ensure good sealing specimens were cut to a nominal length of 7·5mm. To ensure an adequate signal from the detecting coils it was suggested that the specimen weight be in the region of 0·15gm. A specimen consisting of a rectangular prism of dimensions 1·8mm x 1·8mm x 7·5mm complied with this requirement.

To produce these specimens the 1·8mm slices cut from the original ingot were mounted in bakelite and the requisite cuts were made on the carborundum slitting wheel. The specimens were placed in the copper specimen holder and packed in position with silica wool. Hysteresis loops were obtained for various temperatures, measured with a platinum - platinum 13% rhodium thermocouple in contact with the specimen holder. During measurement the apparatus was maintained at a pressure of 5×10^{-3} torr.

CHAPTER IV

IRON - ALUMINIUM - COPPER ALLOYS - RESULTS AND DISCUSSION

The results of this investigation conveniently fall into two catergories, corresponding to the two different alloying additions. The results concerning alloys containing copper will be dealt with in this chapter, whilst chapter V is devoted to alloys with a titanium addition. The chapters are identical in format, presenting first the results obtained by electron microscopy followed by those from magnetic measurements and concluding with a discussion correlating the information from both types of investigation. The effects of the two additions are compared and contrasted in chapter VI.

4:1 Electron microscopy of iron - aluminium - copper alloys

Initially a systematic programme of heat treatments was undertaken with a view to constructing the main outlines of a vertical section through the iron - aluminium - copper ternary diagram, at a constant copper content of 5 atomic %. At a later stage the various transformations were studied in greater detail to enable a comparison to be made with those occuring in the binary system. The results may best be described with reference to Fig. 4:1, which shows the vertical section mentioned above. Each point represents an electron microscopical examination of a specimen directly quenched from 1100°C to the indicated temperature, and subsequently quenched into water. The symbol used to devote these points is indicative of the phases present.

As an introduction to the ordered structures observed in these alloys, two microstructures are shown in Fig. 4:2 and Fig. 4:3 which are characteristic of the $L2_0$ and DO_3

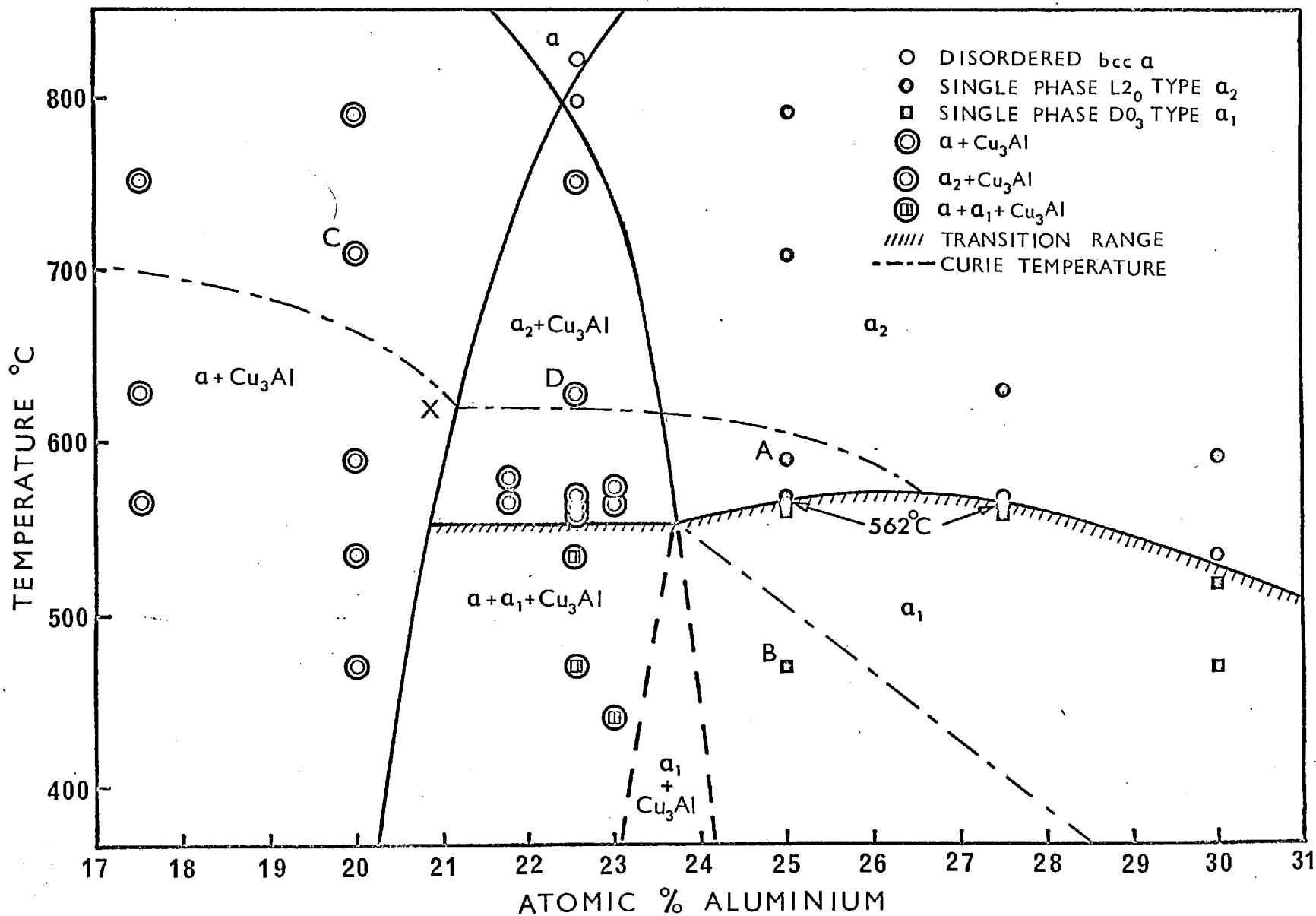

Fig.4:1 Vertical section of the Fe-Cu-Al ternary phase diagram at a constant Cu content of 5 atomic %

FIGURE 4:2

Fig.4:2a ALLOY 25C 1100°C 1hr -591°C 1hr - W.Q. Dark field g = (100) $L2_0$ $\frac{1}{2}a\langle 111\rangle$ antiphase boundaries characteristic of the $L2_0$ structure.

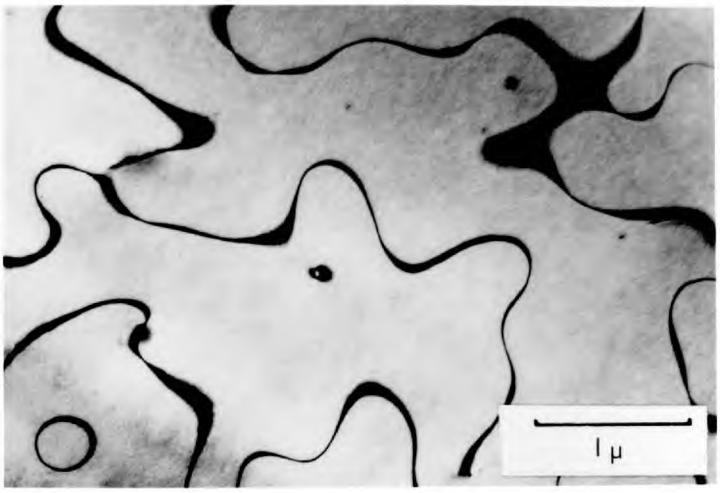

Fig.4:2b As above Dark field g = (111) $L2_0$ Smoothly curving $\frac{1}{2}a\langle 111\rangle$ APBs in a thicker part of the foil.

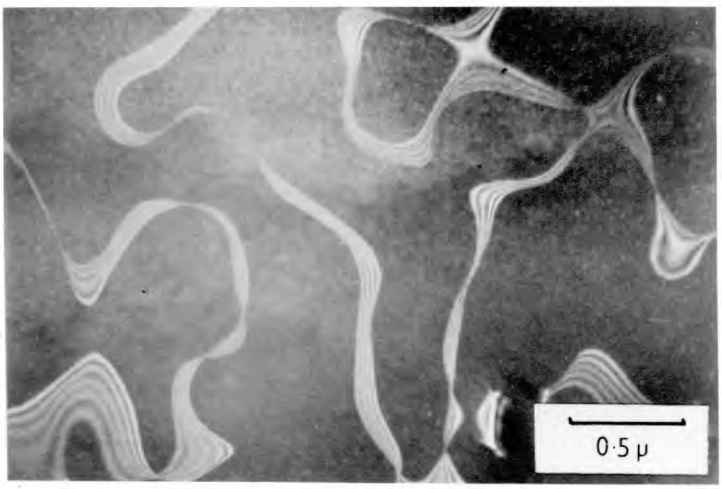

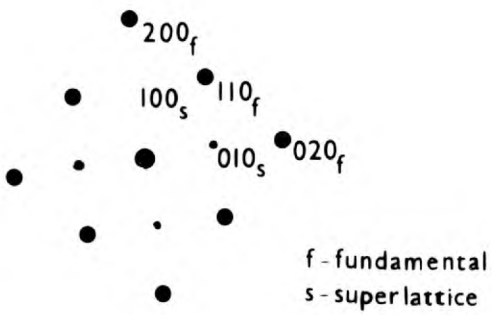

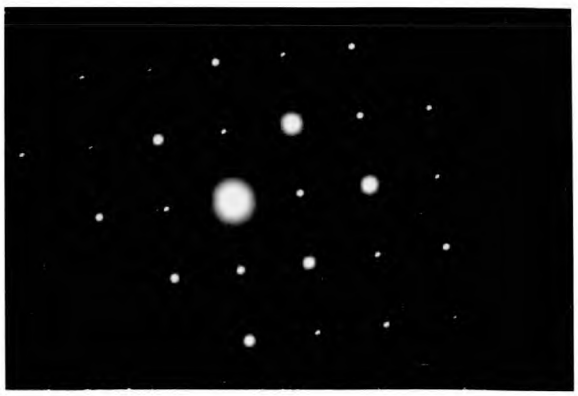

Fig.4:2c Selected area diffraction pattern of Fig.4:2a and key. (indexed with respect to a)

phases respectively. The composition of these specimens was Fe - 25%Al - 5%Cu (alloy 25C), and the corresponding diffraction patterns are shown, the first being indexed with respect to the $L2_0$ lattice parameter (a) and the second with respect to the DO_3 lattice parameter (a'). Figure 4:2a shows a (100)$L2_0$ dark field micrograph in which the $\frac{1}{2}$a <111> antiphase boundaries of the $L2_0$ structure are seen. Observation of these boundaries in a thicker part of the specimen (Fig. 4:2b) indicates their smoothly curving nature, implying a low isotropic antiphase boundary energy. The fringes are observed because of deviation from the Bragg condition, which gives rise to a shorter effective extinction distance. This specimen was heat treated for 1 hour at 591°C as indicated by point A in Fig. 4:1.

By contrast Fig. 4:3 shows the microstructure of a specimen quenched from below the DO_3 critical temperature (point B in Fig. 4:1). The first micrograph, taken with a (200)DO_3 superlattice reflection, shows the $\frac{1}{4}$a' <111> antiphase boundaries, whilst the second shows the $\frac{1}{4}$a' <111> boundaries and also a fine array of the $\frac{1}{2}$a' <100> type. This micrograph was taken with a (111)DO_3 reflection.

The observation of structures similar to those described above has enabled the main outlines of the $L2_0$ and DO_3 phase field to be delineated. The transformation between these two types of ordered structures will now be considered.

4:1:1 The $L2_0$ to DO_3 transformation (α_2 to α_1)

The two previous figures indicated structures occuring in alloy 25C, and the transformation in this alloy will be

FIGURE 4:3

Fig.4:3a ALLOY 25C 1100°C 1hr - 468°C 1hr - W.Q. Dark field g = (200) DO_3. The $\frac{1}{4}a'\langle 111\rangle$ APBs of the DO_3 structure.

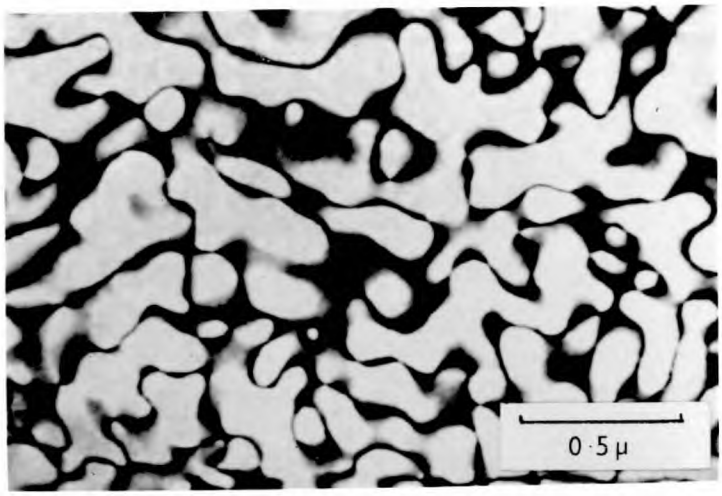

Fig.4:3b As above. Dark field g = (111) DO_3. Both $\frac{1}{4}a'\langle 111\rangle$ and $\frac{1}{2}a'\langle 100\rangle$ APBs are observed.

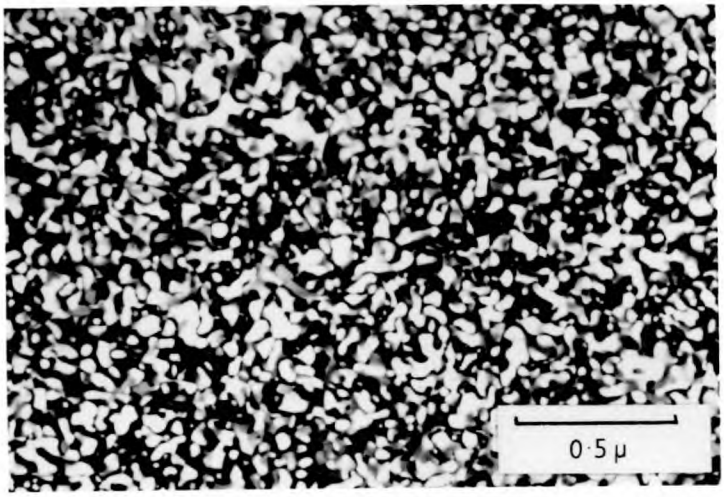

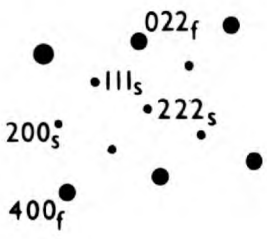

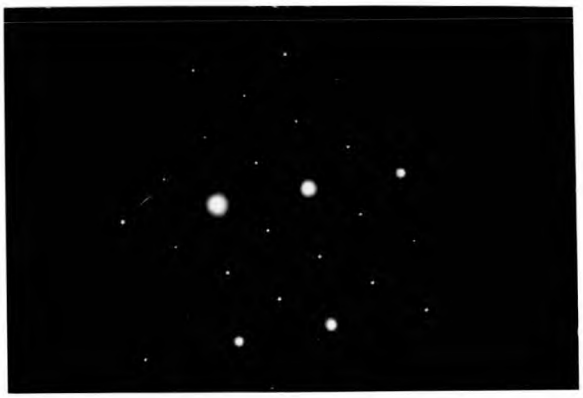

Fig.4:3c Selected area diffraction pattern of figs.4:3a and 4:3b and key. (indexed with respect to a')

considered first. A specimen of the alloy was heat treated for 24 hours at a temperature of 562°C and on examination the structure shown in Fig. 4:4 was observed. A dark field micrograph using a (222)DO_3 reflection indicated a normal $L2_0$ antiphase structure, however, a weak (111)DO_3 reflection was observed in the diffraction pattern. Using this reflection, the dark field micrographs Figs. 4:4b and 4:4c were obtained. These have a mottled appearance and comparison of Figs. 4:4a and 4:4b indicates that the dark lines in the latter correspond to the position of the $\frac{1}{4}$a' <111> domain boundaries. No $\frac{1}{2}$a' <100> boundaries are observed but inside the dark lines, a very high density of DO_3 ordered zones exist in an $L2_0$ matrix. This is best shown in Fig. 4:4c. The dark lines are interpreted as a disordered region at the $L2_0$ antiphase boundaries.

Two points should be made regarding the interpretation of these micrographs:

(i) The fine structure is not formed on the quench as it is not observed in specimens quenched from slightly higher or slightly lower temperatures.

(ii) The structures cannot be confused with the precipitation of the α phase as this would tend to form in high energy regions at the antiphase boundaries and be noticeable in the (222) dark field micrograph (Fig. 4:4a).

The structure observed in a specimen heat treated 3°C lower (559°C) for only 15 minutes is shown in Fig. 4:5. This consists entirely of an array of ordered DO_3 domains in which both types of antiphase boundary are clearly distinguishable. Aging this structure for a longer time merely increased the size of the antiphase domains and did not induce the formation of any other phase.

At the same time as the investigation reported above, a parallel study was made of the $L2_0$ to DO_3 transition in

FIGURE 4:4

Fig. 4:4a ALLOY 25C 1100°C 1 hr - 562°C 24 hrs - W.Q. Dark field g = (222) DO_3. $\frac{1}{2}a$ ⟨111⟩ APBs of the $L2_0$ structure.

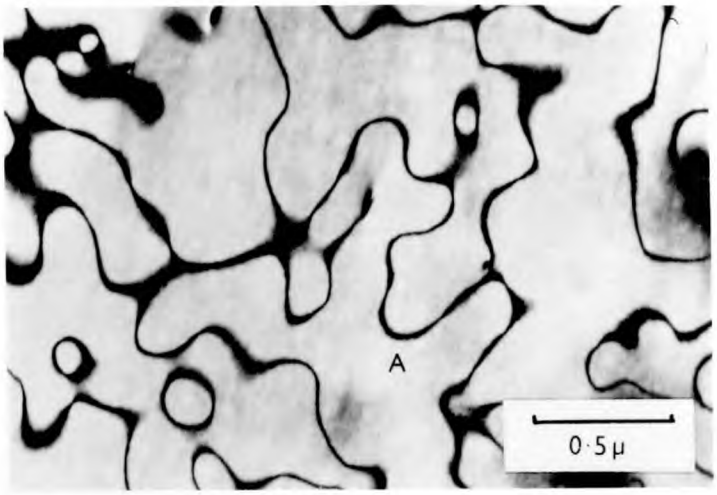

Fig. 4:4b Same area as above (see features marked 'A ') Dark field g = (111) DO_3. Disordered region at APBs and long range order fluctuations within domains.

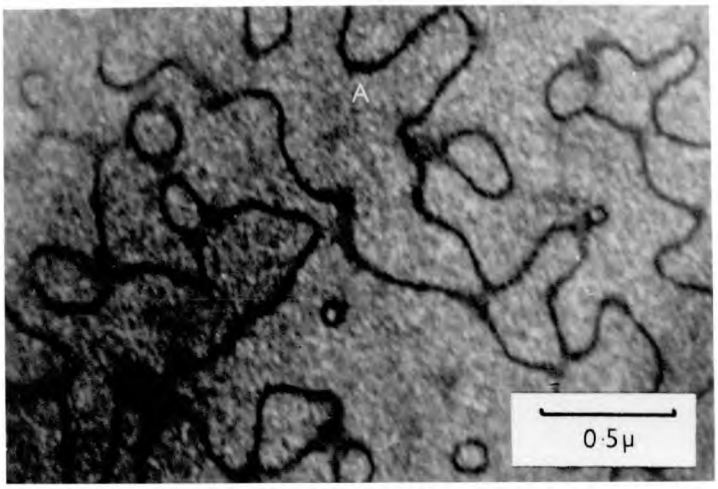

Fig. 4:4c Lower mag., similar to Fig. 4:4b, showing features mentioned more clearly.

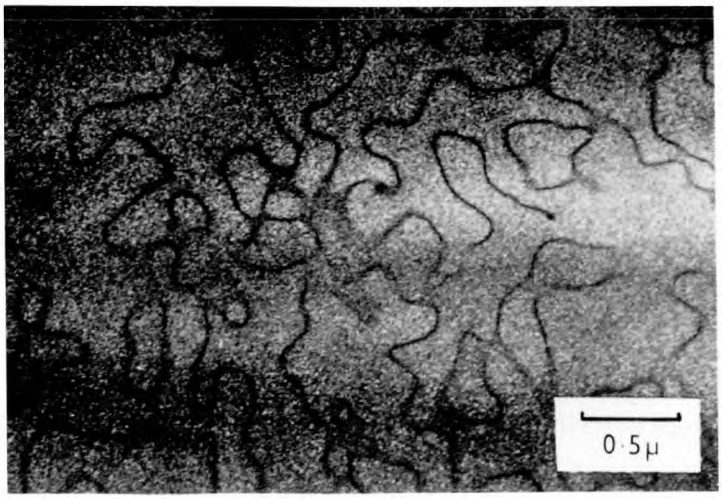

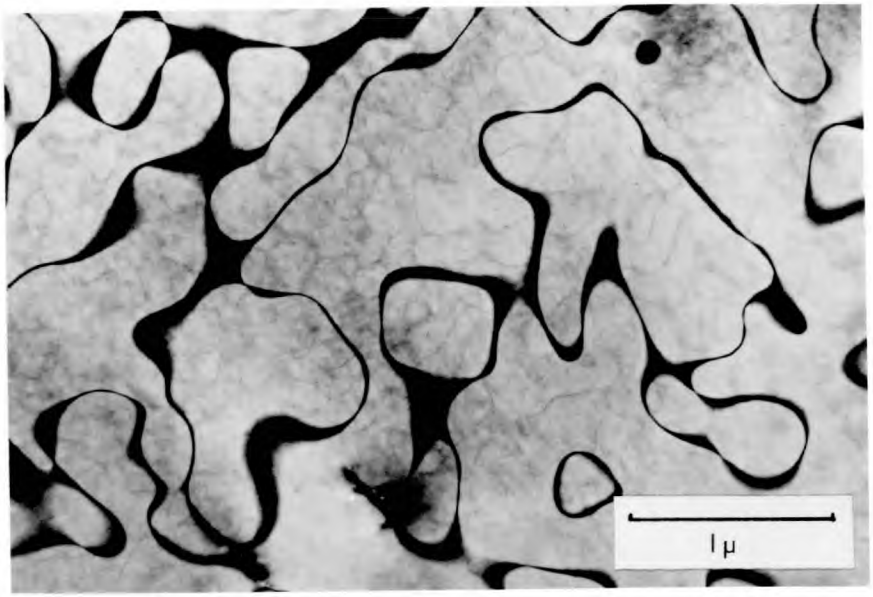

Fig.4:5a

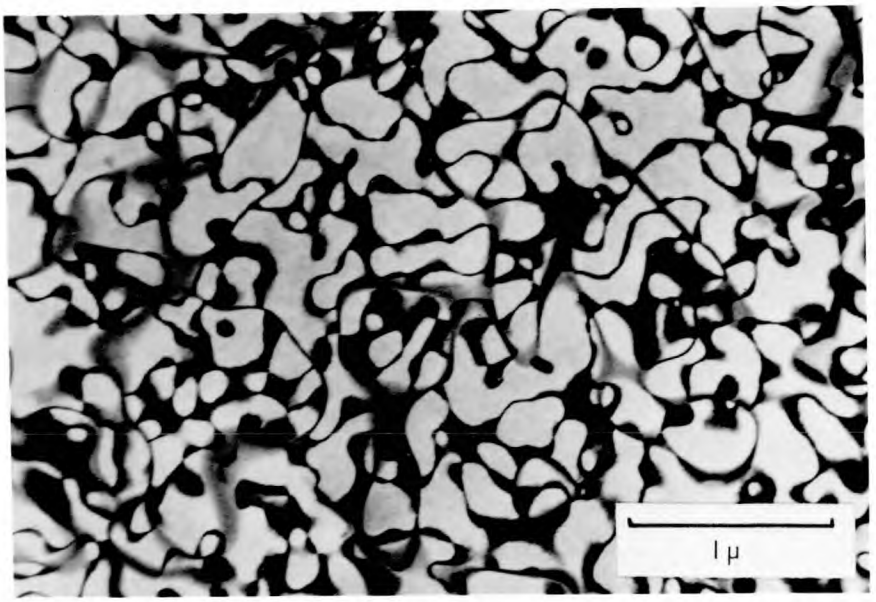

Fig.4:5b

FIGURE 4:5. A pair of dark field micrographs of a single phase DO_3 structure.
Fig.4:5a g = (222) DO_3. Fig.4:5b g = (111) DO_3.

alloy 275C (Fe 27·5%Al 5%Cu). For this alloy the initial heat treatment temperature of 1100°C was found to be below the $L2_0$ ordering temperature. The microstructures of specimens subsequently heat treated at a lower temperature in the α_2 phase field showed only occasional short lengths of $\frac{1}{2}a$ <111> antiphase boundary (APB) as shown in Fig. 4:6a. The structure was almost completely ordered as indicated by the high intensity of superlattice spots and superlattice dislocations were also observed (Fig. 4·6b). The ordering reaction was again followed by a series of (111) dark field micrographs taken of specimens heat treated in the region of the transition. These can be seen in Fig. 4:7.

The specimen shown in Fig. 4:7a was heat treated for 1hr at 566°C. Careful examination of the edge of the foil revealed the diffuse mottled structure observed previously in the 25 atomic % aluminium alloy. This structure is more clearly seen in a specimen heat treated 4°C lower (562°C) for 24 hours, shown in Fig. 4:7b. It is suggested that when this specimen was transferred from the vertical furnace at 1100°C to the salt bath, the temperature initially dropped below the DO_3 critical temperature and $\frac{1}{2}a'$ <100> APBs formed. On holding at the specified temperature, however, the mottled structure developed. In this case the boundaries are diffuse and are observed to consist of a layer of disordered material, whilst inside the domains, ordered and disordered clusters give rise to the speckled effect. The fluctuations in the degree of order appear to be only slightly coarser than those observed 4°C higher in temperature and considering the difference in the duration of heat treatment (1hr at 566°C compared with 24hrs at 562°C) this fact is considered significant.

FIGURE 4:6

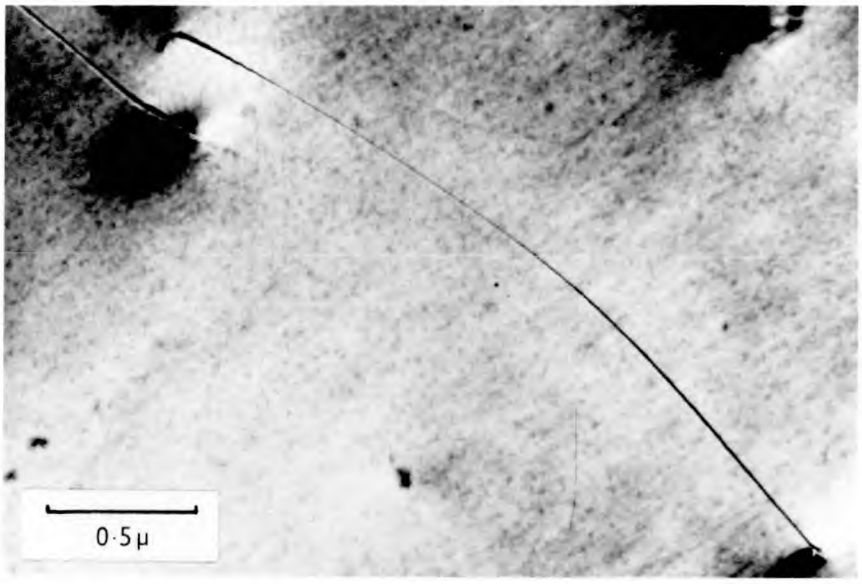

Fig.4:6a ALLOY 275C 1100°C 1hr - 566°C 1hr - W.Q.
Dark field g = (111) $L2_0$.
Segments of $\frac{1}{2}a\langle 111\rangle$ APB.

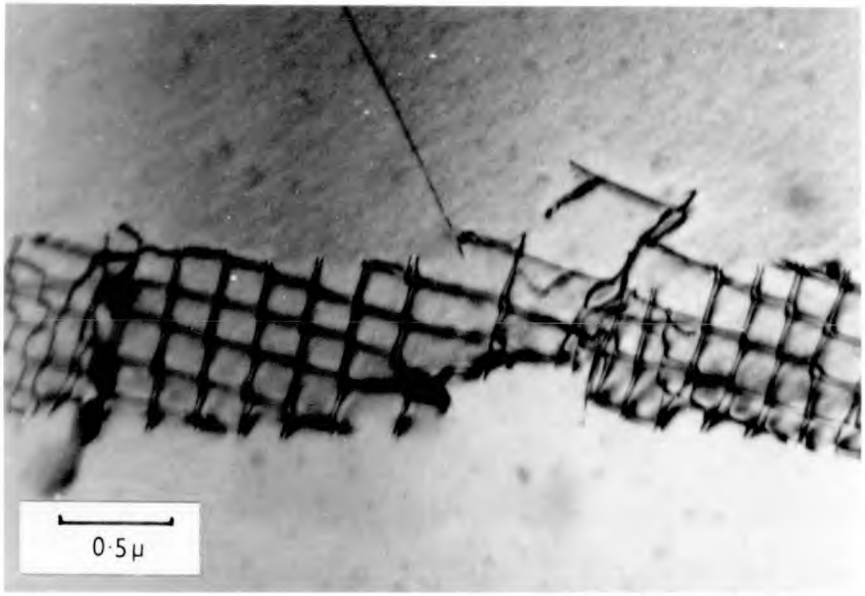

Fig.4:6b ALLOY 275C 1100°C 1hr - 630°C 1hr - W.Q.
Bright field showing a network of superlattice dislocations.

FIGURE 4:7

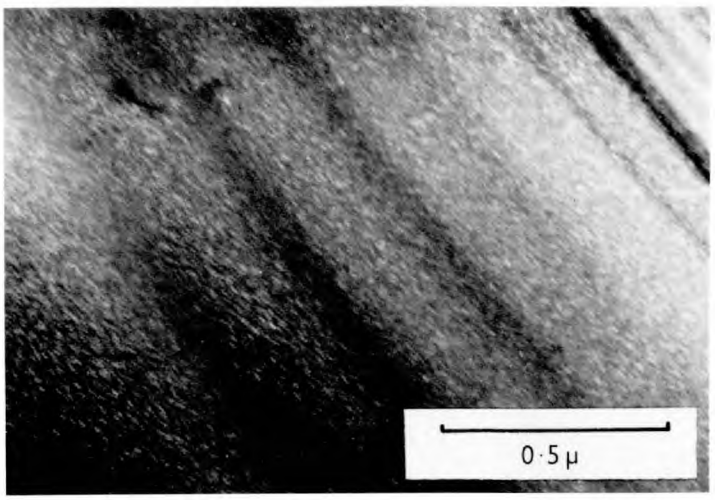

Fig. 4:7a ALLOY 275C 1100°C 1 hr - 566°C 1 hr - W.Q. Dark field g = (111) DO_3. Diffuse, mottled, structure due to long range order fluctuations.

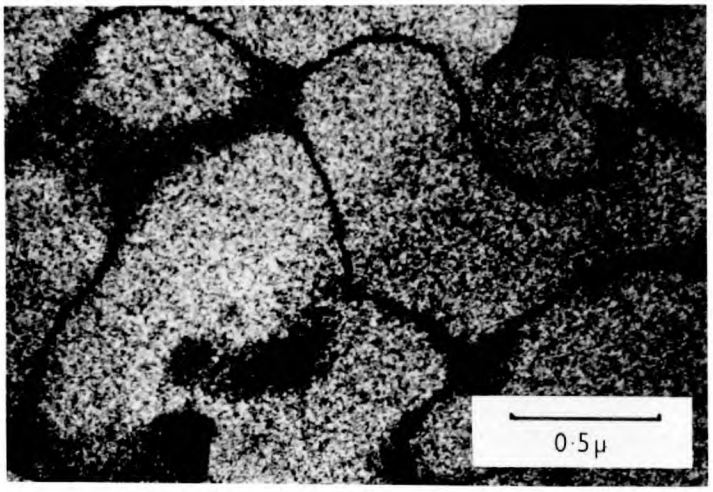

Fig. 4:7b ALLOY 275C 1100°C 1 hr - 562°C 24 hrs - W.Q. Dark field g = (311) DO_3. Broadened ½a' ⟨100⟩ APBs and more pronounced long range order fluctuations within the domains.

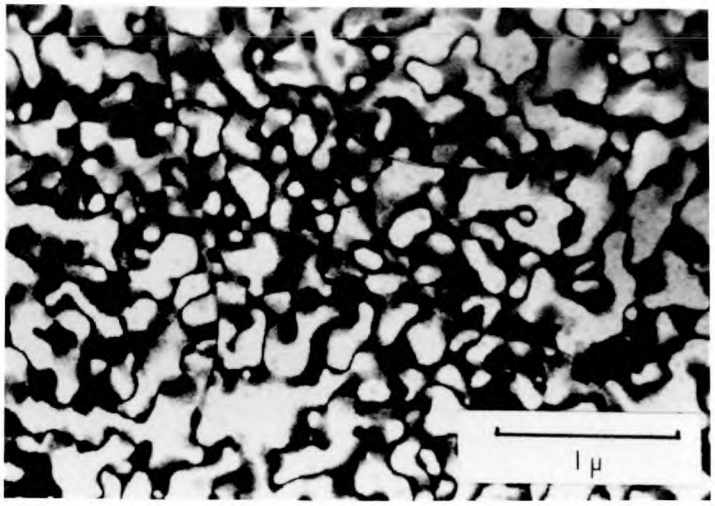

Fig. 4:7c ALLOY 275C 1100°C 1 hr - 559°C 15 mins - W.Q. ½ a' ⟨100⟩ APBs with evidence of slight long range order fluctuations.

A specimen heat treated at 559°C (3°C lower again) for only 15 minutes showed a well developed domain structure characteristic of single phase α_1, having the DO_3 structure (Fig. 4:7c). However, careful examination of this micrograph reveals that these boundaries are somewhat diffuse, which again suggests the presence of critical point fluctuations. The DO_3 critical temperature was found to fall in alloys with aluminium contents higher than 27·5%, as evidenced by observation of structures occuring in alloy 30C. In this case the critical temperature was found to lie between 518°C and 537°C.

4:1:2 Precipitation in the disordered α phase.

The alloys with the lowest aluminium contents of those prepared, i.e. 17.5C and 20C, were found to be disordered at all temperatures studied in the present investigation. They do, however, contain a precipitate not found in the binary system. The behaviour of the two alloys was, essentially, similar. At the highest heat treatment temperatures used, a precipitate was found to form in subgrain boundaries as shown in Fig. 4:8a. This specimen was of alloy 20C, heat treated for 1 hour at 789°C. When heat treated at a lower temperature, corresponding to point C in Fig. 4:1 (1hr at 710°C), the precipitate was nucleated homogeneously and had formed well defined discs. Three orthogonal variants are obvious in Fig. 4:8b.

4:1:3 Identification of the precipitate.

The structure observed in alloy 17.5C after heat treatment for 1hr at 630°C is shown in the $(1\bar{1}0)$ dark field

FIGURE 4:8

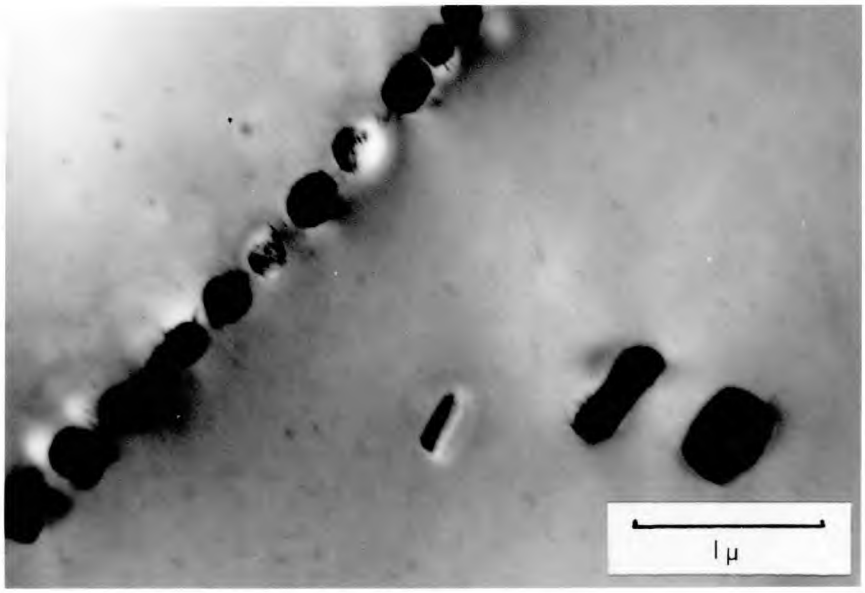

Fig.4:8a ALLOY 20C 1100°C 1hr - 789°C 1hr - W.Q. Bright field showing precipitation on a subgrain boundary.

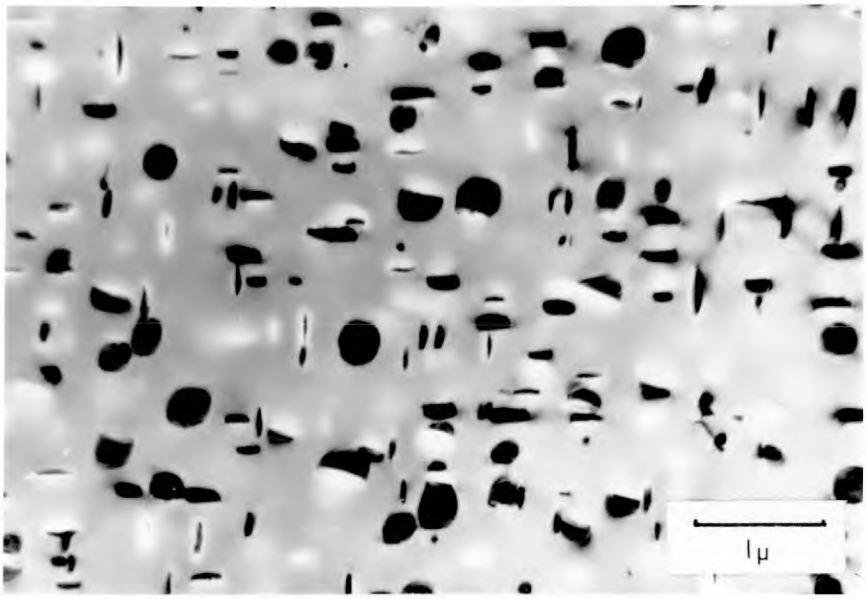

Fig.4:8b ALLOY 20C 1100°C 1hr - 710°C 1hr - W.Q. Homogeneous nucleation showing three orthogonal variants of the disc precipitates.

micrograph, Fig. 4:9a. The corresponding diffraction pattern is shown in Fig. 4:9b. The pattern is that which would be expected of a (111) plane in a disordered α structure, no extra precipitate spots are observed. If this specimen was slightly tilted off the zone, then the spots of the pattern could be seen to be streaked in cube directions (Fig. 4:9d). A dark field micrograph taken with such a streaked spot is shown in Fig. 4:9c. The streaking is thus seen to be due to the three variants of the precipitate lying on cube planes in the matrix. Confirmation of this fact is provided by the streaking present in the diffraction pattern with the incident beam corresponding to the (100) zone axis of a specimen with a similar structure (alloy 20C heat treated for 1hr at 591°C), Fig. 4:10a. In this pattern, however, extra spots are visible in what would be the {100} positions for the matrix. A dark field micrograph using one of these spots (Fig. 4:10b) shows that they arise from the precipitate. Finally the diffraction pattern, Fig. 4:10c, shows a well defined line of precipitate spots, three orders being present between the 000 spot and the 222 spot of the disordered matrix.

The diffraction patterns may be indexed in terms of a coherent precipitate with a lattice parameter very close to that of the matrix. The extra spots observed are precipitate superlattice spots and from these it is possible to say that the precipitate has the DO_3 structure. For this reason the diffraction patterns are indexed with respect to the disordered lattice parameter (a) for the matrix and with a DO_3 parameter, almost exactly double (a), for the precipitate. The morphology and mode of formation of the precipitate indicate that it is not based on Fe_3Al, but is most probably Cu_3Al which has a similar lattice parameter and exhibits $L2_0$ and DO_3 ordering. Investigation of the

FIGURE 4:9

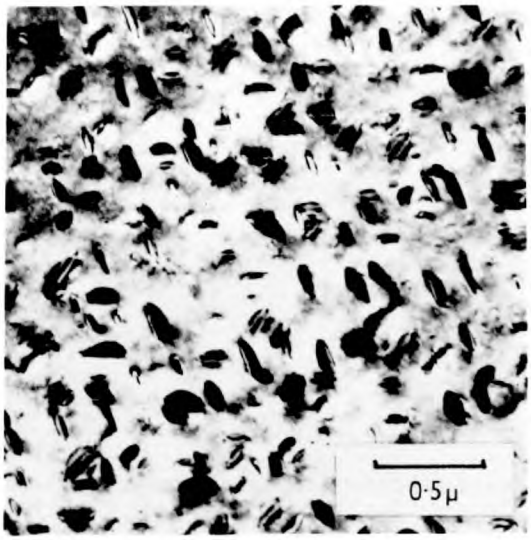

Fig.4:9a ALLOY 175C 1100°C 1hr-630°C 1hr - W.Q.
Dark field g = $(1\bar{1}0)$ $L2_0$
(spot marked 'A')

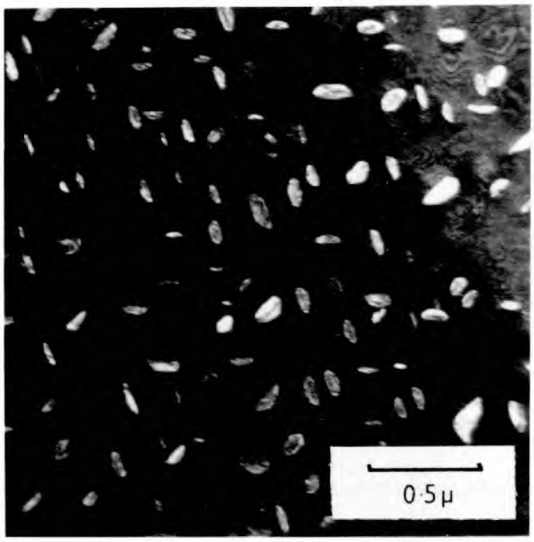

Fig.4:9c As fig.4:9a but slightly tilted. Dark field taken with streaked $(1\bar{1}0)$ spot (marked 'A'). Precipitates lying on cube planes.

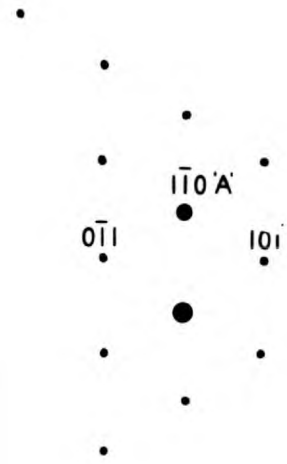

Fig.4:9b S.A.D.P. of Fig.4:9a.

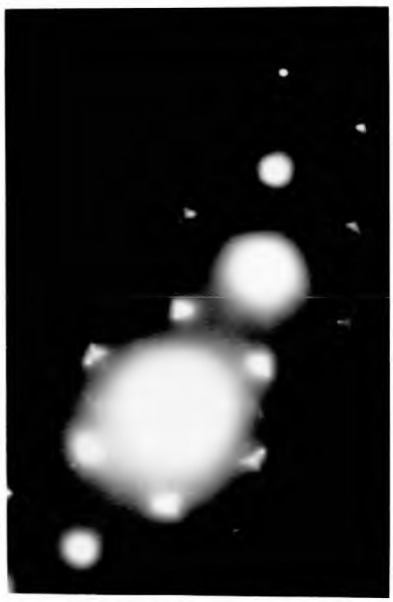

Fig.4:9d S.A.D.P. of Fig.4:9c.
Streaking of spots in cube directions.

FIGURE 4:10

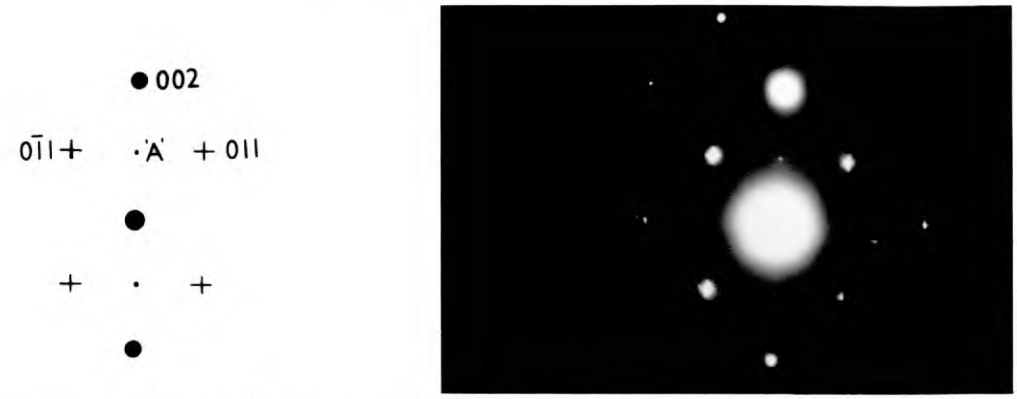

Fig.4:10a ALLOY 20C 1100°C 1hr - 591°C 1hr - W.Q.
S.A.D.P. showing streaking of matrix spots and extra precipitate spots.

Fig.4:10b Dark field
taken with spot marked 'A'

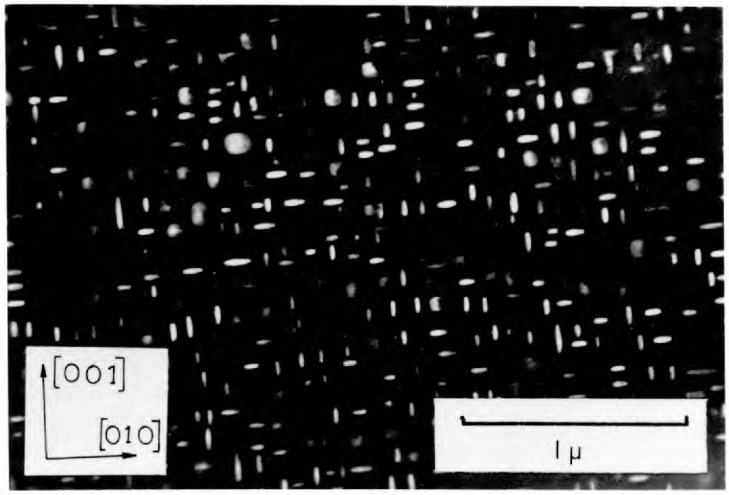

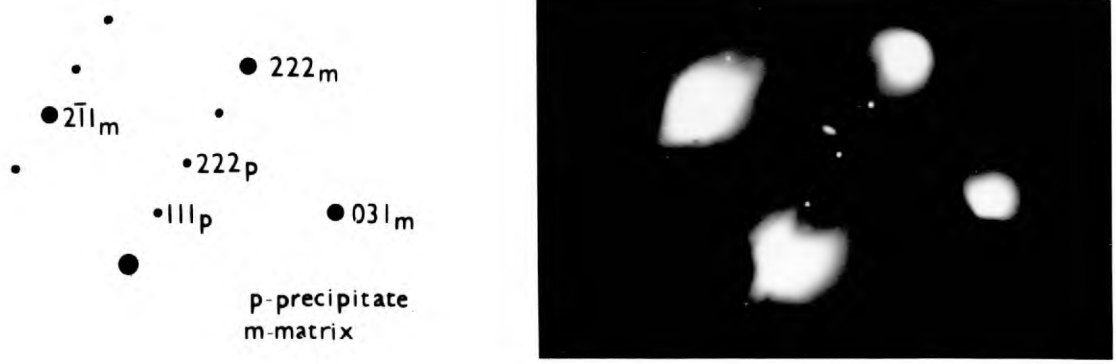

Fig.4;10c S.A.D.P. with lines of precipitate spots, and key.

copper - aluminium system by Swann and Warlimont[72] has shown that DO_3 ordering in Cu_3Al cannot be suppressed by quenching and thus, in the present investigation, it was not possible to say, in any particular case, whether or not the precipitate was ordered at temperature. Confirmation of the fact that comparable lattice parameters of the precipitate and matrix differ only slightly is given by the observation of the moiré fringes shown in Fig. 4:11.

If the interplanar spacings of the two overlapping crystals are d_1 and d_2 Å, and if the planes come into coincidence every x Å, then x/d_2 will be the number of planes with spacing d_2 in this distance. This is also the number of increments $d_1 - d_2$ in the distance d_1 thus:

$$d_1/(d_1 - d_2) = x/d_2$$

$$\text{or } x = d_1 d_2/(d_1 - d_2)$$

The periodic nature of this effect generates a parallel moiré pattern in overlapping crystal structures with slightly different lattice parameters. The fringes will be observed normal to the operating g vector. Well developed fringes are seen in the particle at the top of Fig. 4:11b normal to the [110] direction. This particle is in the exact Bragg condition as evidenced by the presence of the bend contour, which can be seen to be of the (110) type from the diffraction pattern, Fig. 4:11c.

If it is assumed that the precipitate is rich in copper and that the precipitation reaction has reached completion, then the lattice parameter of the matrix may be taken as 2:8970 Å, for the composition Fe 20at% Al. (value from Taylor

FIGURE 4:11

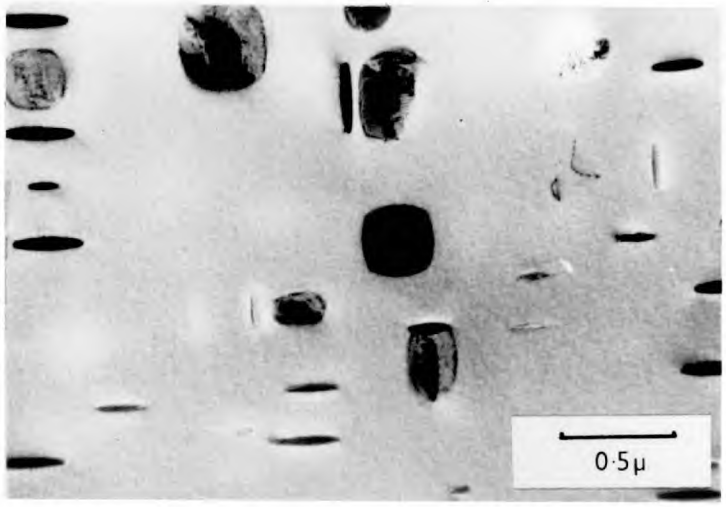

Fig.4:11a ALLOY 20C 1100°C 1hr - 710°C 1hr - W.Q. Discs of precipitate forming on cube planes.

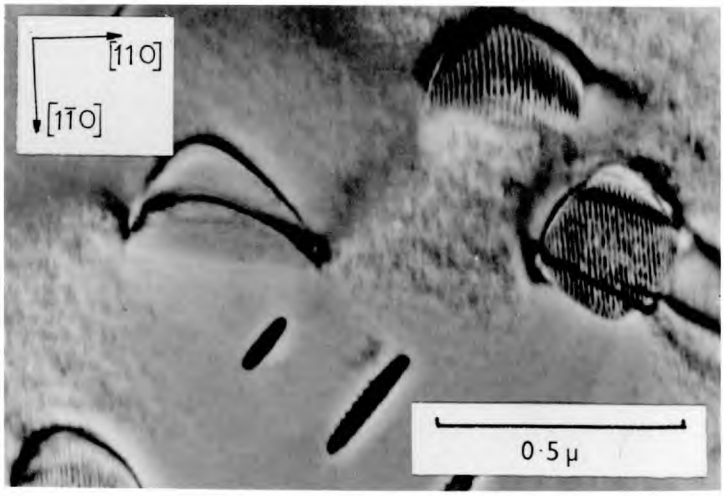

Fig.4:11b Higher mag. micrograph showing moiré fringes in precipitate particles near a (110) bend contour.

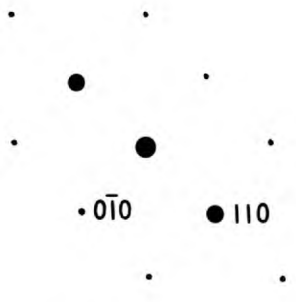

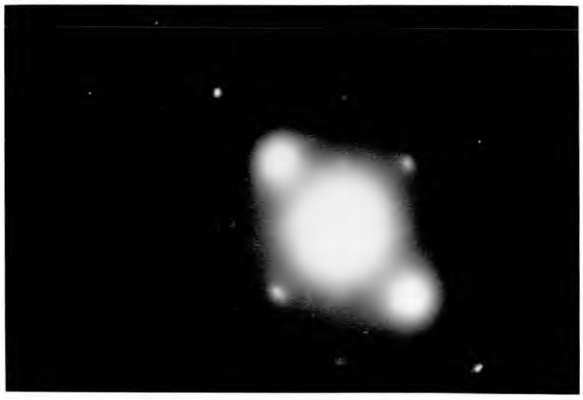

Fig.4:11c Selected area diffraction pattern of Fig.4:11b, and key.

and Jones[16]). This gives a value of 2·049Å for the (110) interplanar spacing. The fringe spacing measured from the above mentioned particle is 139Å. Substituting these values in the above expression we obtain a value for the lattice parameter of the disordered precipitate of 2·94 Å or 5·88 Å for the DO_3 ordered structure, which is in reasonable agreement with the value of 5·84 Å, for Cu_3Al, quoted by Swann and Warlimont[72]. In view of this additional evidence it is concluded that the precipitate is Cu_3Al having the ordered DO_3 structure.

4:1:4 Precipitation in the ordered $L2_0$ phase.

The discussion so far has dealt with those alloys which exhibit only ordering andthose showing precipitation in a disordered matrix. Alloys with a composition between these two extremes exhibit both ordering and precipitation.

The microstructural changes occurring in alloy 225C (Fe 22·5 at % Al 5 at % Cu) are typical of this type of alloy. The structure observed in a specimen of this alloy heat treated for 1hr at 822°C is shown in Figs. 4:12a and 4:12b. The (100)$L2_0$ dark field micrograph shows a fine array of $\frac{1}{2}a$ <111> domain boundaries. The fineness of this structure is regarded as evidence of ordering forming during the quench. The examination of possible preferential nucleation sites, such as the subrain boundaries shown in Fig. 4:12b, indicated that these were free of precipitate. In a specimen of this alloy aged for 1 hour at 751°C, however, segments of APB are seen retained between widely spaced precipitate particles (Fig. 4:12c). Dislocation traces are observed originating from the tips of some of the particles, made visible under these conditions by the lines of APB left behind by the

FIGURE 4:12

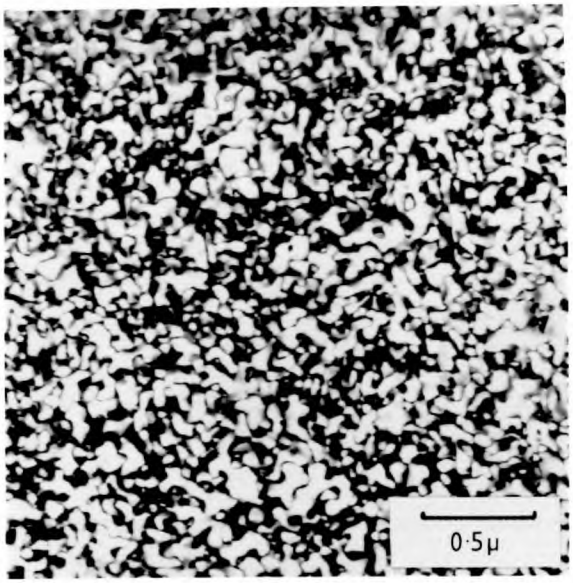

Fig.4:12a ALLOY 225C 1100°C 1hr - 822°C 1hr - W.Q.
Dark field g = (100) $L2_0$. Fine array of $\frac{1}{2}a\langle 111\rangle$ APBs formed on the quench.

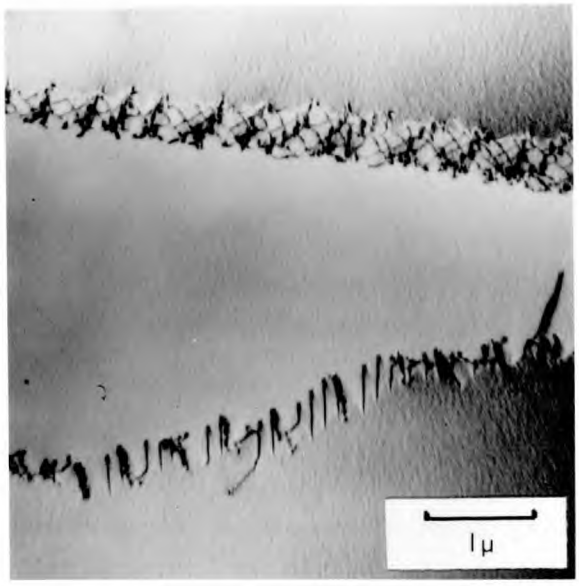

Fig.4:12b Bright field of Fig.4:12a showing subgrain boundaries free from precipitate.

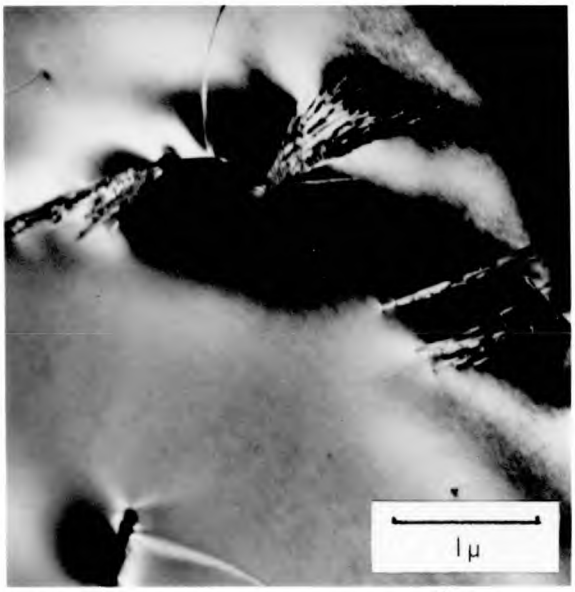

Fig.4:12c ALLOY 225C 1100°C 1hr - 751°C 1hr - W.Q.
Segments of $\frac{1}{2}a\langle 111\rangle$ APBs and dislocation traces associated with precipitate particles.

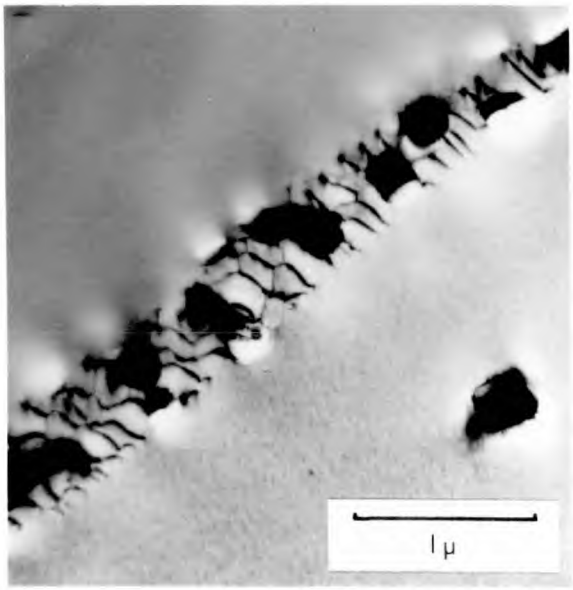

Fig.4:12d Bright field of Fig.4:12c showing precipitation in subgrain boundaries.

moving dislocation. Such dislocation movement is probably a result of interfacial stresses formed on the quench. Precipitation is also observed in low angle boundaries as shown in Fig. 4:12d in contrast to the conditions at higher temperatures indicated in Fig. 4:12b.

At an ageing temperature intermediate between the previous two discussed, 799°C, segments of APB were observed, similar to those shown in Fig. 4:12c, but no precipitate was observed in the bulk of the grains or in grain boundaries. These observations indicate that the $L2_0$ ordering temperature for alloy 225C lies between 799°C and 822°C whilst the first stages of precipitation occur between 751°C and 799°C.

Homogeneous precipitation in an ordered matrix, having the $L2_0$ structure, is illustrated in Fig. 4:13 (225C 1hr 630°C) corresponding to point D in Fig. 4:1. This dark field micrograph is taken with a (100) matrix reflection which corresponds to a (200) precipitate reflection. Under these conditions the matrix is diffracting in a way which exposes the $\frac{1}{2}$a <111> APBs and some precipitate particles can also be seen in bright contrast. A characteristic diffraction pattern from this specimen is worthy of some description, since it clarifies the intensity variations of the reflections operating, (see Fig. 4:13b). The matrix fundamental / precipitate fundamental reflections give rise to the brightest spots observed, whilst the {111} spots characteristic of the DO_3 ordering of the precipitate are very weak. Intermediate intensity is given in positions where superlattic reflections from the precipitate and matrix are superimposed (e.g. the (100) matrix / (200) precipitate spot).

If the heat treatment temperature is decreased further the alloy will be aged in a region below the point of

FIGURE 4:13

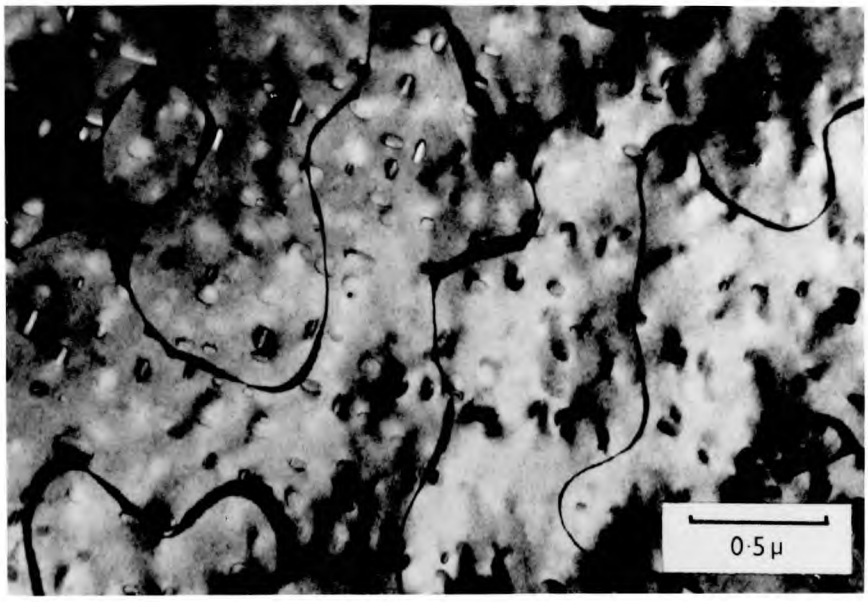

Fig.4:13a ALLOY 225C 1100°C 1hr - 630°C 1hr - W.Q.
Dark field g = (100) $L2_0$
Precipitation in the $L2_0$ superlattice.

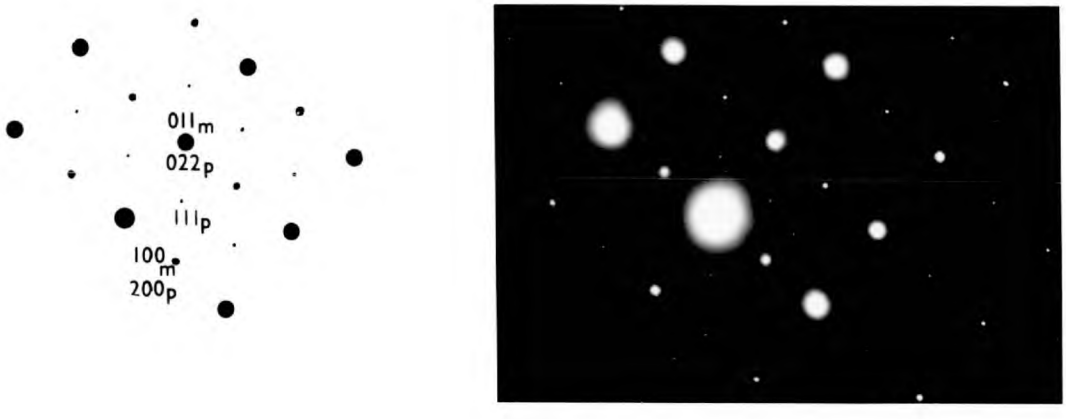

Fig.4:13b Selected area diffraction pattern illustrating the relative intensities of fundamental and superlattice reflections.

intersection of the Curie temperature and $L2_0$ ordering transition lines (point X on Fig. 4:1). Under such conditions in the binary alloys, stable α_m + $L2_0$ two phase structures are formed, as reported by Swann Duff and Fisher[6] and Warlimont, Muhe and Gengnagel[7].

A (100) dark field micrograph taken of a specimen heat treated at 562°C for 24 hours is shown in Fig. 4:14a. If the $\frac{1}{2}$a <111> APBs observed in this structure are compared with those in Fig. 4:13a it will be noted that the former have become preferentially oriented along the traces of {100} planes shown, and seem to be rather thick and diffuse. This indicates that the degree of order in the region of the boundary is low. The micrograph in Fig. 4:14b is taken with a {311} precipitate reflection and shows the Cu_3Al particles but no evidence of DO_3 ordering in the matrix.

It was decided, at this point, to subject the alloy to more prolonged heat treatment in this temperature range and to broaden the investigation to include alloys 2175C (Fe 21·75 at% Al. 5 at% Cu) and 23C (Fe 23 at% Al. 5 at% Cu). The structures resulting from these treatments are shown in Fig. 4·15. The structure observed in alloy 23C after 18 hours at 571°C is almost identical to that shown in Fig. 4:14a, indicating that the diffuse appearance of the $\frac{1}{2}$a <111> APBs, after heat treatment in this range, is not specific to alloy 225C. The volume fraction of precipitate indicated that the heat treatment temperature lay close to the Cu_3Al solvus, as indicated in Fig. 4:1. The other two micrographs shown in Fig. 4:15 are of alloys 225C and 2175C both heat treated for 140 hours at 565°C. The Cu_3Al particles have grown to a such a size that they impede the growth of antiphase domains by pinning the domain boundaries. The

FIGURE 4:14

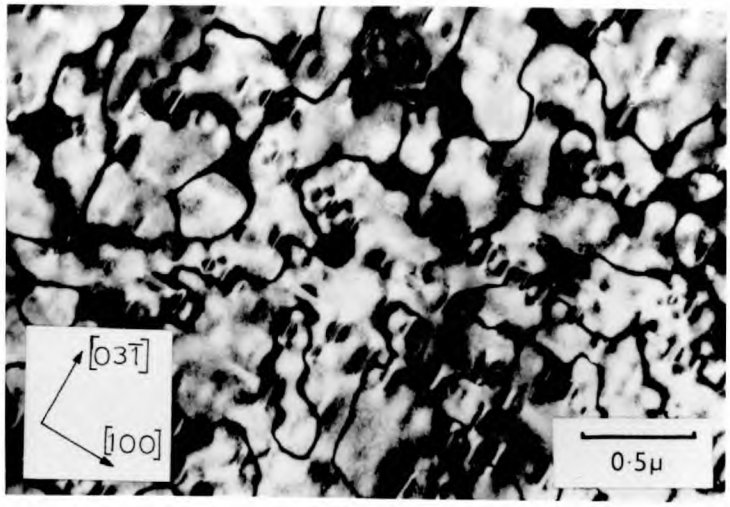

Fig.4:14a ALLOY 225C 1100°C 1hr - 562°C 24hrs - W.Q. Dark field g = (100) $L2_0$. Alignment and broadening of $\frac{1}{2}a\ \langle 111 \rangle$ APBs.

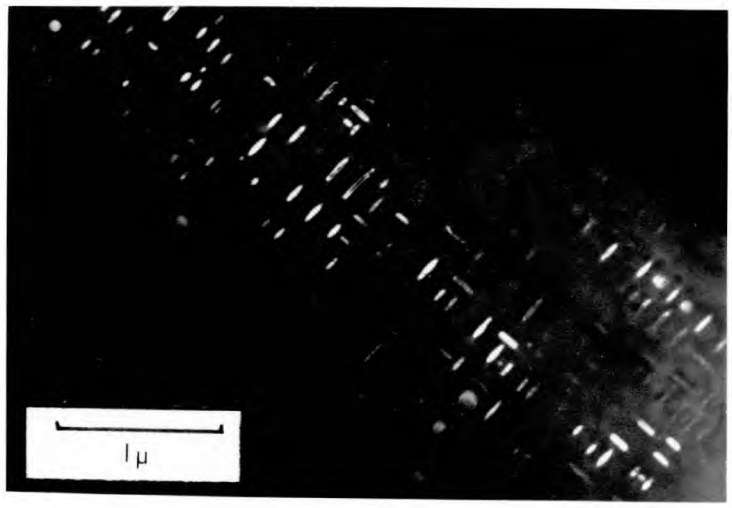

Fig.4:14b Dark field g = (311) precipitate, showing precipitates but no DO_3 ordering of the matrix.

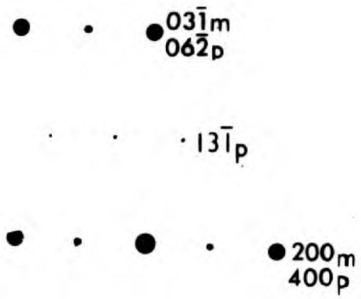

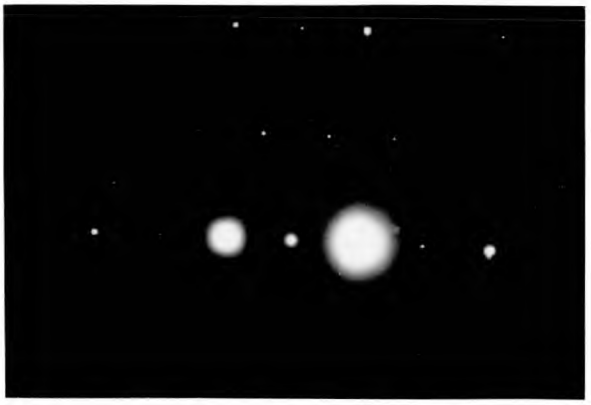

Fig.4:14c Selected area diffraction pattern of this specimen, and key.

FIGURE 4:15

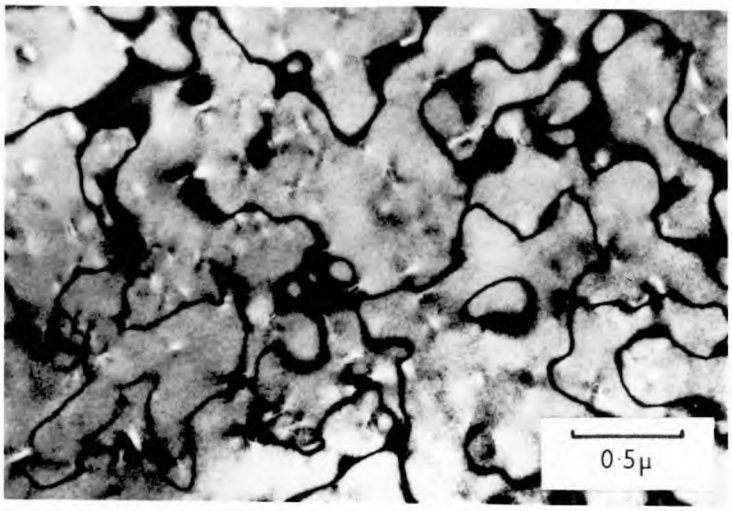

Fig.4:15a ALLOY 23C 1100°C 1hr - 571°C 18hrs - W.Q. Dark field g = (100) $L2_0$. A similar structure to that shown in Fig.4:14a but with a lower volume fraction of precipitate.

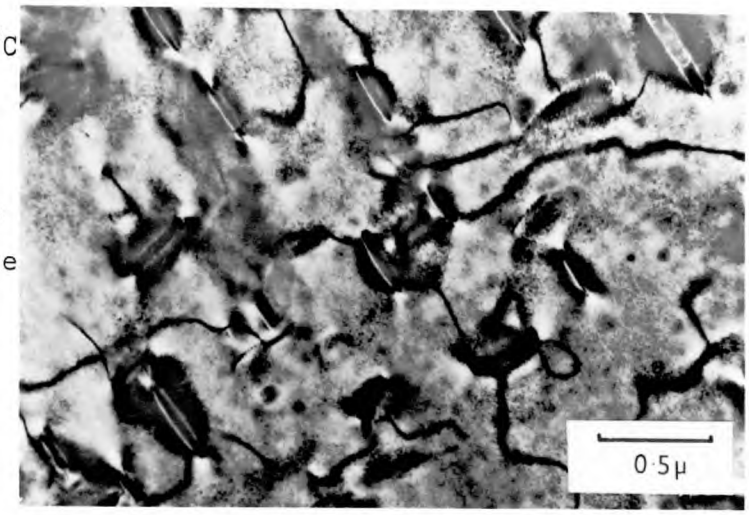

Fig.4:15b ALLOY 225C 1100°C 1hr - 565°C 140hrs - W.Q. Dark field g = (100) $L2_0$ showing diffuse boundaries pinned by large precipitate particles.

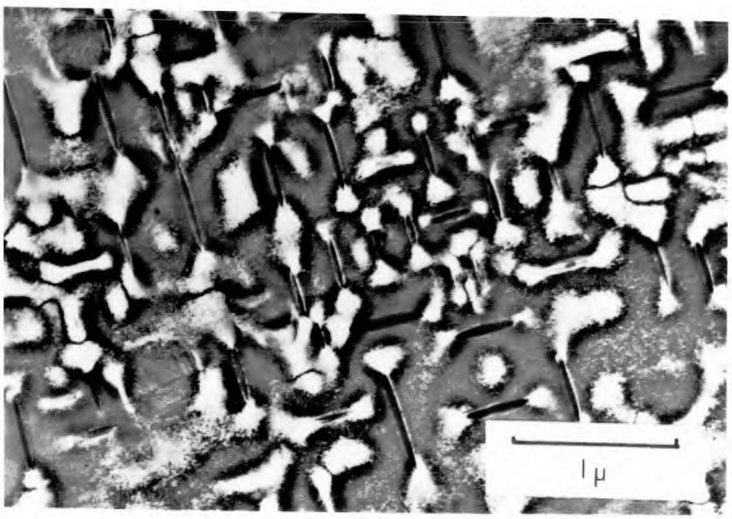

Fig.4:15c ALLOY 2175C 1100°C 1hr - 565°C 140hrs- W.Q. Dark field g = (100) $L2_0$. Strain fields associated with precipitates.

boundaries observed in Fig. 4:15b still exhibit the diffuse appearance seen at shorter heat treatment times and again no discrete particles of the α phase were observed in the bulk of the domains. The contrast conditions in the (100) dark field micrograph, Fig. 4:15c are such that the large strain fields, associated with Cu_3Al particles, are clearly observed and careful examination of this micrograph reveals the presence of moire fringes in the Cu_3Al discs lying in the plane of the foil.

On the basis of this evidence it was concluded that no stable coexistence of the α phase and the $L2_0$ ordered structure occurs in these ternary alloys.

4:1:5 The ($\alpha + \alpha_1$ (Fe_3Al) + Cu_3Al) phase field

Alloys 225C and 23C, heat treated below a certain critical temperature, found to be in the region of 555°C, showed evidence of DO_3 ordering in what has previously been referred to as the matrix. The microstructures characteristic of this region are discussed in this section and the diffraction patterns, in this case, are indexed with respect to a', the α_1 (Fe_3Al) lattice parameter.

Two specimens of alloy 225C were simultaneously quenched from the solution treatment temperature of 1100°C into a salt bath at 538°C. One was water quenched after 15 minutes at this temperature, the other after 24 hours. The microstructures observed are shown in Figs. 4:16 and 4:17 respectively. The (200) dark field micrograph, Fig. 4:16a gives an indication that precipitation has occurred in the bulk of the domains, whilst the boundaries are observed to consist of a layer of disordered material, rather than a sharp division between two highly ordered regions. The

FIGURE 4:16

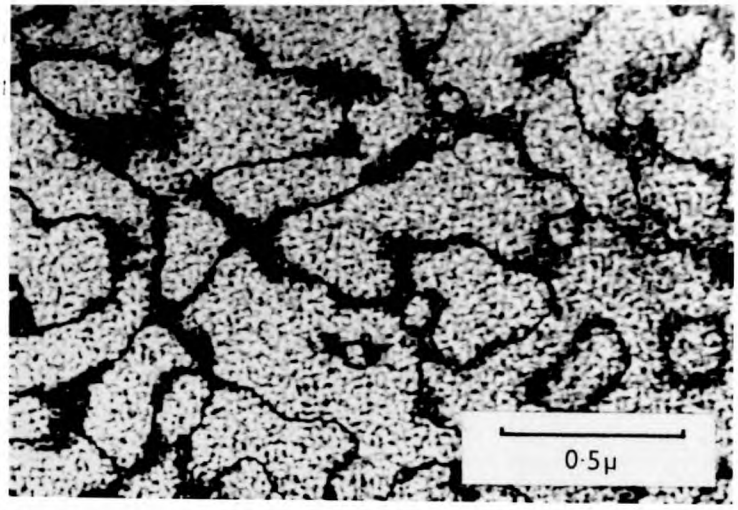

Fig.4:16a ALLOY 225C 1100°C 1hr - 538°C 15mins - W.Q. Dark field g = (200) DO_3. Precipitation on domain boundaries and within the domains of the DO_3 structure.

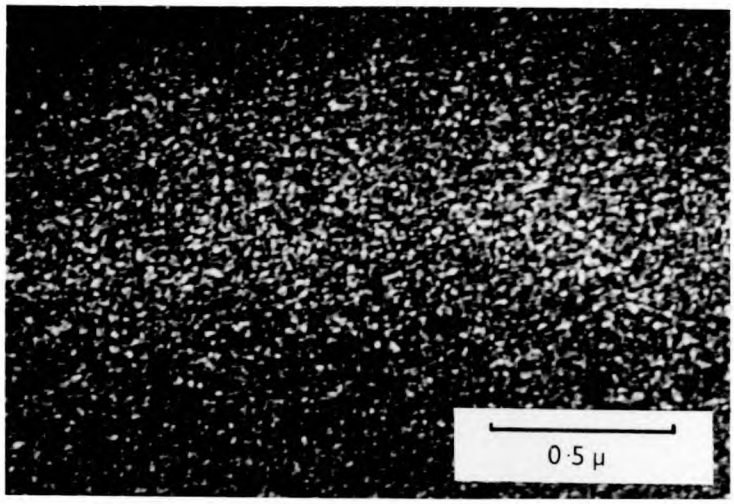

Fig.4:16b Dark field g = (311) DO_3 showing precipitate particles with the DO_3 structure.

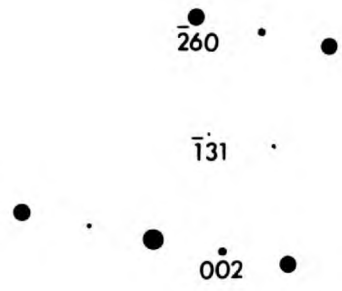

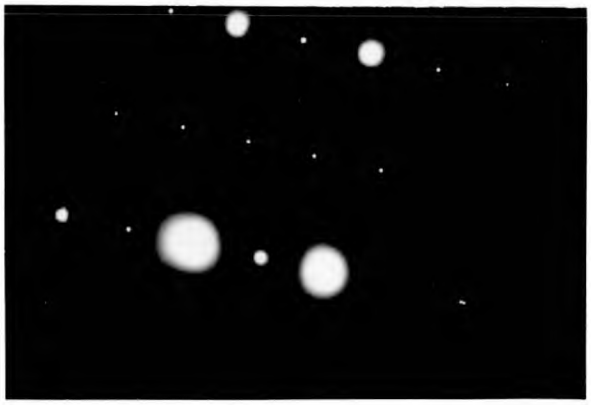

Fig.4:16c Selected area diffraction pattern, and key.

FIGURE 4:17

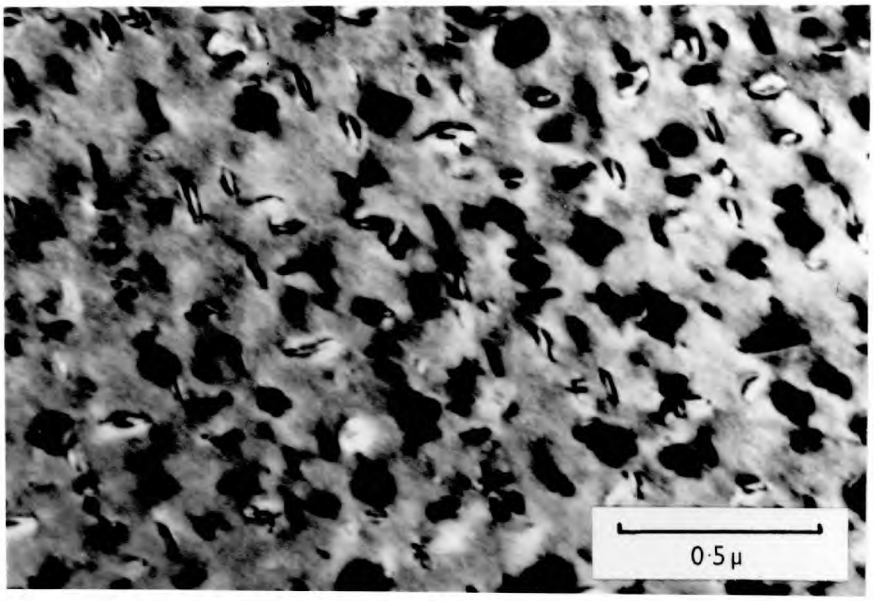

Fig.4:17a ALLOY 225C 1100°C 1hr - 538°C 24hrs - W.Q.
Bright field showing Cu_3Al precipitates.

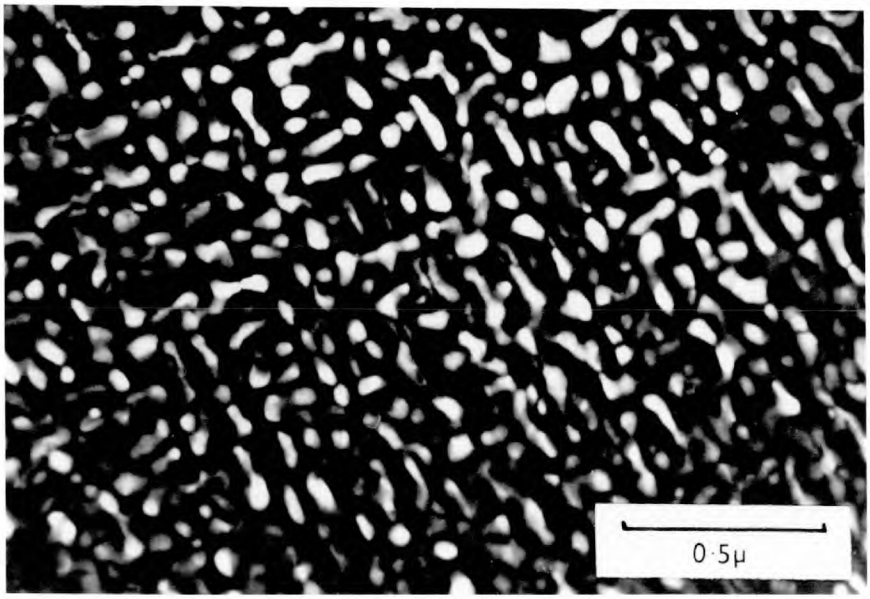

Fig.4:17b Dark field micrograph g = (111) DO_3.
Precipitates of the α_1 phase (Fe_3Al) recognisable by their different morphology.

{311} dark field of the same area shows the precipitate particles, which have the ordered DO_3 structure. At this stage it was not possible to say whether the DO_3 phase observed was α_1 (Fe_3Al) or Cu_3Al or a mixture of both. The presence of α_1 was, however, suspected since the structure in Fig. 4:16b did not show the pronounced <100> directionality associated with the Cu_3Al precipitate.

The position was clarified by observation of the specimen treated for 24 hours. A bright field micrograph of this specimen clearly indicates the presence of the Cu_3Al precipitate Fig. 4:17a, whilst a (111) dark field reveals a precipitate with a completely different morphology. This latter precipitate was identified as the α_1 phase and thus a three phase equilibrium of α, α_1 and Cu_3Al is observed in this region.

Determination of the boundaries of the region at lower temperatures was impeded by a marked retardation of the kinetics below 500°C; some examples of structures observed are, however, shown in Fig. 4:18. A specimen of alloy 225C heat treated at 468°C for 1 hour shows homogeneous precipitation of Cu_3Al and several long straight dislocations are seen (Fig. 4:18a). After aging for 24 hours the structure has coarsened somewhat, and the precipitate has formed preferentially on dislocations. Dark field micrographs of these structures show fine structures which are not easy to interpret and even after 60 hours at 440°C, a specimen of alloy 23C exhibits a relatively small domain size (Figs. 4:18c and 4:18d).

Fig. 4:18c [(200) dark field] indicates discrete areas of DO_3, α_1, phase separated by a layer of disordered α phase. Strain fields, from the Cu_3Al particles present, are

FIGURE 4:18

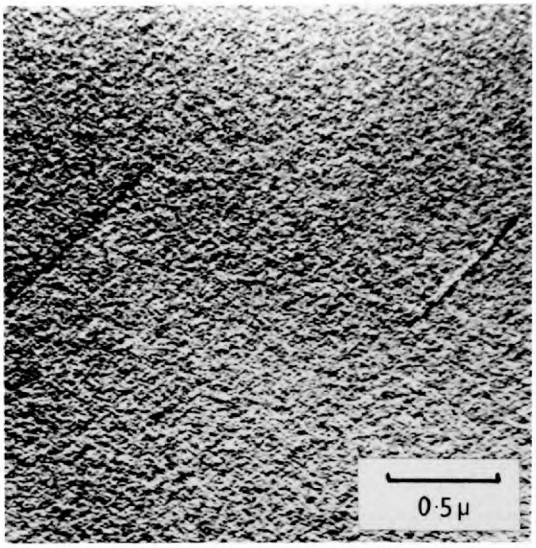

Fig.4:18a ALLOY 225C 1100°C 1hr - 468°C 1hr - W.Q.
Bright field showing precipitation of Cu_3Al in a matrix which contains straight dislocations.

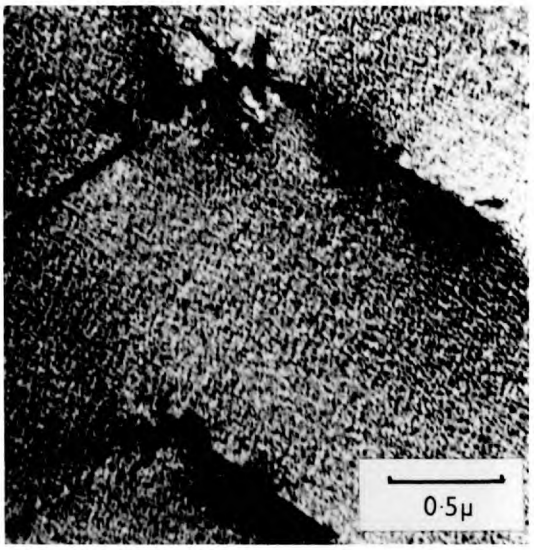

Fig.4:18b ALLOY 225C 1100°C 1hr - 468°C 24hrs - W.Q.
The precipitate has coarsened slightly and formed preferentially on dislocations.

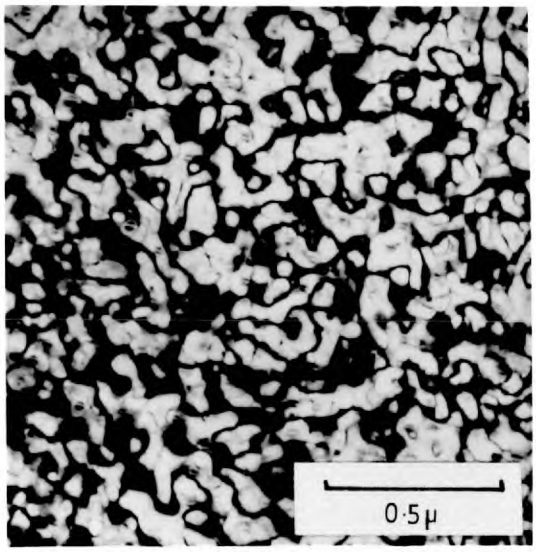

Fig.4:18c ALLOY 23C 1100°C 1hr - 440°C 60hrs - W.Q.
Dark field g = (200) DO_3.
Discrete areas of DO_3 phase surrounded by a disordered layer.

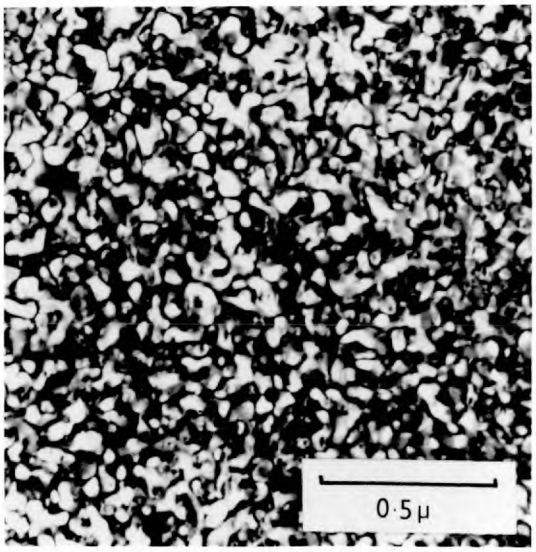

Fig.4:18d As Fig.4:18c but with g = (311) DO_3. This fine domain structure still persists after 60hrs at this temperature.

clearly observed and give rise to rather indistinct bright field micrographs. The {311} dark field (Fig. 4:18d), of the same area, indicates the complex array of both $\frac{1}{4}a'$ <111> and $\frac{1}{2}a'$ <100> present in the structure. Examination of this micrograph suggests that the proportion of α in the structure is relatively low compared with that present at higher temperatures (Fig. 4:17b). This observation is reflected in the position of the phase boundary proposed in Fig. 4:1.

No evidence was obtained for the existence of a two phase (α_1 + Cu_3Al) region, but the proposed curvature of the Cu_3Al solvus would indicate that such an area could exist and would not be observed in any of the heat treatments performed.

As mentioned previously, all the results of the observations by electron microscopy are summarised in Fig. 4:1 and the validity of this diagram will be discussed in section 4:4.

4:2 Results of magnetic balance measurements on alloys containing copper.

A specimen of the iron used in the preparation of the alloys was annealed for 1hr at 750°C and air cooled. This was used as a standard in the magnetic balance measurements and readings were taken at room temperature, of the deflection produced by this specimen in fields ranging from 1,570 Oe to 11,315 Oe. In the initial measurements, using the iron - aluminium - copper alloys, the specimens had been homogenised and air - cooled in

their silica capsules. A comparison of the deflection for each alloy specimen, with the data for the standard, yielded the following results.

For each alloy, the ratio of deflection characteristic of the alloy to that of the standard became approximately constant above 8,000 Oe. The average of seven values for this ratio i.e. σ_s/σ_{Fe} between 8,000 Oe and 11, 315 Oe are shown in Fig. 4:19. The maximum deviation of any individual value from this average value was found to be 0·2%. Absolute values of the saturation magnetic moment per gram (σ_s) for the alloys were obtained by using the published value[74] for σ_{Fe} of 217·75 emu/gm. These results are plotted against the aluminium content of the alloy in Fig. 4:20. This curve shows a discontinuity in the region between 22·5 at % Al and 25 at % Al which is associated with the $\alpha + \alpha_1$ (Fe_3Al) + Cu_3Al phase field (see section 4:4).

Curves of deflection vs temperature were obtained for each of the alloys at three field settings (4,530 Oe, 8, 590 Oe, and 10, 110 Oe) using a constant heating rate of 15°C/min. From these curves and the extrapolation procedure outlined in Appendix B, the Curie points listed in Fig. 4:19 were determined. Examples of the standardised curves obtained at a field value of 8,590 Oe. are shown in Fig. 4:21. In each case the Curie point is marked, although it should be noted that this figure corresponds to the condition of zero applied field. It is observed that the applied field has the effect of stablizing the ferromagnetic state to higher temperatures and the indicated Curie temperature corresponds approximately to the point of inflexion of the curves.

ALLOY	CURIE TEMP. (all values ± 3°C)	MAGNETIZATION VALUES AT 20°C	
		$\frac{\sigma_s(\text{alloy})}{\sigma_s(\text{Fe standard})}$	σ_s(alloy) emu/gm [σ_s(Fe) = 217·75 emu/gm]
175C	699°C	·8331	181·2
20C	664°C	·7907	172·0
225C	618°C	·7198	156·4
25C	603°C 495±5°C	·7157	155·9
275C	403°C	·5721	124·6
30C	316°C	·4366	94·9

Fig. 4:19 Curie temperatures and saturation magnetic moments per unit mass for the iron-aluminium-copper alloys studied.

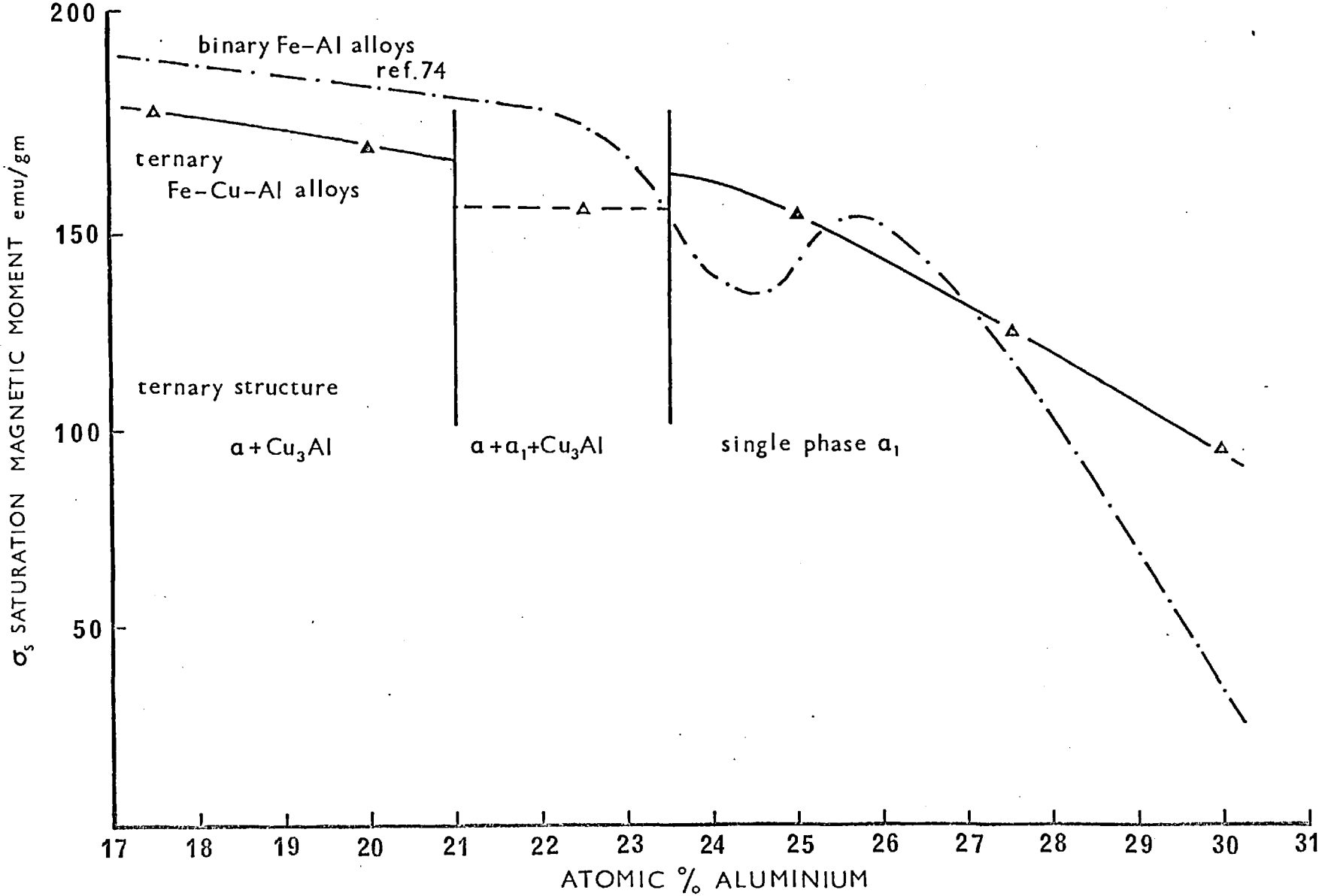

Fig 4:20 The variation of σ_s with composition for alloys containing copper

The variation of σ_s with temperature for alloys 175C and 20C is essentially similar, the heating and cooling curves, both measured at 15°C/min, were almost completely coincident. The general shape of these curves is characteristic of a ferromagnetic material. The equilibrium structure for these alloys, as described in section 4:1, consists of a disordered α matrix with Cu_3Al precipitates, and thus it is apparent that the Curie temperatures indicated refer to the α phase. Any changes in precipitate volume fraction and distribution which occurred during the period of the measurement did not appear to significantly affect the value of σ_s as indicated by the close correspondance of heating and cooling curves.

The curves for alloys 275C and 30C are also similar and again show no measureable thermal hysteresis. The equilibrium structure for these alloys, below 530°C, is single phase α_1 (DO_3 ordered). Since the Curie points of both alloys are below the DO_3 critical temperature, the curves have the shape characteristic of a single phase ferromagnetic material. It should be noted that, in both cases, the alloy was heated to above the DO_3 transition temperature during the measurements, but the magnetization remained at a very low level. In alloy 25C, however, a distinct kink is observed in the curve in the region of 555°C. This feature was reproduceable on repeated heating and cooling of the same specimen, and the temperature at which it occurs coincides approximately with the transition from α_1 to α_2 (DO_3 order to $L2_0$ order) as determined by electron microscopy. The rapid kinetics associated with this reaction were illustrated by the fact that only very slight variations in σ_s were evident when comparing

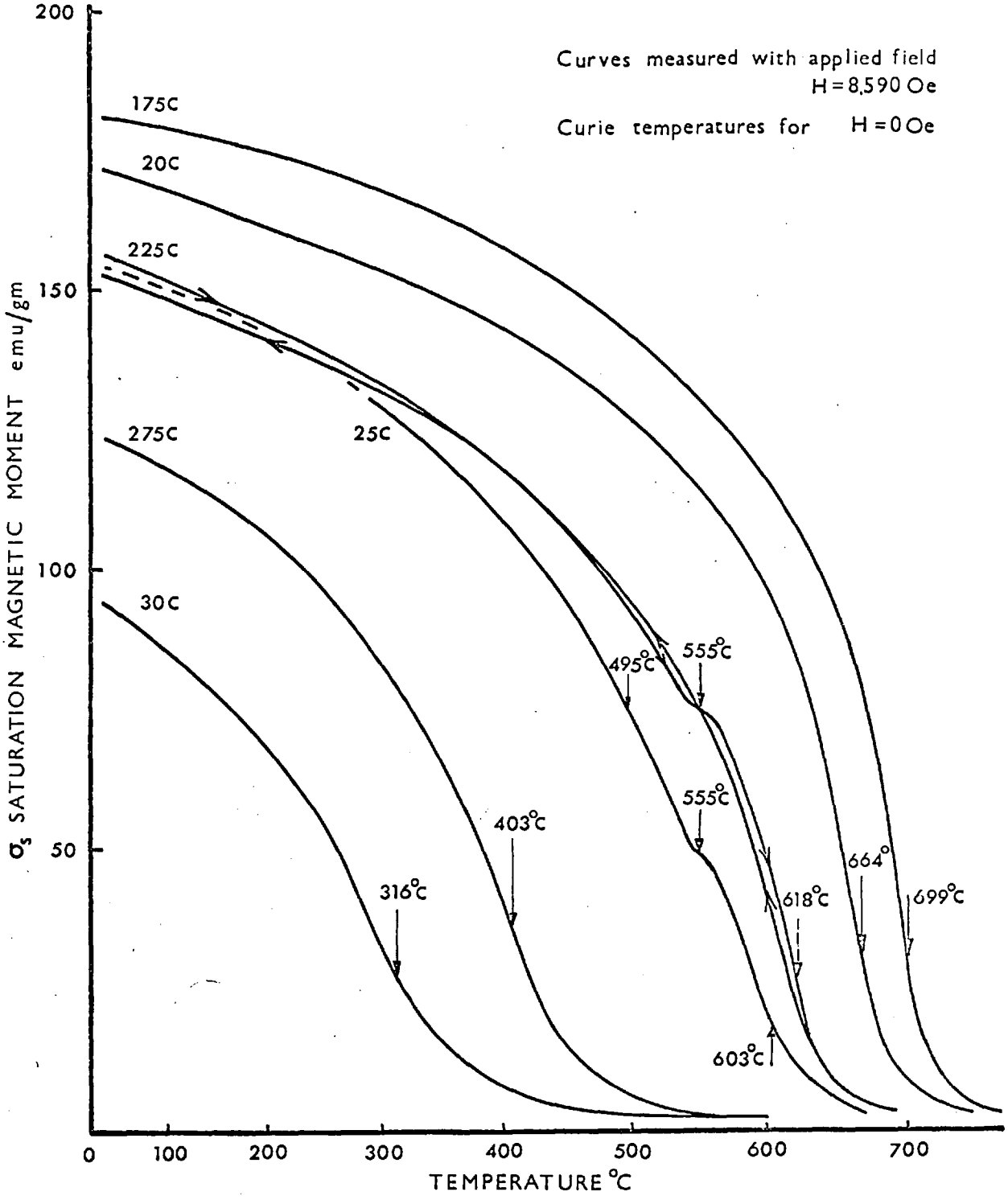

Fig 4:21 The variation of σ_s with temperature for alloys containing copper

the heating and cooling cycles.

From these results it can be seen that alloys which show precipitation of a non - magnetic phase in a disordered matrix, and those with single phase ordered structures give magnetic curves with little or no variation on heating and cooling. This reversibility was not observed in alloy 225C as shown in Fig. 4:21. In the initial heating curve a well defined step occurred, extending from approximately 540°C to 560°C. This feature was not observed in the cooling curve or in any subsequent heating or cooling curves with the same specimen. The anomalous heating curve was, however, observed on initial heating of a second specimen of the same air-cooled alloy. These measurements suggest that the anomaly is associated with a structural change which is irreversible at the heating / cooling rate of 15°C/min used for the measurements. As the anomaly occurs in the region of 555°C it would seem that the structure in question is stable at a relatively low temperature.

To investigate this proposal specimens of two alloys, 225C and 23C, were aged for 24 hrs at 534°C to produce a structure similar to that shown in Fig. 4:17. The thermo-magnetic curves for thses specimens are shown in Fig. 4:22. The general form of the curves is similar to that for the air cooled specimen of alloy 225C but the thermal hysteresis observed in both of these aged specimens was greater in extent. The anomaly for alloy 225C at 555°C was enlarged somewhat and occurred at approximately the same σ_s value whilst for alloy 23C, it occurred over a slightly higher temperature range and lower σ_s value.

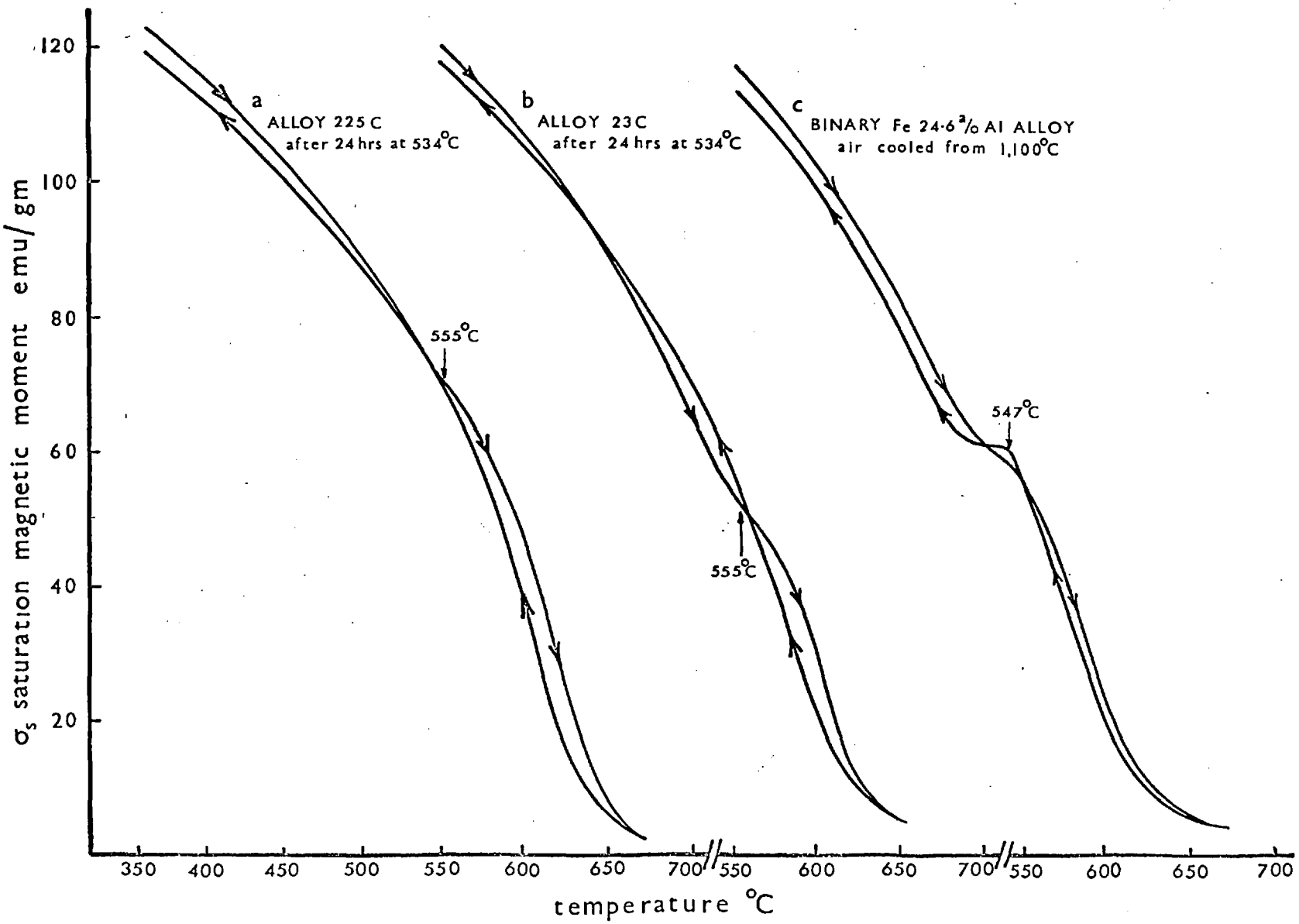

Fig 4:22 Thermomagnetic curves for alloys in which the α and α_1 phases coexist

For the purposes of comparison a thermomagnetic curve was determined for an air cooled specimen of a binary iron - 24·6 atomic % aluminium alloy, and this is included in Fig. 4:22. The initial heating curve is similar to those described for alloys 225C and 23C but the anomaly occurs at a slightly lower temperature. On cooling, however, the curve is markedly different from those observed previously. The anomaly is more pronounced that on heating, in fact σ_s appears to remain constant from 540°C to 520°C. The significance of this curve and the interpretation of the other anomalous effects will be discussed in section 4:4.

4:3 Results of vibrating sample magnetometer measurements on alloys containing copper.

These measurements were made to illustrate the variation in magnetic properties of certain alloys with temperature, as indicated by changes in the shape of the hysteresis loop. Unlike the magnetic balance readings, measurements were not continuous and it was necessary to hold the temperature constant, to $\pm$ 2°C, for several minutes while each curve was recorded. Several features of the design of the apparatus, notably the relatively large thermal mass of the specimen holder and the necessity to maintain the furnace tube under vacuum, restricted the maximum heating rate of the furnace to 5°C/min. On cooling, however, the rate was typically 10°C/min.

The results for an air - cooled specimen of alloy 225C are shown in Fig. 4:23. The σ_s vs temperature curves are seen to closely resemble those obtained from the

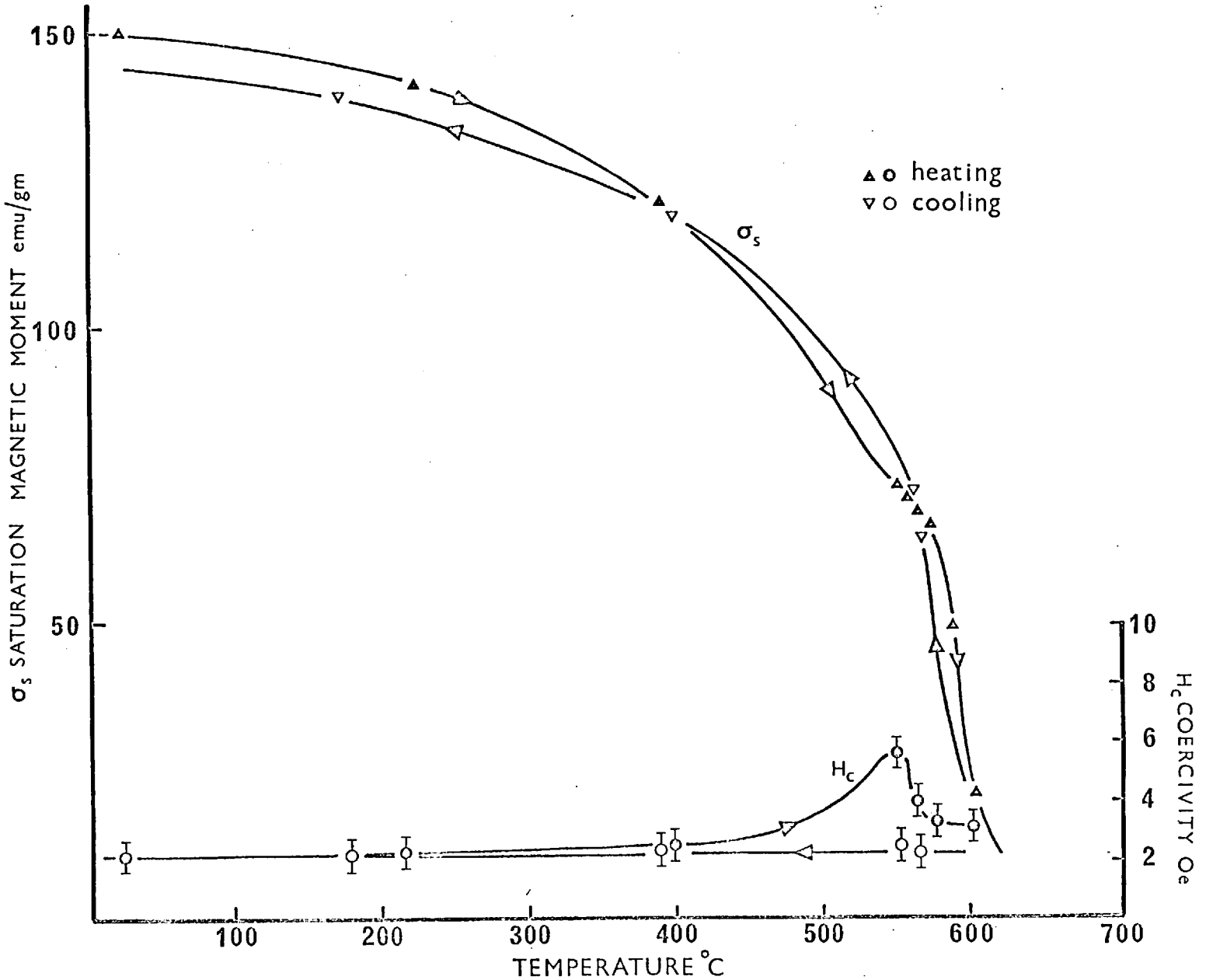

Fig 4:23 THE TEMPERATURE DEPENDENCE OF σ_s AND H_c FOR ALLOY 225C FROM VIBRATING SAMPLE MAG IETOMETER MEASUREMENTS

magnetic balance, and particular attention was paid to the variation of coercivity (H_c) in the region of the anomaly. It was found that a maximum occurred in this quantity at 550°C in the initial heating of the specimen, and did not reappear on cooling. The magnitude of this maximum was 5·5 Oe $\pm$ 0·5 Oe, which, when compared with the initial value of 2·1 Oe $\pm$ 0·5 Oe, is considered significant but certainly not the dramatic increase found in the binary alloys. The coercivity of the alloy appears to fall sharply in the region of 565°C and then decrease gradually to the Curie point at 618°C. A similar investigation with an air - cooled specimen of alloy 25C showed no evidence of a peak in the coervicity, which remained approximately constant at 1·4 Oe $\pm$ 0·5 Oe from room temperature to the Curie point of 603°C.

It should be emphasised that these are absolute values as the apparatus was calibrated with a small copper coil, in place of the specimen, through which a carefully measured current was passed. The total magnetic moment per amp of this dipole was calculated and a calibration curve plotted. This was used to find the σ_s values from the hysteresis loops. The solenoid used to provide the field was calibrated with a Hall effect fluxmeter and was found to give a field of 138 Oe / amp in agreement with the design calculations. This enabled the field axis of the hyseresis loop to be calibrated and hence, absolute values of coercivity to be obtained.

A comparison of corresponding σ_s values from the vibrating sample magnetometer and magnetic balance indicates that the former are, on average, 4% lower than

the latter. This was found to be the case for all the specimens examined by both techniques, and is probably due to the different standards used. As the total magnetic moment of the copper coil used to calibrate the vibrating coil magnetometer may be calculated accurately, the discrepancy would suggest that the saturation magnetic moment per gram of the particular iron specimen used as a standard for the magnetic balance was in the region of 208 emu/gm rather than the "pure iron" value of 217·75 emu/gm. This lower value may be attributed to an inadequate annealing treatment and to a lesser extent, to the impurity content of the iron.

4:4 DISCUSSION OF RESULTS FOR IRON - ALUMINIUM - COPPER ALLOYS.

The vertical section through the iron - aluminium - copper ternary diagram, at a constant copper content of 5 atomic %, was constructed on the basis of evidence from electron microscopy. Since a survey of the literature on the binary iron - aluminium system has shown that the most acceptable version of the binary equilibrium diagram, proposed by Swann et al, was also based on this technique, it is considered that the role of copper as an alloying addition may elucidated by comparison of the proposed vertical section with this version of the binary diagram.

4:4:1 The microstructural changes produced by the copper addition.

The first comparison to be made will be between the single phase α_1 (DO_3) regions in both diagrams. The DO_3 antiphase domain structures observed in alloys with the copper addition are indistinguishable from those occurring in the binary system, but the DO_3 critical temperature is uniformally elevated by approximately 15°C in ternary alloys of corresponding aluminium contents. The maximum in the DO_3 critical temperature, for binary alloys, is at 551·4°C and 26·5 atomic % Al whilst for the ternary alloys the corresponding temperature is approximately 566°C, again at 26·5 atomic % Al. This uniform elevation of the DO_3 critical temperature, which leaves the position of the maximum unaffected, indicates that the copper atoms have

substituted for iron atoms in the DO_3 structure within the composition range 25·3 to 30 atomic % Al. From the experimental evidence obtained by electron microscopy it is not possible to say whether the substitution occurs on a specific iron sublattice in the DO_3 structure, since the atomic scattering factors for electrons, characteristic of iron and copper, are so similar. The identification of the particular sites involved is, however, significant in the interpretation of the magnetic properties of these alloys, which will be discussed later.

The substitution of copper atoms for iron atoms is as expected since both Fe_3Al and Cu_3Al possess the DO_3 structure. The bonding in this structure is characterised by the formation of the maximum number of unlike first and second nearest neighbour pairs, and since the copper addition causes a rise in the DO_3 critical temperature, it is apparent that the interaction giving rise to copper-aluminium bonds is stronger than the corresponding iron-aluminium interaction.

The mode of transformation from the DO_3 to the $L2_0$ structure is unaffected by the copper addition as may be seen by comparison of Figs. 4:4 and 4:7 with micrographs showing critical point fluctuations in the binary system. Although the present investigation of this transition is less detailed than that of Swann et al[4] the same basic features are observed. Close to the critical temperature, the microstructures observed using a DO_3 superlattice reflection adopt a speckled appearance due to long range order fluctuations. The density of ordered clusters is lower in the region of antiphase boundaries which were

present in the DO_3 structure and this decrease in the proportion of ordered material enables the position of such boundaries to be observed as diffuse dark lines when a DO_3 superlattice reflection is used to form the image. This indicates that the critical temperature is lower at the domain boundaries than in the bulk of the domains. As the proportions of DO_3 ordered and disordered (i.e. material with the $L2_0$ structure) phases do not appear to obey the lever rule and since the speckled structures were observed in two alloys, 25C and 275C, it is concluded that no stable two phase field separates the DO_3 and $L2_0$ structures in these ternary alloys.

The $L2_0$ to DO_3 ordering reaction is therefore considered to be non - classical, probably second order, since in the region of such transitions relatively large order - disorder fluctuations can occur with only very small changes in the associated free energy. For these reasons the transition is represented by a single line in Fig. 4:1 with a shaded area representing the transition range. This additional evidence is thus compatible with Swann's observations and the theoretical predictions for the system, and is significant in discounting Warlimont's interpretations of the evidence from electron microscopy, referred to in Cohen's recent review of order - disorder transformations[75]. Whilst Warlimont's diagram, Fig. 2:2h, would predict a single composition at which the ordering reaction would be second order, it cannot account for the observation of critical point fluctuations in two different alloys and hence a second order reaction over a range of composition.

Following the same sequence as was used in presenting the results, the next alloys to be discussed will be those in which precipitation occurs in a matrix which does not exhibit long range order, i.e. alloys 175C and 20C. In these alloys discs of precipitate, having the DO_3 structure, were observed to form on {100} planes of the matrix. The size to which these precipitates maintained coherency (>3,000Å) suggested that their lattice parameter differed only slightly from that of the matrix, in fact no detectable difference could be seen in the electron diffraction patterns. Since a precipitate of such morphology was not found in the binary system, its presence was attributed to the copper addition, and the DO_3 structure indicated that it was probably Cu_3Al. In view of what has already been inferred concerning the relative tendencies of iron and copper atoms to adopt the DO_3 structure when alloyed with aluminium, this interpretation of the composition of the precipitate would appear reasonable.

Additional evidince concerning the nature of the precipitate was provided by the result of a lattice parameter calculation based on the moiré fringe patterns observed. It should be noted that calculations of this type are comparative and thus the lattice parameter difference of 1·48% was based on the assumed value of 2·8970 Å for the matrix parameter taken from the X-ray measurements of Taylor and Jones[16]. This figure refers to the lattice parameter of a binary iron - 20·1 at % aluminium alloy quenched from 600°C and hence its use in a calculation concerning the ternary alloy neglects the

effect of the copper which remains in solid solution in the matrix. Preliminary investigations, indicated that solid solubility in this type of alloy extended to between 1·4 and 2·0 atomic % copper. Since the atomic radii of copper and iron are similar, the effect of this amount of copper in solid solution is not thought to be significant. The discrepancy between the calculated value for the lattice parameter of the ordered precipitate (5·88 Å), and the published value of 5·84 Å for Cu_3Al may be explained by deviations from stoichiometry, however, the inaccuracy in the measurement of the fringe spacing is sufficient to explain such differences. It is therefore concluded that the precipitate is Cu_3Al.

As has been described previously, the precipitate forms as discs on cube planes in the matrix and thus causes streaking in the diffraction pattern (see Fig. 4:10a). The zone azis in this case is near [100] and, as streaking occurs perpendicular to the thickness of the precipitate discs, the spots indexed as $(0\bar{1}1)$ and (011) are streaked in the [001] and [010] directions. Careful examination of this diffraction pattern also reveals streaking in <110> directions which is not due to the precipitate morphology. This effect was more pronounced in alloy 20C than in alloy 175C and appeared to be associated with the background features visible in Figures 4:11a and 4:11b. The possible interpretations of the origin of this fine background structure will now be considered.

In recent years there has been some controversy about the lower composition limit of the $\alpha + \alpha_1$ phase field in the binary iron - aluminium diagram. X-ray measurements

of the relative intensities of fundamental and superlattice reflections indicate the existence of the DO_3 ordered phase to much lower aluminium contents than the results of electron microscopy would suggest. This may be seen from the diagram proposed by Lawley and Cahn[18], Fig. 2:2f, in which a region of short range order is proposed. It is reported[76] that in this region, between 5 and 19 atomic % Al, alloys show an increase in electrical resistivity when quenched and aged and a decrease when quenched and deformed. Alloys possessing such properties are said to show the "K - state". The microstructural features which give rise to such properties are not well understood but the various suggestions indicate that some short range order or clustering phenomenon is responsible.

In a recent investigation Warlimont and Thomas[77] studied alloys showing these anomalous properties by electron microscopy. They reported weak "tweed - like" contrast effects in alloys containing between 10 and 18 atomic % aluminium which had been aged at 300°C. Weak intensity maxima, in characteristic DO_3 positions, were observed in an alloy containing 15·5 at % aluminium and these were more pronounced when the aluminium content was increased to 17·8 at %. Streaking was observed in these diffraction patterns in directions close to <110> and <211> and was observed most strongly at slight deviations from low index zones. Above 18 atomic % aluminium the superlattice reflections were sharp and it was possible to resolve α_1 particles in an α matrix. Unlike the "tweed patterns" these conventional two phase structures responded well to aging treatments and considerable particle growth was observed.

The authors suggest that the "tweed patterns" are formed by overlapping strain field contrast from a high density of coherent precipitate particles, which have the DO_3 structure. The strain is calculated to be approximately 0·5 % and hence the contrast is weak. As a result of the ordering reaction, elastic strains are set up and it is suggested that these account for the streaking of diffraction spots. The direction of streaking is compatible with this explanation since it has been shown[78] that iron-rich iron aluminium alloys show pronounced elastic anisotropy. This would encourage precipitation to occur on the elastically soft {100} planes leading to {110} strain maximum and hence <110> streaking, as outlined by Tanner[79,80] in his work on Cu - Be alloys.

Thomas and Warlimont[77] conclude that the $\alpha + \alpha_1$ phase field should be subdiveded into two regions; the conventional phase field in which the growth of α_1 particles is unlimited, and what has been referred to as the region of short range order in which the growth of α_1 particles is impeded for thermodynamic reasons. They state that if this is the case, the free-energy criteria must depend on the inter-relation of strain energy and particle size in such a way that a minimum in free energy of the system is obtained for a particular dispersion of particles.

The investigation described does, therefore, provide a possible explanation for the peculiarities in physical properties observed in these alloys. This explanation depends on the assertion that the "tweed pattern" contrast observed is due to overlapping strain fields from a high volume fraction of discrete coherent particles which are

too small to be resolved individually. Confirmatory evidence is given in the form of resistivity measurements, about which reservations have already been expressed, (see chapter 2) and which cannot give information on the precise structure of the electron scattering centres involved. The position in this region of the binary system is thus in need of some further clarification.

Any comparison of observations made on binary alloys with those of the present investigation is complicated by the following points. In the ternary alloys 175C and 20C the copper addition leads to the formation of Cu_3Al precipitates, but even if this reaction has reached completion, at the particular aging temperature used, some copper remains in solid solution. The background in Figs. 4:11a and 4:11b, where the aging temperature was 710°C, could therefore be caused by incipient precipitation of Cu_3Al on quenching, due to the decreasing solid solubility of copper with temperature. Alternatively, it may be due to the formation of short range order, on the quench, which might be described on the model suggested by Warlimont and Thomas, i.e. discrete small particles of α_1 in an α matrix. It is recognized, however, that this structural model of short range order is not universally accepted and other "theories", based on pair probability distributions, may be equally applicable in this case.

The observation of diffuse diffraction phenomena from these ternary alloys is of little assistance in determining the nature of the fine background structure since the large Cu_3Al precipitates present, possess the DO_3 structure and give rise to sharp superlattice reflections. These tend to swamp any diffuse maxima which might otherwise be visible in characteristic DO_3 positions. The following

observations are made with respect to the streaking in the diffraction patterns shown:

(i) Fig. 4:10a shows shape - factor streaking of the {110} spots in <100> directions due to the large Cu_3Al precipitates.

(ii) No streaking of {110} spots is seen in Fig. 4:9c but when the specimen is tilted off the zone axis, streaking is observed in <211> directions. The streaking is thus not in the (111) reciprocal lattice plane but may be explained by the projection of <100> shape factor streaks on this plane.

(iii) Figs. 4:9d and 4:10a both show streaking between relpoints in <110> directions which is in agreement with the observations of Warlimont and Thomas[77]. These diffuse streaks are not associated with the shape of the large Cu_3Al precipitates, or with the interaction of their strain fields giving {110} strain maxima; the particles are too widely spaced for this.

In concluding this discussion of precipitation in the "disordered" structure it can be said that a fine structure has been observed in the matrix of alloys 175C and 20C which causes streaking in the diffraction patterns in directions close to <110>. These observations, whilst in agreement with those made by Warlimont and Thomas[77]

using binary iron - aluminium alloys, do not indicate the exact origin of the fine background structure. The elucidation of this point must depend on further developments in the theory of short range order and more comprehensive studies of the binary system.

The composition range between alloys 20C and 25C has proved to be most interesting since it is here that the copper addition has its maximum effect. In alloy 25C the $L2_0$ critical temperature was found to be above 1000°C, whilst that for the binary alloy with the same percentage of aluminium is 770°C (from Fig. 2:3). Similarly, for alloy 225C the critical temperature is between 799°C and 822°C which is well above the temperature corresponding to the onset of ordering in Fe 22·5 at % Al (557°C). The stabilizing effect of copper on the ordered structures in iron - aluminium alloys is thus more pronounced in the case of the $L2_0$ structure than for the DO_3 type already discussed.

This marked stabilizing effect is diminished as the copper comes out of solution and forms the Cu_3Al precipitate, as can be seen by the steeply falling $\alpha/L2_0$ phase boundary, below 22·5 atomic % Al, in Fig. 4:1. In this region the $L2_0$ critical temperature naturally refers to the matrix and during precipitation the composition of this phase gradually changes towards a binary iron - aluminium alloy containing the same percentage of aluminium as the ternary alloy of which it forms a part. This is because the precipitate has approximately the same 3 to 1 stoichiometry as the matrix. The binary composition is not actually reached since there is always some terminal solid solubility of copper in the matrix.

Observations of the structure of alloy 225C at 799°C and 751°C indicated that this was in the first case, single

phase α_2 ($L2_0$) and in the second case α_2 + Cu_3Al. The presence of the disordered α phase was not detected in either case. Also, detailed examination of the $L2_0$ to DO_3 transition has revealed that the copper addition has no detectable effect on the mode of this transformation. In view of the structural similarity between the α_n(disordered) to $L2_0$ and $L2_0$ to DO_3 transformations (each transformation involves only one of the two $L2_0$ sublattices), and the observations mentioned above, it is assumed that the mode of former transformation is also unaffected by the copper addition and remains second order. For this reason the α_n to α_2 ($L2_0$) ordering reaction is represented by a single line in Fig. 4:1.

It is reported by Swann et al[3], that below the Curie point of the disordered phase in the binary system, the α_m to α_2 ($L2_0$) transformation becomes first order and two phase α_m + α_2 ($L2_0$) structures are observed. The suggested explanation is that these structures are stable becuase of the magnetic energy associated with the ferromagnetic α_m particles which form in the paramagnetic ordered structure. This interpretation indicates that a fine balance exists in the system between the ordering energy, which promotes the formation of unlike nearest neighbour bonds, and the magnetic energy associated with iron - iron bonds. This change in the ordering reaction from second order to first order was not observed in alloys with the copper addition. Alloys treated in the relevant area of the ternary diagram (below and to the right of point X in Fig. 4:1) were not found to contain any discrete areas of the α_m phase, even after heat treatment for 140 hrs. On close examination,

however, the antiphase boundaries of the ordered $L2_0$ structure were found to be rather diffuse and were aligned preferentially in cube directions. These observations are similar to those made by Swann et al in binary alloys and indicate the inital stages of decomposition of the ordered structure. Under these conditions the degree of order at the boundary is low and a combination of magneto - crystalline and elastic anisotropy confine these regions of low order to cube planes.

It would appear, therefore, that the copper addition has slightly altered the balance between the ordering and magnetic forces and a situation exists in which regions of low order are stable but decomposition into two distinct phases does not occur. This change is a result of an increase in the energy associated with ordering, due to the formation of relatively strong copper - aluminium bonds, and a decrease in the amount of magnetic energy which decomposition would provide. The former component is independent of any magnetic effects while the latter is a direct result of the elevation of the $L2_0$ Curie temperature which will be discussed in the next section. An effect of the precipitation in the $L2_0$ ordered structure, which has not been mentioned so far, is the interaction between precipitate particles and antiphase boundaries. In Fig. 4:15b the precipitates are seen to be closely associated with APB's but this was not found to be the case at shorter aging times, as may be seen from Fig. 4:13a. The precipitate is, thus, nucleated homogeneously, irrespective of the position of the APBs, but as the particles grow they impede domain boundary migration. This resistance to

domain boundary movement is also a feature of the $\alpha_m + \alpha_1 + Cu_3Al$ phase field as may be seen from the fine structure which still persists in alloy 23C after 60 hrs at 440°C (Fig. 4:18d). In this region the α_1 and Cu_3Al phases were easily distinguished by their different morphologies and observations of the proportions of phases present suggest that the boundaries of the three phase field are as shown in Fig. 4:1. The possible boundaries of an $\alpha_1 + Cu_3Al$ two phase field are also shown in this diagram.

The results of the electron microscopical examination of ternary iron - aluminium - copper alloys are summarised in Fig. 4:1, which indicates the most probable form of a vertical section through the ternary diagram at a constant copper content of 5 atomic %. The vertical section clearly shows the same general outlines as the binary diagram of Swann et al (Fig. 2:3) which was determined by the same technique. (Since both diagrams contain non - classical reactions, the normal phase rule conventions for equilibrium diagrams do not give a satisfactory test of the validity of phase equilibrium under these conditions).

4:4:2 The magnetic properties of iron - aluminium - copper alloys.

In evaluating the results of the magnetic analyses performed in this investigation it is necessary to consider several general factors concerning the way in which the measurements were made. The following comments are, thus, equally applicable to all the alloys studied. The magnetic balance measurements were made at a single constant heating / cooling rate of 15°C / min. This

rate of change of temperature was used to ensure that there was no inherent thermal hysteresis in the apparatus and hence that an accurate value of the Curie temperature was obtained. It was anticipated that under these conditions, certain microstructural changes would occur during heating and that these should be taken into account when correlating magnetic and structural data. This factor is of much greater importance in the vibrating sample magnetometer measurements due to the slower heating rate and the necessity to maintain the specimen at constant temperature for several minutes while each hysteresis loop was recorded.

A second measure which was necessary to ensure that accurate Curie temperates were obtained, was the use of high fields. The extrapolation technique used, illustrates that electronic order can be stabilized by an externally applied field, and the observations of Swann et al[6] indicate that the field can also affect phase equilibria and stability. Thus, the phase diagram, on which any anomalies in the continuous heating curves may be interpreted is expected to differ slightly from the equilibrium diagram, due to the influence of the field.

These two factors are not important in a single phase structure which does not undergo any phase transformations between room temperature and the Curie point and hence the data for the DO_3 structures presents no problems. When two or more phases are present, however, the situation is more complicated. In every case where it was possible to record a magnetization vs temperature curve, one or more Curie points were defined. In a multi - phase situation the exact composition of the phase associated

with the Curie point is uncertain, for the reasons mentioned above. In a binary system this difficulty may be resolved by using the tie line construction and the equilibrium phase diagram. This procedure is not applicable to the present case involving ternary alloys since, in general, the tie lines do not lie in the plane of the vertical section and insufficient information is available to construct the complete ternary diagram. The Curie points determined are therefore marked on the ternary vertical sections (Fig. 4:1 and 5:1) in positions corresponding to the overall alloy composition. Thus, although this representation is inadequate, it does illustrate the general magnetic state of the alloy or more correctly, of one particular constituent phase of the structure. The results of the magnetic measurements on iron - aluminium - copper alloys will now be discussed in the light of these observations.

The variation of saturation magnetic moment with composition, shown in Fig. 4:20, is similar in form to that for the binary iron aluminium alloys[81]. The curve is made up of three sections, the approximately linear disordered region, an anomalous region where structures with two ferromagnetic phases (α and α_1) are stable, and the more steeply falling part associated with the single phase ordered structures. The actual values of saturation magnetic moment per gram in the disordered region are uniformly approximately 9% lower than corresponding values for binary alloys. In the DO_3 ordered region, however, the σ_s value decreases much less sharply in the ternary system than in the case of binary

alloys. This is significant since it would appear that in iron - aluminium alloys with aluminium contents higher than 27 atomic %, if five percent of the iron is replaced by copper, the saturation magnetic moment is increased.

The curves showing the variation of σ_s with temperature for alloys 175C, 20C, 275C and 30C (see Fig. 4:21) are unambiguous and give the Curie temperatures indicated. When these results are plotted in Fig. 4:1, the dependance th Curie temperature on composition in the disordered and DO_3 regions is not significantly different from that in binary alloys. The copper addition, which replaces iron atoms in the DO_3 structure, results in a depression of the Curie temperature by 20°C to 25°C, which is as expected in view of the increased non-magnetic alloy content. By contrast, the copper addition in alloys 175C and 20C is mostly in the form of Cu_3Al. In these alloys the matrix no longer approximates to Fe_3Al and thus the precipitation of Cu_3Al depletes the matrix of aluminium. The extent of this depletion is approximately 1% and if this is taken into consideration when comparing the Curie temperatures in the binary and ternary disordered regions very close agreement is found.

Alloy 25C shows a Curie point at 603°C and a kink is observed in the σ_s vs temperature curve near the DO_3 critical temperature. The deviation marking the start of this anomaly occurs at 530°C, in Fig. 4:21, where curves were measured at 8,590 Oe. Extrapolation of the results for alloys 275C and 30C, suggests that alloy 25C should show a DO_3 Curie temperature at approximately 495°C. Under

the influence of the applied field of 8,950 Oe this Curie temperature would be elevated by 30°C to 40°C and thus appear as an anomaly at 530°C. It was not possible to perform the usual zero field extrapolation procedure on this particular feature since at higher fields the Curie temperature is further elevated to the temperature range in which the DO_3 to $L2_0$ transformation occurs. In view of the structural studies on this particular alloy and the general trend of results in the DO_3 region, it is concluded that the alloy 25C shows two Curie points, characteristic of the DO_3 and $L2_0$ structures at 495°C and 603°C respectively. Alloys 27.5C and 30C were heated through the DO_3 to $L2_0$ transition, as shown in Fig. 4:21 but the $L2_0$ phase at these compositions was not ferromagnetic.

It may be observed from Fig. 4:1 that the DO_3 phase in alloys 22.5C and 23C is ferromagnetic up to the DO_3 to $L2_0$ transition temperature, in contrast to the conditions in a binary system, (see Fig. 2:3). The σ_s vs temperature curves for these alloys are shown in Figs. 4:21 and 4:22 and it is observed that an irreversible reaction occurs during heating. This effect has been noted in the binary system[36] and is associated with the presence of α particles in a DO_3 matrix. To investigate this phenomenon in the ternary system, specimens of two alloys were heat-treated at 534°C for 24 hrs to develop the $\alpha + \alpha_1$ (DO_3) + Cu_3Al structure, shown in Fig. 4:17. Tests on these specimens indicated an increase in the degree of hysteresis between heating and cooling curves associated with the increased volume fraction and change in composition of the α phase. It was also found that the kink in the heating

curve for alloy 23C occurred at much lower magnetization value than that for alloy 225C. This reflects the difference in volume fraction of α between the two alloys.

The curve shown in Fig. 4:22c was recorded for a slowly cooled specimen of a binary iron-24·6 atomic % aluminium alloy and is included for the purpose of comparison. It can be seen that the anomaly, in this case, is more pronounced in the cooling curve than on heating, which is in contrast to the observations with the ternary alloys. The curves may be interpreted as follows. Initially, the microstructure of the binary alloy is $\alpha + \alpha_1$ (DO_3) whilst that of the ternary alloy is $\alpha + \alpha_1$ (DO_3) + Cu_3Al. In both cases the α phase is dissolved on heating and the fast cooling rate supresses its reformation. The difference between the binary and ternary curves is a result of a difference in the Curie point of the respective DO_3 phases. In the binary alloy a region exists, in the heating curve between the DO_3 Curie point, 508°C, and DO_3 critical temperature 547°C in which the structure consists of ferromagnetic α particles in a paramagnetic α_1 matrix. The coercivity in this temperature range has been found by Aptekar and Zusman[42] to reach a value of 90 Oe compared with approximately 1 Oe at room temperature.

In the case of the ternary alloys discussed, the α_1 (DO_3) phase remains ferromagnetic up to the transition to $L2_0$ order which occurs at 555°C. As the upper limit of the phase field is approached, however, the DO_3 phase is nearing its Curie point and hence is only weakly ferromagnetic when compared with the α phase. The coercivity of the alloy was found to show an increase in this region, as may be observed in Fig. 4:23, but the maximum value obtained was

only 5·5 Oe, indicating that considerable flux linkage between α particles, through the matrix, still existed. The peak did not reappear on fast cooling as large α particles were no longer present.

The magnetic curves discussed for alloys 225C and 25C show Curie points associated with the $L2_0$ phase of 618°C and 603°C respectively. These values indicate a marked stabilization of the ferromagnetic state in the $L2_0$ structure as compared with binary alloys, and result in the disappearance of the $\alpha + L2_0$ phase field. This feature, and the increase in room temperature magnetization of the DO_3 phase are the two most significant effects of the copper addition.

In considering the origin of these effects, consideration must be given to magnetic investigations carried out on the binary system. The anomalous magnetic properties measured in the region of Fe_3Al have been explained by Arrott and Sato[82] on the basis of a transition from ferromagnetism to antiferromagnetism with increasing aluminium content. This interpretation would predict a simple antiferromagnetic state for stoichiometric Fe Al and the existance of a mixed ferromagnetic - antiferromagnetic state near Fe_3Al. The theoretical treatment assumes a direct ferromagnetic exchange interaction between nearest neighbouring iron atoms and a 180° antiferromagnetic superexchange interaction between two iron atoms when separated by an aluminium atom. This model offers an explanation of the small temperature dependance of the magnetic susceptibility in Fe Al.

More recently, however, neutron diffraction studies by Nathans and Pickart[83] have failed to show any kind of magnetic ordering in Fe Al. In stoichiometric Fe_3Al they find that the moments of iron atoms on the constituent sub-lattices are different. Those on type I or type II sites

(see Fig. 2:1) have a moment of $1{\cdot}46 \pm 0{\cdot}1\mu_B$ whereas the value for type III sites is $2{\cdot}14 \pm 0{\cdot}1\mu_B$. These values provide evidence for the theory that the moment of an individual iron atom is dependant on the number of nearest neighbour aluminium atoms (n_{Al}). This value is $2{\cdot}2\mu_B$ when n_{Al} is small, decreases more rapidly to zero at $n_{Al} \leqslant 8$. These results are the basis of a treatment by Kouvel[84] which is capable of explaining the experimental observation[82] that, at any given composition, the magnetic moments of the phases follow the sequence

$$\sigma[\text{disordered}] > \sigma[Fe_3Al] > \sigma[FeAl]$$

i.e. the moment is not a montonic function of order.

In considering the effect of the copper addition several observations may be made. The structural observations have suggested that the copper atoms substiute on one of the iron sublattices. If the antiferromagnetic coupling suggested by Arrott and Sato exists it will be increasingly important at high aluminium contents and at room temperature or below. In such an alloy, if a Cu atom were to substitute for an iron atom on a type I or type II site in the DO_3 structure, then this will affect the antiferromagnetic coupling to a much greater extent that the competing ferromagnetic coupling. This could lead to a net increase in the room temperature magnetization and the effect would be more pronounced with increasing aluminium content, which is what has been observed.

As regards the second experimental observation, the elevation of the $L2_0$ Curie point, an explanation based on antiferromagnetic coupling is inapplicable in this case since the temperatures involved are so far above any

proposed Néel temperatures for these compositions. The Curie temperature of an alloy depends on the number of interactions between magnetic atoms as much as on the size of their moments. The copper atoms which substitute for iron in the $L2_0$ structure can do so in one of two positions (see Fig. 2:1). On a type I site (i.e. the sublattice which is wholly iron) the substitution would destroy, on average, four iron - iron and four iron - aluminium nearest neighbour bonds. Alternatively if the copper atom replaces an iron atom on the type II sublattice, eight iron - iron bonds would be broken. Obviously the replacement of a "$1{\cdot}46\mu_B$" iron atom on a type I site is therefore favoured if the Curie temperature is to be maintained. This substitution is also favoured by the affinity of copper and aluminium atoms, which could cause clustering of aluminium atoms on type II sites around each copper atom. The inhomogeneous distribution of aluminium atoms would enable iron atoms to form a greater number of iron - iron bonds and hence the Curie temperature would increase.

This explanation relies on the assertion by Kouvel[84] that the magnetic moment of an individual iron atom is dependent on the nearest neighbour site occupation. A simple power series expression for the μ_{Fe} vs n_{Al} dependence has been formulated for the binary alloys which gives reasonable agreement with experimental observations. This treatment is specific to aluminium atoms and thus does not give any information on the possible effect of an atom with a different electronic structure in solution.

It may be seen, therefore, that two conflicting physical models have been proposed to explain the magnetic

properties of binary iron - aluminium alloys. The neutron diffraction data of Nathans and Pickart[83] is interpreted by Kouvel[84] as evidence for the existance of intrinsic differences in the magnetic moment of an iron atom depending on it's environment. To Arrott and Sato[82], however the results indicate a basic difference in the average magnetization on each sublattice due to a variation in the degree of alignment of the individual identical magnetic moments. Both theories are useful in explaining particular aspects of the effect of a ternary addition of copper but neither is entirely satisfactory.

At the present time, it is not possible to give a more comprehensive account of the effect of copper additions on the magnetic properties of these alloys owing to the limited experimental data for the ternary system and the lack of a satisfactory explanation for many of the anomalous effects found in binary iron - aluminium alloys.

CHAPTER V

IRON - ALUMINIUM - TITANIUM ALLOYS - RESULTS AND DISCUSSION

In the preceding chapter the results obtained from a study of iron - aluminium alloys containing an addition of 5 atomic % copper have been outlined. An additional phase, not present in binary iron - aluminium alloys, was observed and identified as having a composition near Cu_3Al. Once the composition range over which this phase formed was established, the phase equilibria could be understood with reference to the similar conditions existing in the binary alloys. In general, then, it was found that, apart from differences concerning the complex interaction which gives rise to the $\alpha_m + \alpha_{2n}$ ($L2_0$) phase field in the binary alloys, the addition of 5 at % Cu leaves the general shape of the main phase fields largely unchanged. The position regarding iron - aluminium alloys containing 5 atomic % titanium is very different, as will be outlined in this chapter. It is possible to say, with certain reservations regarding the DO_3 structure, that no new phases were observed, but phase equilibria and stability are greatly affected by the addition.

5:1 Electron microscopy of iron - aluminium - titanium alloys.

The results of the electron microscopical investigation of these alloys are summarised in Fig. 5:1 comprising a vertical section through the iron - aluminium - titanium ternary diagram at a constant titanium content of 5 atomic %. Preliminary investigations with alloys 23T (Fe 23 at% Al 5 at% Ti) and 25T (Fe 25 at% Al 5 at% Ti) indicated that neither the $L2_0$ ordering transformation, nor the transformation

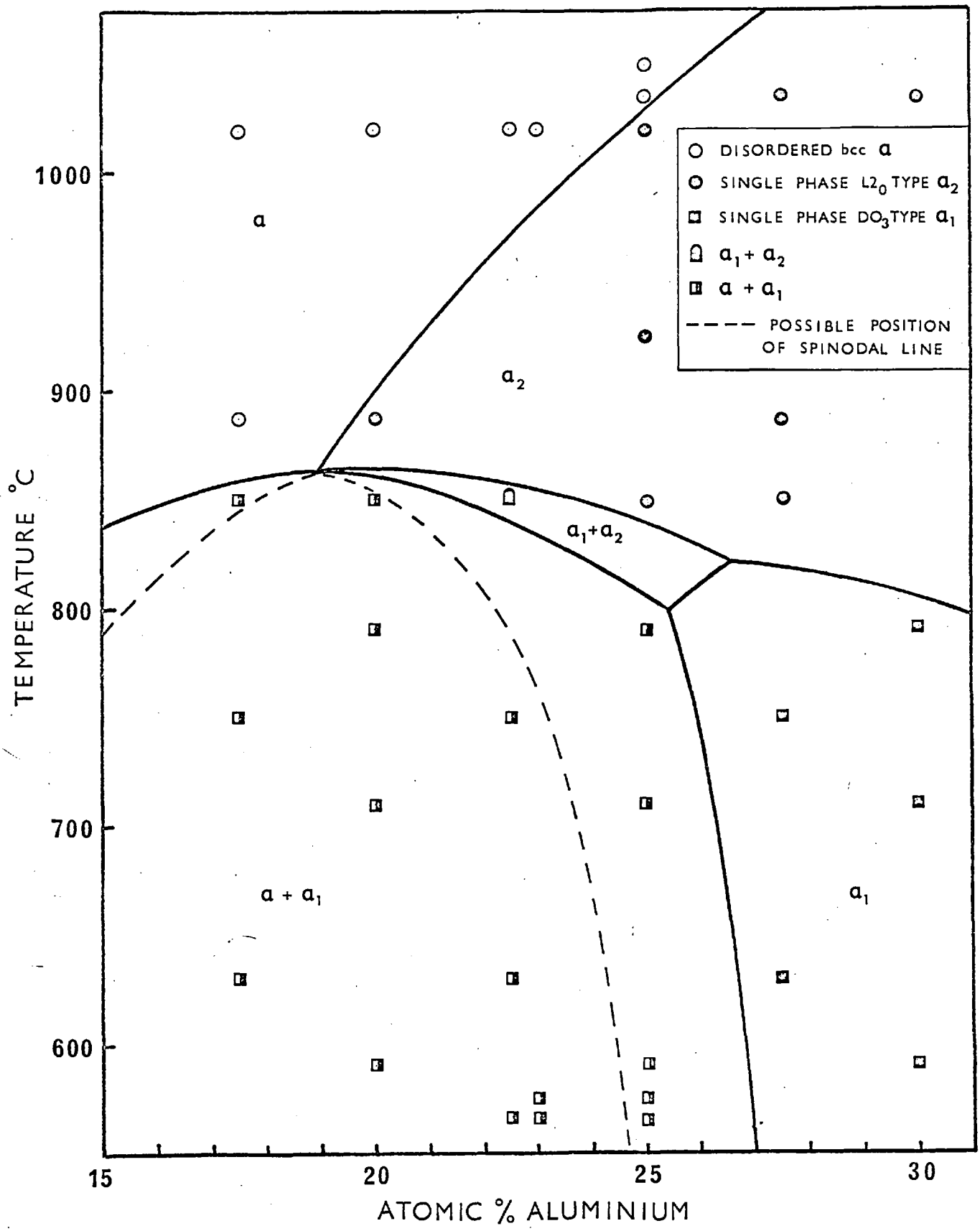

Fig 5:1 Vertical section of the Fe-Ti-Al ternary dia.at a constant Ti content of 5 atomic %

involving the formation of DO_3 type order could be suppressed on quenching from 1100°C, as shown in Fig. 5:2 (the diffracting conditions are described with reference to the DO_3 lattice parameter a').

5:1:1 The α_1 (DO_3) phase field.

The structures observed in alloys 275T and 30T quenced from temperatures below 800°C were similar and consisted of a single phase DO_3 domain structure exhibiting $\frac{1}{2}a'$ <100> APBs. The solution treatment temperature of 1035°C was found to be below the $L2_0$ critical temperature in both cases and hence the alloys had the fully ordered $L2_0$ structure before direct quenching to the ageing temperature. Consequently, no evidence of $\frac{1}{2}a$ <111> boundaries was found in the quenched specimens.

In an attempt to determine the upper limit of the α_1 phase field, specimens of alloy 275T were heat treated at 850°C, 751°C and 630°C for 1 hour. The DO_3 domain size was observed in the series of (111) dark field micrographs shown in Fig. 5:3. The domain structure in Fig. 5:3a was obviously formed on the quench and thus the ordering temperature must lie between 751°C and 850°C. (The mottled appearance of Fig. 5:3c was found to be due to a polishing effect, difficult to eliminate in these alloys.) The observation of a structure similar to that in Fig. 5:3b, in a specimen of alloy 30T quenched from 799°C, indicates that the critical temperature for this alloy is above 800°C. In view of this fact, the ordering temperature of alloy 275T is thought to be in the upper region of the temperature bracket determined i.e. above 800°C.

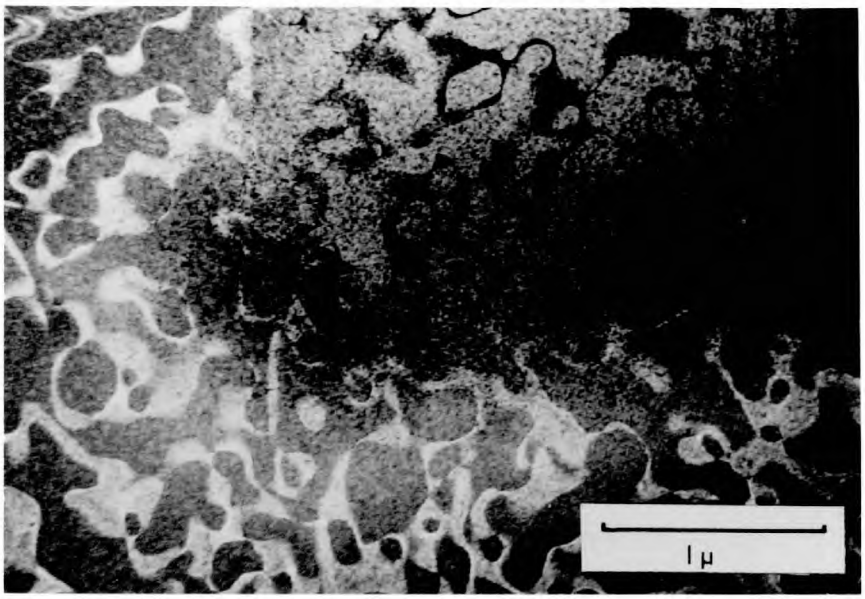

Fig.5:2a Dark field g = (222) DO_3.

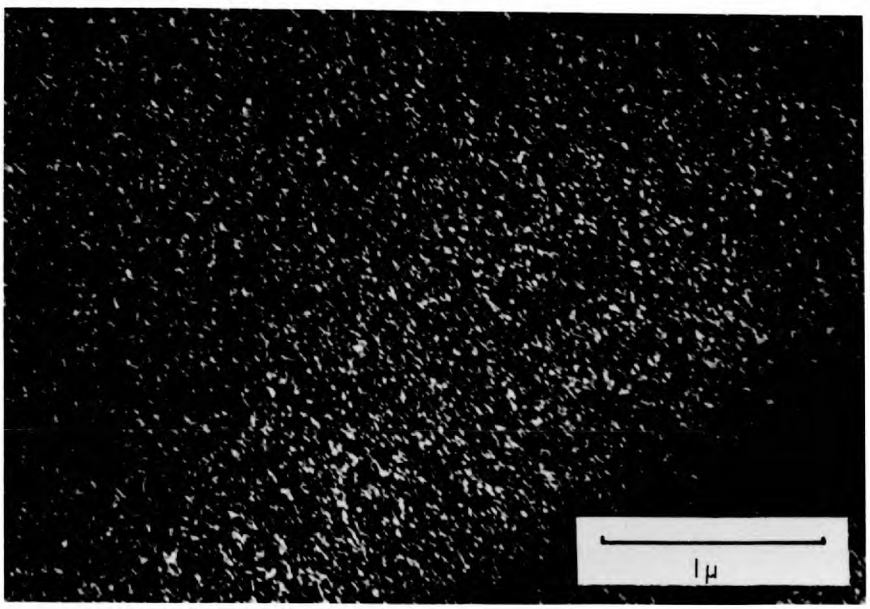

Fig.5:2b Dark field g = (111) DO_3.

FIGURE 5:2 ALLOY 25T 1100°C 1hr - W.Q. An illustration of $L2_0$ and DO_3 ordering formed during the quench.

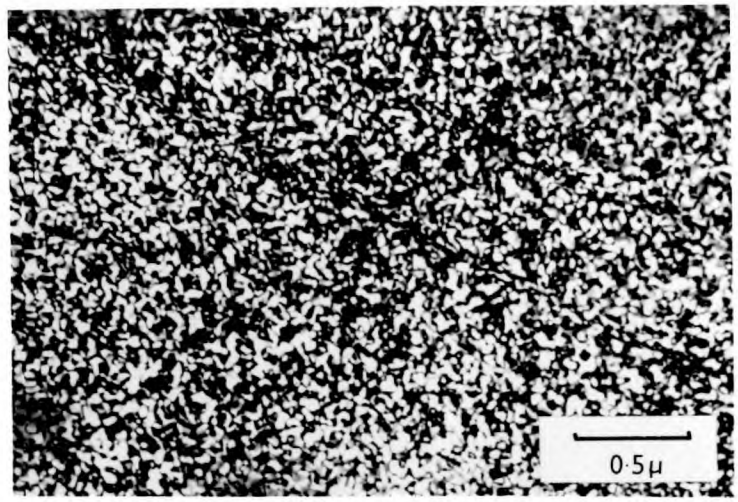

Fig.5:3a ALLOY 275T 1035°C 1hr - 850°C 1hr - W.Q. Specimen quenched from above DO_3 ordering temperature.

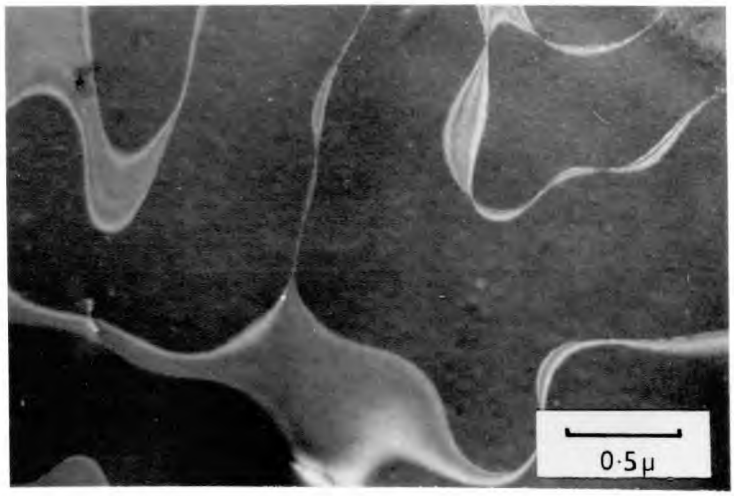

Fig.5:3b ALLOY 275T 1035°C 1hr - 751°C 1hr - W.Q. Specimen quenched from just below DO_3 ordering temperature.

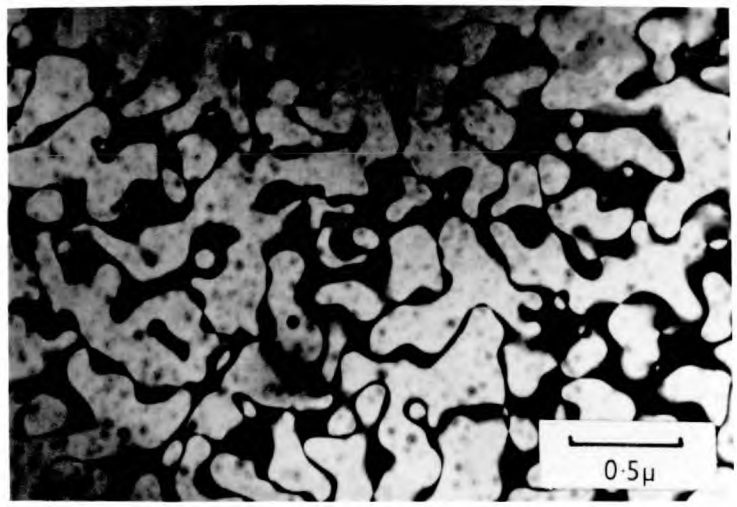

Fig.5:3c ALLOY 275T 1035°C 1hr - 630°C 1hr - W.Q. Specimen quenched from well below DO_3 ordering temperature.

Fig.5:3 The variation of DO_3 domain size with quenching temperature for alloy 275T. Dark field micrograph g = (111) DO_3 revealing $\frac{1}{2}a'$ ⟨100⟩ APBs.

For the purposes of comparison it should be noted that, according to Swann et al[3], a maximum occurs in the DO_3 ordering temperature for binary iron - aluminium alloys at 551·4°C and 26·5 at% Al This indicates the pronounced stabilizing effect that titanium has on the DO_3 ordered phase.

5:1:2 The $\alpha + \alpha_1$ (DO_3) phase field.

In view of the increased temperature range over which the DO_3 phase is stable, as a result of the titanium addition, it was anticipated that the associated ($\alpha + DO_3$) structures would be stable to correspondingly higher temperatures. This was found to be the case and such structures were found to exist over a considerable composition range.

A specimen of alloy 175T was quenched after 1 hour at 630°C and the phases present were identified as α and α_1 by electron diffraction. The structure has a fine uniform texture shown by the bright field micrograph Fig. 5:4a. A clearer indication of the distribution of phases present is given by the (200) DO_3 dark field micrograph Fig. 5:4b. The plane of the foil, here, has been indexed as (001) and the DO_3 particles appear to be aligned along cube directions. The particles themselves are observed to be of a very uniform size and exhibit a cubic cross section under these conditions. Heat treatment at a higher temperature for the same time produced the much coarsened structure shown in the (111) dark field micrograph, Fig. 5:5 (20T, 710°C, 1hr). The plane of the foil, in this case, is (123) and dark lines are seen in three directions in the foil, which have been indexed, as $[2\bar{1}0]$, $[30\bar{1}]$ and $[0\bar{3}2]$. These correspond to the

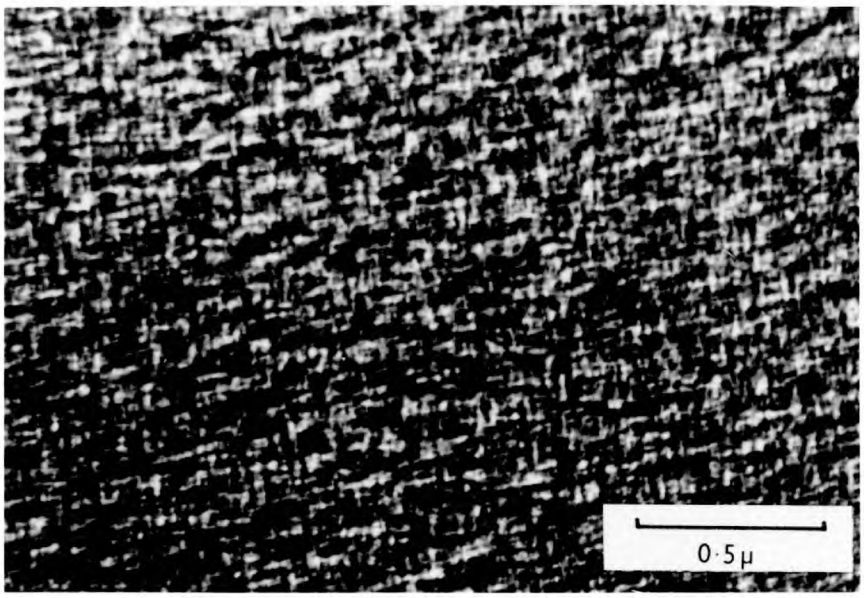

Fig.5:4a Bright field

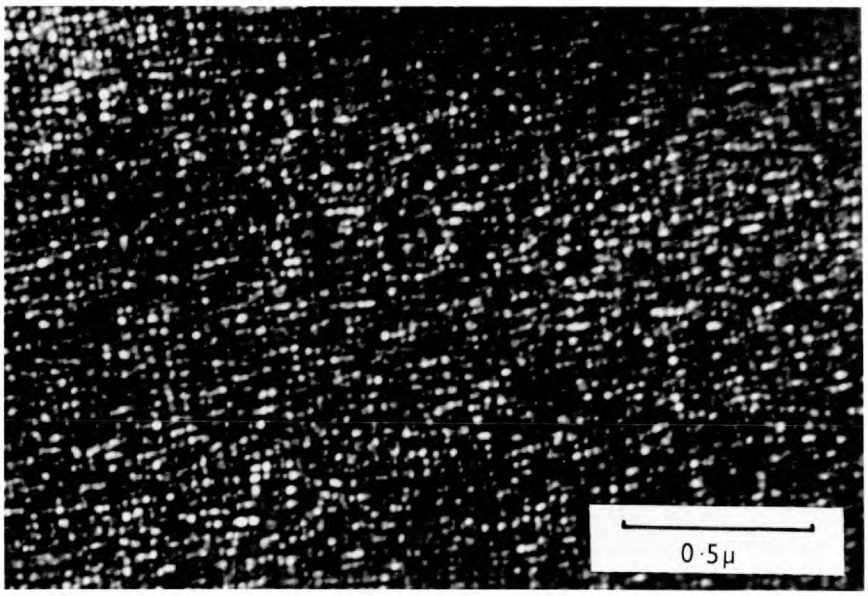

Fig.5:4b Dark field g = (200) DO_3.

FIGURE 5:4 ALLOY 175T 1020°C 1hr - 630°C 1hr - W.Q.
A fine uniform dispersion of aligned cubic α_1 (DO_3) particles in a disordered matrix.

FIGURE 5:5

Fig.5:5a ALLOY 20T 1020°C 1hr - 710°C 1hr - W.Q. Ordered DO_3 precipitates in a disordered matrix. The traces of cube planes and a particular $\{110\}$ plane are shown.

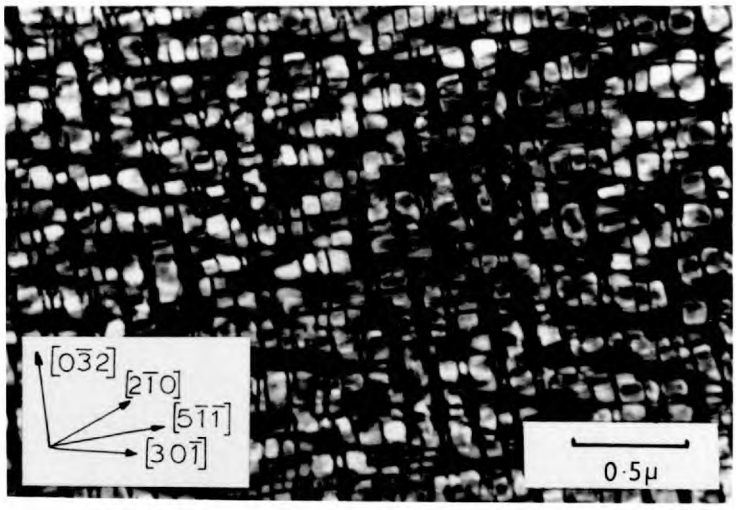

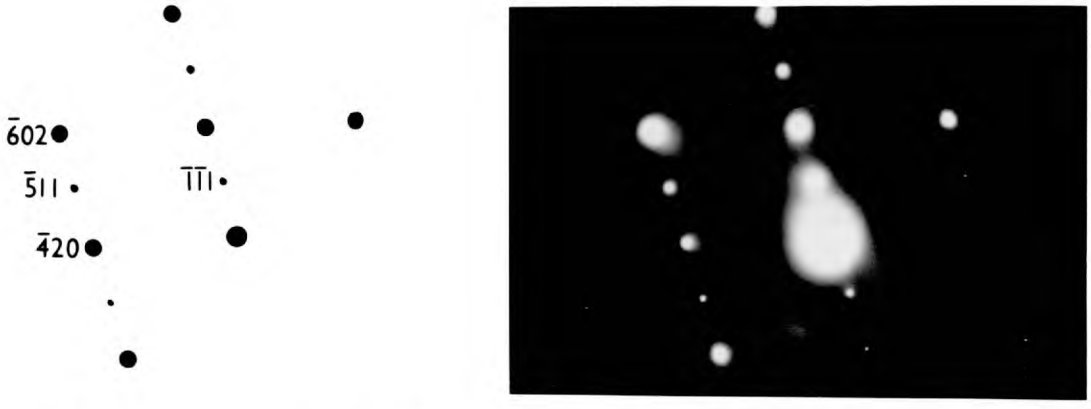

Fig.5:5b Selected area diffraction pattern of fig.5:5a and key.

Fig.5:5c As fig.5:5a but tilted slightly to show the two sets of preferential directions more clearly.

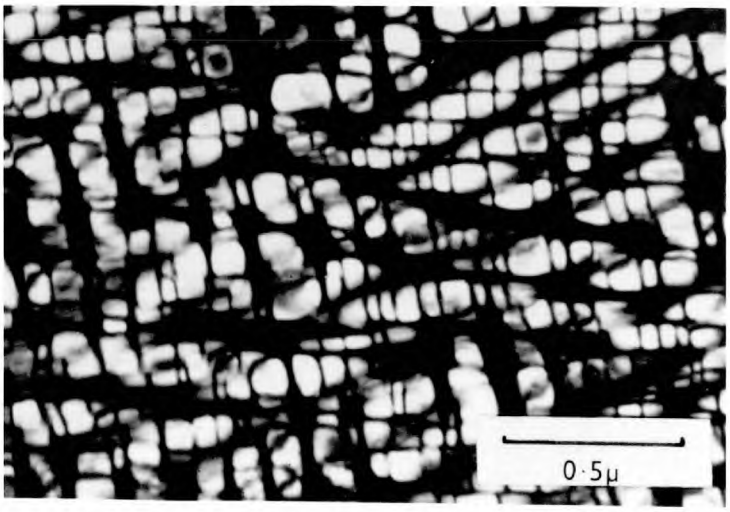

traces formed by the intersection of the (001) (0$\bar{1}$0) and ($\bar{1}$00) planes with the plane of the foil.

A second set of preferential directions between individual particles was observed in the micrograph, for example, parallel to the [5$\bar{1}\bar{1}$] direction. Trace analysis of these directions indicates that they are compatible with alignment of the inter - particle boundaries on {110} planes. The two sets of preferential direcrions are more clearly observed by tilting the specimen off the [123] zone axis about the [$\bar{1}\bar{1}$1]direction as shown in Fig. 5:5c. Under these conditions the alignment on {110} planes gives much sharper traces than that on {100} planes, as may be expected from calculations of the interplanar angles.

Similar micrographs were obtained from alloys 175T and 225T heat treated at corresponding temperatures, and trace analysis of these yielded results which were in agreement with the suggested preferred orientations. Further coarsening of the structure may be attained by heat treatment at higher temperatures as shown in the ($\bar{1}$11) dark field micrographs in Fig. 5:6. The diffraction pattern, Fig. 5:6b, is characteristic of both micrographs and indicates that the plane of the foil in both cases is (110). The precipitates again exhibit cubic morphology with their axes lying along <100> directions in the matrix, and are observed full size along the [00$\bar{1}$] direction and in projection along the [1$\bar{1}$0] direction. Closer examination of the particles in Fig. 5:6a (20T, 789°C, 1hr) indicates that many appear lenticular rather than truly rectangular. This may be attributed to the formation of {110} facets which would intersect the foil parallel to the [1$\bar{1}\bar{1}$] and [1$\bar{1}$1] directions indicated.

Fig.5:6a ALLOY 20T 1020°C 1hr - 789°C 1hr - W.Q. DO_3 particles aligned in cube directions, but showing a tendancy to form {110} facets.

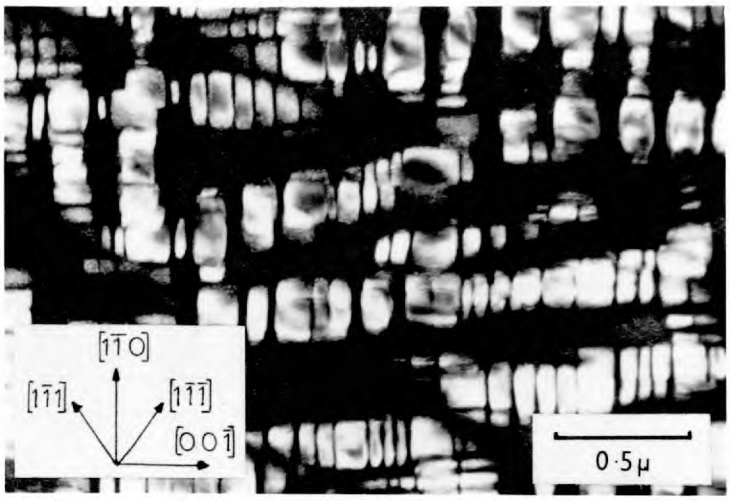

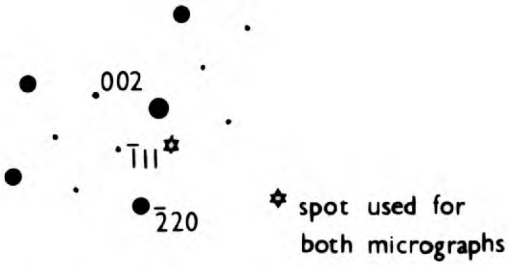

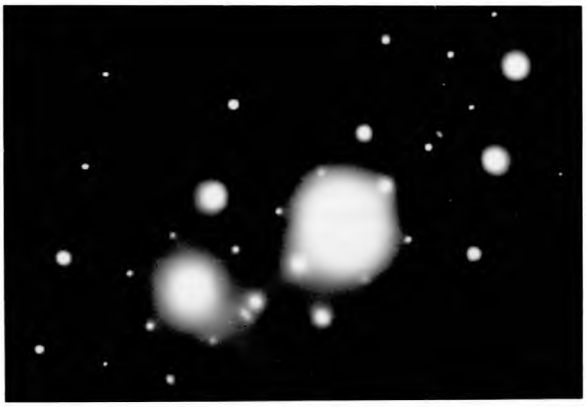

Fig.5:6b Selected area diffraction pattern and key, characteristic of figs.5:6a and 5:6c.

Fig.5:6c ALLOY 20T 1020°C 1hr - 850°C ½hr - W.Q. More pronounced {110} interphase boundaries.

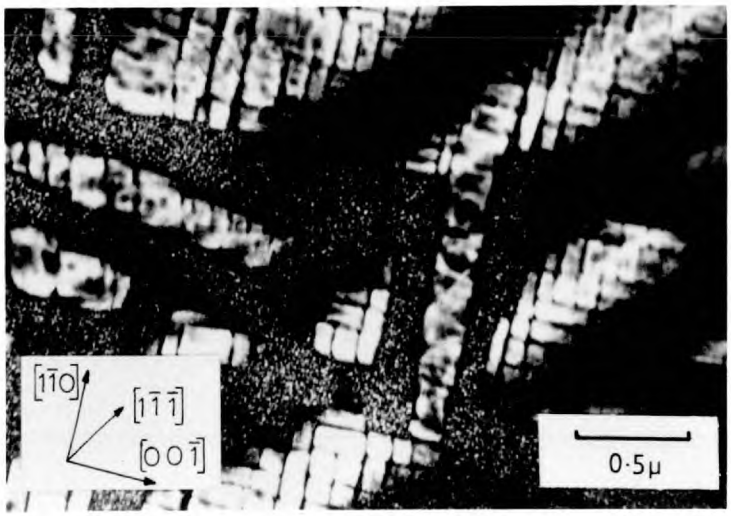

A more striking example of this preferential formation of {110} interphase boundaries is illustrated in a specimen of the same alloy quenched from 850°C after $\frac{1}{2}$ hour, (Fig. 5:6c). The boundaries between individual particles are the same as those described above, and again the lenticular shapes are observed, but lines of particles have formed parallel to the $[1\bar{1}\bar{1}]$ direction affording a {110} precipitate / matrix interface. The speckled appearance of the matrix in both of these micrographs is due to further decomposition to $\alpha + DO_3$, occurring on the quench. This is a result of the broadening of the phase field at temperatures below that used for the heat treatment, which necessitates a composition change, on cooling, of the phases initially present.

The structures described in the section so far have contained comparable amounts of the α and DO_3 phases and may therefore be considered characteristic of the centre of the phase field. The processes which lead to the formation of these structures will be considered in detail in section 5:4, but the conclusion of this assessment of the results may be expressed briefly as follows. It is suggested that initial decomposition of the high temperature solid solution occurs by a spinodal mechanism which gives rise to a composition modulation on {100} planes, as would be expected from the elastic anisotropy occurring in this type of alloy. As the structure coarsens, diffusion allows the phases to assume a configuration which minimises the interfacial energy, in this case, promoting the formation of {110} interfacial boundaries.

In view of the suggested mechanism it was anticipated that, in determining the boundaries of the $\alpha + DO_3$

phase field, the morphology of the structures would change as the spinodal line was crossed. This change, however, is not clearly defined since the nucleation barrier steadily decreases as the line is approached from out side the spinodal and reaches zero at the line itself. As the $\alpha + DO_3$ phase boundary is approached in alloy 175T, the structure assumes the appearance shown in Fig. 5:7a (175T, 850°C hour). The plane of the foil here is (310) and {100} planes give traces parallel to the [100] and [$\bar{1}$30] directions. Some of the particles exhibit facets parallel to [$\bar{1}$3$\bar{1}$] and [$\bar{1}$31] corresponding to the traces of {110} planes, and in the top left-hand corner of the micrograph some almost spherical particles are observed. The spherical particles were observed in other parts of the specimen, most noticeably in association with grain boundaries, although many of these had been polished away preferentially. This was considered evidence of heterogeneous nucleation.

The superlattice spots in the diffraction pattern Fig. 5:7b are much weaker than those observed at lower aging temperatures, which would suggest that the precipitate is only weakly ordered at this heat treatment temperature. This supposition is confirmed by the (200) DO_3 dark field micrograph, Fig. 5:7c, taken in a neighbouring grain, of slightly different orientation. A dark field micrograph taken with a (311) reflection was identical to that using the (200) reflection, indicating that there is no contribution from $L2_0$ ordering in this structure.

It was noted that at low temperatures the structures observed in alloys 175T and 20T were very similar. When treated for hour at 850°C, however, the structures observed in these two alloys are somewhat different, as may be seen

FIGURE 5:7

Fig.5:7a ALLOY 175T 1020°C 1hr - 850°C ½hr - W.Q. Bright field micrograph of specimen heat treated just inside $\alpha + \alpha_1$ (DO_3) phase field. (Traces of {100} and {110} planes are shown)

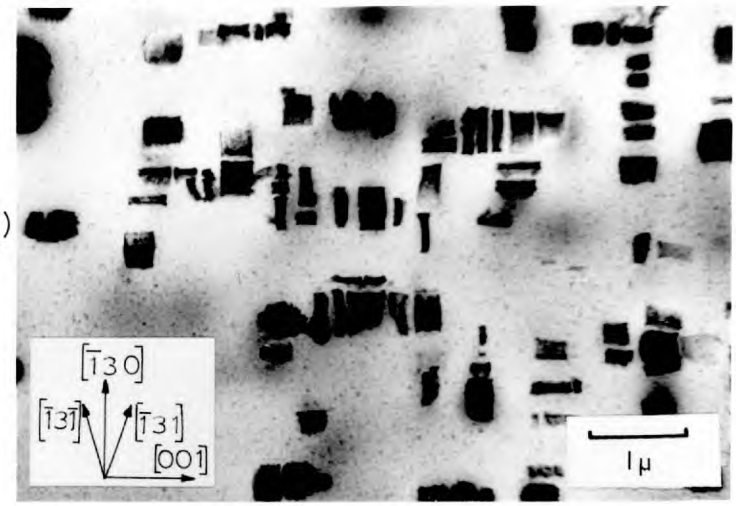

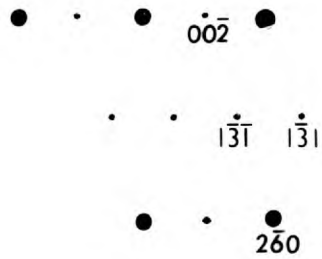

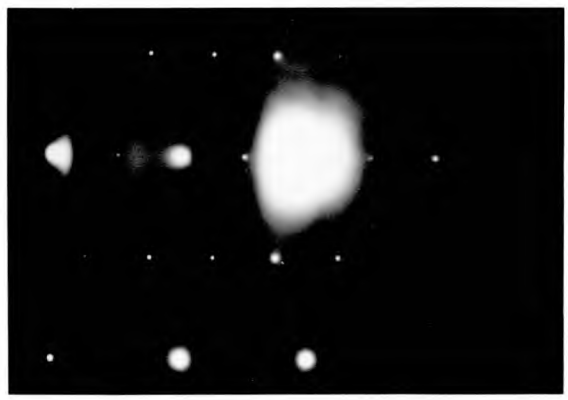

Fig.5:7b Selected area diffraction pattern of fig.5:7a showing weak superlattice spots.

Fig.5:7c Dark field g = (200) DO_3 of similar area to fig.5:7a. The precipitate is only partially ordered at this temperature.

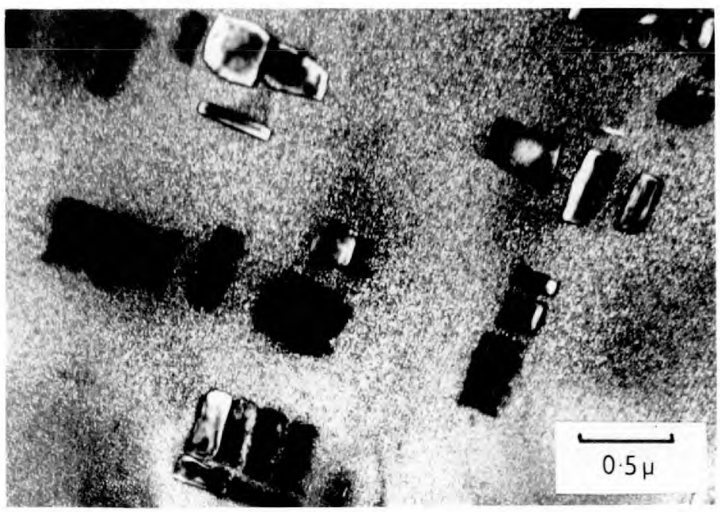

by comparison of Fig. 5:7c and Fig. 5:6c. The heterogeneous precipitation observed in 175T was not present in alloy 20T at this temperature, and the precipitate in the former occupied a smaller volume fraction and was more random. Specimens of both alloys were heat treated for 1 hour at 888°C and here a considerable difference was observed, as shown in Fig. 5:8. The heat treatment temperature was obviously above the $\alpha + DO_3$ phase boundary for both alloys, indicating that the boundary lies between 850°C and 888°C in both cases. A comparison of Figs 5:8a and 5:8c indicates the similarity of these micrographs. Both were taken with reflections characteristic of the DO_3 structure [(111) and (311) respectively] and they show a fine dispersion of ordered particles formed during the quench. This similarity is not observed between micrographs which reveal the $\frac{1}{2}a$ <111> boundaries characteristic of $L2_0$ ordering i.e. Figs. 5:8b and 5:8d. These were taken with reflections for which $(h + k + l)/2$ = odd integer when indexed in terms of the DO_3 lattice parameter [(222) and (200) respectively]. Examination of these structures shows that alloy 175T was in the disordered α phase field prior to quenching, whereas the presence of $\frac{1}{2}a$ <111> boundaries in alloy 20T at the temperature indicates that it is in the $L2_0$ (α_2) phase field. The decomposition on the quench has given the boundaries a diffuse appearance but their smoothly curving shape in many parts of the foil indicates that they were present at temperature, and not formed by dislocation motion on quenching.

The heat treatments outlined above have enabled the $\alpha + DO_3$ phase boundary to be located, at what is considered to be the approximate centre of the phase field. Consideration will now be given to the composition range over which this

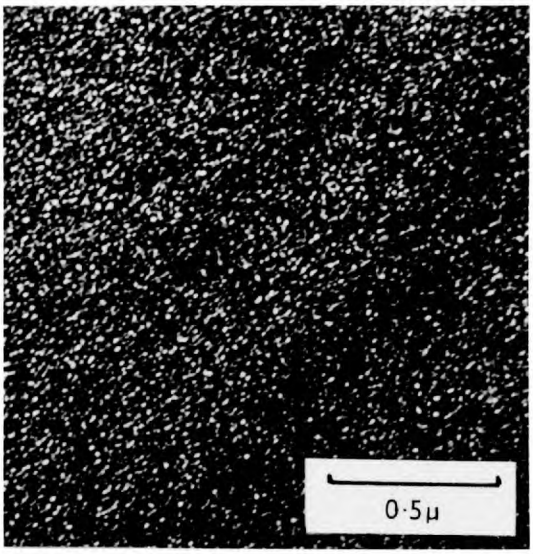

Fig.5:8a ALLOY 175T
Dark field g = (111) DO_3.

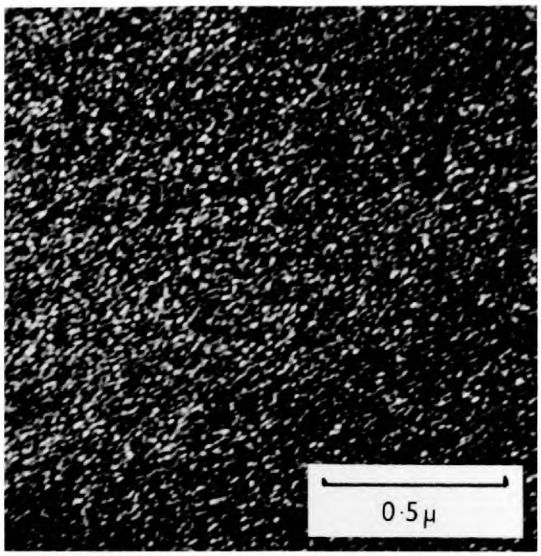

Fig.5:8b ALLOY 175T
Dark field g = (222) DO_3.

DO_3 ordering formed on the quench in both cases.

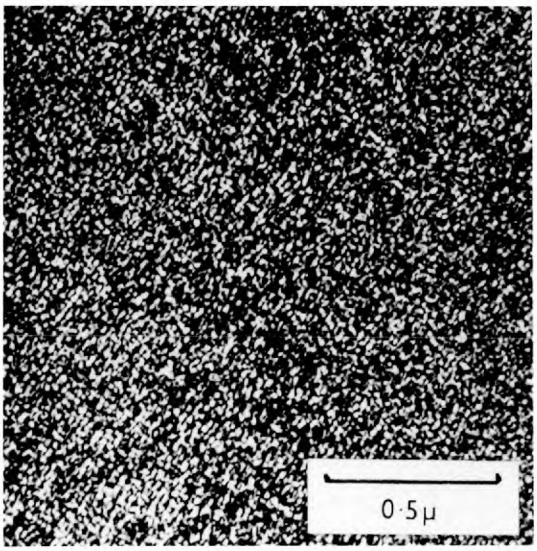

Fig.5:8c ALLOY 20T. Dark field g = (311) DO_3. DO_3 ordering formed on the quench.

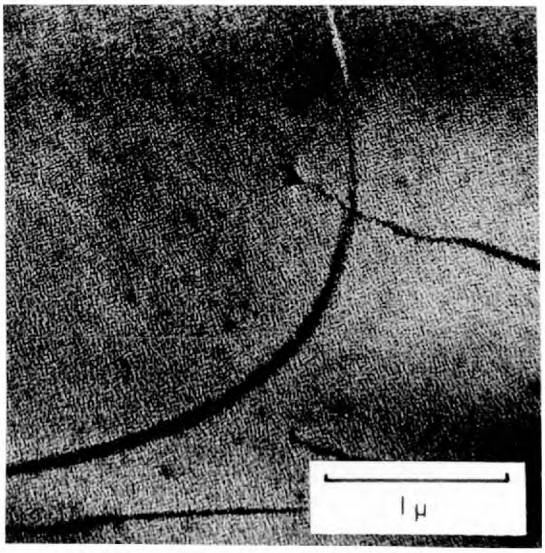

Fig.5:8d ALLOY 20T. Dark field g = (100) $L2_0$. Segments of $\frac{1}{2}a\langle 111\rangle$ APB characteristic of the $L2_0$ structure.

FIGURE 5:8 Heat treatment 1020°C 1hr - 888°C 1hr - W.Q.

two phase structure exists.

It was reported earlier that alloy 275T heat treated at 630°C exhibited the single phase DO_3 structure as shown in Fig. 5:3c and alloy 225T heat treated at 751°C showed a two phase structure which is thought to result from spinodal decomposition (similar to Fig. 5:5a.). The structures observed in an alloy of intermediate composition, 25T, indicate that this alloy lies inside the two phase field, fairly close to the boundary, at temperatures up to about 800°C. An example of this type of structure is shown in Figs. 5:9 and 5:10a (25T, 710°C 1 hour). Analysis of the diffraction pattern, Fig. 5:9b, reveals that the plane of the foil, in the bright field micrograph Fig. 5:9a, is $(\bar{1}13)$. This micrograph has a diffuse tweed-like texture with an orientation in which the $[0\bar{3}1]$ and $[\bar{3}0\bar{1}]$ directions are prominent. These correspond to the traces of the $(\bar{1}00)$ and (010) planes with the plane of the foil. The (111) dark field micrograph of this structure shows strong alignment of $\frac{1}{2}a'$ <100> boundaries on cube planes as evidenced by their correspondence with the $[30\bar{1}]$ and $[0\bar{3}2]$ directions, when the plane of the micrograph is (123), as in Fig. 5:9c. The boundaries, themselves, do not appear sharp which would indicate the presence of an associated disordered layer. This observation is confirmed by the features of the structure revealed by the (200) dark field Fig. 5:10a. The disordered α phase is observed in positions corresponding to the $\frac{1}{2}a'$ <100> antiphase boundaries and takes the form of plates aligned on cube planes. This morphology causes the $\frac{1}{4}a'$ <111> boundaries to also follow cube planes, as shown in Fig. 5:10a. These latter boundaries are related to the $\frac{1}{2}a$ <111> boundaries of the $L2_0$ structure

FIGURE 5:9

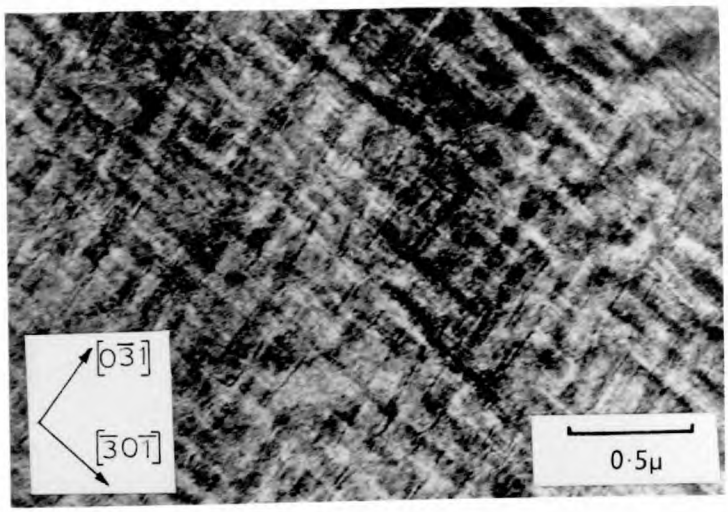

Fig.5:9a ALLOY 25T 1035°C 1hr - 710°C 1hr - W.Q. Bright field micrograph showing diffuse composition modulations following the traces of cube planes.

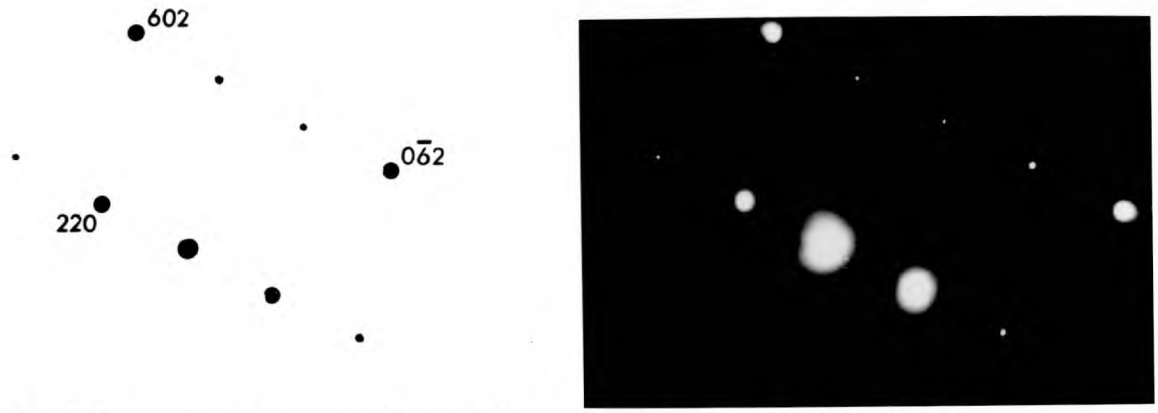

Fig.5:9b Selected area diffraction pattern of fig.5:9a and key.

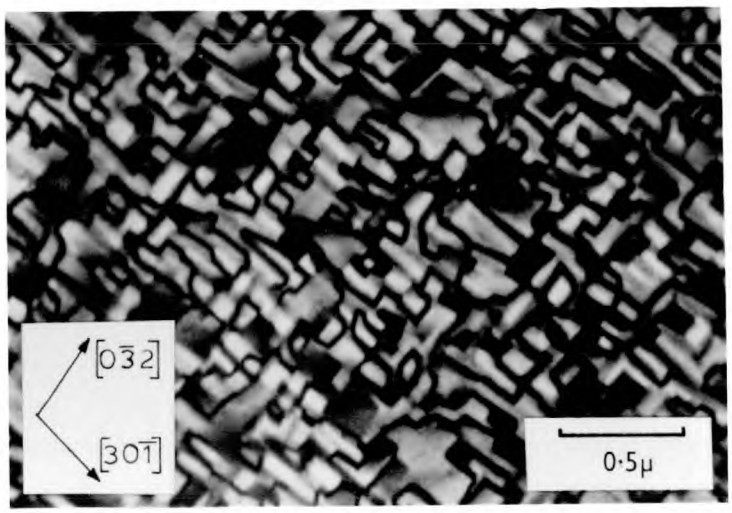

Fig.5:9c Dark field g= (111) DO_3 showing diffuse $\frac{1}{2}a'$ ⟨100⟩ APBs aligned on cube planes.

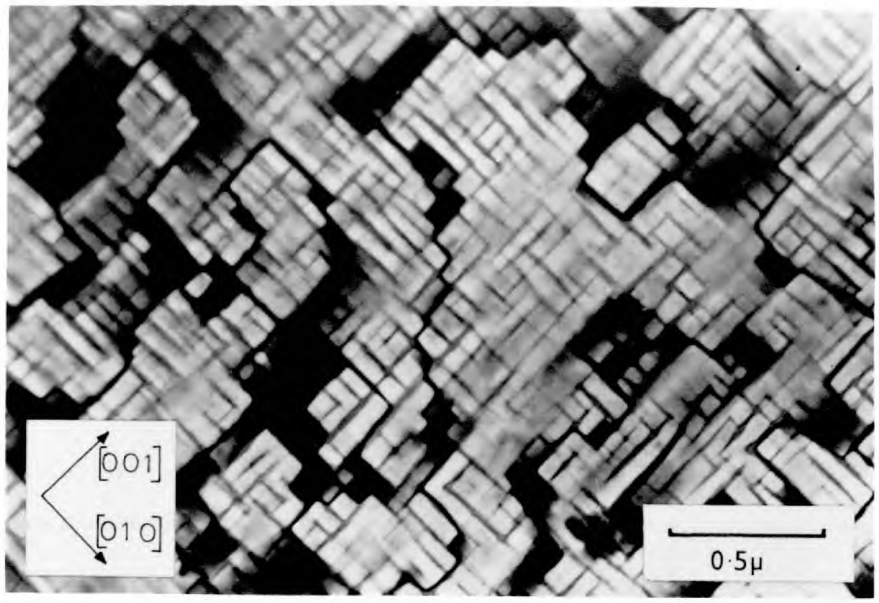

Fig.5:10a 1035°C 1hr - 710°C 1hr - W.Q.
Precipitation of the α phase which causes the
$\frac{1}{4}a'$ ⟨111⟩ APBs to follow cube planes.

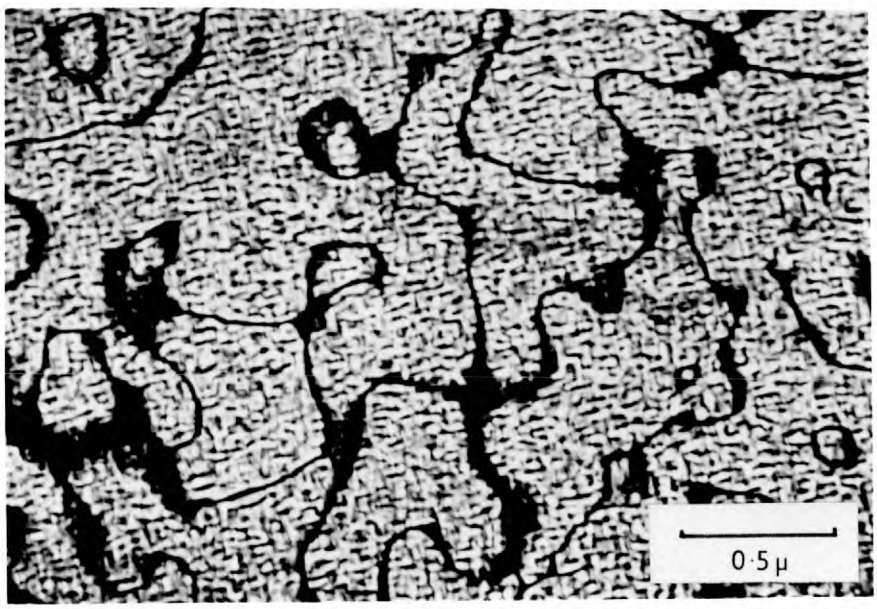

Fig. 5:10b 1035°C 1hr - 563°C 4hrs - W.Q.
The structural anisotropy observed in fig.5:10a is not so pronounced at this lower temperature.

FIGURE 5:10 Dark field g = (200) DO_3 micrographs of alloy 25T.

and indicate that the specimen, which was disordered at the solution treatment temperature of 1035°C, passed through the $L2_0$ phase field on the direct quench to the aging temperature.

The alingnment of $\frac{1}{4}a'$ <111> boundaries is not so pronounced in the second micrograph included here, Fig. 5:10b, which shows the structure after 4 hours at 563°C under similar diffracting conditions. It should be appreciated that both of these structures result from a certain degree of coarsening and thus speculation on the initial stages of decomposition is difficult. It would appear, however, that this morphology is not a result of spinodal decomposition but can be attributed to heterogeneous nucleation on antiphase domain boundaries. This would be compatible with the suggestion that, in this temperature range, these alloys lie inside the $\alpha + DO_3$ phase field, but outside the spinodal line. Two further examples of this type of structure, which are of interest, are shown in Fig. 5:11. The first micrograph is of alloy 25T after 1 hour at 591°C. The important feature here is the large spacing between $\frac{1}{4}a'$ <111> boundaries. This micrograph is not, in fact, typical of a structure in which very few of such boundaries were observed. The solution treatment temperature, in this case, was 1020°C and comparison with Fig. 5:10b, in which the solution treatment temperature was 1035°C, indicates that whilst the alloy at 1035°C is in the disordered α phase field, at 1020°C it is below the $L2_0$ ordering temperature.

A structure similar to that shown in Fig. 5:10b, but with a higher volume fraction of the α phase, was observed in alloy 225T after heat treatment for 1 hour at 630°C

FIGURE 5:11

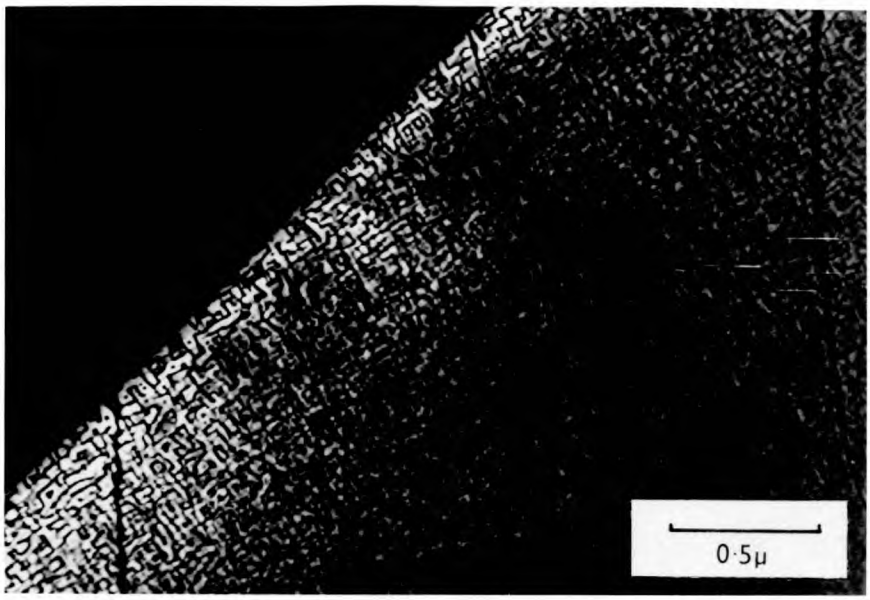

Fig.5:11a ALLOY 25T 1020°C 1hr - 591°C 1hr - W.Q. Dark field g = (200) DO_3. Segments of $\frac{1}{4}a'$ $\langle 111 \rangle$ APBs derived from the large initial $L2_0$ domain size at the solution treatment temperature.

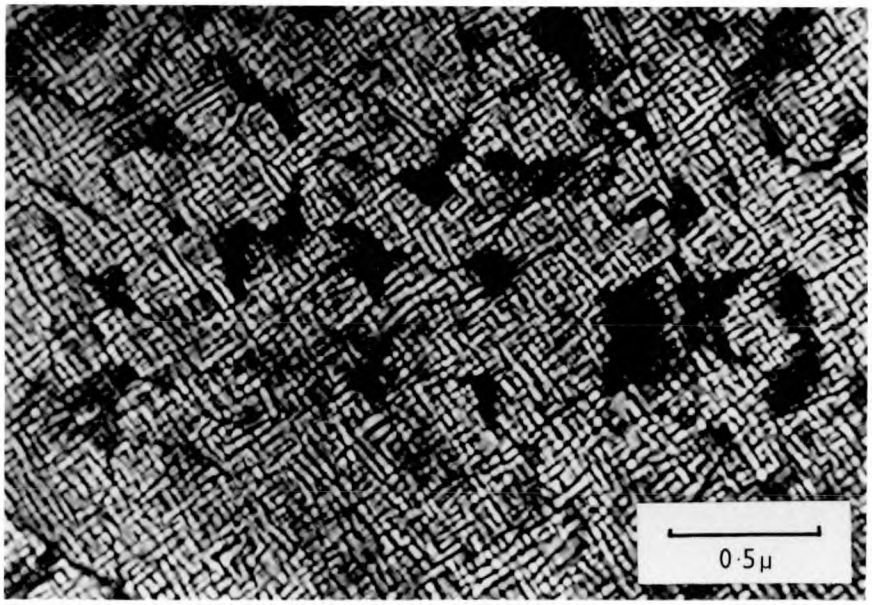

Fig.5:11b ALLOY 225T 1035°C 1hr - 630°C 1hr - W.Q. Dark field g = (200) DO_3. A structure similar to fig.5:10b but with a larger volume fraction of the disordered phase.

(Fig. 5:11b). The micrograph again shows evidence that the alloy was disordered at 1020°C and passed through the $L2_0$ phase field on direct quenching to the aging temperature. All these structures show a pronounced resistance to coarsening and in particular, increasing the aging time at 630°C (for alloy 25T) from 1 hour to 18 hours produced no visible change whatsoever in the structure.

The low volume fraction of α present in the micrographs of alloy 25T discussed so far indicates their close proximity in composition to the α + DO_3 boundary. At higher aging temperatures a coarser structure was formed as illustrated in Fig. 5:12. A higher temperature equivalent of the tweed - like structure, Fig. 5:9a, was observed at 789°C after 1 hour (Fig. 5:12a) and the associated dark field micrographs, from the upper grain, are also shown. The low magnification (111) image shows the alternate bands of α and DO_3 and a close examination of the former phase again indicates further decomposition on the quench, as a result of the broadening of the phase field, which has blurred the phase boundaries. These bands are found to be parallel to the $[10\bar{2}]$ and $[\bar{1}20]$ traces made by the $(0\bar{1}0)$ and $(00\bar{1})$ planes with the plane of the foil which is (211), as shown in Fig. 5:12b. A comparison of (111) and (222) dark field images showed that the $\frac{1}{4}a'$ <111> boundaries e.g. that running from A to B in Fig. 5:12c, followed cube planes only approximately whilst the $\frac{1}{2}a'$<100> APBs in each individual DO_3 band were more accurately aligned.

The observations made for this alloy (25T) at temperatures in excess of 789°C did not show an α + DO_3 structure formed at temperature, and taking into consideration

FIGURE 5:12

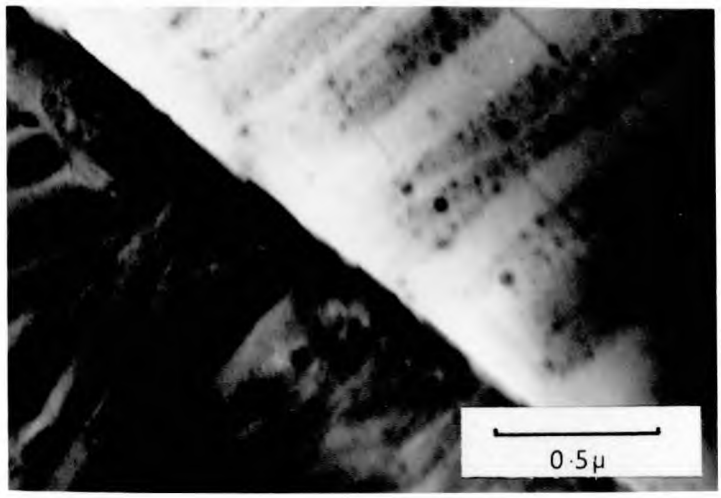

Fig.5:12a ALLOY 25T 1035°C 1hr - 789°C 1hr - W.Q. Bright field micrograph showing a coarse $\alpha + \alpha_1$ (DO_3) structure similar to fig.5:9a.

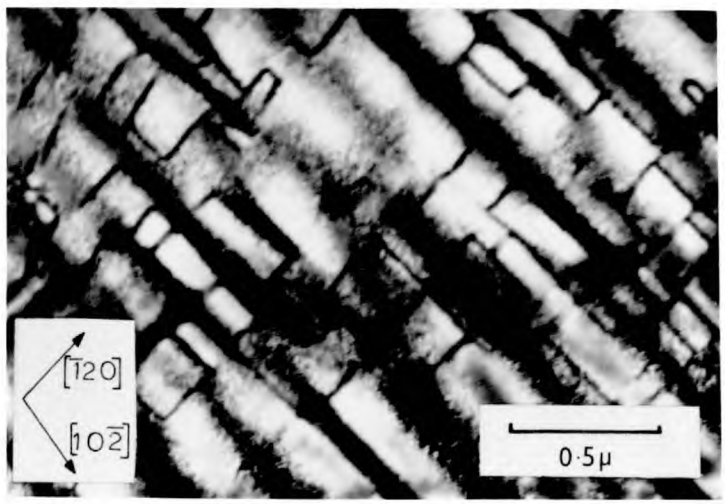

Fig.5:12b Dark field g = (111) DO_3 of upper grain in fig.5:12a showing alternate plates of α and α_1 (DO_3) aligned on cube planes.

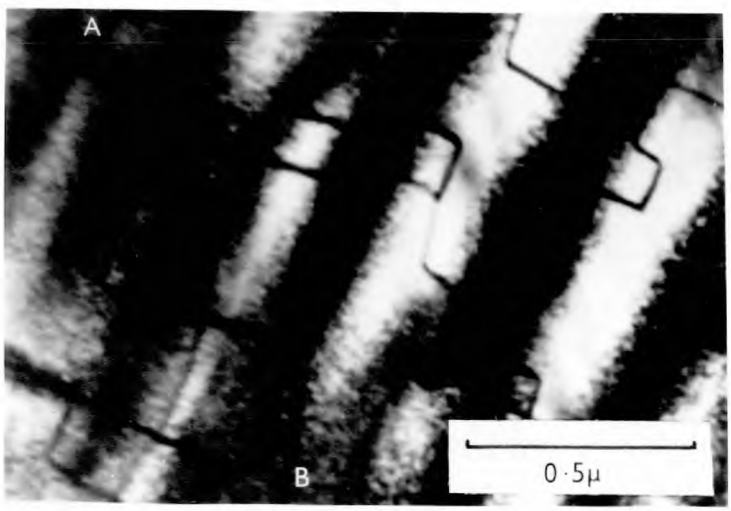

Fig.5:12c Dark field g = (111) DO_3. The $\frac{1}{2}a' \langle 100 \rangle$ APBs in each DO_3 plate are aligned on cube planes and a $\frac{1}{4}a' \langle 111 \rangle$ APB (from A to B) shows similar anisotropy.

all the results of this section the phase boundary was sketched in as shown in Fig. 5:1. A possible course for the spinodal line is also shown, although this is somewhat speculative.

5:1:3 The $L2_0$ phase field.

The evidence for the existence and extent of this phase field has, for the most part, been presented in the preceding two sections. The discontinuity in the $\frac{1}{2}a'$ <100> domain size shown in Fig. 5:3 suggests that the lower limit for the existence of single phase $L2_0$ ordering is in the region of 820°C for alloy 275T, and the upper limit is above 1035°C. In alloy 25T the upper limit was deduced to be between 1020°C and 1035°C by comparison of the spacing of $\frac{1}{4}a'$ <111> antiphase boundaries in specimens with these differing solution treatment temperatures (Figs. 5:10b and 5:11a).

To confirm this interpretation of the results a specimen alloy 25T was solution treated at 1035°C, rapidly transferred to 926°C for 1 hour, and water quenched. As anticipated the bright field image showed evidence of a very fine decomposition reaction, segments of $L2_0$ antiphase boundary of the $\frac{1}{2}a$ <111> type were seen in the (222) DO_3 dark field image, and a fine array of $\frac{1}{2}a'$ <100> APBs was revealed using a (111) reflection. These micrographs are shown in Figs. 5:13a, 5:13b, and 5:13c which has similar appearance to Fig. 5:3a.

Finally the evidence for the existance of $L2_0$ order in alloy 20T at 888°C (Fig. 5:8d) and not in alloy 175T at the same temperature (Fig. 5:8b) places a further restriction on the path of the variation of the $L2_0$

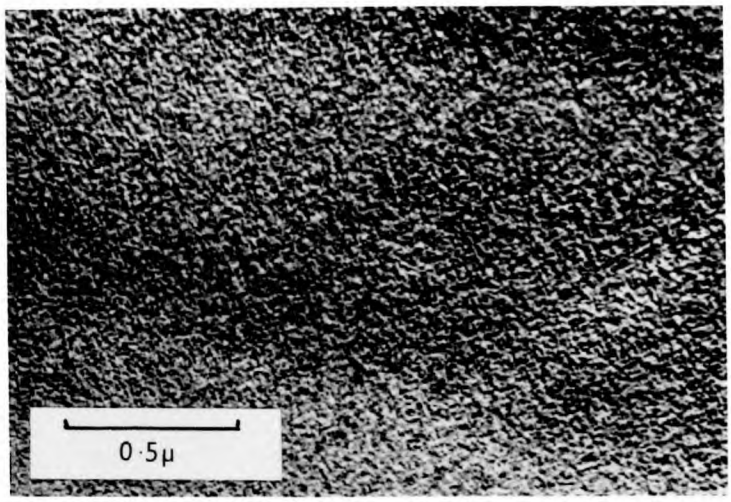

Fig.5:13a ALLOY 25T 1035°C 1hr - 926°C ½hr - W.Q. Bright field micrograph showing the fine decomposition reaction which occured during the quench.

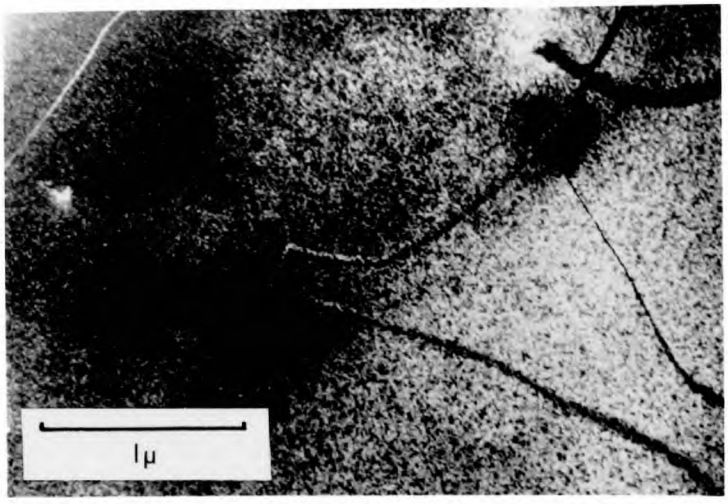

Fig.5:13b Dark field g = (222) DO_3 of fig.5:13a. Segments of the ½a ⟨111⟩ APBs of the $L2_0$ phase (formed at temperature).

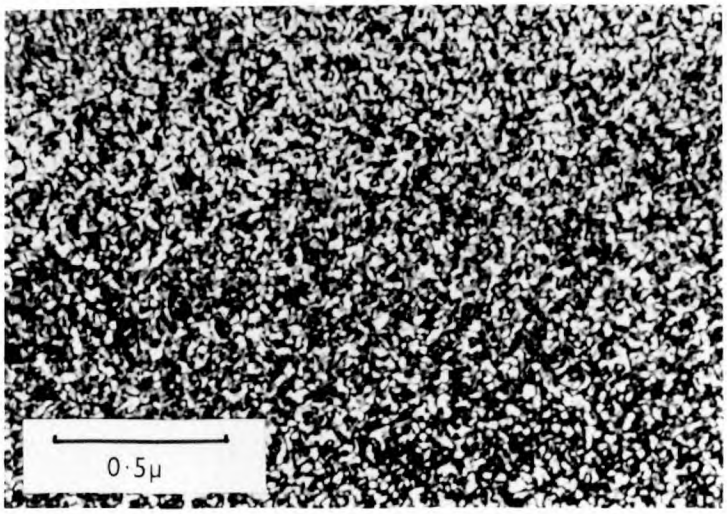

Fig.5:13c Dark field g = (111) DO_3. The fine background of fig.5:13b is observed to be due to the formation of DO_3 ordered regions on the quench.

critical temperature with composition, which would suggest that it follows the line shown in Fig. 5:1.

5:1:4 The transformation from $L2_0$ to $\alpha + DO_3$.

It is apparent, from the binary iron - aluminium diagram proposed by Swann et al, that the transformation from single phase $L2_0$ to $\alpha + DO_3$ does not occur as there is an intervening $\alpha + L2_0$ phase field. It is suggested that this two phase field is stable because of the interaction between $L2_0$ ordering and the magnetic transition. In iron - aluminium + 5 at% copper alloys this interaction is reduced, as outlined in section 4:4, but in the alloys containing titanium, such interaction is impossible because of the greatly differing temperatures at which the two processes occur (see section 5:2 on measurements of Curie points in these alloys.) There is, however, some evidence for an $L2_0 + DO_3$ phase field in these alloys, as will be described below.

A slice of alloy 225T was solution treated for 1 hour at 1020°C, rapidly transferred to 850°C for $\frac{1}{2}$ hour and subsequently water quenched. Several 2:3 mm discs were spark cut from this, as was normal, but contrary to any previous observations, slight structural differences were observed between discs from different parts of the slice, due to inhomogeneity in the composition. The two extreme cases observed are shown in the following pairs of (111) and (222) dark field micrographs, (indexed with respect to the DO_3 structure).

A uniform distribution of DO_3 plate like particles in a $L2_0$ matrix is seen in Fig. 5:14a and 5:14b. The plane of the foil in both cases is (211) and the plates are seen to lie parallel to the $[\bar{1}02]$ $[0\bar{1}1]$ and $[1\bar{2}0]$ directions, which

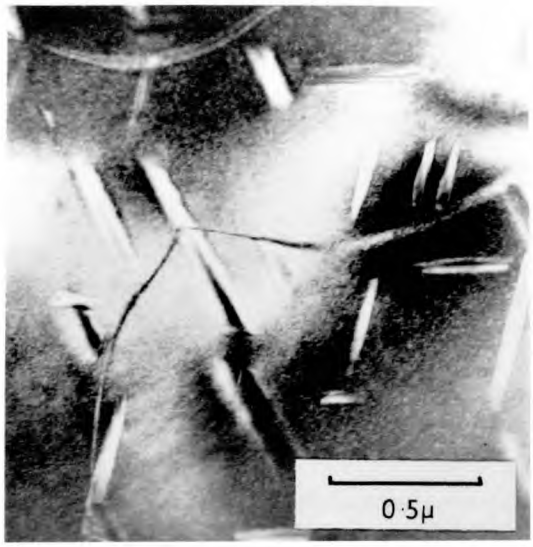

Fig.5:14a Dark field g = (222) DO_3. DO_3 precipitates in a matrix showing $\frac{1}{2}a$ ⟨111⟩ APBs of the $L2_0$ structure.

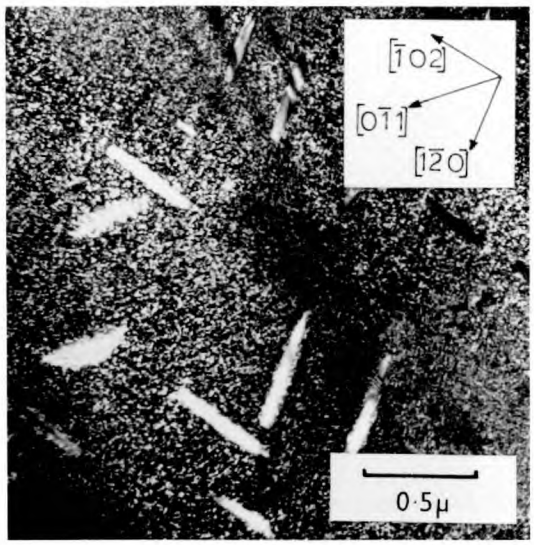

Fig.5:14b Dark field g = (111) DO_3. The fine background is formed on the quench. Traces of cube planes are shown.

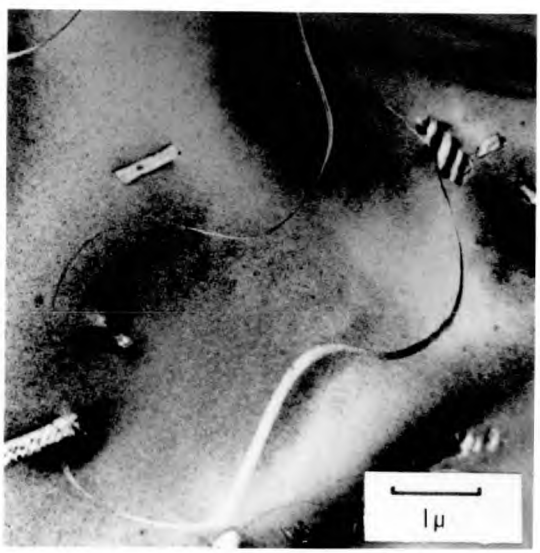

Fig.5:14c Dark field g = (222) DO_3. A region of more irregular precipitation.

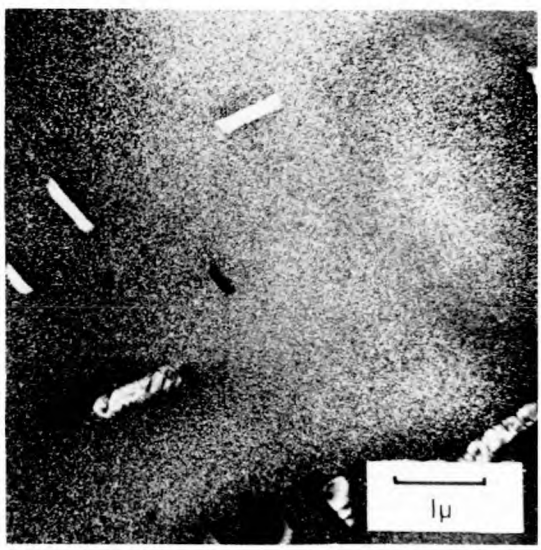

Fig.5:14d Dark field g = (111) DO_3 showing that some of the precipitates are sub-divided.

FIGURE 5:14 ALLOY 225T 1020°C 1hr - 850°C $\frac{1}{2}$hr - W.Q.
Examples of the $L2_0$ + DO_3 structures observed in this alloy.

correspond to the traces of {100} planes with the plane of the foil. These directions are indicated in Fig. 5:14b, and the variant parallel to the [0$\bar{1}$1] direction shows the broadest profile as may be expected from considerations of the interplanar angles involved. The background in this micrograph shows evidence of decomposition on the quench. Fig. 5:14a indicates that the matrix possessed the $L2_0$ ordered structure at the heat treatment temperature as deduced from the presence of $\frac{1}{2}$a <111> APBs.

The second type of structure, as shown in Figs. 5:14c and 5:14d, shows a more random distribution of DO_3 particles which are broader and contain some fine detail. The nature of this fine detail is clarified in the (111) dark field micrographs in Fig. 5:15 and in both cases the traces of {100} planes are indicated, as in Fig. 5:14b. These larger particles are seen to be fragmented, consisting of a group of smaller precipitates seperated by {100} interphase boundaries. These boundaries may arise from broadening of existing $\frac{1}{2}$a' <100> antiphase boundaries, which are unstable in a two phase situation, as will be discussed in section 5:4. This would imply that the morphology results from a cluster of individual nuclei forming in this particular part of the specimen. An alternative suggestion is that, whilst the particles grow on elastically soft {100} planes, they must induce some internal strain, which may be relieved by the formation of 'disordered' bands on planes with low interfacial energy. These bands are 'disordered' with respect to the DO_3 order in the precipitate, but possess the $L2_0$ order of the matrix. The validity of these two proposals will be considered in section 5:4.

A further feature of these micrographs is that decomposition of the matrix, on quenching, has occurred to

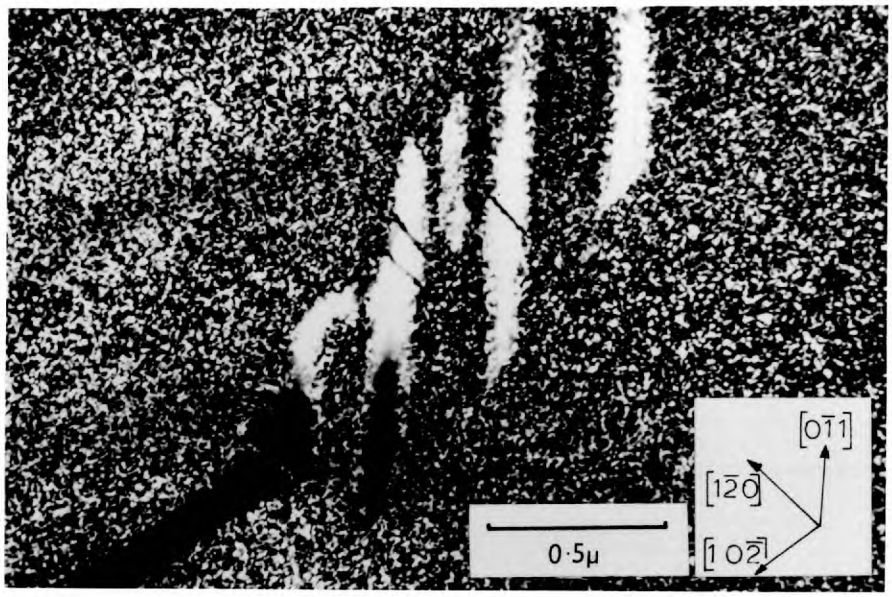

Fig.5:15a

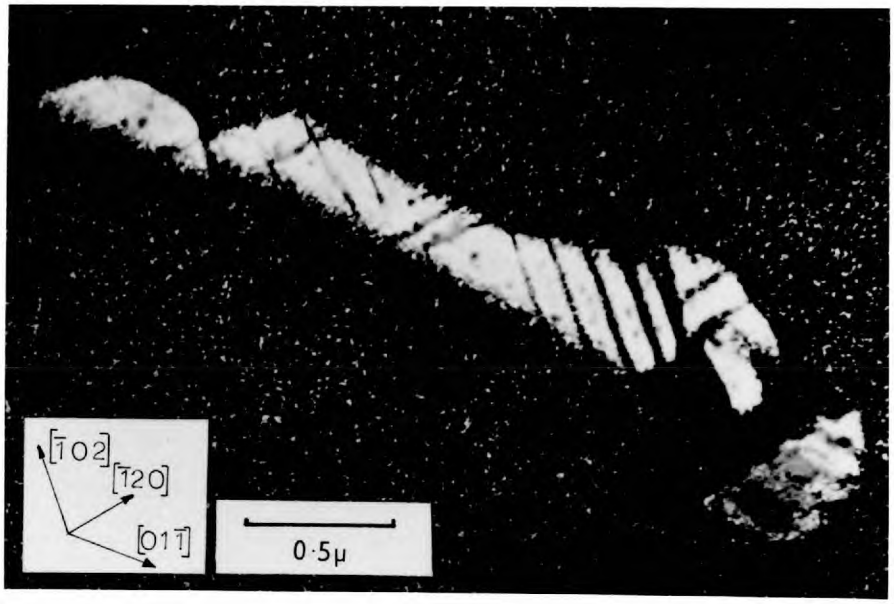

Fig.5:15b

FIGURE 5:15 A high magnification view of individual precipitates from an area similar to that shown in figs.5:14c and 5:14d. Dark field g = (111) DO_3. Traces of cube planes are shown.

a lesser extent close to the large particles, indicating a composition gradient in the matrix. This emphasizes the composition difference between the precipitate and matrix which is a significant factor in accounting for the stability of these two phase structures.

In general, phase equilibria suggested by the form of the vertical section through the iron - aluminium - titanium system (Fig. 5:1) are derived from the normal ternary peritectoid reaction. If the two phase fields 'normally' present between the α and $L2_0$ phases, and the $L2_0$ and DO_3 phases are collapsed to a single line, characteristic of a second order reaction, then the original ternary peritectoid assumes the form shown in Fig. 5:1 (for expansion of this point see section 5:4).

5:2 Results of magnetic balance measurements on alloys containing titanium.

These measurements were carried out with specimens which had been air cooled in silica capsules from the homogenization temperature of 1200°C. The results were standardised with respect to a specimen of the iron used in the preparation of the alloys and the procedure was exactly as described in section 4:2. Initial tests at room temperature gave the σ_s values for each alloy composition shown in Fig. 5:16 and these results are shown in graphical form in Fig. 5:17. A discontinuity is observed between 22·5%Al and 25%Al and comparison with Fig. 5:1 indicates that below this discontinuity the structure is $\alpha + \alpha_1$ (DO_3) whilst at higher aluminium contents the single phase α_1 structure is stable.

The Curie point determination was similar to that described for iron - aluminium - copper alloys in section 4:2 and the curves measured using an applied field of 8,590 Oe are shown in Fig. 5:18. The elevation of the Curie point produced by the applied magnetic field is more pronounced in these alloys containing titanium, as shown in Fig. 5:18.

The variation of the saturation magnetic moment per gram with temperature for alloys 175T and 20T is smoothly curving and unambigous. The Curie point indicated is associated with the disordered α phase and the curve was reproduceable on cooling at 15°C/min. The curves for alloys 225T and 25T shown in Fig. 5:18, do not have the same continuously curving nature, characteristic of a single ferromagnetic phase. Both curves show a change in the sense of curvature at relatively low temperatures (about

ALLOY	CURIE TEMP. (all values ± 3°C unless otherwise stated)	MAGNETIZATION VALUES AT 20°C	
		$\frac{\sigma_s(\text{alloy})}{\sigma_s(\text{Fe standard})}$	σ_s(alloy) emu/gm [σ_s(Fe)=217·75 emu/gm]
175T	711°C	·6518	141·9
20T	680°C	·5682	123·7
225T	664°C 140 ± 5°C	·4835	105·1
25T	656°C 316 ± 5°C	·4420	96·1
275T	181°C	·2068	45·0
30T	<20°C	-	-

Fig. 5:16 Curie temperatures and saturation magnetic moments per unit mass for the iron-aluminium-titanium alloys studied.

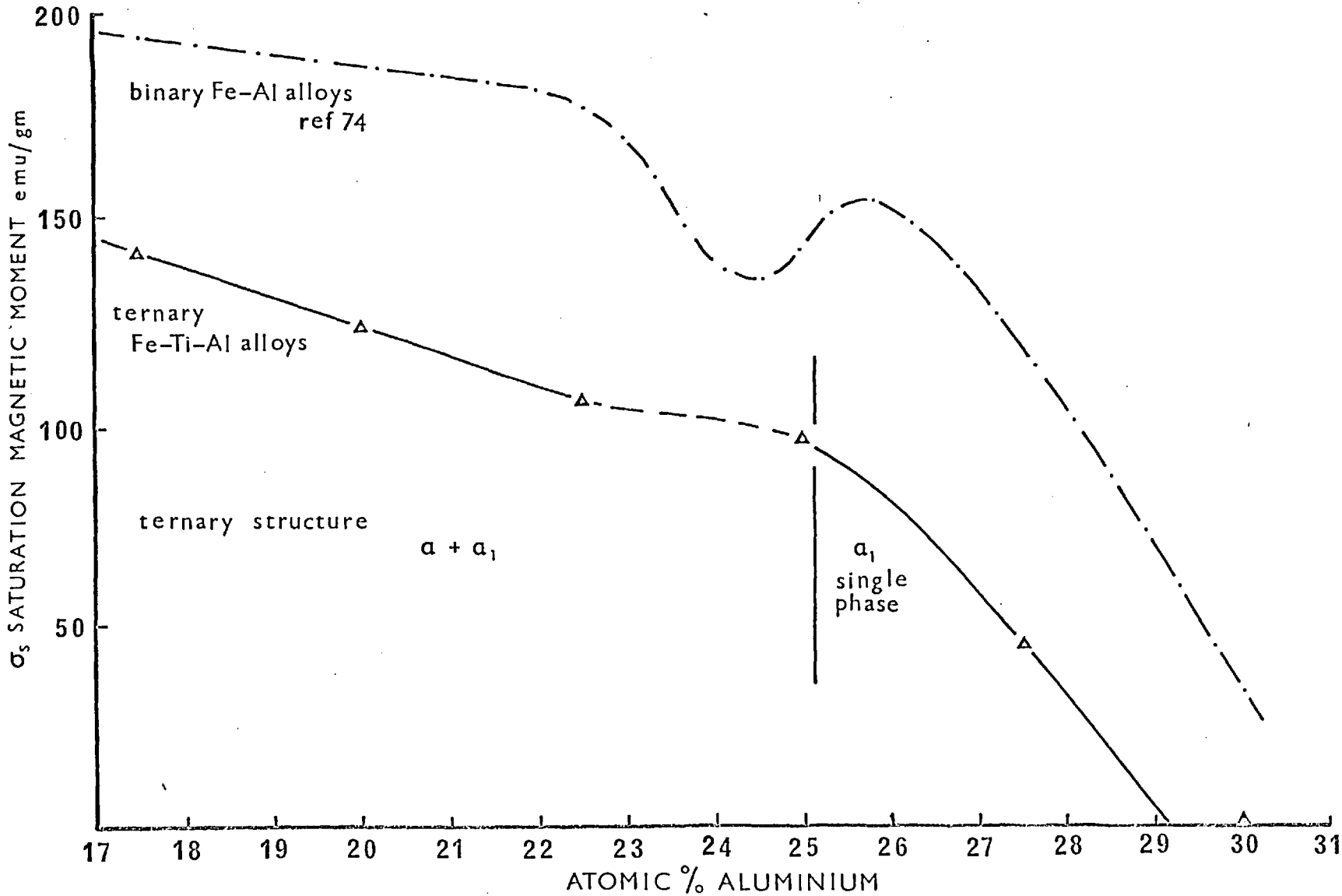

Fig 5:17 The variation of σ_s with composition for alloys containing titanium

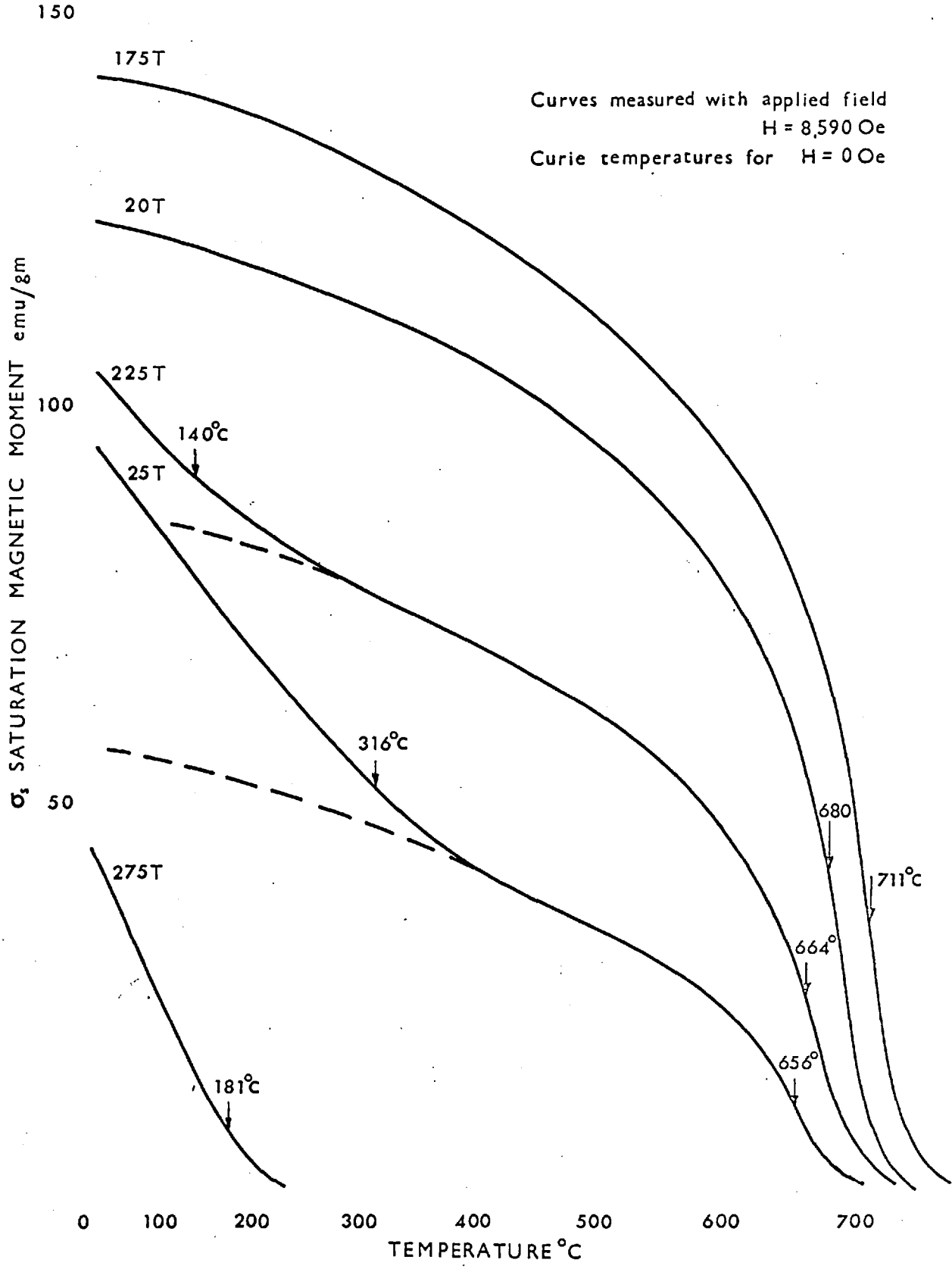

Fig 5:18 The variation of σ_s with temperature for alloys containing titanium

100°C to 200°C in the case of alloy 225T and 250°C to 350°C for alloy 25T) and the curve is considered to show evidence of two ferromagnetic phases with different Curie points. At low temperatures, therefore, the measured curve shows superimposed magnetization variations with temperature for the two phases. In order to seperate the contribution of each phase,the high temperature part of the curve was extrapolated back to room temperature to give a curve of the same general shape as that shown by alloys 175T and 20T (see Fig. 5:18). The low temperature part of the measured curve, in excess of the extrapolated line, was then replotted and the technique described in Appendix B used to determine the Curie point. The two results obtained by this technique, involving an extra extrapolation, are less accurate than those in which a single ferromagnetic phase is indicated, and hence the experimental error is assessed at $\pm$5°C. The determination of the upper Curie points of alloys 225T and 25T was not affected by these low temperature considerations.

Alloy 275T showed a single Curie point at 181°C $\pm$ 3°C and the magnetization fell sharply between room temperature and this point. Alloy 30T was not ferromagnetic at room temperature. No measurable thermal hysteresis was observed for any of these alloys containing titanium at the heating/cooling rate of 15°C/min used in the investigation.

5:3 Results of vibrating sample magnetometer measurements on alloys containing titanium

The magnetic properties of the alloys which showed two Curie points i.e. 225T and 25T, were investigated with particular regard to the relationship between the saturation

magnetic moment per gram (σ_s) and the coercivity (H_c). The discrepancy between σ_s values from the magnetometer and magnetic balance was again of the order of 4%, in confirmation of the proposal, expressed in section 4:3, that the σ_s value for the iron standard, used in magnetic balance measurements, was nearer 208 emu/gm than the pure iron value of 217·75 emu/gm.

The values of σ_s and H_c taken from a series of hysteresis loops, measured at temperatures between 19°C and 635°C for alloy 225T are shown in Fig. 5:19. It is observed that there is a maximum in the coercivity curve in the vicinity of the lower Curie point of the two phase structure, which was found to be 140°C $\pm$ 5°C. The actual value of this maximum from Fig. 5:19 is 120 Oe $\pm$ 1 Oe, which was recorded at 159°C, and from this point the coercivity decreases, in a similar manner to the σ_s value, to below 20 Oe as the upper Curie point is approached. These curves were determined during initial heating of the specimen.

A similar relationship between σ_s and H_c was found for alloy 25T as shown in Fig. 5:20. The curves shown are for both initial heating, and cooling after holding for 1hr at 700°C. In the σ_s curve for initial heating, the position of the lower Curie point, at 316°C, is well defined and the value of σ_s at this point is only 40% of the initial value at room temperature. This would indicate a much larger proportion of the phase with the lower Curie point (α_1) than in alloy 225T. This may be attributed to the relative positions of the two alloys in the phase diagram, Fig. 5:1. The coercivity of alloy 25T, on initial heating, rises from 74 Oe $\pm$ 1 Oe at room temperature to 191 Oe $\pm$ 1 Oe at 341°C and then falls smoothly to 107 Oe $\pm$ 1 Oe at 557°C. The exact position of the maximum of this curve is

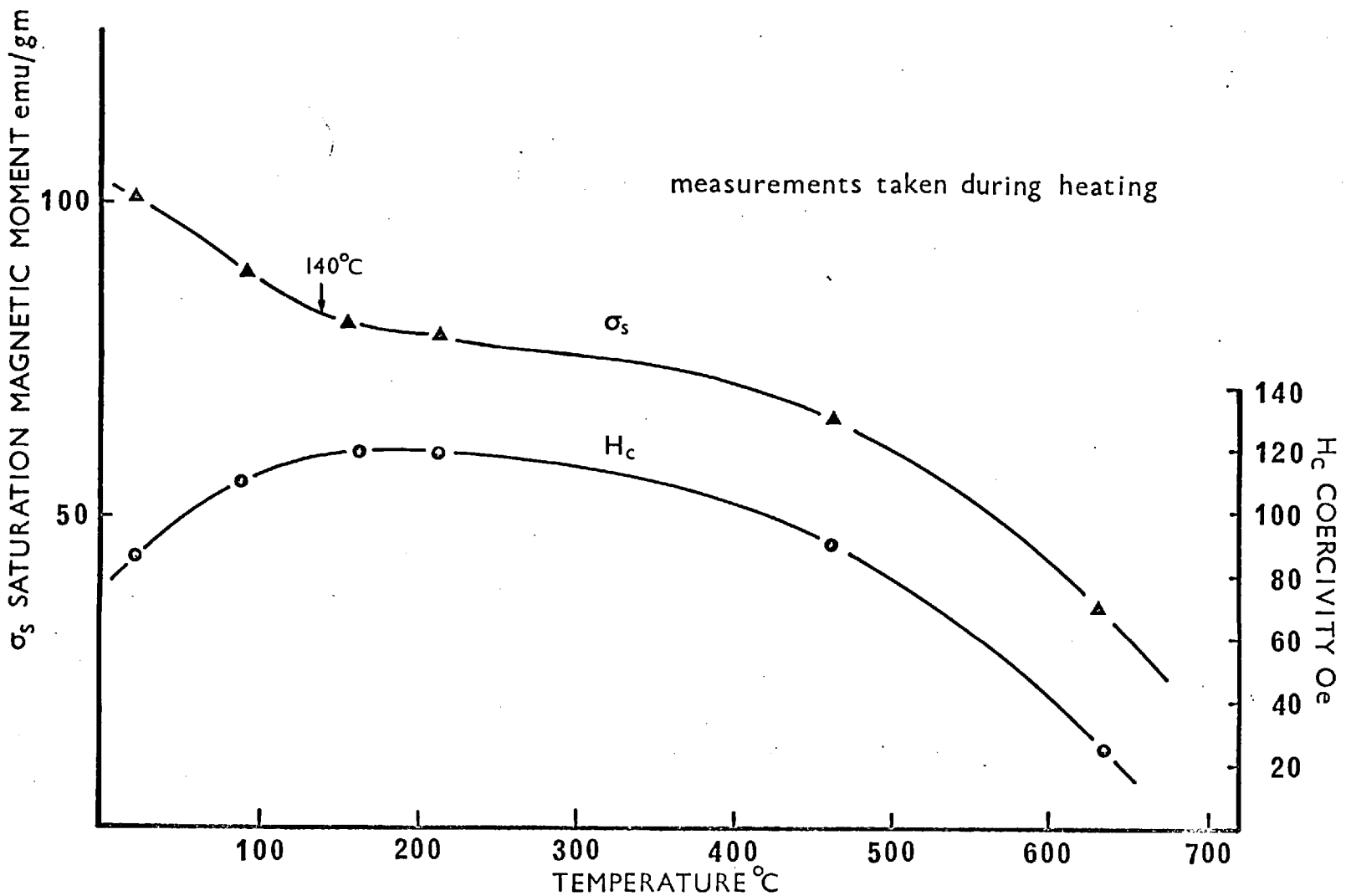

Fig 5:19 THE TEMPERATURE DEPENDENCE OF σ_s AND H_c FOR ALLOY 225T FROM VIBRATING SAMPLE MAGNETOMETER MEASUREMENTS

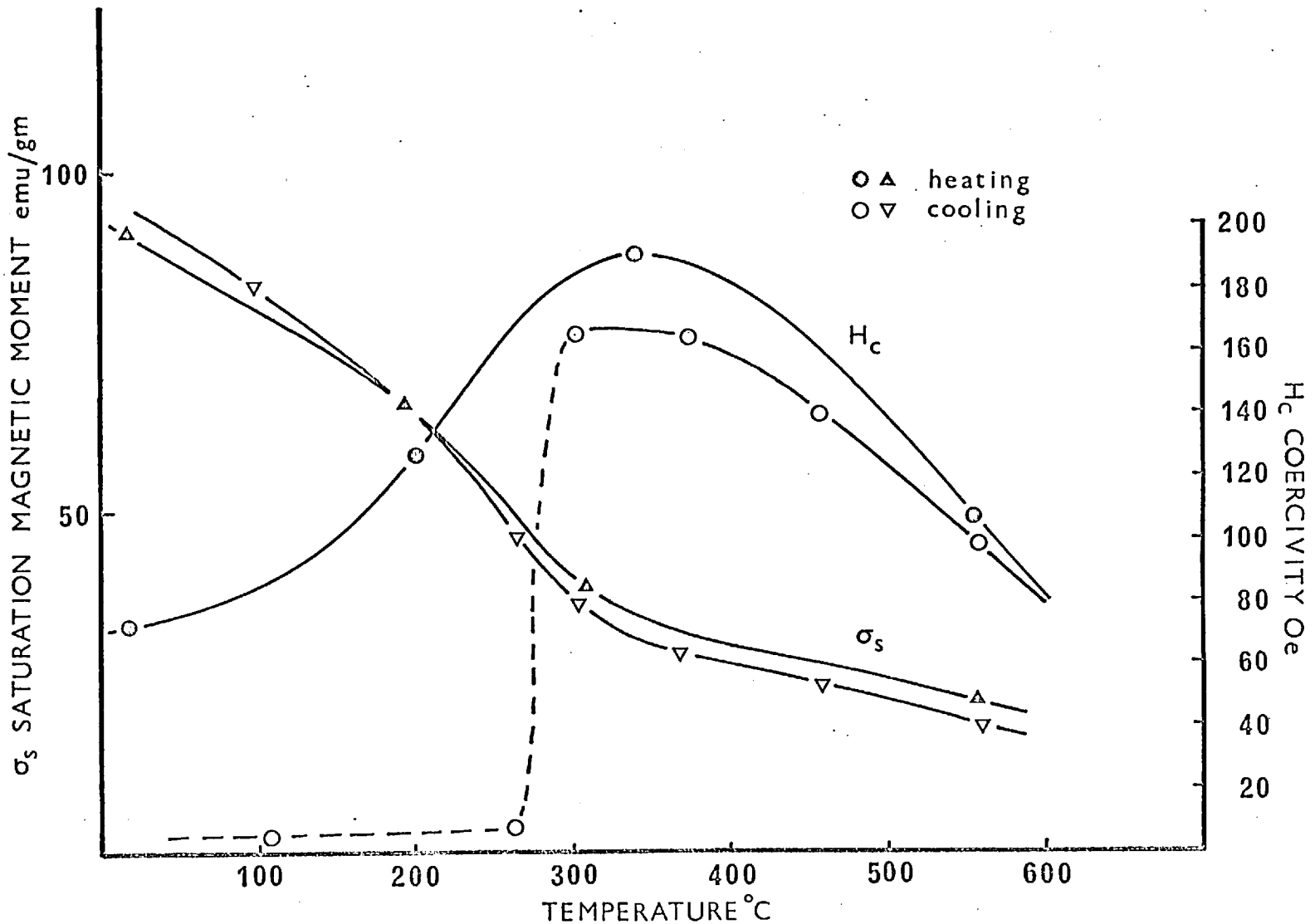

Fig 5:20 THE TEMPERATURE DEPENDENCE OF σ_s AND H_c FOR ALLOY 25T ON INITIAL HEATING, AND ON COOLING AFTER HOLDING FOR 1 HR AT 700°C. VIBRATING SAMPLE MAGNETOMETER MEASUREMENTS

difficult to determine from the small number of readings taken.

The alloy was held at 700°C for 1hr to promote diffusion and coarsening of the structure and measurements were then taken during cooling to room temperature. The σ_s values found between 560°C and 320°C were approximately 8 emu less than the corresponding values on the heating curve, and the lower Curie point was reduced by approximately 20°C. Below 200°C the σ_s value of the structure annealed at 700°C was higher than that for the air cooled alloy.

The depression of the lower Curie point indicates that the annealing treatment at 700°C promotes a change in composition of phases present, which would contribute to the changes in σ_s observed. In addition to this effect, the volume fractions and distribution of the two phases would be affected by the annealing treatment, causing further changes in σ_s. The variation in H_c which accompanies these changes in σ_s is also indicated in Fig. 5:20. The annealing treatment at 700°C produces a reduction in coercivity at all temperatures in this series of measurements. A maximum of 168 Oe $\pm$ 1 Oe was found in the coercivity curve at 305°C and below this temperatures the coercivity fell sharply to a very low value at 269°C. Between 269°C and room temperature accurate measurement of the coercivity was not possible. The low value of the coercivity at room temperature was in marked contrast with the value of 74 Oe $\pm$ 1Oe, recorded before heating was commenced.

The hyseresis loops from which the data for alloys 225C and 225T was taken, showed no irregularities and their relative shapes were characterised by the values reported. The σ_s value expressed the height of the loop

whilst its half width was a measure of the coercivity. These two parameters are, however, insufficient to describe the relative shape changes of loops recorded for alloy 25T as may be seen from Fig. 5:21. This shows a selection of the hysteresis loops, as measured, during heating and cooling, and the relevent temperatures are indicated. The sequence measured on heating was quite normal, and was essentially similar to that recorded for the other two alloys. The loops recorded during the initial stages of cooling remained in character with this sequence, as shown by those measured at 560°C and 375°C, but at 305°C the loop developed the irregular shape shown in Fig. 5:21. Below this temperature experimental difficulties prevented accurate measurements of the centre parts of the loops but there were indications that these had assumed the wasp-waisted form which is reported for perminvar alloys. The experimental difficulty mentioned above, was the inability to produce fields between zero and $\pm$ 20 Oe in the solenoid owing to the "residual current" of the D.C. generator used. This presented no problems with normal loops, as readings could be taken with the current off i.e. zero field, and the linear portions of each half of the loop extrapolated through these points to complete the whole hysteresis curve. Such extrapolations were not possible with the suspected wasp-waisted loops and hence no accurate measure of the coercivity could be obtained.

This discussion has been concerned with measurements of the saturation magnetic moment per gram (σ_s), the coercivity (H_c), and changes in the shape of hysteresis loops. It was possible to assess the first two quantities from the measured hysteresis loops, without applying a correction for the demagnetizing factor of the particular specimen shape. This correction affects the susceptibility, which is

FIG 5:21 HYSTERESIS LOOPS FOR ALLOY 25T FROM WHICH THE DATA FOR FIG 5:20 WAS TAKEN

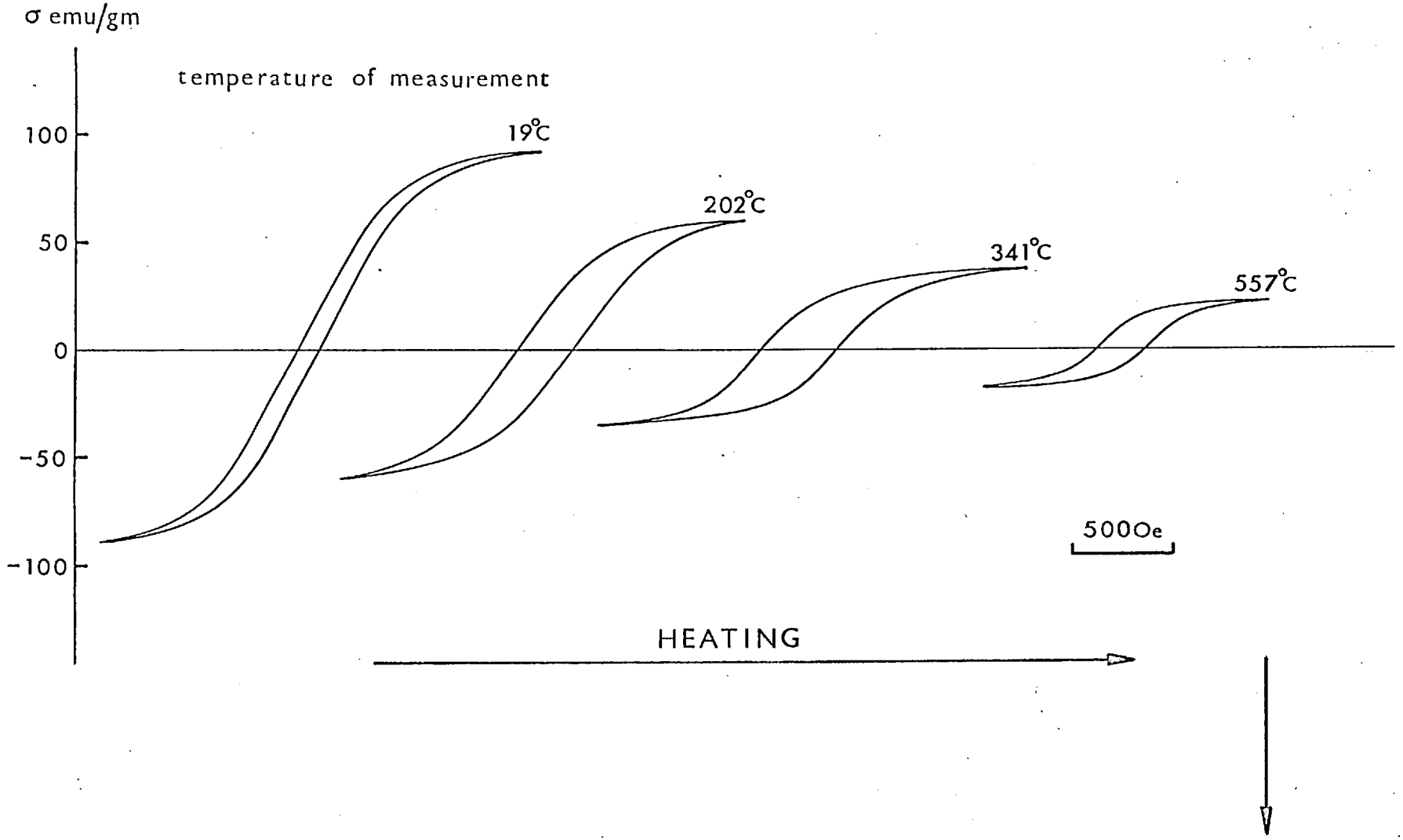

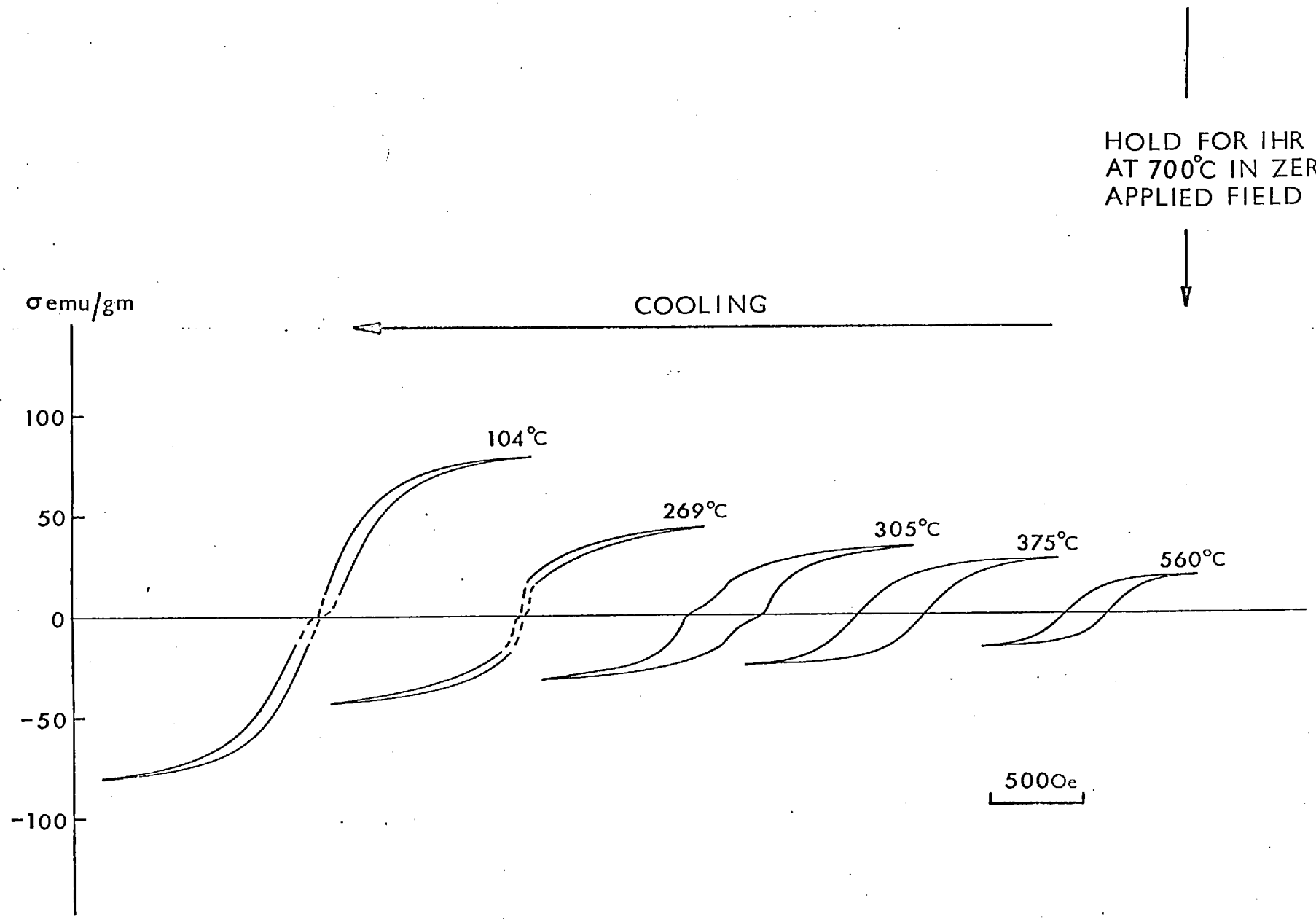
HOLD FOR 1HR
AT 700°C IN ZERO
APPLIED FIELD
σ emu/gm
COOLING
100
50
0
-50
-100
104°C
269°C
305°C
375°C
560°C
500Oe

a measure of the slope of the hysteresis curve, and the apparent values of this quantity, which could be measured from the loops in Fig. 5:21, would be artificially low. The general shapes of the uncorrected loops for each alloy could be compared however, since the same specimen shape was used for all the measurements.

5:4 DISCUSSION OF THE RESULTS FOR IRON - ALUMINIUM - TITANIUM ALLOYS.

As in chapter 4 the discussion will be divided into two parts dealing first with the microstructural observations and then applying these results to the interpretation of the magnetic data.

5:4:1 The microstructural changes produced by the titanium addition.

The structural effect of the titanium addition may be assessed by comparing the ternary vertical section, Fig. 5:1, with the binary diagram, Fig. 2:3. This immediately illustrates the stabilizing effect that titanium has on the ordered phases present. The maximum DO_3 critical temperature is elevated from 551·4°C to above 800°C and the $L2_0$ phase field is affected to a comparable extent. These observations indicate a considerable increase in the 'ordering energy' (E_o) of the system which is related to the critical temperature of the ordered phase (T_c) by an expression of the form[85]

$$E_o = \frac{KT_c}{4}$$

where K is Boltzmann's constant. Titanium also has the effect of elevating and expanding the $\alpha + DO_3$ phase field and, over a small composition range promotes the coexistance of the $L2_0$ and DO_3 phases.

Since no new phases were found in the part of the ternary system studied, it must be concluded that the changes observed result from titanium in solid solution. It is thus important to establish the positions occupied by

the titanium atoms in the ordered structures, since this is obviously the cause of their increased stability.

The addition of titanium to alnicomagnet alloys induces a transformation from $L2_0$ to $L2_1$ in the ordered matrix phase, as outlined in section 2:3:2. In this type of alloy the results of Mason, Ashall and Dean[70] suggest that titanium atoms occupy sites on sublattice III (Fig. 2:1b) in the $L2_1$ structure. This creates a situation where sublattices I and II are equivalent and together form a simple cubic configuration whilst the "body centre" positions, made up of sublattices III and IV, are occupied by titanium and aluminium atoms alternately. This type of structure, characteristic of the Heusler alloy Cu_2 Mn Al, has also been found in iron - silicon alloys with small additions of titanium[86]. In this case the composition of the phase with the $L2_1$ structure was found to be Fe_2 Ti Si. Because of the marked similarity between Fe_3Si and Fe_3Al (both order to $L2_0$ and then DO_3) and in view of the evidence from alnico alloys, it is suggested that titanium promotes the formation of an $L2_1$ structure in the alloys studied. The stoichiometric composition of this phase would be Fe_2TiAl and a continuous transition from Fe_3Al to Fe_2TiAl is expected as the titanium content of the alloy is increased.

The 5 atomic % of titanium added in the present investigation, therefore, substitutes for iron atoms on sublattice III in the DO_3 structure. It can be seen from Fig. 5.1 that this has the effect of stabilizing the α_1 phase and increasing the composition range over which the $\alpha + \alpha_1$ structure can exist. The electron micrographs shown, indicate that this broadening of the two phase field

is accompanied by a change in the morphology of the microstructure. In the binary system the transformation from α_m to $\alpha_m + \alpha_{1m}$ occurs by homogeneous precipitation of coherent, approximately spherical particles of α_1[27]. By contrast the precipitation in the ternary alloys studied, resulted in a modulated array made up of more angular coherent particles. An examination of these structures in alloys 175T and 20T revealed the following features:-

(i) The precipitation reaction cannot be suppressed by quenching.

(ii) The volume fractions of the two phases present are comparable.

(iii) There are pronounced modulations on {100} planes.

(iv) The structure consists of a regular array of coherent particles of a uniform size.

(v) At temperatures well below the $\alpha + \alpha_1$ phase boundary, the regularity of the structure is unaffected in the vicinity of grain boundaries.

The primary objective of the microstructural examination of these alloys was to establish the position of phase boundaries. For this reason the specimens examined were heat treated to give coarsened structures in which the constituent phases were readily identifiable. However, if this fact is taken into consideration, the structural features listed above are compatible with those which would be produced by spinodal decomposition.

A brief account of the theory of spinodal decomposition has been given in chapter 2 section 2:4:1 where it was stated that a solid solution inside the spinodal is unstable to sinusoidal fluctuations of wavelength $2\pi/\beta$ when

$$\frac{d^2f'}{dc^2} + 2k\beta^2 + 2\eta^2\gamma < 0 \qquad \ldots\ldots\ldots\ldots\ldots\ldots (1)$$

The third term in this expression refers to the coherency strains involved and the coefficient, Y, is a function of the degree of elastic anisotropy. The value of Y is a minimum for {100} planes in most cubic materials, including α iron[66], and thus the solid solution first becomes unstable to {100} plane waves. The concept of spinodal decomposition therefore provides an explanation of the composition modulation on {100} planes, observed in the present investigation. Also, the extent to which coarsening has occured may be assessed by comparing the observed wavelength with the initial decomposition wavelength predicted by theory, which is of the order of 30 Å. In these coarsened structures, a further composition modulation on {110} planes, was observed. It is, therefore, important to establish whether this feature is a product of the mode of decomposition or whether it is related to the coarsening process.

It is generally accepted that continuous cooling produces the most uniform spinodal structures, since these conditions allow the principle of "selective amplification" of composition fluctuations to occur. By this means, the fastest growing wavelengths are established in the structure at the expense of all others. In the present investigation, however, the specimens were given an isothermal treatment inside the spinodal. In this situation the solid solution is unstable to all fluctuations with wavelengths above a certain critical value. This spectrum of wavelengths is normally confined to fluctuations on one set of planes; those with the lowest value of Y. But, if the anisotropy of the system is low, fluctuations on

a second set of planes may become operative. Furthermore, in the alloys studied, the {110} planes are the next most favourable after the {100} type.

The degree of elastic anisotropy (A) in a crystal structure may be expressed in terms of the elementary elastic constants; the expression used is

$$A = \frac{2C_{44}}{C_{11} - C_{12}}$$

The measurements of Leamy, Gibson and Kayser[78] have shown that the value of A for binary iron - aluminium alloys ranges from A(10%Al) = 3·2 to A(25%Al) = 6·5 at room temperature. If these results are compared with A values for cubic metals (A (Al) = 1·2; A (α-Fe) = 2·4; A (Ni) = 2·5) it can be seen that iron rich iron - aluminium alloys are highly anisotropic. Thus, on purely elastic considerations, composition fluctuations on planes other than {100} would not be anticipated in the alloys studied.

If the stability criterion for sinusoidal composition fluctuations (equation 1) is re-examined, a second orientation dependant term is found. This is the contribution of the interfacial energy (k). An assessment of the morphology of two-phase microstructures, involving coherent superlattice phases, has been made by Leamy, Schwellinger and Warlimont[87]. Their calculations involved the computation of the atom pair density across a given (h k l) boundary, subdivision of this quantity into values for each pair type and hence, using atomic pair energies, an estimation of the relative boundary energy. Both interphase and antiphase boundaries were considered and the theoretical predictions for iron - aluminium binary alloys were in good

agreement with experimental observations. For the coexistance of α (disordered) and α_1 (DO_3) Leamy et al[87] predict an interfacial energy minimum for {110} planes. The degree of anisotropy is not large for the binary alloys and hence the homogeneous nucleation process leads to approximately spherical particles of α_1 in an α matrix. In the alloys containing titanium, however, the two phase structure is produced by a spinodal mechanism which is more sensitive to such crystallographic factors and the {110} interfaces are clearly observed. It may be predicted that the titanium addition would enhance the degree of anisotropy for the following reason. An examination of Fig. 2:1b reveals that {110} planes contain equal numbers of lattice sites from each constituent sublattice and hence they are the most representative planes of the DO_3 structure. This observation is equally true of the $L2_1$ structure and thus the α/α_1 boundary energy is again expected to show a minimum for {110} planes, although the degree of anisotropy will be greater in this case, since a greater variety of atomic types are involved.

In summary, therefore, it can be said that the $\alpha + \alpha_1$ structures observed in alloys 17ST and 20T are thought to form by spinodal decomposition. The morphology of the structure is dictated by two energy terms which are anisotropic; the elastic energy which is a minimum for {100} planes and the interfacial energy which favours {110} interphase boundaries. During the initial stages of decomposition the pronounced anisotropy of the elastic energy is most important, as the structure coarsens, however, the interfacial energy becomes increasingly

significant. During this stage the particles of the α_1 phase develop {110} facets and seem to resist agglomeration since no antiphase boundaries were observed within α_1 particles in these alloys. This would indicate that the interphase boundary energy is less than half the antiphase boundary energy in agreement with the calculations of Leamy et al[87].

The $\alpha + \alpha_1$ structures which are observed in the alloys with higher aluminium contents do not consist of comparable volume fractions of the two phases and hence the spinodal mechanism cannot operate. This is most noticeable in alloy 25T where the two phase structure obviously develops by the formation of a disordered layer at the APBs of the ordered phase (see Fig. 5:10). The alignment of 1/2 a' <100> boundaries on cube planes is as expected from APB energy calculations[87] and as these planes are also elastically soft, they can accomodate the disordered layer which forms.

The observation of $\alpha_1 + \alpha_2$ structures in these iron-aluminium - titanium alloys provides a further opportunity to test the validity of the boundary energy calculations of Leamy et al[87]. The nature of the interphase boundary energy anisotropy calculated in this case, is similar to that outlined above for 1/2 a' <100> APBs; and thus both interfacial and elastic energy considerations favour precipitates with <100> directionality. This is in agreement with the experimental observations as indicated in Figs. 5:14 and 5:15. Two possible mechanisms for the formation of the {100} boundaries separating individual α_1 particles have been proposed in section 5:1:4. The

first involves the alignment on {100} planes, and subsequent broadening of existing 1/2 a' <100> APBs. If such a boundary were present, this would be energetically favourable in a two phase situation. However, it is difficult to envisage the nucleation and growth process to account for the existance of the APBs.

No such difficulties arise with the second suggested mechanism in which a band of α_2 is formed on a plane with low interfacial energy, to relieve the elastic strain built up by the growth of an α_1 particle. Groups of particles are therefore formed in rows or fragmented plates on {100} planes to minimise the total elastic distortion of the lattice. This mechanism therefore offers a reasonable explanation of how the observed $\alpha_1 + \alpha_2$ structures form but does not give any indication of why they are stable.

In binary iron - aluminium alloys the transition from $L2_0$ to DO_3 is by a second order reaction which is represented on the phase diagram by a single line. The reaction involves ordering of one of the two simple cubic sublattices of the $L2_0$ structure, and hence the chemical composition of both ordered phases is identical. In the ternary iron - aluminium - titanium alloys, however, evidence for the coexistance of α_1 and α_2 has been found. Since the interfaces in these structures show pronounced directionality, in agreement with theoretical calculations, it must be assumed that the interfacial energy has a finite value, which may be attributed to a difference in chemical composition between the two phases. This arises because of the important role played by titanium in stabilizing the DO_3 structure, which has already been discussed. It is therefore considered that the α_1 (DO_3) phase is

titanium rich compared with the α_2 ($L2_0$) phase with which it coexists.

In conclusion of this section on the structure of the iron-aluminium-titanium alloys studied, it can be said that the experimental observations have enabled the position of phase boundaries to be established in the vertical section, Fig. 5:1. It should once more be emphasized that the α to α_2 reaction and α_2 to α_1 transition above 27 atomic percent aluminium are considered second order and are thus represented by single lines. The diagram shown is thus related to a ternary peritectoid situation in which two of the component reactions are second order. The stability of the ordered phases was found to be due to the tendency of titanium to occupy the alternate body centre sites (type III in Fig. 2:1b) which, if sufficient titanium were added, would lead to the formation of a compound Fe_2TiAl with the $L2_1$ structure. The morphology of the structures observed could be understood with the aid of the elasticity data of Leamy, Gibson and Kayser[78] and the interfacial energy calculations of Leamy, Schwellinger and Warlimont[87].

5:4:2 The magnetic properties of iron - aluminium - titanium alloys

The magnetic results obtained for these alloys are subject to the introductory remarks made in section 4:4:2 concerning microstructural changes during the measurement, and these have been taken into consideration in the following assessment.

The variation of saturation magnetic moment with composition, shown in Fig. 5:17, is once again similar to

that for binary iron - aluminium alloys. The curve is made up of three sections and, by reference to the phase diagram, Fig. 5:1, and the table of Curie points in Fig. 5:16, the structures in each of these regions may be deduced. Between 17 and 21 atomic % aluminium the structure is two phase $\alpha + \alpha_1$ but only the α phase is ferromagnetic at room temperature. The first section of the curve in Fig. 5:17 therefore shows an almost linear decrease in σ_s due to the increasing dilution of the α phase with aluminium. In the region between 22 and 25 at % Al the structure is still composed of α and α_1 but both are ferromagnetic and hence the curve is seen to rise slightly. Above 27·5 at % Al the structure is single phase α_1 and, as in the case of binary alloys, the magnetization falls of steeply.

The absolute values of σ_s, in the composition range studied, show a very marked decrease due to the titanium addition, as may be seen from Fig. 5:17. This fact is significant if considered in the light of the results of Nathams and Pickart[83] and Kouvel[84] which have been outlined in section 4:4:2. This experimental evidence indicates that the magnetic moment of an iron atom in the DO_3 structure depends on the nature of its nearest neighbours. Thus an iron atom on a type I or II site has a magnetic moment of $1{\cdot}46 \pm 0{\cdot}1\ \mu_\beta$ while those on type III sites have a moment of $2{\cdot}14 \pm 0{\cdot}1\ \mu_\beta$. It may therefore be appreciated that the substitution of titanium atoms for iron atoms on type III sites, as proposed in section 5:4:1, has a much more potent effect on the saturation magnetic moment than if substitution were to occur on type I or type II sites. The magnitude of the decrease in σ_s produced by the titanium addition

is thus further evidence for specific site substitution leading to the formation of an $L2_1$ structure, based on Fe_2Ti Al, in these alloys. The curves showing the variation of σ_s with temperature, for the alloys containing titanium (Fig. 5:18), are easier to interpret than those determined for alloys containing copper. This is because none of the alloys undergoes a phase transformation on heating to the Curie point and hence the curves do not show any measurable thermal hysteresis. The single Curie temperatures indicated for alloys 175T and 20T and the upper Curie temperatures for alloys 225T and 25T are obviously characteristic of the disordered α phase. The values show a slight decrease with increasing aluminium content from 711°C for alloy 175T to 656°C for alloy 25T. The composition of the α phase in each case is, however, unknown and may not be deduced from the vertical section Fig. 5:1 since the lever rule construction is inapplicable in this ternary situation. This is equally true of the lower Curie points characteristic of the α_1 phase in alloys 225T and 25T, but in the case of alloy 275T the structure is single phase α_1 (DO_3), and thus the composition is accurately known.

The σ_s vs T curves obtained for alloys 225T and 25T, which show that the alloy contains two ferromagnetic phases, are similar to those obtained for alnico alloys, and this type of curve is shown schematically in Fig. 5:22a. In this case the total saturation magnetization is given by

$$I = v_1 I_1 + v_2 I_2 \quad \ldots\ldots\ldots \quad (i)$$

where I_1 and I_2 are the saturation magnetizations and v_1 and v_2 the volume fractions of the two phases. A brief

description of alnico alloys has been given in section 2:3:2 where it was noted that they owe their good magnetic properties to a structure consisting of a fine uniform dispersion of elongated single - domain ferromagnetic particles in a less magnetic matrix. Stoner and Wohlfarth[69] derived the following relationship for a group of ellipsoidal single - domain particles all oriented in the same direction

$$H_c = p(1 - p)\,(N_2 - N_1)\frac{(I_1 - I_2)^2}{I_s} \quad \text{.....(ii)}$$

(for definition of symbols see section 2:3:2)

If values of I_1, I_2 and the average saturation magnetization, I_s, are estimated from the I vs T curve (Fig. 5:22a) and substituted in equation (ii), the temperature dependance of the coercivity may be determined. This procedure gives an H_c vs T curve of the type shown in Fig. 5:22b which is in agreement with the experimental observations of Iwama[88] on Alnico 5. Since the magnetization vs temperature curve for alloy 225T was of the same shape as the the general curve used in the theoretical treatment, the coercivity measurements were expected to show the type of temperature dependance depicted in Fig. 5:22b. This was, in fact, found to be the case, as shown in Fig. 5:19 but it should be noted that the lower Curie point and hence the corresponding coercivity maximum are blurred due to the stabilizing effect of the applied field. The Stoner - Wohlfarth equation has been successfully used in the case of magnetically heat treated alnico alloys by Bronner et al[9]. However, the basic model on which the equation was based

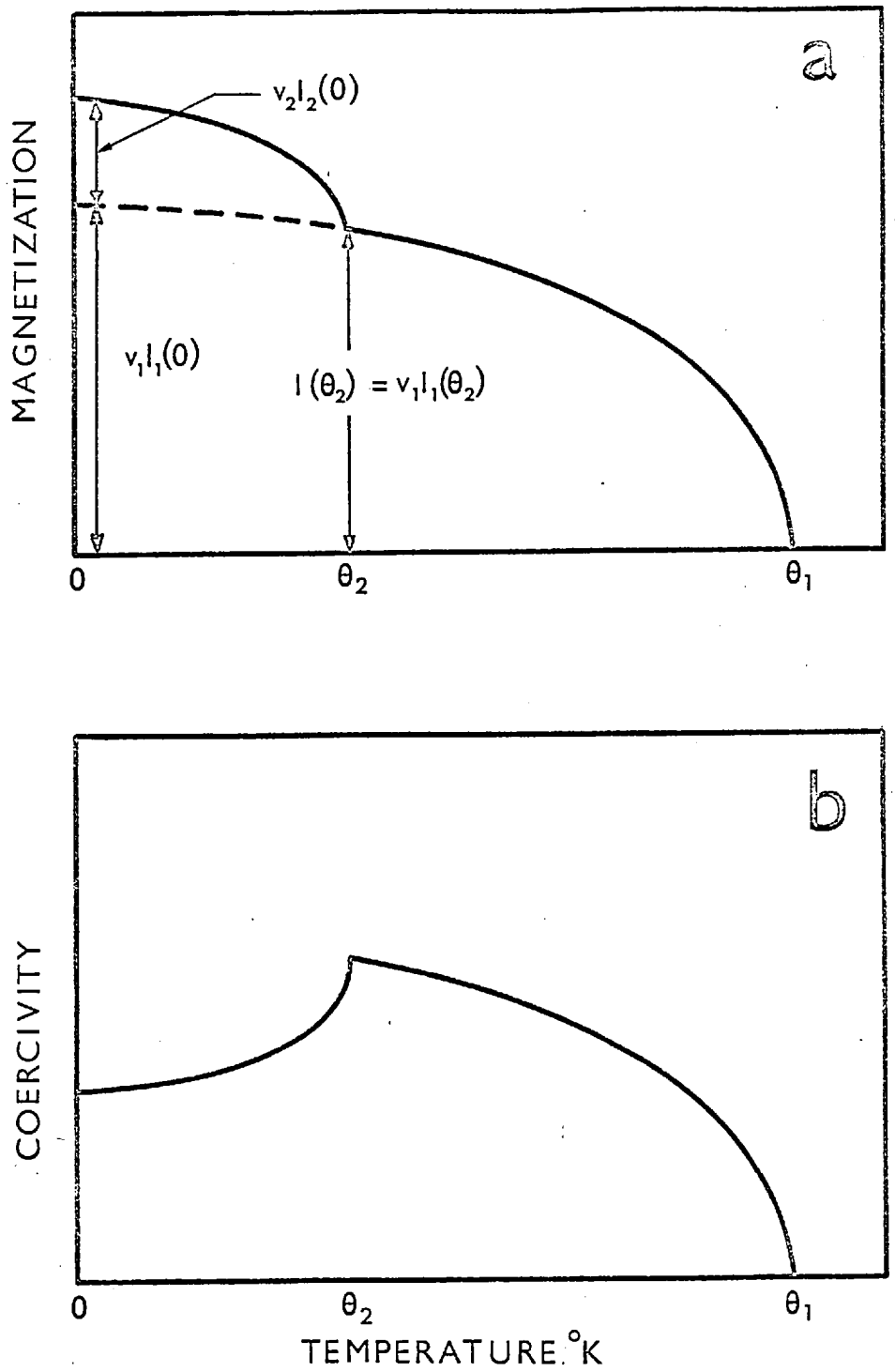

Fig 5·22 (a) I–T curve and (b) H_c–T curve for an idealized material consisting of two ferromagnetic phases; here the H_c–T curve is calculated by Eq (ii) using the data of curve (a) (from ref 88)

precludes its use as a means of estimating absolute values of coercivity in the present case of a randomly oriented polycrystalline specimen.

The measured coercivities for alloy 225T, which vary from H_c = 86 Oe at 19°C to a maximum of H_c = 120 Oe at 160°C, may be put in perspective by comparing them with the coercivity of a simple alnico alloy in the as cast condition. A typical value for such an alloy, Alnico 5 (Fe - 24Co - 14Ni - 8Al - 3Cu) is H_c = 220 Oe measured at room temperature. It should be emphasized that it is possible to increase the coercivity of Alnico 5 to about 600 Oe by a complex thermo - magnetic treatment. The experimental results for alloys 225T and 25T will therefore be examined to establish whether their magnetic properties are susceptible to improvement by such treatments.

It may be seen from Fig. 5:1 that alloy 225T lies inside the spinodal and thus during air cooling the solid solution would rapidly decompose to form an $\alpha + \alpha_1$ structure. The thermomagnetic curve for this structure indicates that the Curie temperature of the α phase is 664°C and that of the α_1 phase is 140°C. Since the Curie temperature of the α_1 phase in these alloys is very sensitive to small changes in composition it may be concluded that the α_1 phase is similar in composition to alloy 275T, which shows a single Curie point at 181°C. To compensate for this enrichment of the α_1 phase, the α phase in alloy 225T is correspondingly depleted in titanium and aluminium. The diffusional processes which account for the establishment of such extensive composition differences on air cooling are characteristic of spinodal decomposition.

In alloy 25T, however, the microstructural observations

of the $\alpha + \alpha_1$ structure would seem to indicate decomposition by heterogeneous nucleation and growth on antiphase boundaries. The kinetics of this process are expected to be slower than those of spinodal decomposition, and hence less pronounced composition differences would be produced on air cooling. This is confirmed by the thermomagnetic curve for alloy 25T which indicates the coexistence of α and α_1 for which the Curie temperatures were 656°C and 316°C respectively. The α_1 phase in this case occupies a greater volume fraction and is less depleted in iron than the α_1 phase formed in alloy 225T.

The curves indicating the temperature dependence of σ_s and H_c show the same inter-relationship as was found previously. However, the maximum coercivity recorded on initial heating of the specimen, 191 Oe at 341°C, was considerably greater than the maximum for alloy 225T. This reflects a lower degree of inter-connection of the α particles in the former case as indicated by electron microscopy.

The modification of the magnetic properties, produced by holding the specimen for 1 hr at 700°C, may be attributed to changes in composition and hence saturation magnetization of the constituent phases, due to the narrowing of the $\alpha + \alpha_1$ phase field. In addition, the heat treatment produces growth and coalescence of some α particles which cannot be considered as single magnetic domains. These two factors both help to remove bariers to magnetic domain wall movement in these two phase alloys and hence account for the low coercivities measured on cooling below the Curie point of the α_1 phase. It was in this region, however, that the measured hysteresis loops were found to have the unusual shape normally associated with Perminvar alloys.

The name "Perminvar" refers to the type of Fe - Ni - Co alloy in which these wasp waisted or constricted loops are most pronounced,but they have been observed in other systems. Of particular interest in this context are the findings of Zusman[40] and of Mazzetti, Montalenti and Soardo[89] who have observed such loops in binary iron - aluminium alloys. The irregular shape of the loops is obviously due to the existance of a low energy, stabilized, configuration of magnetic domains within the structure, but the factors governing the developement of such a configuration are not well understood.

Zusman has stated that his results may be satisfactorily explained by the theory of directional order which was developed independently by Neel[90] and by Taniguchi and Yamamoto[91]. The fundamental assumption of this theory is that there exists an energy which depends on the angle between the direction of the local magnetization and the axis of a nearest neighbour pair of iron atoms. At a temperature below the Curie point but high enough for diffusion to occur, the pair axes will not be distributed at random, but will show some preffered direction with respect to the local magnetization. If the temperature of the system is lowered until diffusion no longer occurs at an appreciable rate, this structural anisotropy with its associated magnetic domain configuration is 'Frozen in'. The occurrence of constructed loops is therefore attributed to this stabilized domain structure, with each domain wall at a local energy minimum. However, in their recent review of directional ordering, Chikazumi and Graham[92] note that the simple theory, based solely on nearest neighbour interaction, does not give an adequate explanation of the

anisotropy found in substitutional alloys with the b.c.c. structure. In this context they quote the experimental results of Wakiyama which indicate that for binary iron - aluminium alloys, the directional order anisotropy coefficients (k_1 and k_2) show sharp maxima in the composition range 20 - 25 at % Al, whilst theory predicts k_1 should be zero. This marked difference between the experimental results[40, 89, 92, 93] and predictions based on the concept of directional ordering is ascribed, by various authors[92,93], to over - simplification in the derivation of the theory. They maintain that a better agreement may be obtained if both second nearest neighbour interactions and variations in the magnetic moment of iron atoms with their environment are taken into consideration.

The principal defect of this explanation for the origin of low energy, stabilized, domain structures in iron aluminium alloys is that it takes no account of the microstructure of the alloys concerned. It can be seen from the binary phase diagram that alloys containing between 20 and 25 atomic % Al, in which the most pronounced Perminvar effects are found, lie inside the $\alpha + \alpha_1$ phase field at temperatures where diffusion is appreciable. The importance of this observation may be illustrated by consideration of the structural condition of the specimens used by Mazzetti et al. They observed abnormalities in the hysteresis loop of an iron - 22 at % aluminium alloy which had been heat treated in a weak magnetic field at 500°C, and subsequently cooled to below 300°C whilst remaining in the field. At 500°C the alloy is in the $\alpha + \alpha_1$ phase field above the Curie point of the α_1 but well below that of the α phase. During heat treatment and cooling

the phases will therefore adopt an anisotropic configuration due to the presence of the samll applied magnetic field. A structure produced in this way will have a low energy domain configuration in the direction of the original applied field, which will be shown up in the hysteresis loop. Further correlation of the reported magnetic results with the phase diagram indicates that the alloys of lower aluminium content, in which Zusman found constricted loops, are those which also exhibit 'K state' properties.

The recognition that binary iron - aluminium alloys can show the relatively large scale structural anisotropy does not completely negate the case for directional order. Therefore, in these alloys a better understanding of the origins of magnetic anisotropy may be obtained if contributions from both phase distribution and directional order in the structure are considered jointly.

In the present investigation Perminvar loops were observed in alloy 25T after holding for 1 hr at 700°C and cooling to below the Curie point of the α_1 phase. The structure of the specimen after such a treatment would be similar to that shown in Fig. 5:10a which exhibits pronounced directionality due to the formation of the α phase on antiphase boundaries following cube planes. The low energy domain structure causing the Perminvar properties is therefore largely associated with the structural anisotropy found in this case. The contribution, if any, from directional order cannot be assessed from these measurements made using polycrystalline specimens.

The possibility of improving the magnetic properties of iron - aluminium - titanium alloys by suitable heat treatments can now be considered in the light of the

foregoing discussion of the structures of alloys 225T and 25T. The observation of Perminvar loops in alloy 25T is significant since alloys which show this behaviour on cooling in the absence of an external field, generally respond to thermomagnetic treatment. In specifying such a heat treatment the following factors should be taken into consideration if the optimum properties of a hard magnetic material are to be obtained.

(i) Cahn[57] has estimated that the anisotropy in elastic energy usually exceeds by far the magnetostatic energy anisotropy, except near the Curie temperature. Consequently, to maximize the effect of the magnetic field, annealing should take place as near tothe Curie temperature of the original homogeneous alloy as possible. In practical terms, since permanent magnet alloys are usually slow cooled in the magnetic field, this means that the Curie point of the homogeneous phase must be just above the miscibility gap.

The importance of this factor in the binary iron - aluminium system has been illustrated by Swann et al[6] in their study of alloys with the $\alpha + \alpha_2$ structure.

(ii) After cooling in a magnetic field the alloy should be subjected to an annealing treatment to induce compositional changes in the phases present. The purpose of this treatment is to reduce the Curie point of the less magnetic phase to room temperature, since this results in the coercivity maximum also occuring at room temperature. An example of the exploitation of this fact may be found in the experimental determination of the optimum annealing temperature for Alnico 5 reported by Iwama[88].

In the case of the iron - aluminium - titanium alloys, 225T and 25T, the following observations may be made concerning the points mentioned above. In both cases

decomposition to the $\alpha + \alpha_1$ structure can occur above the Curie point of the α phase formed, and hence thermomagnetic treatment would be ineffective during the critical initial stages of particle formation. This is of great importance in the case of alloy 225T, where rapid decomposition by the spinodal mechanism occurs, but less significant for alloy 25T where the prospect exists of supressing decomposition to below the α Curie point.

The application of a suitable annealing treatment offers more obvious scope for improvement in the properties of these alloys, since the Curie temperature of the α_1 phase has been shown to be remarkably sensitive to small changes in composition.

In conclusion, therefore, it can be said although the room temperature coercivity of these iron - aluminium alloys containing 5 atomic percent titanium may be improved by annealing, the alloys are not expected to be particularly suitable for thermomagnetic treatment. There is a distinct possibility that an alloy containing less than 5 atomic percent titanium might prove more susceptible to such a treatment since a more favourable relationship between the upper limit of the $\alpha + \alpha_1$ phase field and the Curie temperature may be established.

Finally it should be emphasized that, although this discussion of magnetic properties has been concerned with maximizing the coercivity of the alloys studied, a more meaningful assessment of the quality of a permanent magnet is the maximum energy product (BH_{max}). Thus, a second important advantage of reducing the titanium addition to the alloys discussed, would be an increase in the induction component (B) of the maximum energy product.

CHAPTER VI

CONCLUSIONS AND SUGGESTIONS FOR FUTURE WORK.

In order to assess the effect of ternary additions on the ordering reactions in iron - aluminium alloys it was necessary to establish the conditions which exist in binary alloys. A comprehensive surves of the literature on this system has indicated that the phase diagram proposed by Swann et al shows the best agreement with all the experimental data.

The structure of the ordered phases has been referred to throughout with reference to the unit cells shown in Figs.2:1a and 2:1b. Thus for the $L2_0$ structure which exists in alloys with aluminium contents near 25 atomic %, sublattice I is occupied by iron atoms while sublattice II is occupied by equal numbers of iron and aluminium atoms distributed at random. In the larger unit cell characteristic of the DO_3 superlattice, iron atoms occupy type I, II and III sites with aluminium atoms on the fourth sublattice.

CONCLUSIONS

ALLOYS CONTAINING COPPER

Phase Stability

The effect on phase stability of adding 5 atomic % copper to alloys with compositions near Fe_3Al is summarised in the vertical section of the ternary phase diagram, Fig. 4:1. This indicates that:-

1. Copper stabilizes the ordered phases. The $L2_0$ critical temperature in an alloy containing 22·5% Al is elevated by

about 250°C whilst that for the DO_3 structure is raised uniformally by 15°C over the composition range 25 to 30 at % aluminium. As this alloying addition causes no shift in the position of the DO_3 phase field with respect to aluminium content, it is concluded that copper atoms are substituting for iron in the ordered structures.

2. No evidence of the interesting $\alpha + \alpha_2(L2_0)$ phase field, which occurs in the binary alloy system, was found in these alloys containing copper. In the region of the ternary phase diagram where the formation of such structures might have been anticipated, the antiphase boundaries of the $L2_0$ structure were found to be somewhat diffuse and showed a tendancy to align on cube planes. This type of behaviour normally precedes the formation of a discrete layer of the α phase at the APB. However, since prolonged ageing failed to produce this effect, it was concluded that no stable $\alpha + \alpha_2$ structures can exist in these alloys.

3. When the copper addition is made to alloys on the iron rich side of stoichiometry, a precipitate is formed which is not found in the binary system. This precipitate has the DO_3 structure and has been identified as Cu_3Al.

Morphology.

1. The Cu_3Al precipitate forms as coherent discs on cube planes with
$\{100\}_{ppte} // \{100\}_{matrix}$ and $\langle 100\rangle_{ppte} // \langle 100\rangle_{matrix}$.
The precipitate thus complies with the condition for minimum elastic strain energy in a highly anisotropic matrix.

Due to the small difference in lattice parameter between the precipitate and matrix, coherency can be maintained to precipitate diameters in excess of 3,000 Å.

2. No evidence was found of a two phase region separating the $\alpha_2(L2_0)$ and α_1 (DO_3) phase fields. As the transition temperature was approached, however, critical point fluctuations were observed at two different alloy compositions. It is concluded that, as in the binary system, the transformation from α_1 to α_2 is by a non - classical phase change.

Magnetic Properties.

1. The addition of 5 atomic % copper to alloys which do not order, causes a reduction of 9% in the room temperature saturation magnetic moment and a slight reduction in the Curie temperature.

2. In alloys with the DO_3 structure, the addition results in a slight decrease in Curie temperature, but the saturation magnetic moment does not fall off so rapidly with composition, as in the case of the binary alloys.

3. The Curie temperature of alloys with the $L2_0$ structure is elevated by the copper addition. This feature in conjunction with an increase in the ordering energy of the system, affects the delicate balance which exists between the ordering and magnetic energies. The result of this change is that decomposition to $\alpha + \alpha_2$ is no longer energetically favourable.

4. The two previous observations, concerning the elevation

of the $L2_0$ Curie point and the increase in DO_3 magnetization produced by the copper addition, are examined in the light of the alternative suggestions that an antiferromagnetic state exists in the alloys or the magnetic moment of an iron atom is dependent on its environment. Neither theory gives an entirely satisfactory explanation of the experimental observations but both suggest that copper atoms substitute for iron atoms on either of the equivalent sublattices (denoted I and II in Fig. 2:1b) in the DO_3 structure, and on the wholly iron sublattice in the $L2_0$ structure (sites marked I in Fig. 2:1a).

ALLOYS CONTAINING TITANIUM

Phase Stability.

As before, the effect of an addition of 5 atomic % titanium is summarised in the form of a vertical section of the ternary phase diagram (Fig. 5:1). This indicates that:-

1. Titanium stabilizes the ordered phases. The $L2_0$ critical temperature in an alloy containing 27·5 atomic % Al is increased by about 250°C whilst the DO_3 critical temperature is elevated by 280°C. The upper limit of the $\alpha + \alpha_1$ phase field is similarly affected and the range of composition over which these two - phase structures can exist is considerably broadened.

2. Evidence has been found of a two phase $\alpha_1 + \alpha_2$ region separating the α_2 and $\alpha + \alpha_1$ phase fields. In the binary iron-aluminium system α_1 and α_2 do not coexist since both experimental observation and theoretical

predictions indicate that the transition from $L2_0$ to DO_3 is a non-classical phase change. The present observations indicate that a marked composition difference between the α_1 and α_2 phases is responsible for their coexistance in this case.

Morphology

1. The titanium addition changes the mode of formation of the $\alpha + \alpha_1$ structures from normal homogeneous nucleation and growth, to a process which shows all the characteristics of spinodal decomposition. Thus the random distribution of spherical precipitates of α_1 observed in binary alloys, is transformed into a modulated array of evenly spaced, angular, particles of the ordered phase, in a disordered matrix.

2. On initial decomposition, composition modulations on {100} planes are observed in the $\alpha + \alpha_1$ structure. In a system with such pronounced elastic anisotropy, decomposition by three orthogonal {100} plane waves produces a two phase structure with the minimum elastic strain energy. Thus this set of modulations are compatible with the mechanism of spinodal decomposition.

3. In coarsened structures a second modulation on {110} planes is observed. Under these conditions diffusion has promoted the formation of {110} facets on α_1 particles since this represents the minimum interfacial energy condition between precipitate and matrix. In the $\alpha_1 + \alpha_2$ structures both the elastic energy and the interfacial energy favour {100} precipitate / matrix habits and hence no {110} facets are observed.

Magnetic Properties.

1. The titanium addition produces a marked reduction in the saturation magnetic moment of the alloys. The extent of the reduction is dependant on composition but is of the order of 30% to 50%.

2. The Curie temperature of the DO_3 phase falls off rapidly with composition, thus an alloy containing 5 atomic % Ti and 30 at %.Al was not ferromagnetic at room temperature.

3. Alloys with the $\alpha + \alpha_1$ structure can exhibit high coercivities of the order of 200 Oe. This property is associated with a structure consisting of strongly ferromagnetic α particles in a weakly ferromagnetic, or paramagnetic α_1 matrix. These alloys are related to alnico permanent magnet materials and are expected to show some response to thermomagnetic treatment. When cooled in the absence of a magnetic field the alloys exhibit the waisted hysteresis loops characteristic of Perminvar alloys. It is suggested that this property results from the pronounced directionality associated with the two phase structure. As the α_1 phase present, possesses a high degree of long range order, an explanation of the Perminvar properties on the basis of directional order is ruled out.

4. By analogy with the results of other investigations on similar systems[70, 86], and taking into account the evidence from structural and magnetic studies, it is concluded that titanium substitutes for iron atoms on sublattice III in the DO_3 structure. This implies a continuous transformation

from Fe_3Al with the DO_3 structure to Fe_2TiAl with the $L2_1$ sturcture. In a structure where the magnetic moment of an iron atom is reported to be dependant on its environment, the replacement of an iron atom having eight iron nearest neighbours, has a maximum effect on the saturation magnetization and the Curie temperature. The tendancy to form an $L2_1$ structure also accounts for the composition difference between the α_1 and α_2 phases which stabilizes the $\alpha_1 + \alpha_2$ two phase field.

These conclusions clearly illustrate the effects produced by the two alloying elements studied in this investigation. Copper produces a precipitate of Cu_3Al in the system but otherwise leaves the phase stability and magnetic properties of the alloys largely unchanged. By contrast, the titanium addition is retained in solid solution over the whole composition range studied and it produces marked changes in phase stability and magnetic properties.

The dissimilarity between the two cases may be ascribed mainly to a difference in the particular sites at which substitution occurs in the ordered structures.

SUGGESTIONS FOR FURTHER WORK

This investigation has indicated that many of the apparent anomalies reported in the magnetic and other physical properties of binary iron - aluminium alloys may be explained by microstructural changes not considered by the authors. Of particular interest is the region in which the binary alloys show K state properties accompanied by streaking of the electron diffraction patterns. It is therefore suggested that an investigation involving the joint use of high temperature magnetic measurements and electron microscopy would do much to clarify the situation.

The elevation of the $L2_0$ Curie temperature, and increase in DO_3 magnetization produced by the copper addition are not fully understood. A better interpretation depends on a detailed assessment of the electronic structure which characterises the ferromagnetic state in these alloys.

The potential of iron - aluminium - titanium alloys as relatively cheap permanent magnet materials has been pointed out in the course of this discussion. In this connection it would be interesting to investigate the response to thermomagnetic treatment of an alloy with composition Fe 22 at % Al 3 at % Ti. In addition the alloy Fe_2TiAl should be examined to confirm that it has the $L2_1$ structure.

Finally the influence of structural anisotropy on the magnetic domain configuration in alloys with two ferromagnetic phases should be investigated by Lorentz microscopy. This technique may also prove useful in establishing whether directional order is an important feature of alloys in the α phase field which do not show long range order.

ACKNOWLEDGEMENTS

I wish to express my gratitude to my supervisor, Dr. P.R. Swann, for his guidance and advice throughout the course of this work. I also wish to thank my colleagues in the Physical Metallurgy Department for their many helpful discussions and suggestions.

I am most grateful to members of the college technical staff, particularly Mr. W. Bishop for processing electron microscope plates and Miss. P. Martins for printing the photographs for this thesis.

I am indebted to Professor J.G. Ball for the provision of laboratory facilities and the Science Research Council for their financial support.

Finally, I would like to thank my wife for her encouragement and assistance throughout the course of this research project.

References

1. W.F. Barrett, W. Brown and R.A. Hadfield
   Sci. Trans. Roy. Dublin. Soc. 7 67-126 1900
2. C. Sykes and H. Evans, J.I.S.I. 131 225 1935
3. P.R. Swann, W.R. Duff and R.M. Fisher, Trans A.I.M.E.
   245 851 1969
4. P.R. Swann, W.R. Duff and R.M. Fisher, Phys. Stat. Sol.
   37, 577 1970
5. P.R. Swann, W.R. Duff and R.M. Fisher,
   to be published Trans. A.I.M.E. 1971
6. P.R. Swann and R.M. Fisher, Appl. Phys. Letters
   9 279 1966
7. H. Warlimont, H. Muhe and H. Gengnagel,
   Z. angew Phys. 26 301 1969
8. K.J. de Vos, Thesis, University of Eindhoven 1966
9. C. Bronner, J. Sauze, E. Planchard, J.M. Drapier,
   D. Coutsouradis and L. Habraken
   Cobalt No.36 123 1967
10. I. Pfeiffer Cobalt No. 44 115 1969
11. P.P. Ewald and C. Hermann, Strukturbericht I
    Akademische Verlagscesellshaft M.B.H.,
    Leipzig 1936
12. M.J. Marcinkowski and N. Brown, J.Appl.Phys. 33 537 1962
13. Metals Handbook - American Society for Metals
    p 1161 1948
14. A.J. Bradley and A.H. Jay, Proc. Roy. Soc. A136 210 1932
15. M. Hansen and K. Anderko,
    'Constitution of Binary Alloys' McGraw-Hill
    New York 1958
16. A. Taylor and R.M. Jones, J.Phys. Chem. Solids
    6 16 1958
17. F. Lihl and H. Ebel, Arch. Eisenhuttenwes
    32 483 1961

18. A. Lawley and R.W. Cahn J. Phys. Chem. Solids 20 204 1961
19. L. Rimlinger, A. Pianelli and R. Faivre C.R. Acad. Sc. Paris, 260 148 1965
20. T. Eguchi, H. Matsuda, K. Oki, S. Kiyoto and K. Yasutake Trans. J.I.M. 8 174 1967
21. W.D. Bennett J.I.S.I. 171 372 1952
22. M.J. Marcinkowski and R. Smoluchowski, J. Phys. Chem. Solids 26 185 1965
23. H.J. McQueen and G.C. Kuczynski Trans A.I.M.E. 215 619 1959
24. R.G. Davies J. Phys. Chem. Solids 24 985 1963
25. A.V. Seybolt Trans. Amer. Inst. min.(metall)Engrs. 218 570 1960
26. L. Rimlinger C.R. Acad. Scl. Paris 261 4090 1965
27. G. Lutjering and H. Warlimont Acta. Met. 12 1460 1964
28. G. Lutjering and H. Warlimont Z. Metallkunde 56 1 1965
29. H. Warlimont Z. Metallkunde 60 195 1969
30. L. Rimlinger C.R. Acad. Sc. Paris 267 1206 1968
31. P. Morgand and J.M. Gjurasevic C.R. Acad. Sc. Paris 263 1492 1966
32. P. Morgand and J.M. Gjurasevic C.R. Acad. Sc. Paris 264 1577 1967
33. P. Morgand and J.M. Gjurasevic C.R. Acad Sc. Paris 265 448 1967
34. P. Morgand, P. Mouturat and G. Sainfort Acta Met. 16 867 1968
35. L.D. Landau and Ye. M. Lifshits, Statistical Physics, published by Pergamon Press London 1958

36. L. Rimlinger Mem. Sci. Rev. Metall 64 847 1967
37. V.I. Ivanovski and P.P. Denison
Fiz. Metal. Metalloved. 4 550 1957
38. L. Pal and T. Tarnoczi
J. Phys. Chem. Solids 6 16 1958
39. T. Shinohara J. Phys. Soc. Japan 19 51 1964
40. Sh.I. Zusman Fiz. Metal. Metalloved 9 41 1960
41. Sh.I. Zusman Fiz. Metal.Metalloved 9 635 1960
42. I.L. Aptekar' and Sh. I. Zusman
Fiz. Metal.Metalloved 12 350 1961
43. I.L. Aptekar' Fiz. Metal.Metalloved 12 197 1961
44. P. Ehrenfest Proc. Kon. Acad. Amsterdam 36 153 1933
45. M.A. Krivoglaz and A.A. Smirnov
The Theory of Order Disorder in Alloys
published by Macdonald 1964
46. D. Chipman and B.E. Warren
J. Appl. Phys. 21 415 1941
47. Ye. M. Lifshits Zh. Eksperim. i. Teor. Fiz. 11 269 1941
48. L. Guttman Solid State Physics
Academic Press New York 3 145 1956
49. J.W. Christian "The Theory of Transformations in
metals & alloys" (Pergamon) 1965
50. W.L. Bragg and E.J. Williams
Proc. Roy. Soc. A151 540 1935
51. H. Bethe Proc. Roy. Soc. A150 552 1935
52. C.N. Yang J. Chem. Phys. 13 66 1945
53. P.S. Rudman Acta Met. 8 321 1960
54. H. Sato Tohoku Univ. Res. Insts. Sci. Rep. A1 71 1951
55. C.R. Houska J.Phys. Chem. Solids 24 95 1963
56. D.A. Lavis and G.M. Bell Phil. Mag 15 587 1967
57. J.W. Cahn J.Appl. Phys. 34 3581 1963
58. T. Mishima Ohm 19 353 1932

59. D.A. Oliver and J. W.Sheddon Nature
142 209 1938
60. N.V. Philips, Brit. Pat. 522 731 1938
61. J. Harrison and W. Wright
Cobalt 35 63 1967
62. K.J. De Vos "Magnetism & Metallurgy" Vol I ed
A. Berkowitz and E. Kneller
Academic Press New York 1969
63. R.D. Heidenreich and E.A. Nesbitt
J. Appl. Phys 23 352 1952
64. M. Hillert Acta Met 9 515 1961
65. J.W. Cahn and J.E. Hilliard
J.Chem Phys. 28 258 1958; 31 688 1959
66. J.W. Cahn Acta Met 9 795 1961; 10 179 1962
67. J.W. Cahn Trans A.I.M.E. 242 166 1968
68. R.B. Nicholson and P.J. Tufton
Z. Angew. Physik 21 59 1966
69. E.C. Stoner and E.P. Wohlfarth
Phil.Trans.Roy.Soc. (A) 240 599 1948
70. J.J. Mason, D.W. Ashall and A.V. Dean
Cobalt 46 23 1970
71. K.M. Creer, A.de Sa and W.O'Reilly
J. Sci. Instum. 44 133 1967
72. P.R. Swann & H. Warlimont
Acta Met 11 511 1963
73. H.O. Ali, R. Adams and P.R. Swann
To be published
74. R.M. Bozorth "Ferromagnetism"
Van Nostrand 54 1951
75. J.B. Cohen "Phase Transformations"
A.S.M. 581 1970
76. H. Saito and H. Morita
J. Japan. Inst.Metals 30 930 1966

77. H. Warlimont and G. Thomas
Met. Sci.J. 4 47 1970
78. H.J. Leamy, E.D. Gibson and F.X. Kayser
Acta. Met. 15 1827 1967
79. L.E. Tanner Phil. Mag. 14 111 1966
80. L.E. Tanner Phys. Stat. Solidi 30 685 1968
81. R.M. Bozorth Ferromagnetism Van Nostrand 216, 1951
82. A. Arrott and H. Sato Phys. Rev. 114 1420 (1959)
83. R. Nathans and S.J. Pickart as reported by
Nathans "Magnetism" (ed. G.T. Rado
& H. Suhl) Vol 3 235 Academic Press
New York 1963
84. J.S. Kouvel "Magnetism and Metallurgy"
(ed A.E. Berkowitz & E. Kneller)
Academic Press New York 1969
85. N.S. Stoloff and R.G. Davies Progress in Materials
Science 13 14 1966
86. D.H. Jack Met. Sci. J. 4 22 1970
87. H.J. Leamy, P. Schwellinger and H. Warlimont
Acta Met 18 31 1970
88. Y. Iwama. Trans.Japan Inst. Metals 8 18 1967
89. P. Mazzetti G. Montalenti and G.P. Soardo
IEEE Trans on Magnetics
2 407 1966
90. L. Neel J. Phys. Radium 15 225 1954
91. S. Taniguchi and M. Yamamoto
Sci. Rept. Res. Inst. Tohoku Univ.
A6 330 1954
92. S. Chikazumi and C.D. Graham,Magnetism and Metallurgy
(ed A.E. Berkowitz and E. Kneller)
Academic Press New York 596 1969

93. G.W. Rathenan and G. de Vries
Magnetism and Metallurgy
(ed A.E. Berkowitz and E. Kneller)
Academic Press New York 596 1969

APPENDIX A

POLISHING TECHNIQUE

Introduction:- Principles.

To facilitate the preparation of the large number of electron microscope specimens used in this investigation it was necessary to devise a rapid but reliable electro-polishing technique. The apparatus described here fulfills these conditions and is based on the jetted electrolyte method. The purpose of the jet is to increase the rate of polishing, prevent build up of the anode products and prevent local overheating of the electrolyte near the specimen.

Description of polishing apparatus.

The apparatus may best be described with reference to the photographs (Figs. A1 and A2) and the sectional view (Fig. A3). It can be seen that there are two main components as described below:-

(i) The main body of the polisher is hinged in two sections. Each contains a jet assembly and an identical flow - path for the electrolyte. Situated behind the jets are a light and photo - sensitive resistor, these are protected from the electrolyte by two glass windows. The body of the polisher provides the cathode during electro-polishing.

(ii) The specimen holder (Fig. A2) contains the anode connection and is located between the two halves of the polisher body by its tapered outside faces. When in position the large surface area of the taper forms a good liquid seal and ensures alignment of the specimen with the jets and detection system. The holder itself is made

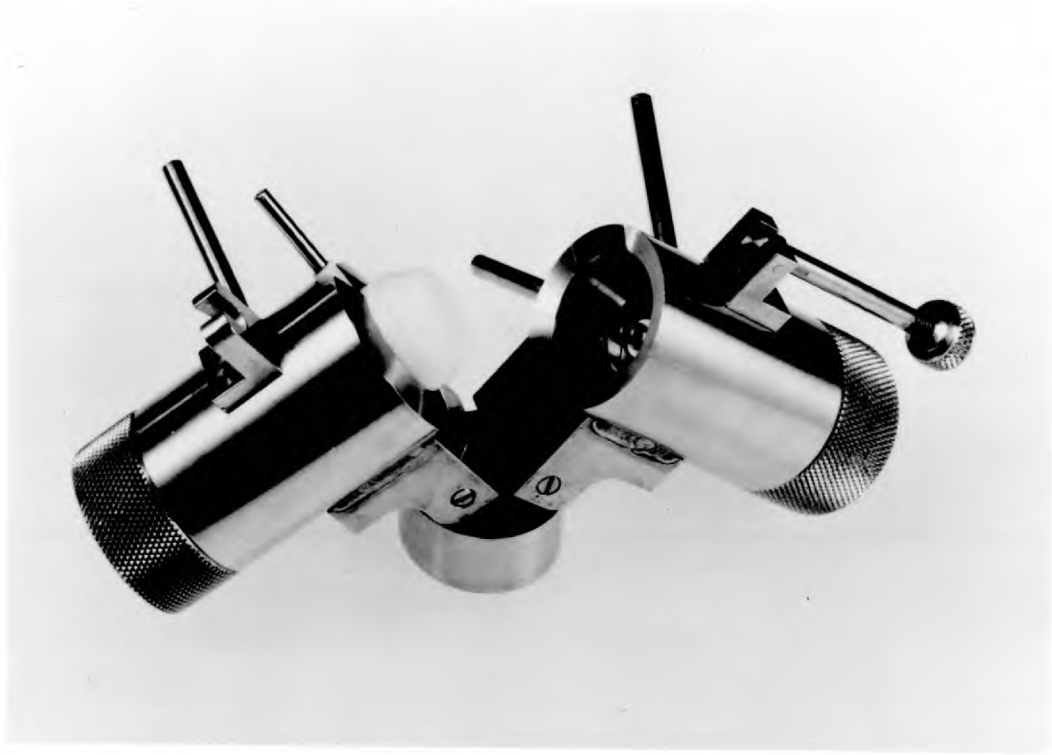

Fig. A1. General view of jet polishing apparatus.

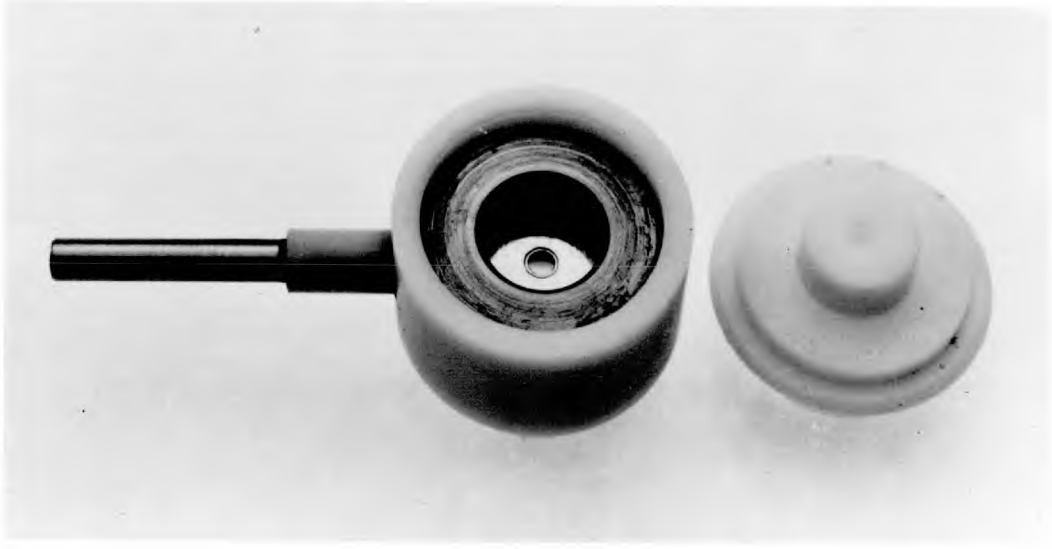

Fig. A2. Specimen holder in position for loading disc.

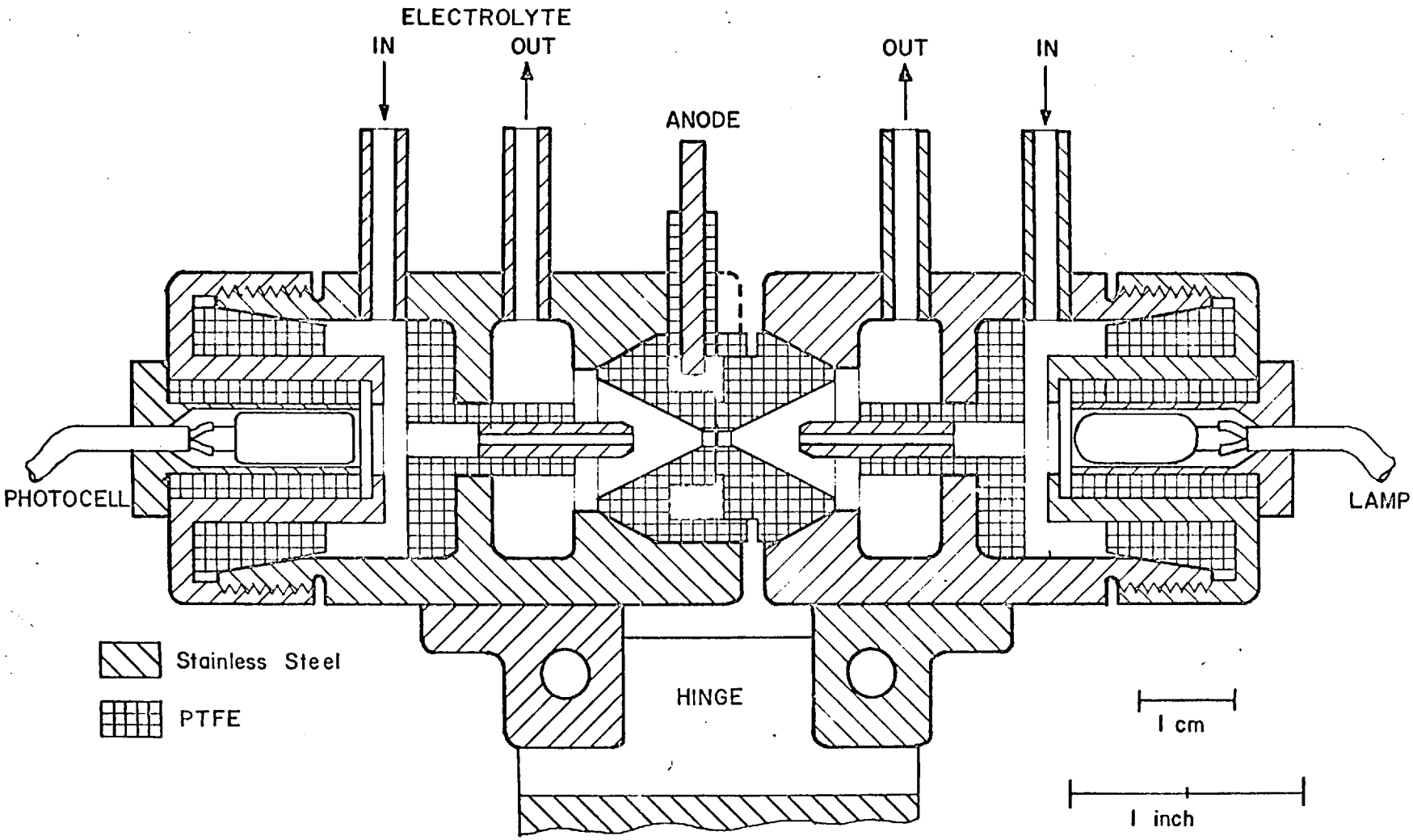

FIG.A3 SECTIONAL VIEW OF JET POLISHING APPARATUS

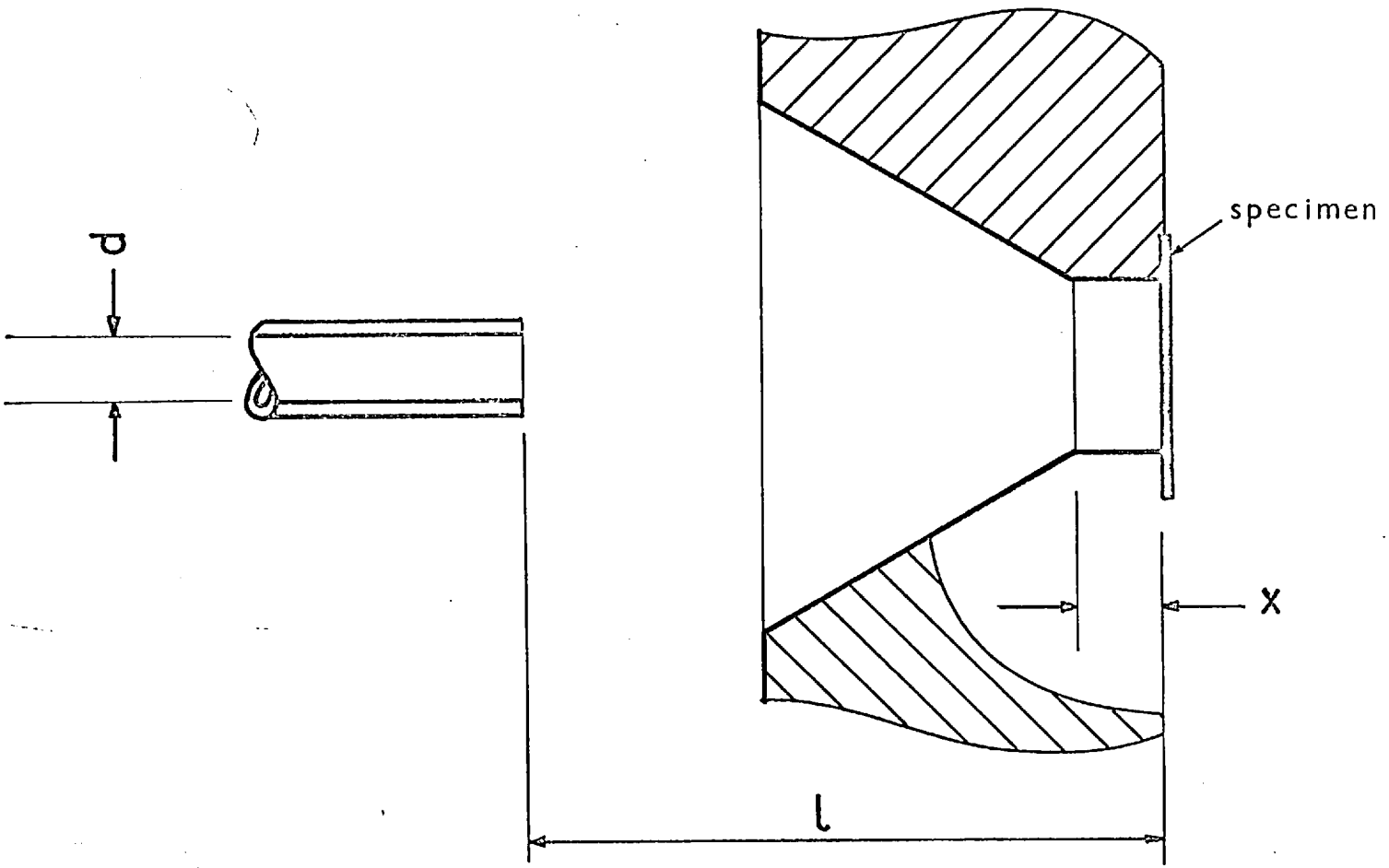

FIG. A4 VARIABLE PARAMETERS OF THE JET POLISHER DESIGN

in two parts as shown in Fig. A2. With the holder in the position shown, the 2·3 mm disc specimen is loaded into the left hand part so that it rests in a stepped hole in the platinum sheet, which forms the anode connection. The two halves of the holder are then fitted together, and the whole assembly is placed in the main polishing body (see Fig. A3).

During electropolishing, electrolyte flows from a reservoir at a height h above the polisher, through jets of diameter d terminating at a distance 1 from either side of the specimen and is recirculated by a peristaltic pump. The specimen holder has a lip of thickness x on either side of the specimen to promote the formation of a good profile. These dimensions are indicated in Fig. A4. The effect of variation of these parameters on the specimen profile was the subject of a recent study using this apparatus, the results of which are in publication[73]. The optimum values found for iron - aluminium specimens were

x = 0·4 mm
h = 150 mm equivalent to 150 ml/min
d = 2 mm
1 = 9 mm

Detection circuit

The photo - sensitve resistor and light arrangement was used to detect the inital perforation of the specimen, trigger the alarm system and turn off the polishing current. The circuit employed is shown in Fig. A5. The two variable resistors enable the voltage on the base of the transistor to be adjusted during the early stages of polishing, so

APPENDIX A. POLISHING TECHNIQUE

FIG. A5

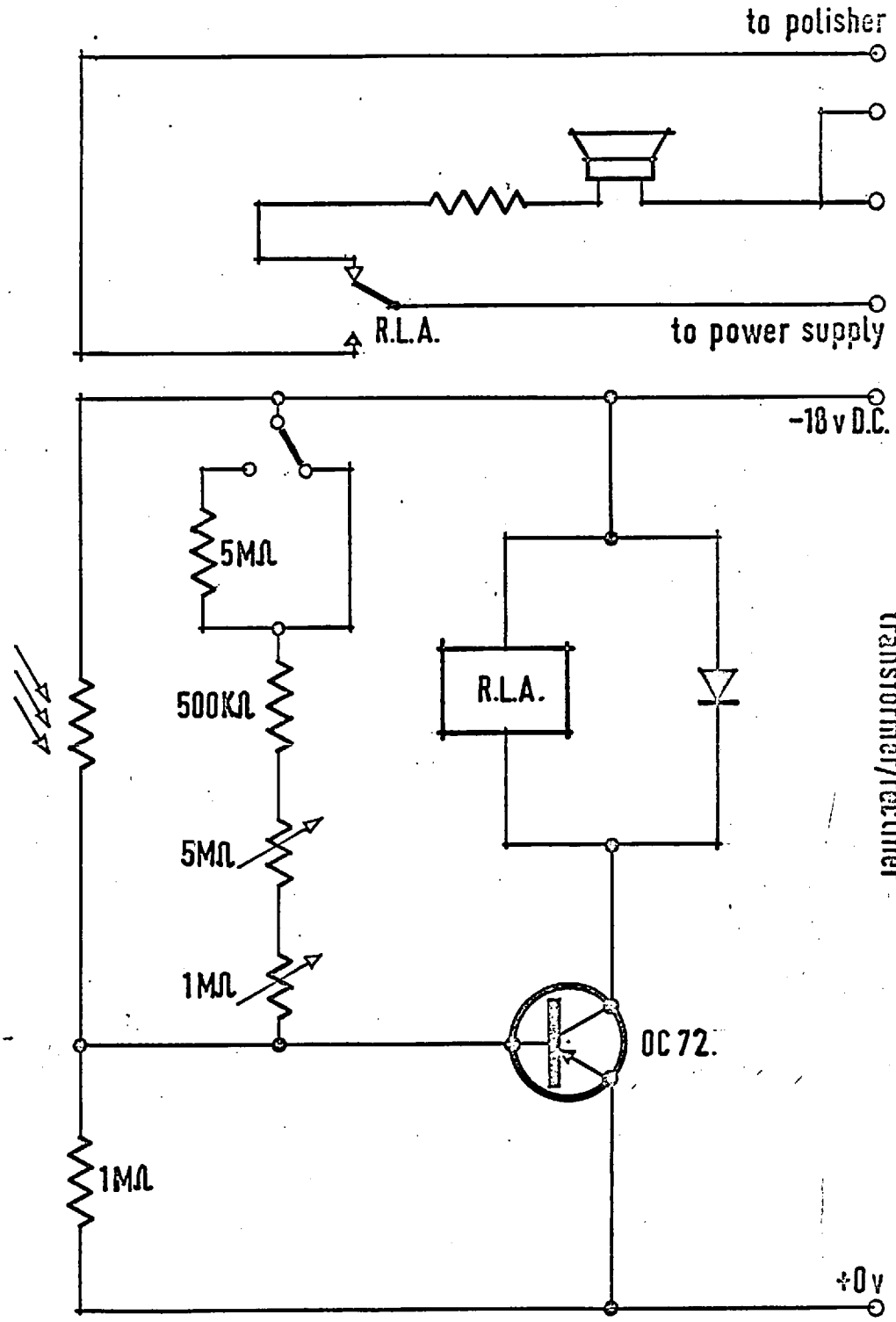

photo-sensitive resistor = Clairex CL603AL

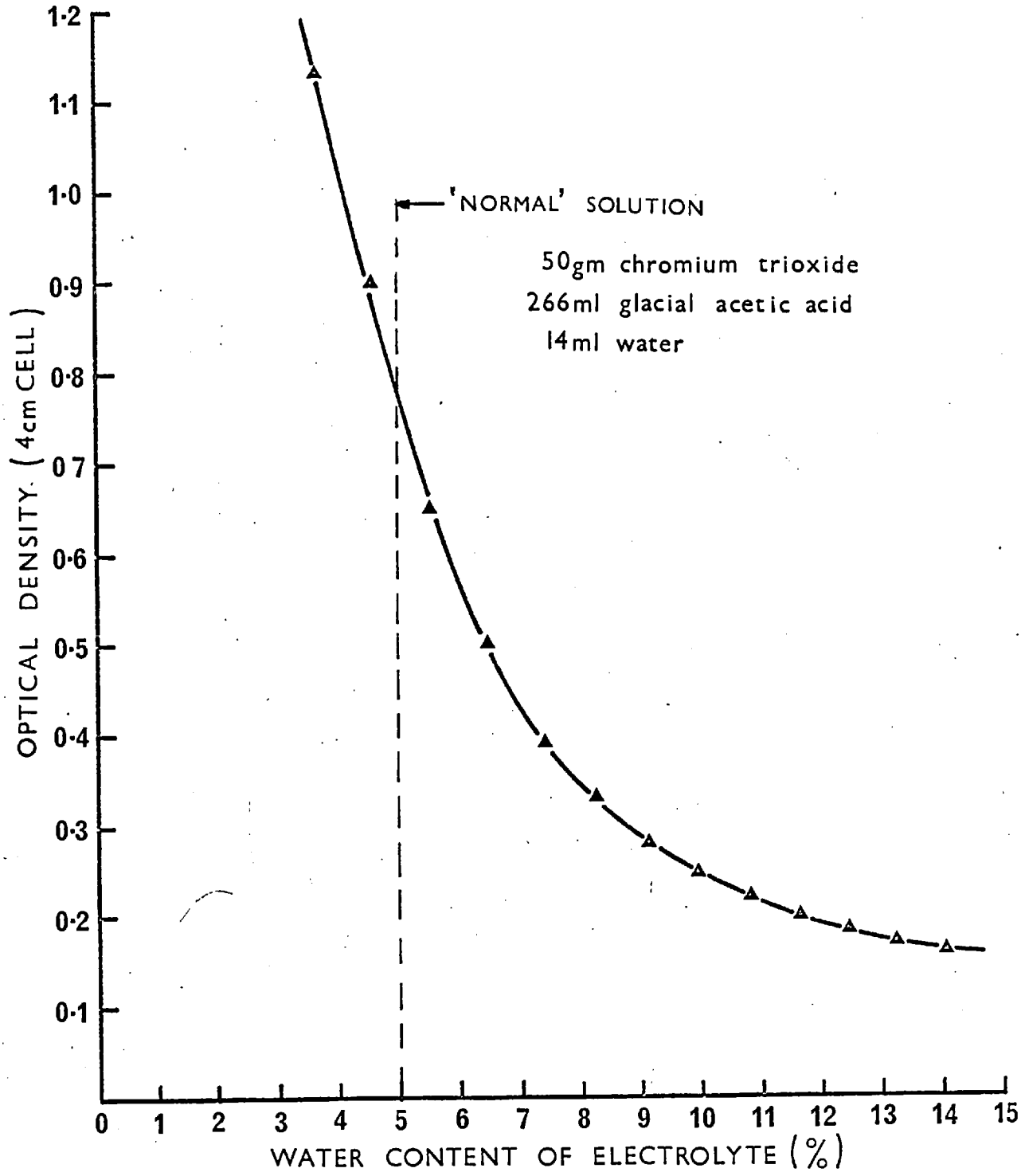

FIG A6 THE VARIATION OF OPTICAL DENSITY WITH WATER CONTENT OF THE ELECTROPOLISHING SOLUTION

that a small change of resistance in the photo-sensitive resistor causes the transistor to fire and the relay to operate.

The Electropolishing solution.

A chromic - acetic acid electrolyte was used with the basic composition 266 ml glacial acetic acid 50 gm CrO_3 and 14 ml water. Although this solution is opaque to the eye, spectrophotometry indicated a good transmission in the infra red range and a marked dependance of the optical density on water content, as shown in Fig. A6. In view of these results the photo-sensitive resisotr chosen for this for this application (Clairex CL603AL) was red-sensitive and the following procedure was adopted to determine the optimum water content of the solution. The apparatus was assembled without a specimen in position and the electrolyte was circulated. With the light on the resistance of the photo - sensitive resistor was noted, and water added drop by drop until a precipitous drop in resistance was observed. This was the electrolyte composition used; further addition of water were found to be detrimental to the quality of the polish.

Summary.

Using this technique specimens with large electron - transparent areas could be rapidly and reliably produced. Loading and washing the specimen were facilitated by the removable specimen holder and the automatic detection system ensured reproducable results and a considerable saving in time over more conventional preparation techniques.

APPENDIX B

Curie Point Determination

The modified Weiss theory indicates that in high fields, at temperatures near the Curie point, the curve relating the saturation magnetization (I_s) to the absolute temperature (T) is given by

$$\frac{I_s}{I_o} = \tanh \frac{I_s / I_o + H/NI_o}{T/\theta}$$

Where I_o is the saturation magnetization at T = 0
N is the molecular field constant
θ is the Curie temperature
H is the field.

The measurements must be made at high fields to ensure that all domains in the specimen are oriented parallel to the direction of the field. In this condition the local magnetization within a domain (I_s) is equal to the magnetization (I) of the specimen as a whole. The high field applied, however, has the affect of slightly increasing the domain magnetization over its spontaneous value in weak fields. Weiss and Forrer obtained curves of σ_s ($=^{Is}/d$) vs temperature at various high field strengths as shown in Fig. B1a. They selected points on the curves for a constant σ_s value and extrapolated back to find the curve for H = 0. This extrapolation was found to be linear for high field values in agreement with theory. From the curve so constructed σ_s values, corresponding to various temperatures, were read off and σ_s^2 was plotted against T as shown in Fig. B1b. The temperature at which the curve reaches the axis i.e. at $\sigma_s^2 = 0$ and therefore $I_s^2 = 0$, is defined by Weiss as the Curie point.

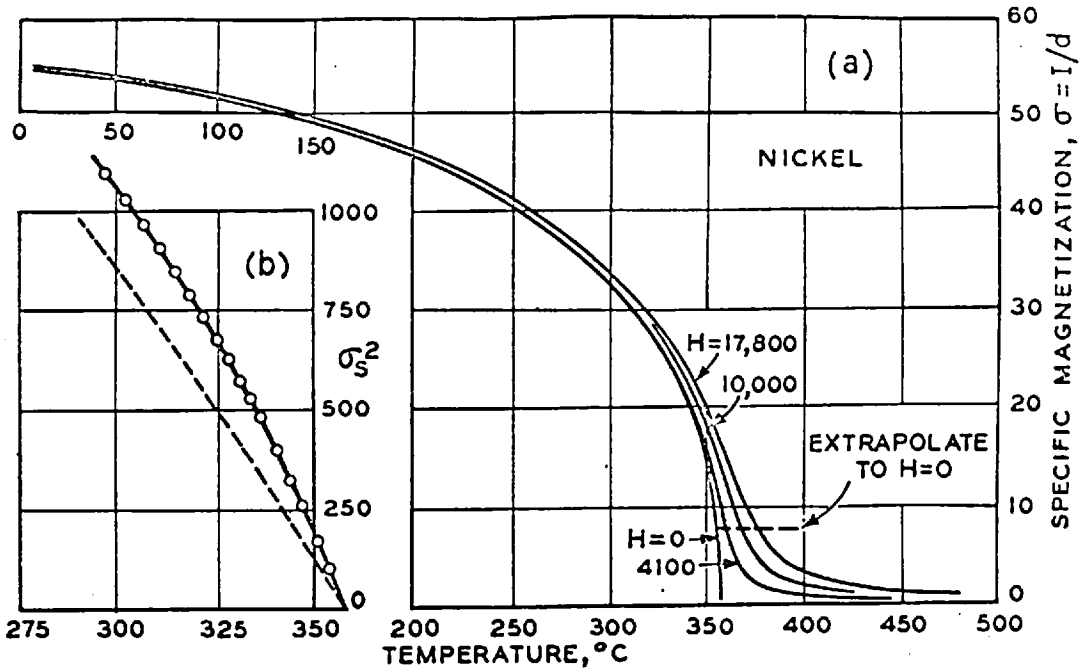

Fig B1 Method of determining the saturation magnetization, σ_s, and the dependence of σ_s^2 on the temperature to determine the Curie point.
after Weiss and Forrer[81] p717

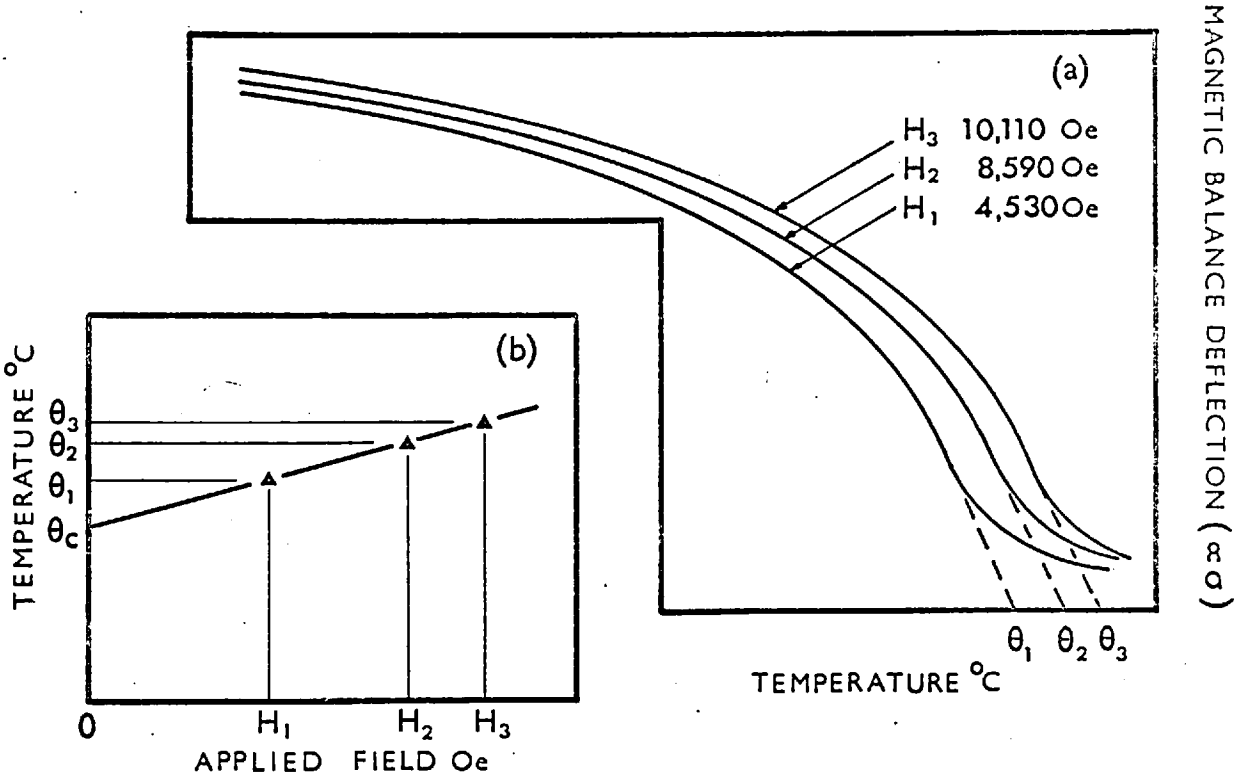

Fig B2 Simplified method of Curie temperature determination used in this investigation

In the present investigation the curves obtained were of transducer deflection (D) vs temperature. This deflection is proportional to the force on the specimen (F) which is related to σ by the following expression

$$D \propto F = \sigma m \, dH/dx$$

In each measurement the specimen was at the position od maximum dH/dx and the location of this maximum for the apparatus was stationary for all field values used (H.Smith Ph.D thesis London University 1968). The absolute value of dH/dx for different field settings is, however, different and thus absolute values of σ can only be obtained by comparison of the measured deflection with the deflection produced by the same mass of iron at the same temperature. This is a lengthy process and thus for this investigation the following technique was adopted.

The steeply falling section of each curve was extrapolated to zero deflection as shown in Fig. B2a giving a value of temperature characteristic of each field value. These points were then plotted against the field strength and extrapolated linearly to zero field Fig. B2b. Thus instead of obtaining a curve of σ vs T for zero field, only one point was obtained which was taken as the Curie point. Experiments with pure iron and pure nickel, using this technique gave the Curie temperatures shown below, the generally accepted values are shown in brackets.

Curie point of pure iron 768 $\pm$ 3°C (770°C)
Curie point of pure nickel 360 $\pm$ 3°C (358°C)

The accuracy of the method is governed by the individual extrapolations involved but in view of the large temperature

scale used on the X - Y recorder and the steepness of the curves approaching the Curie point an accuracy of $\pm$ 3°C is considered appropriate.